Subchannel Thermal-Hydraulic Experimental Program (STEP)
Volume 2: Void Fraction by Gamma Scattering

NP-1493, Volume 2
Research Project 765

Final Report, August 1980

Prepared by

THE BABCOCK & WILCOX COMPANY
Alliance Research Center
Research & Development Division
Alliance, Ohio 44601

Principal Investigators
L. A. Zielke, Program Manager
K. W. Grant, Data Analysis
J. G. MacKinnon, Experimentation

Prepared for

Electric Power Research Institute
3412 Hillview Avenue
Palo Alto, California 94304

EPRI Project Managers
D. Cain
H. A. Till

Water Reactor System Technology Program
Nuclear Power Division

ORDERING INFORMATION

Requests for copies of this report should be directed to Research Reports Center (RRC), Box 50490, Palo Alto, CA 94303, (415) 965-4081. There is no charge for reports requested by EPRI member utilities and affiliates, contributing nonmembers, U.S. utility associations, U.S. government agencies (federal, state, and local), media, and foreign organizations with which EPRI has an information exchange agreement. On request, RRC will send a catalog of EPRI reports.

NOTICE

This report was prepared by the organization(s) named below as an account of work sponsored by the Electric Power Research Institute, Inc. (EPRI). Neither EPRI, members of EPRI, the organization(s) named below, nor any person acting on their behalf: (a) makes any warranty or representation, express or implied, with respect to the accuracy, completeness, or usefulness of the information contained in this report, or that the use of any information, apparatus, method, or process disclosed in this report may not infringe privately owned rights; or (b) assumes any liabilities with respect to the use of, or for damages resulting from the use of, any information, apparatus, method, or process disclosed in this report.

Prepared by
The Babcock & Wilcox Company
Alliance, Ohio

EPRI PERSPECTIVE

PROJECT DESCRIPTION

This is the final report of Phase II (RP765) of the Subchannel Thermal-Hydraulic Experiment Program (STEP). Phase II was designed to measure void fractions for selected heat transfer conditions in a simulated pressurized water reactor fuel rod bundle. Phase I was designed to study the mixing characteristics of mass and energy for a reactor fuel rod bundle; its results are presented in Volume I of EPRI Final Report NP-1493. Both experiments were conducted to help improve subchannel fluid flow and heat transfer codes. Little is known about the exact type of two-phase flow taking place in high-pressure systems. Improved accuracy in predicting void fraction and heat transfer will result in more accurate pressure drop and flow distribution calculations.

PROJECT OBJECTIVE

The objective is to characterize the void fraction in fuel subchannels to improve void fraction and subcooled models. These models will ultimately be used to improve reactor core analysis codes. The measurements used an improved gamma-ray scattering technique.

PROJECT RESULTS

The results indicate that significant void distributions can exist across a subchannel. The voids tend to distribute in the center of the flow channel. Vapor generation and void fraction were compared to results produced by several subcooled, boiling, and void-fraction models. The ones that most closely predict the experimental data are identified.

The information is of interest to those involved in core and reactor systems analysis.

H. Till, Project Manager
Water Reactor System Technology Program
Nuclear Power Division

ABSTRACT

This volume provides a description of the gamma-scattering technique for the measurement of local void fraction within complex geometries. The technique was applied to measurements in the center subchannel of a 4 x 4 array of electrically heated rods with four heated walls.

Over 300 data points were obtained covering thermal-hydraulic conditions typical of light water reactors. Results indicate a large variation of void fraction within the center subchannel and a measured-average void fraction higher than predicted by the COBRA IV computer code.

CONTENTS

CONTENTS (CONT'D)

CONTENTS (CONT'D)

ILLUSTRATIONS

ILLUSTRATIONS (CONT'D)

TABLES

TABLES (CONT'D)

NOMENCLATURE

A	atomic mass
A	cross-sectional area
a	constant in void distribution model
A_G	cross-sectional flow area
b	constant in void distribution model
C	compton scatter factor
C	constant in collimator set 2 weighting functions
C, C_1, C_2, C_3	detector response calibration coefficient
C_1, C_2, C_3	correlation constants
C_o	distribution parameter in drift flux model
C_p	specific heat at constant pressure
D	constant in collimator set 2 weighting functions
d	rod diameter
D_h	hydraulic diameter
E	constant in collimator set 2 weighting function
E	energy of the incident gamma
E	relative error (see Eq. 3-26)
E	energy of the reflected gamma
F	constant in collimator set 1 weighting function
f	geometry factor in quality calculation
f_0, f_1, f_2	attenuation factors (see Eq. 3-8 and 3-9)
f_I, f_T	rod scatter correction factors for magnetic rod bow and temperature expansion, respectively
Fr	Froude number
G	mass flux
$\bar{G}$	average bundle mass flow rate
g_0, g_1, g_2	geometry ratio (see Eq. 3-8 and 3-9)
g_c	gravitational constant
HBE	heat balance error
h	enthalpy
h	rod bundle depth dimension
h_f	saturated liquid enthalpy
h_g	saturated vapor enthalpy
h_ℓ	liquid enthalpy
I	intensity of a gamma beam
i	material index (see Eq. 3-3)
j	volumetric flux
K_1, K_2	density ratios (see Eq. 3-12 and 3-13)
m	number of materials (see Eq. 3-3)
$\dot{m}$	mass flow rate
M_1, M_2, M_3	material designators (see Figure 3-2)
N_o	rate gammas are emitted from the source
N_{m2}, N_{m3}	rod scatter contribution to the count rates of detectors 2 and 3, respectively
N_{mo2}, N_{mo3}	empty vessel rod scatter contribution to the count rates of detectors 2 and 3, respectively
N_T, N_B, N_S	total count rate, background count rate, and signal count rate (see Eq. 3-27)
N_1, N_2, N_3	count rates on detectors 1, 2, and 3, respectively
P	pressure
P	subchannel pitch
Pe	Peclet number
P_h	heated perimeter
Pr	Prandtl number
P_ϕ	heated perimeter
Q	proportionality constant (see Eq. 3-31 and 3-32)
Q	volumetric flow rate
q_2, q_3	geometry calibration coefficients for detectors 2 and 3, respectively
R	radius
R	regression coefficient
Re	Reynolds number
RSS	residual sum of squares
S	slip ratio
S,So	strength of a gamma beam
s	channel exterior width dimension
T	temperature
T	transmittance
t	time
V	velocity
$\mathcal{V}$	volume
V_{gj}	weighted mean relative drift velocity
W	weighting function
w	rod bundle width dimension

NOMENCLATURE (CONT'D)

We	Weber number
x	quality
x	measure of distance
x	distance in direction of incoming gamma beam
x_d	equilibrium quality at bubble departure
x_{eq}	equilibrium or thermodynamic quality
x_t	true or mass flow quality
x_0	center of collimator set 2 gap measurement
x_0, x_1, x_2, x_3	total distance through water that the gamma beam travels to and from the scatter volume. Subscripts 0, 1, 2, 3 refer to the direction from the scatter volume to the source and detectors 1, 2, and 3, respectively
Y_B^+	dimensionless bubble diameter
Z	atomic number (see Eq. 3-7)
Z	distance in the direction of flow
α	void fraction
β	mixing coefficient
β	volumetric flow fraction
$\overline{\Delta h}$	bundle enthalpy rise
Δh_{sc}	subchannel enthalpy rise
δ	liquid film thickness
ϵ_1, ϵ_2	detector efficiencies
θ	angle between incident and scattered gammas
μ	mass attenuation coefficient
μ	viscosity
μ_c	compton scatter coefficient
μ_1, μ_2	mass attenuation coefficient of gammas in water for incident and scattered gammas, respectively
ρ	density of a material
ρ	fluid density
ρ_e	density of the fluid in the exterior water
ρ_f	saturated liquid density
ρ_g	saturated vapor density
ρ_ℓ	liquid density
$\rho_0, \rho_1, \rho_2, \rho_3$	average fluid density in the paths to and from the scatter volume. Subscripts 0, 1, 2, 3 refer to the directions from the scatter volume to the source and detectors 1, 2, and 3, respectively
$\overline{\rho}_1, \overline{\rho}_2, \overline{\rho}_3$	total average density of the fluid in all paths between the source and detectors 1, 2, and 3, respectively (see Eq. 4-3)
$\rho_m, \rho_{m2}, \rho_{m3}$	Fluid density in the paths of gammas scattered off the rods. Subscripts 2 and 3 refer to gammas counted by detectors 2 and 3, respectively
$\rho_{s2}, \rho_{s3}, \rho_s$	scatter volume density seen by detectors 2 and 3, and in general
σ	surface tension
$\sigma_1, \sigma_2, \sigma_3$	total density attenuation coefficient for the fluid paths between the source and detectors 1, 2, and 3, respectively (see Eq. 4-3)
$\sigma_{e1}, \sigma_{e2}, \sigma_{e3}$	total density attenuation coefficient for the distance through the exterior water region for gamma paths between the source and detectors 1, 2, and 3, respectively
$\sigma_m, \sigma_{m2}, \sigma_{m3}$	density attenuation coefficient in the fluid for gammas scattered off the rods. Subscripts 2 and 3 refer to gammas counted by detectors 2 and 3, respectively
$\sigma_T, \sigma_B, \sigma_S$	standard deviation in the total counts, background counts, and signal counts, respectively (see Eq. 3-28)
σ_w	density attenuation coefficient for gammas traveling through the equivalent distance in water as they actually travel through the rods (see Eq. 4-6 and 4-7)
τ_w	wall shear stress
ϕ	heat flux
$\overline{\phi}$	average bundle heat flux
ϕ_{sc}	subchannel heat flux
Ω	measure of solid angle (see Eq. 3-7)

Superscripts

e	value during experimental run
r	value during reference run

Subscripts

ax	complete mixing
b	bulk
cs	center subchannel
d	bubble departure
f	saturated liquid
g	saturated vapor
in	inlet condition
ℓ	liquid

Subscripts (Cont'd)

m	measured
nx	no mixing
sat	saturation
sc	subchannel
v	vapor
2-c	collimator set 2 center
2-g	collimator set 2 gap

SUMMARY OF PHASE II

Refer to Volume I, "Mixing in a Pressurized Water Reactor (PWR) Rod Bundle", for summaries of the Subchannel Thermal-Hydraulic Experimental Program (STEP) and the Phase I test project.

OBJECTIVE

The objective of this project was to apply a new technique to the measurement of void fraction in a simulated nuclear reactor rod bundle.

BACKGROUND

The gamma scattering technique for void fraction determination was conceived by N. N. Kondic. Three experiments followed that preceded this project effort. First, an unpressurized, low temperature benchscale test was performed to assess the feasibility of using the scattering concept in determining fluid density. The second and third tests were attempts to refine the successful benchscale concept into a laboratory tool capable of making density or void fraction measurements on electrically simulated fuel bundles operating at reactor-like flows, pressures, and temperatures.

The technique of measuring void fraction allows accurate measurements in selecting regions of the flow channel without disturbing the flow. Gammas scatter out of a beam projected into a fluid at a rate proportional to the fluid density. After correcting for beam attenuation in the fluid and scatter from the rods, the gamma detection rate measures the density in a volume defined by the intersection of the exterior (i.e., source and detector) collimator projections. Density is converted to void fraction using the liquid and vapor phase densities.

Void fraction is one of the important parameters involved in the calculation of two-phase pressure drop and nuclear reactivity. A review of the open literature has revealed that there is a wide variety of models available to predict void fraction in two-phase flow. However, due to the complex nature of two-phase

flow, nearly all of these models must rely on experimental data to evaluate some key constant or parameter. Frequently, these parameters cannot be measured directly and are inferred from bulk void fraction data. The measurement of void fraction and other two-phase flow parameters in a heated rod array is an expensive and time-consuming task. As a result, the data base that makes up such an important part of the development of existing models is largely derived from experiments involving much simpler geometries. Thus, void fraction measurement by gamma scattering within a reactor-like geometry at reactor conditions facilitiate a greater understanding of thermal-hydraulic behavior unique to nuclear fuel assemblies.

PROJECT DESCRIPTION

Void fraction was measured in the center subchannel of a 4 x 4 array of electrically heated rods (0.963 cm OD; 1.273 cm pitch) with four heated walls.

Measurements were made at the end of a 1.83-meter uniformly heated test section. Thermal-hydraulic conditions covered the following ranges:

Pressure - 6.90 to 16.90 MPa

Heat Flux - 158 to 1260 kW/m^2

Mass Flux - 204 to 3122 $kg/m^2 \cdot sec$

During the experiment, void fraction was measured in two specific regions of the center subchannel. One area was the gap between the two rods; the other was the central region of the subchannel. Tests were conducted by holding pressure, mass flux, and heat flux constant and taking measurements over a range of inlet temperatures.

RESULTS

- Over 300 void fraction data points were obtained using the previously stated thermal-hydraulic conditions.

- Measurement times were about five minutes -- a significant improvement over previous gamma scattering experiments.

- Analysis of the collimator set 1 and collimator set 2 data has shown that the void fraction versus quality curves demonstrate several general trends predicted by existing void fraction and subcooled boiling models. In the subcooled boiling region, the data show that the void fraction at a given quality is highest for high heat flux to mass flux ratios. In the bulk boiling region, the void fraction at a given quality is highest for the lowest pressure.

- The data from collimator set 2 demonstrate that as boiling begins the void fraction in the gap between the rods is higher than in the center of the subchannel. As the quality is raised, a transition occurs and the void fraction becomes highest in the center of the subchannel. In general, this transition occurs at higher qualities as the pressure increases or the mass flux decreases.

- The data from collimator set 2 also show that under certain conditions steep void fraction profiles exist across a subchannel. The magnitude of these distribution effects appear to be strongly related to the mass flux and, to a lesser extent, also related to pressure. The void distribution effects were seen to be small at pressures greater than about 13 MPa and at mass fluxes greater than 680 $kg/m^2 \cdot sec$.

- A void distribution model has been developed which describes the void fraction in the center subchannel as a function of position. The data from collimator set 2 were used to evaluate constants in the model. Integration of the void distribution function has provided a subchannel average void fraction which can be compared with the predictions of existing models.

- In the bulk boiling region, the observed subchannel average void fractions are higher than existing models, including the homogeneous model, predict. Slip effects would tend to give void fractions lower than the homogeneous model.

- A worst case analysis showed that under conditions of idealized annular flow, the calculated subchannel average void fraction could be higher than the actual subchannel average by as much as $\sim$0.10 in void fraction. However, when this additional uncertainty was taken into consideration, even the highest non-homogeneous model still did not fall completely within the error bands for much of the data.

- In the subcooled boiling region, there are several models which provide a good fit to the data.

- A lack of knowledge about void fractions in neighboring subchannels and the uncertainty in equilibrium quality prevented precise quantification of the effects of lateral vapor motion.

CONCLUSIONS

- The gamma scattering technique was successfully applied to the measurement of regional void fractions within the 4 x 4 rod bundle operating at reactor-like conditions.

- In general, the technique cannot be applied to fast transients. However, under specific conditions of a relaxed accuracy requirement, a large scatter volume, and a very active gamma source, measurement times could be reduced to the point where slow transient void fractions are measurable.

- Application of the technique required considerable front-end engineering, preparation, control, and calibration. The amount of effort is dependent on the application. Effort was particularly acute in this experiment because gamma scattering off the heated rods interfered with the simple fluid scattering measurement. In applications where interference scatter is negligible, implementation of the technique is considerably simplified.

- The analysis of the void fraction data obtained in this program demonstrates that significant void distributions can exist across a subchannel. At higher qualities and void fractions, the vapor phase can be seen to concentrate in the center of the center subchannel.

- The relationship of the data with respect to existing models indicates that this vapor concentration effect may also occur on a bundle-wide basis.

RECOMMENDATIONS

- The gamma scattering technique is recommended as a laboratory tool for nonintrusive, steady-state, regional measurements of density in complex geometries where test conditions justify the expense and effort involved in implementing the technique.

- Several techniques are recommended to simplify the implementation of the gamma scattering technique:

  -- Tungsten collimators should be used to minimize the uncertainty in defining the scatter volume caused by gamma penetration of the collimators.

- -- A high energy gamma source should be used to minimize attenuation. Cesium is a good choice because of its cost and availability.

- -- A high activity source is recommended to minimize measurement times required to obtain a specified accuracy.

- -- Considerable attention to fixing the source-detector-test geometry is recommended to minimize misalighnment problems.

- -- Shielded detectors are recommended to minimize interference from large magnetic fields that accompany electrically-heated test sections.

- -- The avoidance of scatter off of fixed objects that interfere with the detection rate of gammas scattering off the fluid is recommended.

- The data obtained in this program should not be used to develop a new void - quality model for thermal-hydraulic codes such as COBRA. Currently, these codes do not include a perferential liquid/vapor exchange mechanism which may be necessary to describe two-phase flow in rod bundles.

- The evidence for lateral vapor motion between subchannels suggests that further development of subchannel codes must center on a more complete description of the interactions across subchannel boundaries.

- Two fluid models, which use separate sets of conservation equations for each phase, are currently being developed for accident analysis. In order to further improve the prediction of steady-state thermal-hydraulic conditions in rod bundles, these models should be investigated for their ability to properly incorporate a net liquid/vapor exchange process.

Section 1

INTRODUCTION

The objective of this program is to provide basic data on local values of subchannel enthalpy and void fraction obtained from electrically-heated rod bundles at reactor-like conditions. Volume I of this report reviews the subchannel enthalpy measurements taken in the two-phase mixing experiment. Here, Volume II covers the experimental details, analysis, conclusions, and recommendations of the void fraction project.

Historically, the gamma scattering technique was conceived by N. N. Kondich. Three experiments followed that preceded this project effort. First, an unpressurized, low temperature benchscale test was performed to screen the feasibility of using the analytical concept to determine density. The second and third tests were attempts to refine the successful benchscale concept into a laboratory tool capable of making density or void fraction measurements on electrically simulated fuel bundles operating at reactor-like flows, pressures, and temperatures.

The general concept of measuring density by gamma scattering uses the same principles as the more commonly used simple attenuation principles for measuring average density. In a sense, the scattering technique merely views the gamma radiation scattered from a particular region and observes the attenuation of the scattered radiation as well as the attenuation of the primary beam. Such a scattering technique is, of course, not restricted to the particular rod bundle geometry encountered here, but may be used for a variety of other two-phase flow investigations.

The test section geometry used for this project's experimental void fraction determination is a heated shroud, 4 x 4 rod matrix simulating the fuel bundle of a pressurized water reactor's open lattice core. Similar rod bundle test sections are typically used for critical heat flux tests and emergency core cooling studies. The rod bundle is housed in a pressure vessel; the system has been designed to operate at typical reactor pressures, temperatures, and flow rates so that the void fraction data will be representative of typical conditions and geometries.

Section 2

FACILITY DESCRIPTION

1.8 MW HEAT TRANSFER FACILITY

The tests were carried out in the 1.8 MW Heat Transfer Facility shown in Figure 2-1. The facility is a closed-circuit test loop consisting of a pressurizer system, a circulating pump, flow control valves, flow measurement elements, a test section, inlet fluid heaters, and a heat removal system. Test section power is supplied by two 900-kW silicon-diode rectifiers connected in parallel. Loop water is monitored and controlled for conductivity, pH, and oxygen content.

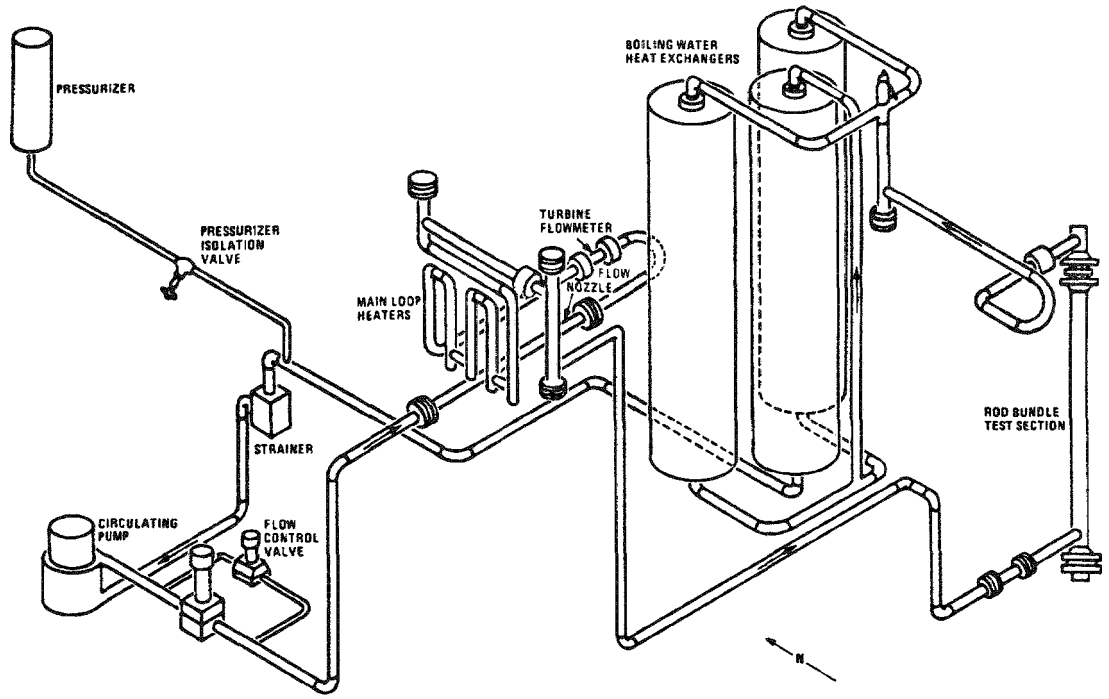

Figure 2–1. 1.8 MW heat transfer facility

VESSEL AND BUNDLE

General Description

The test bundle hardware was designed to simulate a B&W Mark C reactor core geometry (Table 2-1). Pressurized water flowed vertically through a 16-rod (4 x 4) array. (See Figure 2-2.) These rods and the bundle walls were uniformly electrically heated over a 1.83-meter section. The resultant boiling water produced two-phase flow at the exit of the heated length. The void fraction was measured in the center channel of the 4 x 4 array at a point 2.86 cm below the end of the heated portion of the bundle. The bundle and loop were designed to produce a wide range of steady-state conditions simulating normal pressurized water reactor (PWR) and boiling water reactor (BWR) operating conditions.

Table 2–1

BUNDLE GEOMETRY

Bundle Geometry	4 x 4, Heated Wall
Rod OD	0.963 cm
Pitch	1.273 cm
Rod - Wall Gap	0.457 cm
Heated Wall Width	4.475 cm
Flow Channel Size	5.695 x 5.695 cm
Wall to Rod Heat Flux Ratio	Collimator Set 1 - 0.795; Collimator Set 2 - 1.000
Heated Length	1.83 meters
Grid Spacing	38.1 cm
Void Fraction Measurement Location	2.858 cm Below End of Heated Length

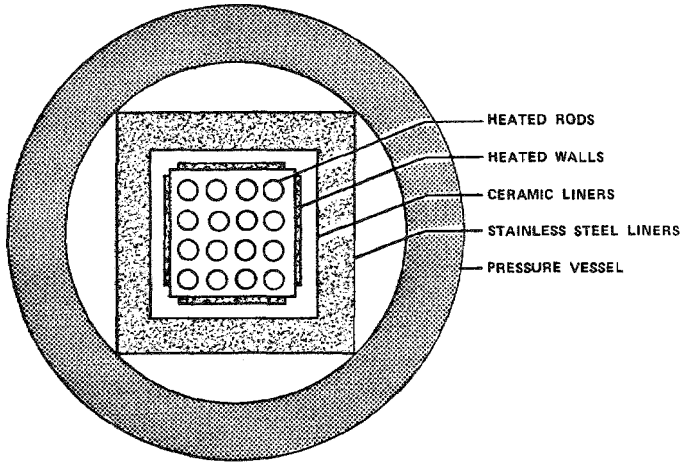

Figure 2–2. 4 x 4 rod bundle with heated walls

The parameters that determine void fraction are pressure, heat flux, flow rate, and enthalpy. However, these parameters could not all be varied independently of each other. The primary constraint was critical heat flux (CHF) which was avoided to prevent the heated rods from melting. CHF was avoided in several ways. First, some of the tubes were instrumented with thermocouples to detect sharp increases in temperature. Also, the heated wall was designed to produce a heat flux of 82.9% of the rod heat flux in order to avoid CHF on the uninstrumented walls. Finally, the test matrix was checked against a CHF correlation and conditions were kept out of the CHF range.

The gap between the heated wall and the outer rods was designed to produce a reasonably flat radial flow and enthalpy profile within the constraint of avoiding CHF on the heated walls. A flat profile minimized the effect of mixing on the center channel flow and enthalpy.

A ceramic liner surrounded the heated walls to define the flow geometry and electrically insulate the rod bundle from a stainless steel liner used to give the bundle support. A pressure vessel surrounded the entire test bundle and formed the pressure boundary. Between the inner wall of the pressure vessel and the stainless steel liner was a cavity filled with stagnant water.

The normal thickness of the vessel wall and steel liner wall would prohibit gammas from passing through effectively. To circumvent this problem, special features were designed into the pressure vessel and stainless steel liner to facilitate the gamma traverse from outside the vessel into the center channel of the bundle and back out of the vessel. Ports were designed into the vessel and liner which considerably reduced the steel thickness at the entry and exit directions of the gamma beam while still maintaining a reliable pressure boundary.

Hardware

Rods. All rods were identical except for minor differences in the lengths of the end connectors to aid in the installation and connection of electrical leads. The rods extended through both ends of the vessel and were divided into four sections according to material. The lower section was solid copper and extended from the lower end of the heated length out through the vessel to the bottom electrical connectors. The copper was nickel plated to retard corrosion. The next section was the Inconel X-750 heated portion, as described by Table 2-2.

Table 2–2

HEATED RODS
(Heated Portion)

Material	Inconel X-750
Length	1.83 meters
OD	0.963 cm
ID	0.818 cm

The high resistivity and the thin wall in the heated section combined to produce efficient resistance heating when current was applied. Above the heated portion was a thick-walled nickel section that was used to electrically connect the upper end of the heated section with the nickel connector plate. The nickel plate was used to conduct the electric current from outside the vessel into the rods that hung from the plate. Above the nickel plate, a stainless steel instrumentation lead passed from inside the rods out through the upper seals of the vessel. The inner cavity of the rod was open to the atmosphere.

Assembled rods were hydrostatically tested, and the length of the heated portion and its resistance were checked according to Alliance Research Center (ARC) Quality Assurance procedures.

Shrouds. The four heated walls (or shrouds), one for each side of the bundle, were made up of a middle section (used for heating) and upper and lower connections. The middle section was composed of a thin strip of Inconel 600 which, like the rods, had a high resistivity to facilitate electrical heating.

There were two sets of shrouds used in this test. The first set, used in runs up to No. 592, was attacked by electrolysis and had to be replaced. The replacement set was slightly thicker and was used on all subsequent runs. The loss of the shroud was sudden and did not affect any of the data preceding the replacement of the shroud. A description of the shrouds is given in Table 2-3.

Table 2–3

HEATED SHROUDS
(Heated Portion)

Material	Inconel 600
Length	1.83 meters
Width	4.74 cm
Thickness	0.470 mm (First Set); 0.584 mm (Second Set)

These strips did not meet at the corners since this would have caused overheating in the small corner channel. The strips, therefore, rested in shallow slots in the ceramic liner. The depth of the slot was about equal to the thickness of the strips thus producing a square channel with no discontinuities at the edge of the strip. At regular intervals, the shroud was bolted to slots in the ceramics. This prevented the magnetic attraction of the rods and flow effects from peeling the shroud away from the channel wall. The bottom of the heated strip was welded to a thicker nickel strip section, which in turn was connected to a section consisting of two copper rods similar to those on the heated rods. These copper ends passed through the lower seals and connected to the electrical leads below the vessel. The copper portions were plated to retard corrosion. The upper end of the heated strip was welded to a thicker Inconel 600 strip section which in turn was connected to a section represented by two solid Monel 400 rods.

These rods electrically connected the heated strips to the top conductor plate from which the entire shroud assembly hung. Since the shrouds were not instrumented, no connectors from the shroud extended beyond the connector plate. Shroud thickness and the width and length of the heated portion along with its resistance were kept within tolerances and checked according to ARC Quality Assurance procedures.

The shrouds and rods were designed so that the voltages at all grid locations, including those located on the electrical connector extensions, matched. This prevented current cross-flow through the grids between the rods and the shroud.

Ceramic Liners. Aluminum oxide ceramic liners formed the outer boundary of the flow channel and electrically insulated the heated wall and rods from the rest of the test section parts. The liners were molded into "L"-shaped sections, four of which combined to form a square channel. The ceramic liners also supported the heated walls which were periodically bolted to the ceramics in such a manner that they could thermally expand independently of the ceramics.

Stainless Steel Liners. Four 1.9 cm thick stainless steel liner strips were bolted together into a square around the ceramic liners to form a rigid support for the flow channel. Circular plates bolted at the top and bottom of the liner assembly were sized to the inner diameter of the pressure vessel and centered the bundle within the vessel.

This design divided the inside of the vessel into four volumes as shown in Figure 2-3. Above the upper plate was the upper cavity and below the lower plate was the lower cavity. Between the plates was the flow channel located inside the liners with the middle cavity on the outside.

The liners were too thick to allow efficient passage of the gamma radiation. Instead, holes were cut into the liner at the entrance and exit paths of the gamma beam. To prevent water from flowing through these holes from the middle cavity into the flow channel, a thin disc was welded over the inner edge of the holes.

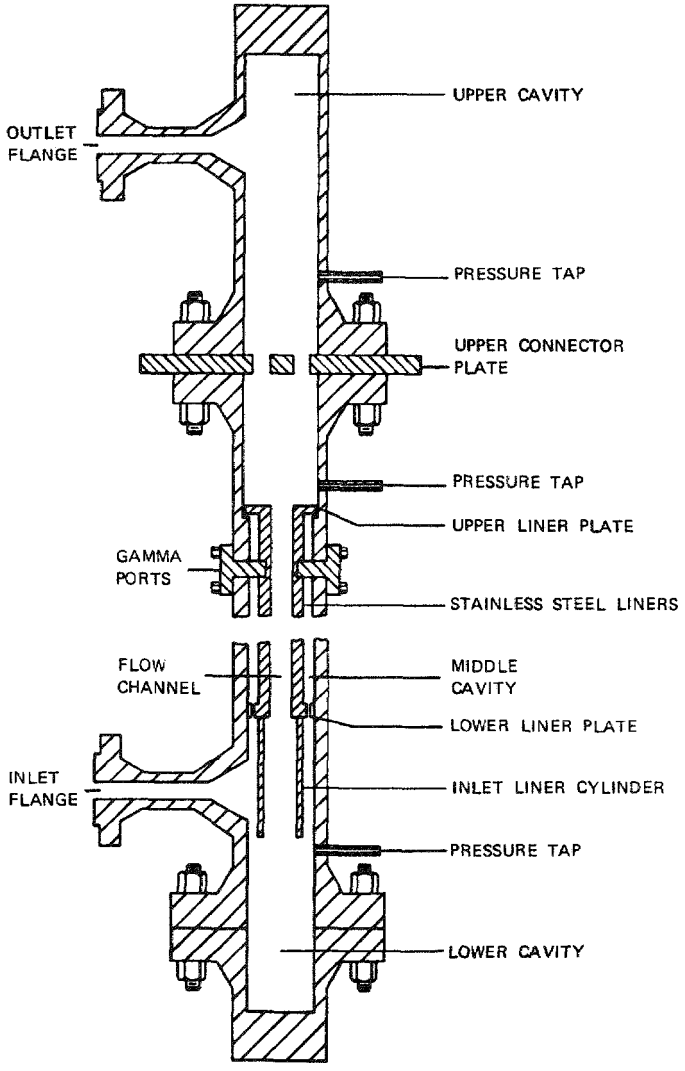

Figure 2–3. Arrangement of bundle liner within the pressure vessel (ceramic, rods, and grids not shown)

The liner extended below the lower plate in the form of a cylinder. The water inlet to the vessel was located at this level. During operation, the water entered the lower cavity, impinged on the cylinder walls, and was directed downward outside the cylinder. The water reversed direction at the bottom of the vessel and traveled up through the center of the cylinder and into the flow channel to produce an even flow distribution. The calming length prior to the heated section was about 12 times the hydraulic diameter.

Gamma Ports. The gamma port design served two purposes. One was to reduce the amount of material the gammas must traverse as they passed into the center channel of the bundle and back out. The second was to form and direct (collimate) the gamma beam into the center channel.

Without a special port design, the amount of material the gamma beam would have had to traverse would have been considerable. The beam would have had to travel through 2.5 cm of vessel wall, 2.5 cm of water in the middle cavity, and 1.9 cm of metal liner to reach the ceramic liner. After scattering, the beam would again have had to pass through these materials on its way out. This process would have reduced the intensity of the gamma beam to 0.17% of its ideal value based on traversing no metal or water. The object of the port design was to minimize the reduction in the beam intensity while maintaining a reliable pressure boundary between the water and the isotopic gamma source.

Without a special port design, gamma beam formation would also have been inefficient. Collimation would have occurred outside the vessel wall -- far from the scatter volume. Figure 2-4 shows the effect of positioning on beam efficiency. Because of the spreading beyond the outer edge of the collimator, a small collimator hole would have been required without the port. This would have reduced the strength of the beam and also produced a nonuniformity in the beam. A further difficulty would have been the problem of aligning the beam to intersect the center subchannel. The closer the collimator was to the scatter volume, the easier it was to line up the source and collimators with the scatter volume.

Two series of four ports were used in the experiment. Each series produced different scatter volumes within the rod array. The first series formed a scatter volume that allowed a detailed examination of the void fraction in the central region of the center subchannel. The second series formed scatter volumes that allowed a determination of the void fraction gradient within the subchannel.

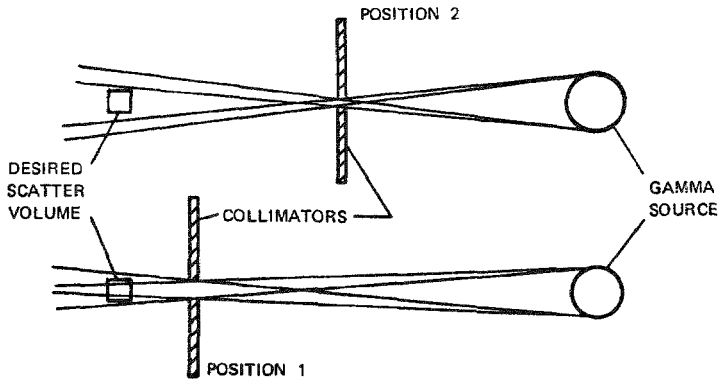

Figure 2–4. Effect of collimator position on gamma beam

Each port consisted of a concentric barrel and flange assembly as shown in Figure 2-5. The flange was bolted onto the side of the vessel. The barrels contained at least one vertical tapered slit through its length to allow gamma passage. The flange end was open to the atmosphere; the other end was covered with a 0.152 cm thick stainless steel strip that formed the pressure boundary.

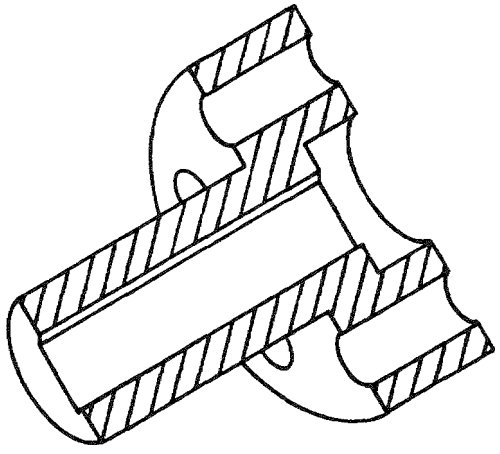

Figure 2–5. Cutaway view of port assembly

A cross-sectional view of the assembly for the collimator set 1 ports is shown in Figure 2-6. While maintaining a reliable pressure boundary, this design caused the gamma beam to reduce to only 60% of its ideal value during entering and exiting of the bundle compared to 0.17% without the ports.

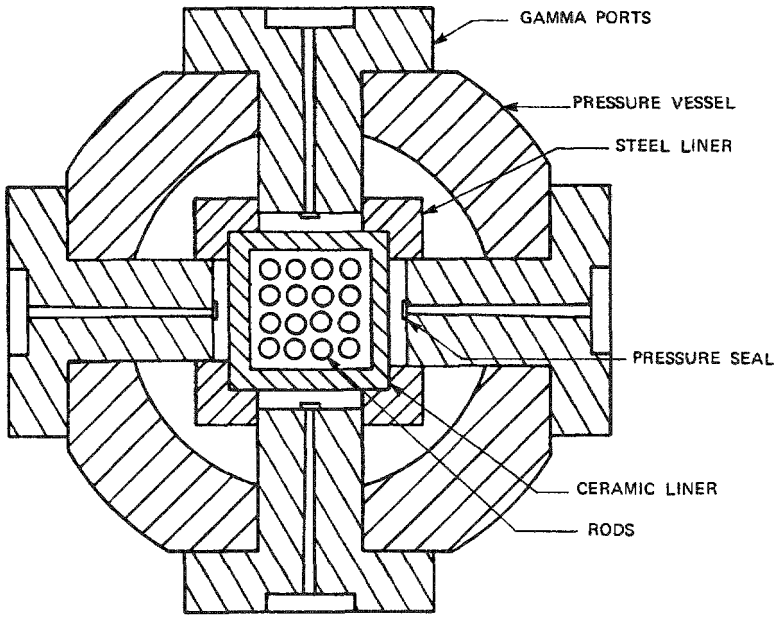

Figure 2–6. Port assembly for collimator set 1

Blast Deflector. A steel shield was placed between the upper flange and the gamma source. If the upper gasket failed on the side of the gamma source, the force of the blowdown would have been redirected away from the gamma source.

Insulation. The entire surface of the vessel was insulated with approximately 5.1 cm of fibrous insulating material, except for a small area at the entrance to each of the gamma ports.

Loop Instrumentation and Calibration

Two distinct instrumentation systems were used in this experiment. One system collected the thermal-hydraulic data; the other collected the gamma data.

Thermal-hydraulic data were read by various instruments that produced a voltage output. This output was read by a high-speed voltage reader which converted the reading to a digital signal and sent the data to a computer. A listing of instruments used is contained in Table 2-4.

Table 2–4

INSTRUMENTS

Description	Manufacturer and/or Model Number
Inlet/Outlet RTDs	Rosemount 78-69-29
Outlet Pressure Transducer	BLH 402469
Flow Nozzle (2-inch)	Bailey
Flow Nozzle (3-inch)	Bailey
Flow Transducer (0 - 25 inches)	Barton 367-183
Flow Transducer (0 - 100 inches)	Barton 295-164
Flow Transducer (0 - 125 inches)	Bailey BQ55221
Flow Transducer (0 - 400 inches)	Barton 295-165
Current Shunt	Esterline Angus 20000 AMP
RTD Resistance Standard	Leeds & Northrup 4030B
Low Level Analog Input System	Computer Products

Temperature Monitoring. Temperatures at various points were monitored by thermocouples. These readings were used in several capacities not directly related to the collection of test data. Calibration of the thermocouples was provided by the manufacturer. Traceability to the National Bureau of Standards (NBS) was not required.

- Thermocouples were placed on the vessel surface at several locations to correlate heat loss data.
- Thermocouples were placed on the inlet and outlet lines that carry cooling water to and from the lower seals. Since current conducting rods passed through the lower seals, a certain amount of heat was generated in this region. The water conducted excess heat away. The thermocouples were monitored by a computer for abnormal readings.
- Thermocouples were placed inside some of the tubes at a point 0.953 cm below the top of the heated length to monitor CHF indications.

Pressure. Pressure taps were located at three points in the vessel wall as shown in Figure 2-2. One was located in the lower cavity just above the lower flange. Another was located in the upper cavity just above the inlet liner plate. The last tap, also in the upper cavity, was located above the upper flange. The middle tap was used for data collection and monitoring of pressure. The pressure differences between this tap and the other two were checked for abnormal readings that could indicate a possible flow blockage. The pressure transducers were calibrated by standard procedures using a NBS traceable dead-weight tester.

Temperature. Two resistance temperature detectors (RTDs) were located at the inlet to the test vessel and two at the outlet. The RTDs were used to measure temperature rise across the bundle and absolute temperature for use as data and for monitoring. Calibrations certified traceable to the NBS were provided by the manufacturer.

Flow Rate. Flow rate was measured using a 3-inch flow nozzle for the high flow rates and a 2-inch nozzle for the low flows. The pressure drop was read by several transducers covering different ranges. Both the flow nozzles and the transducers were calibrated traceable to NBS. The flow nozzles were calibrated by using weigh tanks with pressure drops measured by transducers and manometers. The pressure transducers were calibrated with a dead-weight tester. An RTD was located in the fluid line near the flow nozzle to measure the fluid temperature.

Voltage. A set of voltage taps was placed in each of two tubes. One lead of the set was attached to the bottom of the heated length; the other to the top. Two other sets of voltage taps were placed on the buss connectors to measure the overall voltage across the bundle. A third location for voltage taps was at the lower flange and sparkplate where the readings were checked for shorts across the lower gasket.

Current. The electric current into the test vessel was measured by a voltage drop across a current shunt. The resistivity of the current shunt was calibrated traceable to the NBS.

Voltage Dividers. The high speed voltage reader was limited to a maximum voltage of 1 volt. Some of the outputs of the transducers and voltage taps were greater than this. Voltage dividers were used to step the voltage down to measureable levels. These dividers were calibrated traceable to the NBS. The resistivity of the dividers was chosen so as not to interfere with the measurement.

GAMMA PRODUCTION AND DETECTION SYSTEM

General Description

The void fraction measuring technique is based on the proportionality between water density and the scatter rate of gamma rays. The conversion of density to void fraction is discussed in Section 4 (Data Acquisition and Reduction). To measure the local density at a given point, a gamma beam is directed at that point and the

number of gammas scattered from that point are counted. There were three major features incorporated in this design to facilitate the technique -- the source, collimators, and gamma detectors. The arrangement of these is shown in Figure 2-7.

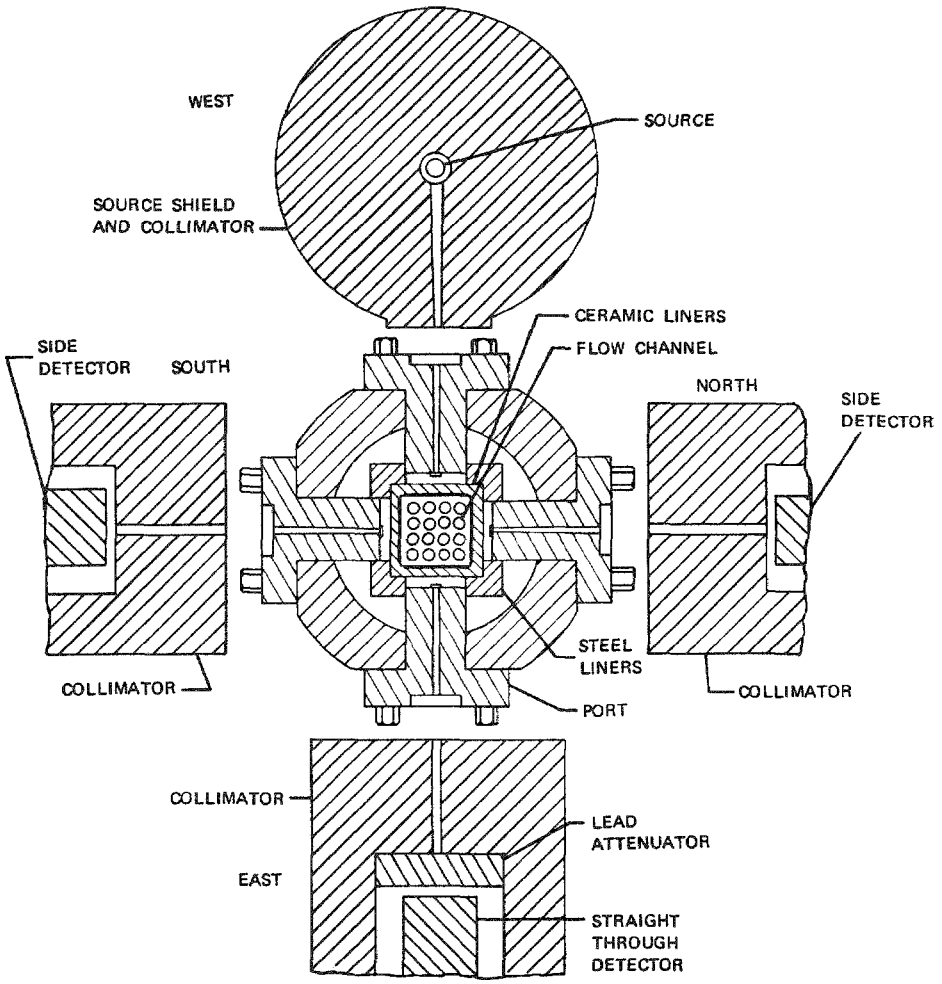

Figure 2–7. Gamma production and detection system arrangement

The gamma source consisted of a cylinder containing radioactive cesium. Since the source emitted gammas equally in all directions, the formation of the gamma beam was simply the process of screening out all gammas not properly directed by shielding and collimation. In the present arrangement, about 1 in 20,000 gammas was emitted in the right direction. Because of their common direction, gammas directed toward the center flow channel constituted the beam. As the beam entered the bundle, gammas collided with electrons in the coolant and bundle material and scattered in all directions out of the beam at a rate proportional to the electron

density and the strength of the beam. The process continued as the beam passed through the local scatter volume of interest. Since the objective was to measure the gammas that scattered out of this chosen volume alone, a further screening was required so that the detectors were exposed only to gammas emitted from the scatter volume. About 1 in 100 gammas that reached the vessel pressure boundary scattered out of the scatter volume.

The isolation of a specific scatter volume and the selection of a specific scatter angle was done simultaneously using collimators passing out of the test vessel on both sides of the vessel at 90° with the source beam. This screening reduced the numbers of gammas detected by a further factor of 1 in 5000.

In addition to the side detectors which detected the compton scatters, a detector located in the forward direction detected the gammas that passed through the vessel. The reasons for the forward detector were as follows. Density affected the side detectors by two mechanisms. One was by compton scattering; the other was the reduction in beam strength caused by passing through the water. The forward detector was affected only by the second mechanism. The forward detector was used to correct for the reduction in beam intensity, thus leaving essentially a linear relation between density in the scatter volume and the detection rates of the side detectors.

A consequence of the compton scatter technique was that relatively long counting times were required to accumulate enough gamma counts in the detectors to reduce statistical errors. The combination of scattering rates, screening, and passage through bundle parts and water caused only about one gamma in 2×10^{10} gammas emitted from the source to reach the side detectors. Consequently, it was necessary to use a source far more active than that used in conventional gamma densitometry and to limit testing to steady-state conditions.

Hardware

Gamma Source. The gamma source was 130 Curies of Cesium 137 that produced 4.31×10^{12} gammas a second at an energy of 661.6 keV. This source strength permitted typical counting times on the order of 5 minutes per data point. At this energy, the intensity reduction of a gamma beam traveling through room temperature water would be about 20% per inch and through stainless steel would be about 80% per inch. The cesium was doubly encapsulated in stainless steel with each wall being 0.05 cm thick. The material formed a cylinder inside the

capsule nearly 5.1 cm high with a 1.0 cm diameter. The source capsule was contained within a vertical tube surrounded by at least 10.2 cm of lead. The capsule was connected to an apparatus which allowed it to move up and down within the tube upon manual or electrical activation. In the deactivated (down) position, the source was surrounded on all sides by lead. In the activated (up) position, lead surrounded the source except for a slit aimed at the vessel to form the gamma beam.

Gamma Selection Hardware. A cross-sectional view of the densitometer plane showing the vessel internals, the gamma source, shielding, and detectors is as shown in Figure 2-7. The significant feature is the passage that connected the source and detectors to the rod array. These passages collimate and screen the gammas: that is, they allowed a selection of gammas to travel from the source into the rod array and back out to the detectors.

Two complete series of collimators were used in the experiment. One defined a scatter volume which was located at the center of the central subchannel. This first series (collimator set 1) is the one shown in Figure 2-7. A second series of collimators (collimator set 2) was installed to determine the difference in density between the center of this subchannel and the gap region between the rods.

Detectors. The gamma detectors were germanium-lithium (GeLi) detectors that were chosen for their insensitivity to magnetic fields. The detectors produced an electrical pulse proportional to the energy of each detected gamma. Sodium-iodide detectors were found to be too sensitive to the magnetic fields produced by their proximity to the electric current in the rod array and buss bars.

Peripherals. The material in the shields around the detectors was lead. Because of the high operating temperatures of the nearby vessel and low melting point of lead, a copper tube circulated cold water through the shields. Thermocouples were located on the lead surface to monitor the temperature.

The liquid nitrogen supply to the detectors was kept in tanks associated with each detector and was replenished every few days. In the interest of safety, a remote filling system was used to eliminate the need to enter the vessel room.

The source and each detector with its associated shielding sat on adjustable tables that allowed each of them to move in any direction in the horizontal plane independent of the other. These tables were in turn mounted on a single rotating frame which allowed the source-detector unit to rotate as a whole around the vessel a total of 3° in either direction. Adjustments in the alignment of the source and detectors were made easily.

Section 3

GAMMA MODEL DEVELOPMENT

This section describes the development of the mathematical model that describes the response of the gamma detectors to the fluid density. From this model, the procedures used to obtain density during experimentation are developed and are later described in the portion of Section 4 entitled "Void Fraction From Density".

In this section (Section 3), the following discussions are presented:

- A general description of the behavior of gamma rays interacting with matter. This behavior forms the basis for the gamma scattering technique.
- Development of the equations describing an idealized gamma scattering technique and an examination of the errors introduced by the assumptions that simplify the development. These equations are derived for the present project. Other approaches and mathematical descriptions can be found in papers by Kondic (1) and Kondic and Lassahn (2).
- Development of the equations further to account for scattering off the rods that are part of the 4 x 4 flow geometry. The equations developed in this section are the ones used in the data reduction.

THE INTERACTIONS OF GAMMA BEAMS WITH MATTER

Gamma Beam

The characteristic of a gamma beam that is of concern is its interaction with matter. For the purpose of this analysis, the gamma beam can be adequately described as a collection of particles traveling in roughly the same direction. Matter is best described as a random collection of particles uniformly distributed in space and separated by very large distances relative to their diameter.

As a beam of gammas enters matter, the beam begins to attenuate. Attenuation is the macroscopic result of the random collisions between the gamma particles and the particles of the material. The attenuation at the energies of gammas that concern us in this report is caused by two mechanisms that compete with each other.

One is absorption, technically known as the photoelectric effect. In this case, the gamma collides with an electron, imparting all of its energy to the electron, which in turn diffuses the energy about the surrounding material. The second mechanism is compton scattering. In this case, the gamma imparts only part of its energy to the electron in a billiard ball-type collision. The gamma then scatters at a degraded energy.

At the energy of gammas emitted from cesium, the attenuation process is almost entirely by compton scattering. See Table 3-1. As the gammas pass into a material, the fraction of gammas that have undergone at least one collision begins to rise and would soon overwhelm the original uncollided beam except for three mitigating effects:

1) The scattering mechanism redirects the gamma out of the beam so that multiple scatters are required to return to the gamma to the beam.

2) As the gammas collide, they lose energy. The detector discriminates the energy level and so discriminates against scattered gammas.

3) As the energy of a gamma decreases, the probability of an absorption rises sharply (i.e., by photoelectric effect), hence eliminating scattered gammas after several collisions.

Table 3-1

ATTENUATION COEFFICIENTS
(cm^2/gm)

	Energy (MeV)					
	0.05	0.1	0.2	0.4	0.6	0.8
Water						
Absorption	0.024	0.002	small	small	small	small
Compton	0.188	0.164	0.136	0.106	0.0896	0.0786
Total	0.212	0.166	0.136	0.106	0.0896	0.0786
Iron						
Absorption	1.762	0.206	0.024	0.0031	0.0012	0.0005
Compton	0.156	0.138	0.114	0.0888	0.0750	0.0659
Total	1.918	0.344	0.138	0.0919	0.0762	0.0664

For clarity, the following two quantities are defined:

- The strength of a gamma beam is the total number of gammas in the beam per unit time.
- The intensity of a gamma beam is the number of gammas per unit area per unit time in the beam.

The attenuation rate of a monoenergetic beam of gammas passing through matter is equal to the product of the strength, S, of the beam, the density of the material, ρ, and an attenuation coefficient, μ, that is characteristic of the material:

$$\frac{dS}{dx} = \mu\rho S \tag{3-1}$$

The attenuation coefficient, μ, varies slightly from element to element and is dependent on the energy of the gamma. (See Table 3-1.) For a compound material, μ is equal to the sum of the coefficients of the element weighted by their partial mass fractions. The solution of Eq. 3-1 is:

$$S = S_0 \exp(-\mu\rho x) \tag{3-2}$$

where S_0 is the strength of the beam with no material present. This equation applies to an infinitely thin, parallel beam of gammas passing through a single medium. In many cases, the application of the exponential attenuation characteristic can be applied outside these restrictions without introduction of significant error. This can be clarified by examining each restriction in detail.

- Multiple Media: A beam passing through several materials in series obeys Eq. 3-2 with the exponent replaced by a summation over all the materials between the source of the beam and a given point:

$$S = S_0 \exp\left(-\sum_{i=1}^{m} \mu_i \rho_i x_i\right) \tag{3-3}$$

Two conclusions can be drawn from the form of this equation:

1) The order of the materials has no effect.

2) The effect of each material on the beam is independent of the others. It makes no difference to a material whether the source intensity is reduced by a factor of ten by the intervening materials or whether the source itself is ten times weaker. The source and intervening materials can be lumped together and the transmitted gammas considered the source.

This combining of materials is used to simplify the gamma scattering model to be developed later. In passing from the source, the emitted gammas must pass through the cesium, its stainless steel capsule, air, three layers of metal, and a layer of water before entering the flow channel. In the analysis, the attenuating effect of materials other than the water are lumped together into a single factor which is the ratio of gammas actually entering the flow channel to those that would enter if there were none of these materials intervening. Similar factors are given for the materials between the detectors and the flow channel.

- Wide Beam: The restriction of an infinitely thin beam can be relaxed if each ray of the beam passes through identical media. In this case, the form of the exponential equation does not change. The form does change if the media are not identical. In the latter case, an integration is made over each ray which individually obeys the exponential form. This integration must be weighed by the intensity, I, of the ray:

$$S = \int_{A_o} I(A) \exp(-\mu\rho x)\, dA \qquad (3\text{-}4)$$

where:

$$\int_{A_o} I(A)\, dA = S_o$$

A_o is the total cross-sectional area of the beam, and I is the intensity. The loss of the exponential form is illustrated in the following example. Assume a uniformly intense beam, half passing through a material whose product $\mu\rho$ is 5 and half passing through a material whose product $\mu\rho$ is 2. The beam strength is found by summing the behavior of the individual parts:

$$S = \frac{S_o}{2}\left[\exp(-2x) + \exp(-5x)\right] \qquad (3\text{-}5)$$

This form cannot be simplified further and is clearly nonexponential. The loss of an exponential form would severely complicate the analysis. While the technique could still be applied, calibration and data reduction would be considerably more involved and the conceptual simplicity lost. Although not true in general, the particular geometry used in the project allowed the assumption of an exponential attenuation despite a finite width beam. The effect of this assumption will be examined in more detail later after a more thorough description of the geometry and the technique.

- Non-Parallel Beam: The final restriction given on the application of the exponential attenuation law is that of a parallel beam. For an isotopic source, the assumption of a parallel beam is only a simplification that applies over short distances far from the source. A real beam diverges as distance from the source increases. This has two effects. The first effect is the inverse square law. For a point source, the intensity of gammas coming from the source decreases as the square of the distance from the source. For a finite dimensional source, the intensity is a result of integrating the inverse square law over the entire source. The second effect is illustrated in Figure 3-1.

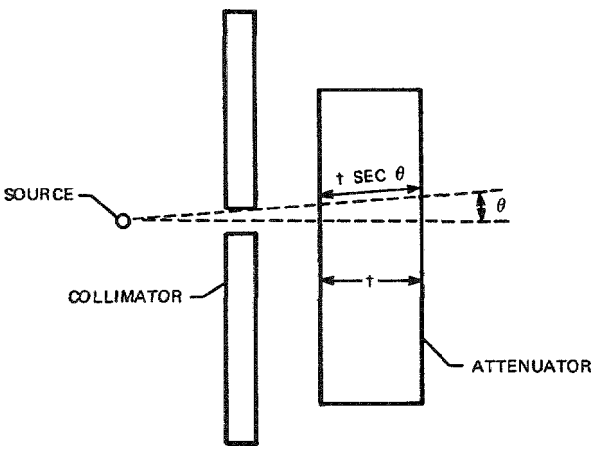

Figure 3-1. Effect of a diverging beam - each path through the attenuator is of unequal lengths

The distance through the attenuator is not the same for each ray of the beam. The true beam attenuation is the integrated effect over all the solid angle, and the result is not a simple exponential. In this experiment, the maximum angle that a ray could diverge from zero was about 2.6°. The relative increase in the amount of material traversed by this ray was 0.1%. The integrated effect of all rays was much smaller and the final effect on the calculation of the density was at least an order of magnitude below that. The assumption of exponential attenuation using the perpendicular distance was applied to the analysis with negligible error.

Compton Scattering Mechanism

Consideration so far has been confined to a monoenergetic beam of gammas. To fully understand the experimental technique, the compton scattering process must also be understood, and in context, a spectrum of gamma energies.

As mentioned above, the primary mechanism for the removal of gammas from the gamma beam is compton scattering. The gammas colliding with the electrons are scattered in all directions. The energy of the gamma emerging from the collision (E') is found from:

$$E' = \frac{E}{1 + E(1 - \cos\theta)/0.511} \tag{3-6}$$

where E is the energy of the incident gamma and θ is the angle between the incident and scattered gammas. The scattering is not isotropic but is forward-directed. The rate gammas are scattered into a differential solid angle, $d\Omega$, is:

$$d\mu_c = \frac{Z}{A}\left(\frac{E'}{E}\right)^2\left(\frac{E}{E'} + \frac{E'}{E} - \sin^2\theta\right) d\Omega \tag{3-7}$$

where $d\mu_c$ is the differential compton scatter coefficient. It should be noted that the variables E, E', and θ in Eq. 3-7 are not independent of each other but are related by Eq. 3-6. Detailed discussions of the compton effect are available in most textbooks on particle physics and nuclear shielding (3).

In the present experiment, only gammas scattered within a certain tolerance of 90° in the horizontal plane are able to pass through the collimator holes and reach the detector. While the incident gammas are monoenergetic, the scattered gammas that reach the detector vary slightly in energy. This is because the energy is dependent on the scattering angle which ranges slightly about the average value of 90°. For the experiment, the angle range was within 2.6° of 90°. The effect of this is illustrated in Table 3-2.

Since the scattered gammas do not have the same attenuation coefficient, the beam as a whole will not obey the exponential attenuation equation. However, the error introduced by assuming that the attenuation coefficient at 90° applies over the whole range is on the order of 1 part in 100,000 and is clearly negligible.

Table 3-2

ATTENUATION COEFFICIENTS
FOR VARIOUS ANGLES OF SCATTER

Angle (°)	Energy (MeV)	Water Attenuation Coefficient (cm^2/gm)
87.4	0.2959	0.1185
90.0	0.2883	0.1193
92.6	0.2811	0.1212

THE COMPTON SCATTER MODEL

In its simplest form, the model of the density measuring technique is easy to understand. The large number of variables should not detract from the concept since most of these drop out after the first few steps of the development. A simple model will first be developed with the assumptions clearly stated. These assumptions will then be examined to determine the size of the error they introduce when used in the present experiment.

Derivation of the Model

Figure 3-2 is a diagram of the horizontal plane showing the gamma beams entering and leaving the scatter volume. Only one side detector is shown since the analysis applies equally to both. The assumptions made in this figure and in the subsequent analysis are as follows:

1) All gamma beams are infinitely thin; the scatter volume is a point.

2) All materials, except water, located between the flow channel and the source and the detectors are lumped into single materials, M_0, M_1, and M_2.

3) The thin layers of water located between the outer edge of the flow channel and the inner edge of the collimator are lumped into the flow channel water.

4) The average density of water along each beam segment, 0, 1, and 2 in Figure 3-2, is equal.

5) The water density does not vary in time.

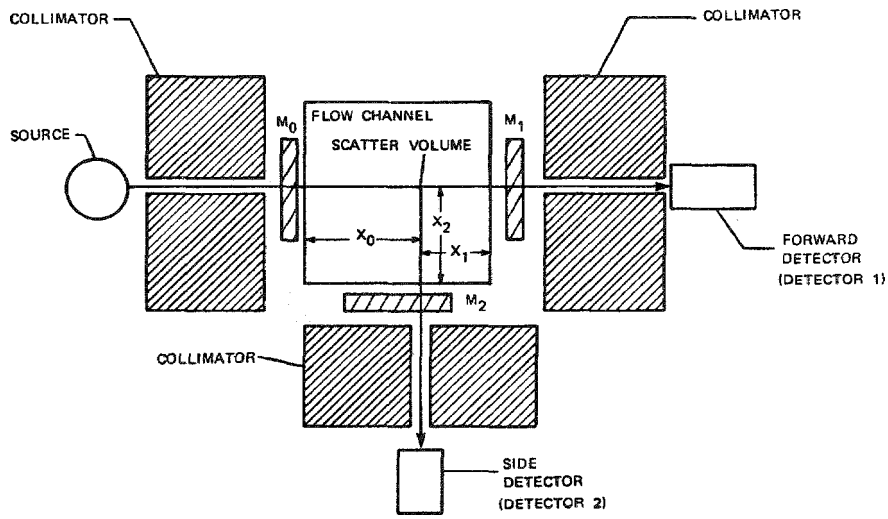

Figure 3-2. Schematic diagram of gamma beam geometry

The following quantities are defined:

N_0 is the rate that gammas are emitted from the source.

N_1 is the rate that gammas are detected by the forward detector.

N_2 is the rate that gammas are detected by a side detector.

x_i is the total distance through water that the beam travels to and from the scatter volume. It includes water inside the flow channel and in the thin stagnant area between the flow channel and the collimator. The subscripts 0, 1, and 2 refer to the directions corresponding to the source, forward detector, and side detector, respectively.

g_0 is a geometry ratio relating the rate gammas that would enter the scatter volume if only the collimators are present to form the beam and no material fills the space on a direct line between the source and scatter volume to the rate that gammas are emitted by the source.

g_1 is a geometry ratio relating the rate that gammas would enter detector 1 if only collimators are present to the rate that gammas are emitted by the source.

g_2 is a geometry ratio relating the rate that gammas would enter detector 2 if only collimators are present to the rate that gammas are scattered in the scatter volume.

f_0 is the attenuation factor due to all materials except water between the source and the scatter volume. The materials are lumped into M_0 in the figure.

f_1 is the attenuation factor due to all materials except water between the source and detector 1. These materials include M_0 and also other materials lumped into M_1 in the figure.

f_2 is the attenuation factor due to all materials except water between the scatter volume and detector 2 (M_2 in the figure).

μ_1 is the mass attenuation coefficient in water of the uncollided cesium gammas (661.6 keV).

μ_2 is the mass attenuation coefficient in water of the gammas scattered at 90° (288.3 keV).

C is the compton scatter factor. It is the ratio of gammas scattered out of the scatter volume to the incident gammas per unit density in the scatter volume.

ρ_s is the density of water in the scatter volume.

ρ_0 is the average density of water between the scatter volume and flow channel wall on the source side according to the following equation where $\rho(x)$ is the density of water at x:

$$\rho_0 = \frac{1}{x} \int_{\text{Scatter Volume}}^{\text{Source}} \rho(x)\ dx$$

ρ_1 and ρ_2 are defined similar to ρ_0:

$$\rho_1 = \frac{1}{x_1} \int_{\text{Scatter Volume}}^{\text{Detector 1}} \rho(x)\ dx$$

$$\rho_2 = \frac{1}{x_2} \int_{\text{Scatter Volume}}^{\text{Detector 2}} \rho(x)\ dx$$

ρ_0, ρ_1, and ρ_2 in this analysis include water located in the flow channel and in the water layers located outside the flow channel.

ε_1 is the efficiency of detector 1. It is the ratio of detection rate to the rate that gammas enter the detector.

ε_2 is the efficiency of detector 2.

Using these definitions, the number of gammas detected by detector 1 is:

$$N_1 = N_0 f_1 g_1 \varepsilon_1 \exp(-\mu_1 \rho_0 x - \mu_1 \rho_0 x_0) \tag{3-8}$$

The number of gammas detected by detector 2 is:

$$N_2 = N_0 f_0 f_2 g_0 g_2 \varepsilon_2 \rho_{s2} \; C \; \exp(-\mu_1 \rho_0 x_0 - \mu_2 \rho_2 x_2) \tag{3-9}$$

In the density measuring procedure, the detector rates are compared to the rates determined from a known density. If e and r refer to experimental and reference quantities, respectively, the following results from the above equations:

$$\frac{N_1^r}{N_1^e} = \exp\left[\mu_1 x_1 (\rho_1^e - \rho_1^r) + \mu_1 x_0 (\rho_0^e - \rho_0^r)\right] \tag{3-10}$$

$$\frac{N_2^r}{N_2^e} = \frac{\rho_{s2}^r}{\rho_{s2}^e} \exp\left[\mu_2 x_2 (\rho_2^e - \rho_2^r) + \mu_1 x_0 (\rho_0^e - \rho_0^r)\right] \tag{3-11}$$

In deriving these equations, the following quantities were assumed constant:

N_0, f_0, f_1, f_2, g_0, g_1, g_2, ε_1, and ε_2.

The source strength, N_0, is assumed constant because the cesium source is in a sealed capsule and has a half-life of 30 years. (The source strength is reduced by only 0.1% in 16 days.) The attenuation factors, f_0, f_1, and f_2, did not change since the material did not change. The geometry factors and efficiency factors are also assumed constant.

Now, by defining the quantities K_1 and K_2 as:

$$K_1 = \frac{\rho_1^r - \rho_1^e}{\rho_0^r - \rho_0^e}$$

and

$$K_2 = \frac{\rho_2^r - \rho_2^e}{\rho_0^r - \rho_0^e}$$

and then substituting them into Eq. 3-10 and 3-11 yields:

$$\frac{N_1^r}{N_1^e} = \exp\left[\mu_1(\rho_0^e - \rho_0^r)(xK_1 + x_0)\right] \tag{3-12}$$

$$\frac{N_2^r}{N_2^e} = \exp\left[(\rho_0^e - \rho_0^r)(\mu_2 x_2 K_2 + \mu_1 x_0)\right] \tag{3-13}$$

Solving Eq. 3-12 for $(\rho_0^e - \rho_0^r)$ yields:

$$\rho_0^e - \rho_0^r = \frac{1}{\rho_1(x_1K_1 + x_0)} \log\left(\frac{N_1^r}{N_1^e}\right) \tag{3-14}$$

Now, substituting Eq. 3-14 into Eq. 3-13 gives:

$$\frac{N_2^r}{N_2^e} = \frac{\rho_{s2}^r}{\rho_{s2}^e}\left(\frac{N_1^r}{N_1^e}\right)^{q_2} \tag{3-15}$$

where:

$$q_2 = \frac{\mu_2 x_2 K_2 + \mu_1 x_0}{\mu_1(x_1K_1 + x_0)}$$

Finally, rearranging Eq. 3-15 yields:

$$\rho_{s2}^{e} = \rho_{s2}^{r} \frac{N_2^{e}}{N_2^{r}} \left(\frac{N_1^{r}}{N_1^{e}} \right)^{q_2} \tag{3-16}$$

The exponential term, q_2, is not independent of water density because of the terms, K_1 and K_2, which relate the water densities in the directions outward from the scatter volume. In the foregoing discussion, K_1 and K_2 are assumed to equal 1. An analysis of this assumption is given later in the report. This leads to the fundamental equation of the compton scatter technique for measuring density:

$$\rho_{s2}^{e} = \rho_{s2}^{r} \frac{N_2^{e}}{N_2^{r}} \left(\frac{N_1^{r}}{N_1^{e}} \right)^{q_2} \tag{3-17}$$

where:

$$q_2 = \frac{\mu_2 x_2 + \mu_1 x_0}{\mu_1 x_1 + \mu_1 x_0}$$

With this equation, an unknown density can be found in terms of a known density and the detection rates of the detectors.

These equations were developed for side detector 2 only; a parallel set of equations apply to side detector 3. The final equation for this derivation is:

$$\rho_{s3}^{e} = \rho_{s3}^{r} \frac{N_3^{e}}{N_3^{r}} \left(\frac{N_1^{r}}{N_1^{e}} \right)^{q_3} \tag{3-18}$$

where:

$$q_3 = \frac{\mu_2 x_3 + \mu_1 x_0}{\mu_1 x_1 + \mu_1 x_0}$$

Of the assumptions made at the start of this model development, assumptions 2 and 3 are not restrictive at all. Combining material placed in series is a valid simplification that introduces no errors. This was indicated by the form of Eq. 3-3. The other assumptions intrduce errors which will now be examined in detail.

The Effect of Imperfect Collimation

The nature of exponential attenuation is such that the intensity is never reduced to zero -- regardless of the amount of material placed in the beam. The process used to form the gamma beam does not produce a sharp-edged beam but rather reduces the intensity of the radiation emitted from the source to a very low level in all but the desired direction. To be completely accurate in the model development, each differential ray from each differential source volume would need to be followed to determine its contribution to the detection rates. However, this would be impractical and unnecessary in many real applications of gamma rays. A 2.5 cm thickness of stainless steel reduces the intensity of the cesium gamma beam by a factor of 5. A second 2.5 cm thickness reduces this by another factor of 5. In many cases, this could be sufficient to model the material as being infinitely dense, thus eliminating all gammas entering the material.

The situation arising in this experiment makes this assumption very difficult to apply. The problem is illustrated in Figure 3-3 and further explained as follows.

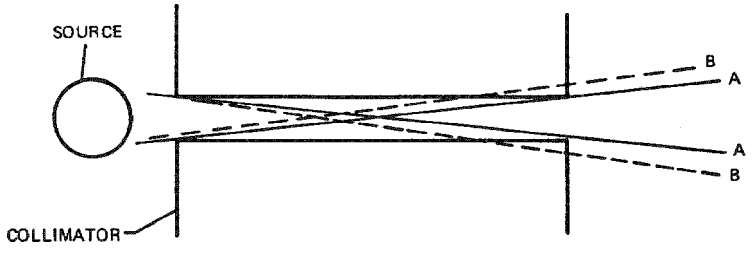

Figure 3-3. Gamma penetration through collimators

A small number of gammas were always able to penetrate the collimators (as shown by the rays marked "B") producing a low intensity fringe on the beam. Ordinarily, the beam could be modeled as lying within the rays marked "A" because the intensity of the beam drops rapidly beyond these rays. However, in this experiment, the beam was so narrow that the fringe contained a significant portion of the gammas. The fringe had the effect of widening the scatter volume so that its corners encompassed the heated rods.

The effect of scatter off the heated rods is discussed later. However, for the purpose of this model, there is generally little or no effect on the model equations that have been derived. As long as this effect is properly accounted for in the design of the collimators and in the definition of the scatter volume size, no errors are introduced into the experiment.

Another potential problem comes from the fact that only a very small fraction of gammas follow the model defined paths and are detected. Of all the gammas emitted from the source, about 1 gamma in 20,000 is directed toward the specified scatter volume that forms a 90° angle between the source and one of the detectors. There is a potential for 20,000 times more gammas entering the detectors at the correct energy from locations other than the planned scatter volume. Adequate shielding must be provided around the source and detectors to minimize this interference. In the experiment, 17.8 cm of lead was used to separate the source from the detectors. This would attenuate a straight-through beam by a factor of at least 10 billion. The attenuation is so great that interference will not come from the direct route between the source and the detector but rather from a myriad of tortuous paths involving multiple scattering within the test section, ultimately lining up with the collimator paths to permit detection. Fortunately, this multiple scattering contribution was easily distinguished by energy discrimination from the desired single scatter rate and presented no problem.

The Effect of Density Asymmetry

The assumption that K_1 and K_2 equal 1 is the largest potential source of error in measuring water density so it will be examined in greater detail. What is sought is the relative error, E, between the calculated value of the scatter volume density, $\rho_s e$ and the actual density of the scatter volume, $\rho_s' e$. We have assumed that K_1 equals 1. From the definitions therefore:

$$1 = \frac{\rho_1^r - \rho_1^e}{\rho_2^r - \rho_0^e}$$

The method of obtaining reference densities allows:

$$\rho_0^r = \rho_1^r = \rho_2^r = \rho^r$$

Therefore, our assumption leads to:

$$\rho_1^e = \rho_0^e$$

Similarly, from K_2:

$$\rho_2^e = \rho_0^e$$

This implies that the average density of water is the same in any direction from the scatter volume out to the source or to any of the detectors. Specifically, it is the error in this assumption that we are analyzing. The error estimate proceeds by assuming an experimental density, calculating the actual detector rates, and then applying these to the equation containing the assumption to generate a calculated density which is compared to the original assumed density. In the data reduction, we apply the following equation:

$$\rho_s^e = \rho_s^r \left(\frac{N_2^e}{N_2^r}\right)\left(\frac{N_1^r}{N_1^e}\right)^{q_2} \tag{3-19}$$

where the assumption is found in the exponent, q_2, as:

$$q_2 = \frac{\mu_2 x_2 + \mu_1 x_0}{\mu_1 x_1 + \mu_1 x_0}$$

The relative error, E, is found by relating the calculated density and the assumed density:

$$E = \frac{\rho_s'^e - \rho_s^e}{\rho_s'^e} \tag{3-20}$$

$$= 1 - \frac{\rho_s^e}{\rho_s'^e}$$

Eq. 3-10 and 3-11 give the expressions for the ratios found in Eq. 3-19. Making the substitution:

$$\rho_s^{\,e} = \rho_s^{\,r} \frac{\rho_s'^{\,e}}{\rho_s'^{\,r}} \exp\left[-\mu_2 x_2(\rho_2^{\,e} - \rho_2^{\,r}) - \mu_1 x_0 (\rho_0^{\,e} - \rho_0^{\,r})\right] \qquad (3\text{-}21)$$

$$\exp\left[(\mu_1 x_1 (\rho_1^{\,e} - \rho_1^{\,r}) + \mu_1 x_0 (\rho_0^{\,e} - \rho_0^{\,r}) \quad q_2\right]$$

Now, substituting the value of q_2 found in Eq. 3-19 and remembering that

$$\rho_0^{\,r} = \rho_1^{\,r} = \rho_2^{\,r}$$

leads to the following expression after simplification:

$$\frac{\rho_s^{\,e}}{\rho_s'^{\,e}} = \exp\left[\frac{1}{x_1 + x_0}\left((\rho_1^{\,e} - \rho_2^{\,e})\,\mu_2 x_1 x_2 + (\rho_1^{\,e} - \rho_0^{\,e})\right.\right. \qquad (3\text{-}22)$$

$$\left.\left.\mu_1 x_1 x_0 + (\rho_0^{\,e} - \rho_2^{\,e})\,\mu_2 x_0 x_2\right)\right]$$

If the absolute value of the term in the brackets is much less the 1.0, then the exponential expression can be approximated by its Taylor series truncated to two terms. Substituting this into Eq. 3-20 and simplifying gives:

$$E = \frac{1}{x_1 + x_0}\left[(\rho_1^{\,e} - \rho_2^{\,e})\,\mu_2 x_1 x_2 + (\rho_1^{\,e} - \rho_0^{\,e})\,\mu_1 x_1 x_0\right. \qquad (3\text{-}23)$$

$$\left. + (\rho_0^{\,e} - \rho_2^{\,e})\,\mu_2 x_0 x_2\right]$$

Clearly if the assumption of equivalent densitites were true, the density differences would be zero leading to a zero error.

For the first collimator series (collimator set 1), the geometry was designed symmetrical. In a geometrical sense, at least, the error was minimized. Hypothetical asymmetric conditions were programmed into the thermal-hydraulic code COBRA IIIC (4) to determine possible density variations from symmetry for the 4 x 4 rod array. The asymmetric condition consisted of a 10% power spike on selected rods and heated walls as shown in Figure 3-4. The selection was made to maximize the asymmetry.

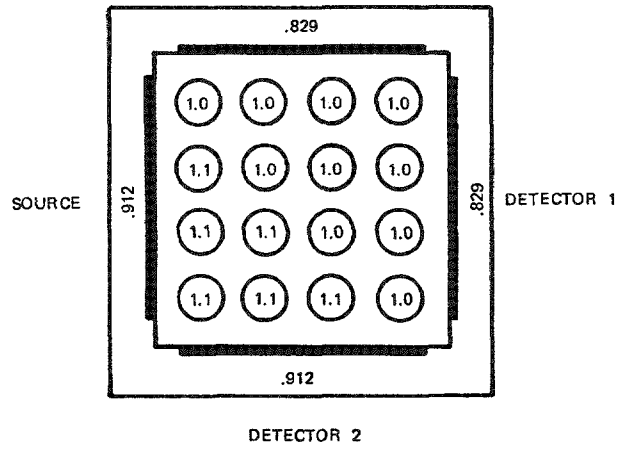

Figure 3-4. Forced asymmetry - numbers indicate relative heat fluxes

COBRA calculated the water density in each subchannel. The results were applied to Eq. 3-23 which predicted a density error in the range of 0.2% to 0.4%. Although these errors are small, actual errors were much smaller since actual rod heat fluxes did not vary more than 1% and then did so randomly.

For the second collimator series (collimator set 2), the design was not symmetrical. For the detector that examined the gap region of the subchannel, the exiting gamma beam was directed through the rods. (See Figure 4-7 in Section 4.) Clearly, the water density that this beam sees is not the same as the straight-through detector sees. The side detector sees densities that are approximately the same as the gap density while the straight-through detector sees both the gap density and center of subchannel density. Measurements indicate an upper limit of about 160 kg/m^3 between the two densities of the subchannel. This leads to a density difference of about 80 kg/m^3 between the two exiting gamma paths. Through the use of Eq. 3-23, the error due to this nonsymmetry was calculated to be 0.9% of the density measurement. This maximum deviation is within the acceptable error.

The Effect of Dynamic Bias

Dynamic bias is a deviation in the gamma detection rate that results from a fluctuating density in the gamma beam paths and scatter volume. The analysis of dynamic bias is involved. A complete determination of its effect on this experiment is given in Appendix A. The conservative analysis concluded that the dynamic bias is less than 1.25% of the density measurement and only existed in the limited flow regimes where slugging in the subchannels occurred.

The Effect of a Finite Scatter Volume

In Figure 3-2, it was assumed that the width of the beam was infinitely thin. If this requirement is relaxed, an error is introduced at the scatter volume. Figure 3-5 is an illustration of a scatter volume assumed square for simplicity. The figure shows the incident and scatter beams as well as the thin beam "A" assumed in the earlier analysis.

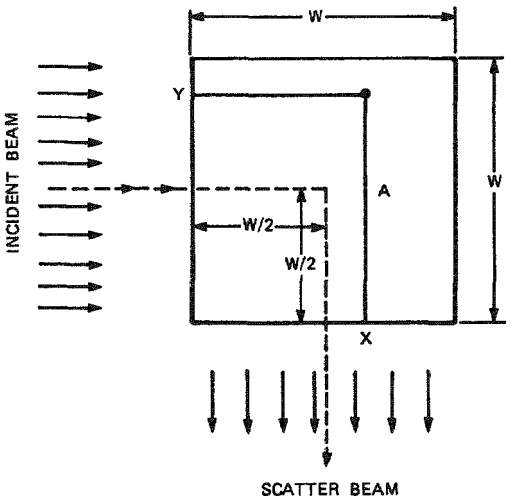

Figure 3-5. Finite scatter volume

For the thin beam case, the strength of the scatter beam just leaving the actual finite scatter volume is related to the strength of the incident beam just entering the scatter volume by Eq. 3-24 where C is the compton scatter factor:

$$S_1 = S_0 C \rho \exp(-\mu_1 \rho \frac{W}{2} - \mu_2 \rho \frac{W}{2}) \qquad (3\text{-}24)$$

where:

S_0 is the strength of the incident beam

S_1 is the strength of the scatter beam

For the actual case, an integration must be performed over the entire scatter volume:

$$S_1' = \frac{S_0 C\rho}{W^2} \int_0^W \int_0^W \exp(-\mu_1 \rho_x - \mu_2 \rho_y) \; dx \; dy$$

$$S_1' = S_0 C\rho \left(\frac{1 - \exp(-\mu_1 \rho W)}{\mu_1 \rho W} \right) \left(\frac{1 - \exp(-\mu_2 \rho W)}{\mu_2 \rho W} \right) \qquad (3\text{-}25)$$

The relative error is:

$$E = 1 - \frac{S_1}{S_1'}$$

If the exponential terms are expanded in a Taylor series, the following expression approximating the error results from truncation and simplification:

$$E = \frac{\left(\mu_1^2 + \mu_2^2\right) \rho^2 W^2}{24} \qquad (3\text{-}26)$$

Typical values for these constants are:

ρ = 1.0 gm/cm^2

μ_1 = 0.0860 cm^2/gm

μ_2 = 0.1204 cm^2/gm

W = 0.6 cm

The density, ρ, is given its cold atmospheric water value; the attenuation coefficients are for the unscattered and 90° scattered values for gammas emitted from cesium and passing through water. All of this leads to an error of:

E_{max} = 0.03% ,

which is clearly negligible.

The Effect of Gamma Counting Statistics

The production and interaction of gamma rays is a stochastic process. Under otherwise steady-state conditions, the number of gammas counted by the detectors will vary over any set time interval. For large total counts, the variation is approximated by a normal distribution about the mean. The standard deviation is equal to the square root of the mean. For example, if in a given time interval the detectors count 10,000 gammas, one is 68% confident that the mean lies within 100 counts of 10,000 or 95% confident that the mean lies within 200 counts of 10,000.

The total count rate is a combination of background gammas that are of interest. To obtain the signal gammas, the background must be subtracted from the total. Letting N_T, N_B, and N_S denote the total count rate, background count rate, and signal count rate, we have:

$$N_S = N_T - N_B \tag{3-27}$$

If σ denotes the standard deviation, then according to the laws of error propagation:

$$\sigma_S = \sqrt{\sigma_T^2 - \sigma_B^2} \tag{3-28}$$

If t denotes time, this can be simplified:

$$\sigma_S = \sqrt{t(T + B)} \tag{3-29}$$

This last step comes from the fact that the standard deviations σ_T and σ_B are equal to the square root of the total count, Tt and Bt.

In this experiment, a 95% confidence that the count rate is within 1% of the mean was sought on each of the side detectors. Mathematically, this requires that:

$$\frac{2\sigma_S}{St} \leq 0.01 \tag{3-30}$$

To meet this criteria with the count rates experienced in this project, 400 seconds were required for the first collimator set and 1000 seconds were required for the second collimator set.

THE COMPTON SCATTER MODEL WITH ROD SCATTER

Shortcomings of the Simple Model

The preceding section developed the general concept behind the compton scatter technique and developed a model to apply the techniques to actual experiments. This section will first show why the simple model cannot be immediately applied to the geometry of this experiment and will then develop the required changes.

Although many assumptions were required in the development of the simple model, most lead to insignificant error. The one assumption that introduces an error that cannot be ignored is the thin beam assumption. A wide beam can lead to two variations in the original model illustrated in Figure 3-6. The flow channel contains 16 heated rods in a 4 x 4 array. Water occupies the space between the rods and air occupies the space inside the rods. Shown is a sample beam that illustrates the effects of a wide beam. The first effect results from a scatter volume that encompasses part of the heated rods within its defined volume. In this case, part of the gammas counted by the side detectors do not scatter off the density-varying water but off the constant density rods. The second effect results from a beam that travels through different materials in parallel. In getting to and from the scatter volume, part of the beam travels only through water while another part travels through the rods in addition to the water. This effect was introduced in general in an earlier section wherein it was concluded that there were two consequences: One was an alteration in the exponential form of the attenuation curve; the other was a change in the attenuation coefficients. Each of these will now be examined in greater detail.

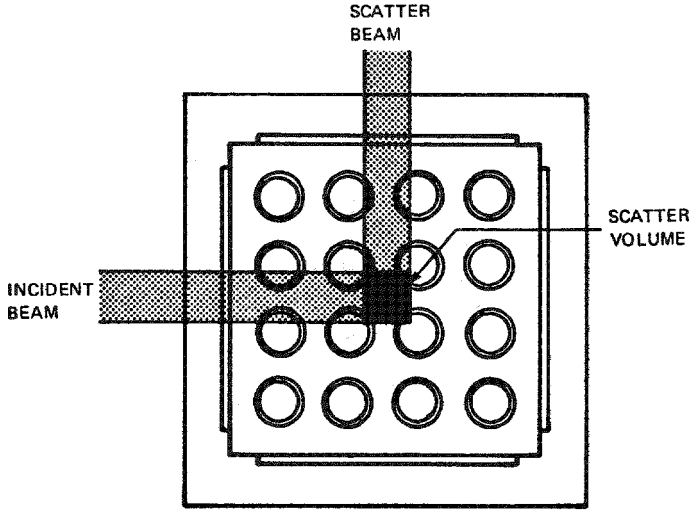

Figure 3-6. Wide gamma beam within flow channel

The Effect of Non-Exponential Attenuation

To place an upper limit on the magnitude of the error involved in assuming an exponential curve, an extreme case will be calculated. The worst case was not chosen since excessive analysis is involved in finding it. The one chosen is obviously sufficiently severe that the actual cases have less effect. Two beam paths are chosen. One travels through the maximum possible amount of water; the other through the minimum amount. Any real beam used in this experiment will consist of rays between the two extremes. The variance in the amount of water crossed by the rays will be less in a real beam than by one that concentrates at the two extremes. The deviation from the exponential form is dependent on the variance. Consequently, the real beams can be more closely approximated by an exponential. The paths used in this extreme case analysis are illustrated in Figure 3-7. Each path contains equal intensities of gammas. Data pertaining to each path are given on the figure.

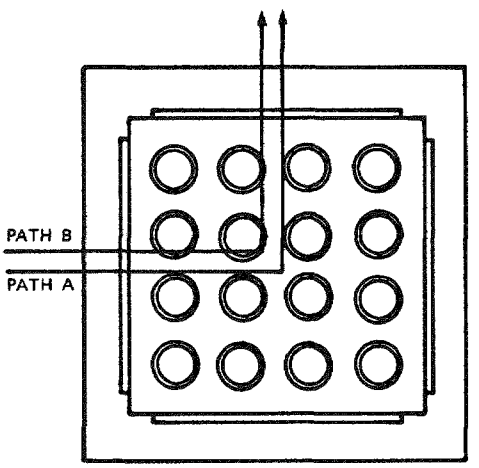

	DISTANCE THROUGH ROD MATERIAL INCOMING OR OUTGOING	DISTANCE THROUGH ROD CAVITY INCOMING OR OUTGOING	DISTANCE THROUGH WATER INCOMING OR OUTGOING
PATH A	—	—	3.002 cm
PATH B	0.455 cm	0.963 cm	1.189 cm

ATTENUATION COEFFICIENTS

	INCOMING	OUTGOING
ROD MATERIAL	0.638 cm^{-1}	0.890 cm^{-1}
ROD CAVITY	—	—
WATER	0.0860 cm^2/gm	0.1204 cm^2/gm

Figure 3-7. Two gamma ray paths - severe case for non-exponential attenuation

The detection rate of the side detectors is simply the addition of the rates caused by the two individual rays.

Each ray obeys Eq. 3-9. Applied to each ray, this equation becomes:

$$N_{2A} = Q\, f_A\, \rho(-\mu_1\, \rho x_{0A} - \mu_2\, \rho\, x_{2A}) \tag{3-31}$$

$$N_{2B} = Q\, f_B\, \rho(-\mu_1\, \rho x_{0B} - \mu_2\, \rho\, x_{2B}) \tag{3-32}$$

where Q replaces the constant terms of Eq. 3-9 and f_A and f_B are factors to account for the intensity reduction caused by attenuation in the rods. The density is assumed uniform in the bundle to simplify the analysis. From Figure 3-7, we have:

$$f_A = \exp(0) = 1$$

$$f_B = \exp(-0.638 * 0.455 - 0.890 * 0.455) = 0.499$$

$$x_{0A} = x_{2A} = 3.002 \text{ cm}$$

$$x_{0B} = x_{2B} = 1.189 \text{ cm}$$

$$\mu_1 = 0.0860 \text{ cm}^2/\text{gm}$$

$$\mu_2 = 0.1204 \text{ cm}^2/\text{gm}$$

Substituting these values into Eq. 3-31 and 3-32 and using the fact that the detection rate is the sum of the rates from the two individual paths, we have:

$$N_2 = N_{2A} = N_{2B}$$

$$N_2 = Q\rho \left[\exp(-0.620\rho) + 0.499(-0.245\rho)\right] \tag{3-33}$$

This equation is not a simple exponential, but in order to maintain the simplicity of the original compton scatter model, we wish to approximate this expression by an exponential and determine the size of the error introduced. During calibration, a fit is made to two points. One point is at zero fluid density; the other point is at the density of room temperature water, 1.0 gm/cm^3. The actual response of

the side detector to these two points is given by Eq. 3-33, $Q_\rho(1.499)$ and $Q_\rho(0.9285)$, respectively. An exponential fit to these bracketed factors leads to the following equation:

$$N_2 = Q_\rho \left[1.499 \exp(-0.479\rho) \right] \qquad (3\text{-}34)$$

The maximum difference between Eq. 3-33 and 3-34 is about 0.4% over the range of water density. This is an upper limit given for a severe case. Actual differences are below 0.1% of the actual side detector rate. We can conclude that the beam attenuation can be modeled as exponential.

The Effect of Changed Attenuation Coefficients

The effective water attenuation coefficients change because the rods that the beam passes through decrease the importance of the water in attenuating the beam. In the simple model, the coefficients could be found in tables of attenuation coefficients. For the complex model, the coefficients are found by calibration. The calibration procedure is discussed in Section 4.

The Effect of Rod Scatter

The collimators for this project were designed such that portions of the heated rods fell within the scatter volumes. The intensity of the gamma beam is greatly reduced at this outer edge of the scatter volume, but the density of the rods is about 16 times greater than water and so causes about 16 times as much scattering as would water in the same location. It is important then to determine the form of the equations that take into account the effect of rod scatter. In the analysis that follows, the first collimator series is used as a basis.

For collimator set 1, the modeling of the gamma beam to include parallel materials and collimator penetration to predict rod scatter is too complex to be done analytically, so a computer was used to numerically analyze the geometry. Although only the behavior of the rod scatter is strictly required, modifications to the computer programs to completely model the density measuring technique were so minor that they were incorporated. The approach was to integrate the effect of each ray connecting each point on the source and each point in the detectors with each point in the scatter volume.

The results of the computer simulation are given in Table 3-3. Shown are the tabluated normalized count rates of the forward and side detectors for discrete values of the density of water in the flow channel. The side detector rate is separated into the contributions given by the rods and by the water. The effect of rod scatter will be discussed in subsequent subsections. First, some of the sidelights of the analysis that verifies earlier analysis are examined.

Table 3-3

COMPUTER SIMULATION OF DETECTOR COUNT RATES

Density (gm/cm^3)	Forward Rate	Side Rate	Rod Contribution	Water Contribution
0	1.00000	0.01699	0.01699	0
0.09992	0.94561	0.04503	0.01630	0.02874
0.19985	0.89417	0.06957	0.01564	0.05393
0.29977	0.84555	0.09093	0.01500	0.07593
0.39970	0.79957	0.10941	0.01439	0.09502
0.49962	0.75611	0.12528	0.01381	0.11148
0.59955	0.71501	0.13881	0.01325	0.12556
0.69947	0.67616	0.15022	0.01271	0.13751
0.79940	0.63942	0.15972	0.01220	0.14752
0.89932	0.60468	0.16750	0.01170	0.15580
0.99924	0.57184	0.17374	0.01123	0.16251

Empirical Fits to the Computer-Generated Rates:

Forward Rate:

$$\frac{N_1^r}{N_1^e} = \exp\left[15.49(\rho^r - \rho^e)\right]$$

Water Contribution:

$$\frac{N_{2w}^r}{N_{2w}^e} = \frac{\rho^r}{\rho^e} * \exp\left[17.54(\rho^e - \rho^r)\right]$$

Rod Contribution:

$$N_m = 0.01699 \exp\left[-11.47\ \rho\right]$$

Simple Compton Scatter Model Predictions:

$$\frac{N_1^r}{N_1^e} = \exp\left[15.77(\rho^e - \rho^r)\right]$$

$$\frac{N_{2w}^r}{N_{2w}^e} = \frac{N_2^r}{N_2^e} = \frac{\rho^r}{\rho^e} \exp\left[18.92(\rho^e - \rho^r)\right]$$

As predicted, a simple exponential will not fit any of the rates exactly; however, exponential fits to the tabulated values were made and are given at the bottom of Table 3-3. A quantitative comparison between the tabulated data and the empirical fit indicated that the difference in all cases is less than 0.1% of the tabulated value. This result lends support to the simple exponential model for the purposes of the present application.

Table 3-3 also presents the equations predicted by the simple compton scatter model. The coefficients given for the new model are slightly less due to decreased importance of water caused by the presence of the rods in the beam. The actual attenuation coefficients for the forward rate and the water contribution were found by calibration. If N_1' is defined as the calibrated value of the attenuation coefficient for the forward detector, the fit can be generalized to:

$$\frac{N_1^r}{N_1^e} = \exp\left[\mu_1' (\rho^r - \rho^e)\right] \tag{3-35}$$

If we define N_2' as the attenuation coefficient for the side detector path, the fit can be generalized to:

$$\frac{N_{2w}^r}{N_{2w}^e} = \frac{\rho_r}{\rho_e} \exp\left[\mu_2' (\rho^r - \rho^e)\right] \tag{3-36}$$

The computer simulation predicts a small contribution to the total side detection rate by the rod scatter. The dependence of rod scatter is accurately modeled as exponential. The equation governing the rod scatter can be generalized to:

$$N_m = N_{mo} \exp(-\mu_m \rho) \tag{3-37}$$

For the second collimator series (collimator set 2), the geometry is actually less complex. In the center region measurement, no rod scattering was observed. For the gap region measurements, the rod scattered gammas traveled approximately the same paths as the water scattered gammas. It can be shown for this case also that the forms for the equations above apply equally to the second collimator series.

The Effect of Magnetic Attraction and Rod Temperature

The electric current in the rods produced a magnetic field that caused the rods to defect inward. This resulted in a slight increase in the total rod volume within the scatter volume. The increase in temperature also causes a slight geometry distortion with the net effect being a decrease in rod scatter. The complete general equation governing the rod contribution to the side scatter is:

$$N_m = N_{mo} f_I f_T \exp(\sigma_m \rho_m) \tag{3-38}$$

The factors f_I and f_T account for the effect of the magnetic attraction and rod temperature, respectively. In this test, the rod contribution is small. A conservative estimate of f_I and f_T indicates a possible deviation of 10% from the nominal value of unity.

The error introduced into the calculation of void fraction caused by neglecting these adjustments depends to a large extent on the test conditions. The error in void fraction ranges between 0 and 1%, which means that our calculated values could be slightly lower than the actual values.

The Model with Rod Scatter

Eq. 3-37 is used in the data reduction. Applied to side detector 2 and side detector 3, the equation becomes:

$$N_{m2} = N_{mo2} \exp(\sigma_{m2} \rho_{m2}) \tag{3-39}$$

and

$$N_{m3} = N_{mo3} \exp(\sigma_{m3} \rho_{m3}) \tag{3-40}$$

where the subscripts 2 and 3 identify the side detectors. Eq. 3-17 from the simple model, modified for gamma scatter off the rod, becomes:

$$\rho_{s2}^{e} = \rho_{s2}^{r} \left(\frac{N_2^{e} - N_{m2}^{e}}{N_2^{r} - N_{m2}^{r}} \right) \left(\frac{N_1^{r}}{N_1^{e}} \right)^{q_2} \tag{3-41}$$

for side detector 2, and

$$\rho_{s3}^{e} = \rho_{s3}^{r} \left(\frac{N_3^{e} - N_{m3}^{e}}{N_3^{r} - N_{m3}^{r}} \right) \left(\frac{N_1^{r}}{N_1^{e}} \right)^{q_3} \qquad (3\text{-}42)$$

for side detector 3.

These are the equations used in the data reduction.

Section 4

DATA ACQUISITION AND REDUCTION

TEST MATRIX

In this experiment, average density in a local volume was measured. Void fraction can be determined from the average density and the individual liquid and vapor densities (See Eq. 4-2). Two series of tests were conducted to measure density within the center subchannel of a 4 x 4 rod bundle. The goal was to obtain the average density across the entire subchannel. The first series was designed to obtain base data. The scatter volume during these measurements was the largest obtainable portion of the subchannel that could be achieved within the constraint of limiting the rod scatter contribution to a reasonable fraction. Figure 4-1 illustrates this volume.

SHOWN ARE THE CONSTANT WEIGHT LINES OF THE SCATTER VOLUME LOCATED IN THE CENTER SUBCHANNEL. THESE LINES ARE ANALOGOUS TO CONSTANT ELEVATION LINES ON A TOPOGRAPHIC MAP.

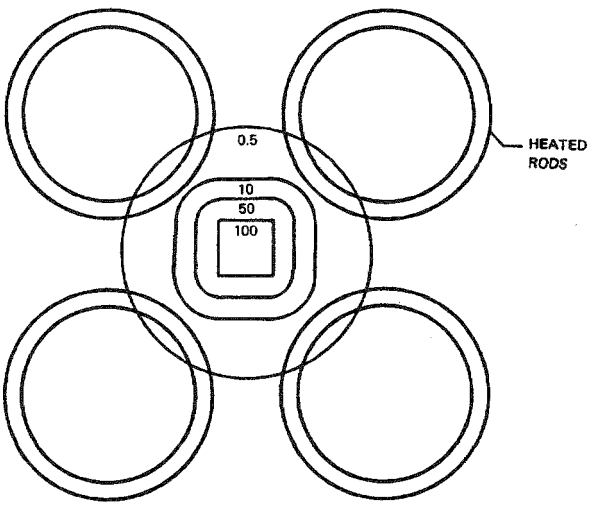

Figure 4—1. Scatter volume — collimator set 1

The second series of data was designed to determine the size of the subchannel gradients so that an appropriate factor could be applied to the base data, allowing them to be applicable to the subchannel as a whole. Figure 4-2 illustrates the volumes measured.

SHOWN ARE THE CONSTANT WEIGHT LINES OF EACH SCATTER VOLUME. SOLID LINES DEFINE THE SCATTER VOLUME SEEN BY DETECTOR 2. DASHED LINES DEFINE THE SCATTER VOLUME SEEN BY DETECTOR 3. THESE LINES ARE ANALOGOUS TO CONSTANT ELEVATION LINES ON A TOPOGRAPHIC MAP.

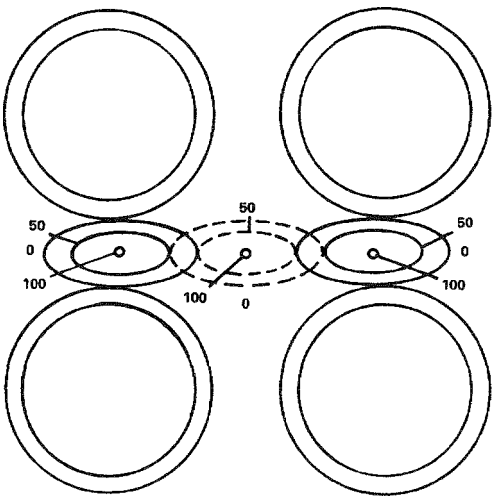

Figure 4–2. Scatter volume – collimator set 2

Data were taken by holding pressure, flow rate, and heat flux constant while varying inlet temperature (subcooling) to obtain a range of void fractions. Nominally, the complete void fraction range from single-phase liquid to single-phase vapor was sought. As a practical matter, approaching pump cavitation, critical heat flux, or heat exchanger capacity constrained test conditions. The actual test data matrix is given in Table 4-1.

Table 4–1

TEST MATRIX

Pressure MPa	Flow Rate $kg/m^2 \cdot sec$	Heat Flux $kW/m^2 \cdot sec$			
		1262	631	315	158
16.90	3122	1	1		
	1357		1	1	
	679				
	407			1	
	204				1
15.17	3122	1	1,2		
	1357		1,2	1,2	
	679		1,2		
	407		1	1	
	204				1
13.79	3122	1	1		
	1357		1	1,2	
	679		1		
	407			1	
	204				
11.03	3122	1	1,2	1	
	1357	1	1,2	1,2	
	679		1,2	1,2	
	407			1	
	204				1
6.90	3122	1	1,2	1	
	1357	1	1,2		
	679		1,2	1	
	407		1		
	204			1	

NOTE:

1 = Completed Curves - Collimator Set 1

2 = Completed Curves - Collimator Set 2

GENERAL PROCEDURES

Prior to a series of experimental runs, a reference run at a known density was required. Theoretically, there are no restrictions on the fluid conditions for this run except for the specification of single-phase. In practice, two problems were encountered that forced tighter restrictions on this procedure.

The magnetic field associated with the electrically-heated rod bundle affected the gamma detector count rate about 2% over the range of power. This problem affected density calculations only where reference runs and experimental runs were not taken at the same approximate power level. The original procedure called for reference runs to be made at zero power so that the reference temperature could be easily determined from inlet or outlet temperature. The procedure was changed to take reference runs at the power level of the experimental runs and at the highest flow rate achievable. This minimized enthalpy rise through the bundle and allowed the best determination of the reference density with power on.

It was also noticed that small changes of about 2% in detector count rate were produced by moving the source in and out of its safety position. Apparently, the operating position was not repeatable. This problem was solved by changing the calibrating procedure to repeat reference runs each time the source was moved.

Conditions for the reference run were set such that the fluid remained single-phase. The density of the fluid was determined from ASME subcooled water equations. The temperature and pressure of the water are measured at the exit of the bundle. Counting time was 3000 seconds thus giving a standard deviation in the net counts of about 0.1%.

Following the reference run was a series of experimental runs that were used to determine the void fraction under two-phase conditions. The facility pressure, flow, and power were held constant as the inlet temperature was brought to a preselected level. When conditions were steady (about 5 minutes), the data acquisition was initiated. Data were accumulated for 400 seconds for the first collimator series and 1000 seconds for the second collimator series. This counting period assured a standard deviation of gamma counts in the neighborhood of 0.5%.

THERMAL-HYDRAULIC DATA

In general, data acquisition proceeded as planned. Only one significant problem was encountered. Detector 2 malfunctioned and was out of service until its replacement for Runs 468 to 492. In as much as detector 2 measurements were duplicated by detector 3, the effect was minimal.

Transducers

All transducers used to collect data for this report were traceable to the National Bureau of Standards (NBS). In many cases, duplicate measurements were made. A listing of the comparisons follows.

Standard facility procedures were used for the thermal-hydraulic data collection and reduction. These included, but were not limited to:

1) Measurement of and correction for AC component ripple factor
2) Calculation of rod bow due to magnetic attraction
3) Pressure tap head corrections
4) Measurement of zero power heat loss
5) Measurement of energy balance at each single-phase data point
6) Selection of "best-fits" from multi-term fits to transducer calibration data
7) Measurement of rod gap sizes
8) Resistivity and dimension checks for each rod and wall and the assembled bundle

The transducers were connected to a high-speed analog-to-digital converter that transferred the signals to an on-line computer. The computer constantly displayed thermal-hydraulic conditions converted to engineering units in the facility control room. Data acquisition was totally automated. At the achievement of steady-state operation, data acquisition was initiated by a switch at the control panel. Thermal-hydraulic data were read approximately every 12 seconds for the duration of the test point. Mean and standard deviations of the readings were calculated and stored by the computer.

Subchannel Enthalpy and Flow Distribution

Bundle average heat flux is determined by dividing total power to the heated section of the bundle by the total heated area. The heat flux was axially uniform and of equal value on all 16 rods. The heat flux on the four heated walls was lower for most runs in order to reduce the chance of critical heat flux occurring on the uninstrumented wall. For the last set of runs, a different heated wall was used with a somewhat higher heating rate because of damage to the original heated walls by electrolysis. The relationship between the heat flux on the walls, ϕ_w, and rods, ϕ_r, and the average bundle heat flux, $\overline{\phi}$, is summarized as:

	$\phi_w/\overline{\phi}$	$\phi_r/\overline{\phi}$
Runs 69 - 492	0.844	1.061
Runs 512 - 608	1.000	1.000

Table 4-2 summarizes the thermal-hydraulic parameters for each of the subchannels and for the bundle as a whole. The subchannel designations refer to Figure 4-3 which illustrates the locations of the subchannels. Note that the hydraulic diameter is nearly the same value for each of the subchannels. This design produced a flat mass flux profile across the bundle. Also shown in the table is the ratio of the average subchannel heat flux, ϕ_{sc}, to the average bundle heat flux, $\overline{\phi}$. The values in the last two columns are for information only to show the sensitivity of the center subchannel enthalpy to subchannel mixing. These values are the ratio of two numbers. The denominator is the bundle enthalpy rise rate, $\overline{\Delta h}$, determined from:

$$\overline{\Delta h} = \frac{\overline{\phi}\, P_\phi}{\overline{G}\, A_G} \qquad (4\text{-}1)$$

where:

$\overline{\phi}$ = bundle average heat flux

$\overline{G}$ = bundle average mass flux

P_ϕ = bundle heated perimeter

A_G = total bundle flow area

Table 4–2

SUBCHANNEL THERMAL–HYDRAULIC DESIGN PARAMETERS

Subchannel Designation	Number of Subchannels	Flow Area cm^2	Wetted Perimeter cm	Heated Perimeter cm	Hydraulic Diameter cm	$\phi_{sc}/\bar{\phi}$		$\Delta h_{sc}/\overline{\Delta h}$	
						Runs 69 - 492	Runs 512 - 608	Runs 69 - 492	Runs 512 - 608
1	1	0.8916	3.025	3.025	1.178	1.061	1.000	1.111	1.047
2	4	0.8916	3.025	3.025	1.178	1.061	1.000	1.111	1.047
3	4	0.8916	3.025	3.025	1.178	1.061	1.000	1.111	1.047
4	8	0.8303	2.784	2.784	1.194	0.962	1.000	0.995	1.035
5	4	0.8303	2.784	2.784	1.194	0.962	1.000	0.995	1.035
6	4	0.6994	2.634	1.684	1.062	0.941	1.000	0.700	0.744
Bundle Total	25	20.787	71.168	67.368	1.168				

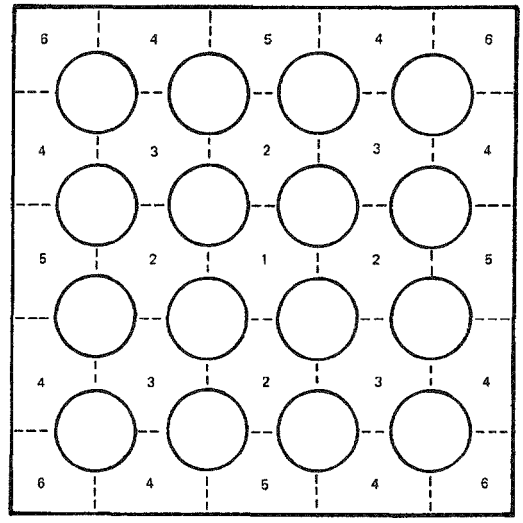

NOTE:
THERMAL-HYDRAULIC PARAMETERS FOR THESE SUBCHANNELS ARE GIVEN IN TABLE 4-2.

Figure 4–3. Subchannel designations

The numerator is the individual subchannel enthalpy rise rate, Δh_{sc}, determined as in Eq. 4-1 but with subchannel values replacing average bundle values. It was assumed for the calculations of the values in Table 4-2 that the mass flux in each subchannel equaled the average mass flux. This assumption results from nearly identical hydraulic diameters in all of the rods. The ratios given in these columns are not exact because mixing between the channels affects the enthalpy rise rate in each subchannel. These values represent the enthalpy rise rates, assuming the absence of any interactions between the subchannel, and they indicate the relative thermal profile across the rod bundle. Note that the

enthalpy rise rate in the subchannel where the void fraction measurements were made -- the center subchannel -- is 11.1% greater than the bundle average for the first set of data. For the second set, the enthalpy rise rate is 4.7% greater. These numbers show that the enthalpy profile is fairly flat; therefore, the enthalpy rise rate in the center subchannel is not very sensitive to subchannel mixing.

Quality from Inlet Temperature

The quality listed in the data tables of this report is the bundle average equilibrium quality. To correlate the void fraction measured in the center subchannel, the center subchannel quality is desired. This quality was originally intended to be calculated by using the COBRA IV computer code. Flow, pressure, inlet temperature, and bundle heat flux would be input for the code. However, an unforeseen difficulty arose. The quality calculated by the code was not compatible with the void fraction data obtained. This incompatibility is addressed later in the report. Essentially, slip factors less than unity were required to correlate the measured void fractions and the predicted qualities. The conclusion is that the COBRA IV code has not correctly handled the mass transfer between the subchannels, resulting in an underprediction of the center subchannel quality; void drift is postulated as the reason. This results from the homogeneous modeling used in the code which is generic to most subchannel codes and is not a problem peculiar to the COBRA IV code alone.

DENSITY DETERMINATION

Void Fraction from Density

Void fraction, α, is calculated from density, ρ, by:

$$\alpha = \frac{\rho_\ell - \rho}{\rho_\ell - \rho_g} \tag{4-2}$$

where ρ_g is the saturated vapor density and ρ_ℓ is the liquid density. The liquid density cannot be approximated as the saturated liquid density since this will lead to unacceptable errors in the calculation of void fraction in the subcooled boiling region. To determine the liquid density, a method was used which

incorporates information about the center subchannel enthalpy. The method proceeds by seeking thermodynamic agreement between the values of liquid enthalpy, liquid density, center subchannel enthalpy, and center subchannel density as follows:

1) Guess $\rho_\ell > \rho_f$

2) $\alpha = \dfrac{\rho_\ell - \rho}{\rho_\ell - \rho_g}$

3) $x = \dfrac{1}{1 + \dfrac{\rho_\ell}{\rho_g}\dfrac{1-\alpha}{\alpha}}$

4) $h_\ell = \dfrac{h - xh_g}{1 - x}$

5) $\rho_\ell = \rho\ (\rho,\ h_\ell)$

6) Repeat steps 2 to 5 until convergence is reached.

The terms used in the above method are defined as:

α = void fraction

ρ = measured density

ρ_ℓ = liquid density

ρ_g = saturated vapor density

x = quality

h = calculated center subchannel enthalpy

h_ℓ = liquid enthalpy

h_g = saturated vapor enthalpy

p = pressure

This method fails to be meaningful if the calculated enthalpy is so large that the liquid enthalpy, h_ℓ, necessary to solve the equations is greater than the saturated value, h_f. Physically, this could occur if slip is not unity as is assumed in step 3. A check is made in the iteration scheme for a liquid enthalpy greater than saturation, in which case the liquid density, ρ_ℓ, is assumed the saturated value, ρ_f.

Multichannel Analyzer

The signals for the three gamma detectors were routed to three of four quadrants of a 4096-channel multichannel analyzer. Each quadrant contained 1024 channels with each channel corresponding to a particular gamma energy. When a gamma is detected, the count total in the channel corresponding to the gamma energy is raised by one. At the end of a run, the stored counts are displayed graphically. This histogram of counts versus channel represents the energy-intensity spectrum of gammas entering the detectors.

Figure 4-4 graphically represents the counts stored in the second quadrant of the multichannel analyzer. This particular curve was taken during a calibration run in which the vessel had been filled with cold water and counted for 3000 seconds. The figure illustrates the basic shape of the scatter collection curve. The sharp peak in the center represents the gammas collected as a result of a single scatter. The wider base position of the curve results from multiple scattering. It is possible to predict the edges of this base from compton scatter theory. The base portion decreases with density but not as fast as the central peak. This is a result of the multiple scattering that occurs on the rods that remain when the vessel is empty. The energy resolution of the peak can be calculated from the fact that the channel energy width is about 2.0 keV. The width at half max was about 7 keV.

In practice, only a small portion of the curve shown in Figure 4-4 was sent to the computer. This portion was 60 channels wide with the peak approximately centered. Counts were accumulated over a 400-second interval. A typical curve taken with a density of about 420 kg/m^3 is shown in Figure 4-5. Several things must be considered in an algorithm to reduce this histogram to a single number representing the detector count rate. First, the location of the peak may vary by several channels from run to run. Second, the width of the peak may vary. Third, the base count rate is neither constant nor a fixed ratio of the peak count

rate. Lastly, one must be careful to minimize the effect of statistical deviations. For example, searches for maximum and minimum points in the curves must be based on the trends observed in many consecutive channels. A simple channel-to-channel search for a minimum may result in "statistically-caused" minimums rather than "true" minimums.

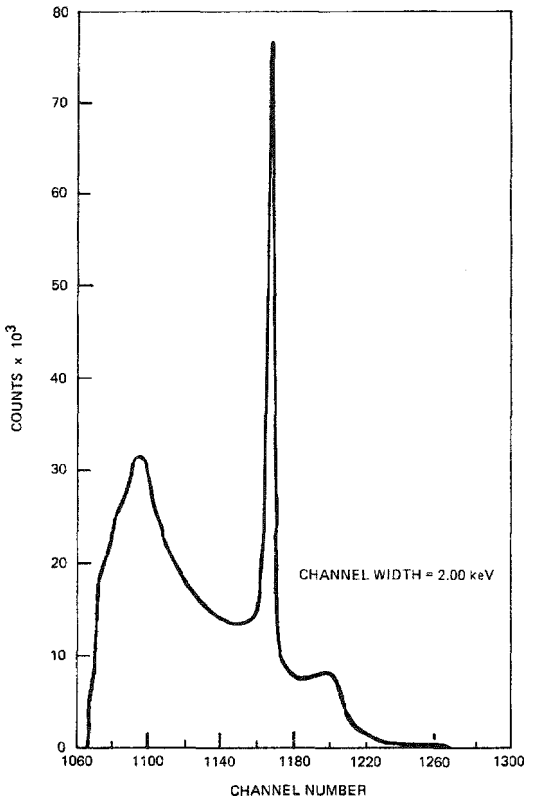

Figure 4–4. Gamma counts for detector 2 indicated by the multichannel analyzer

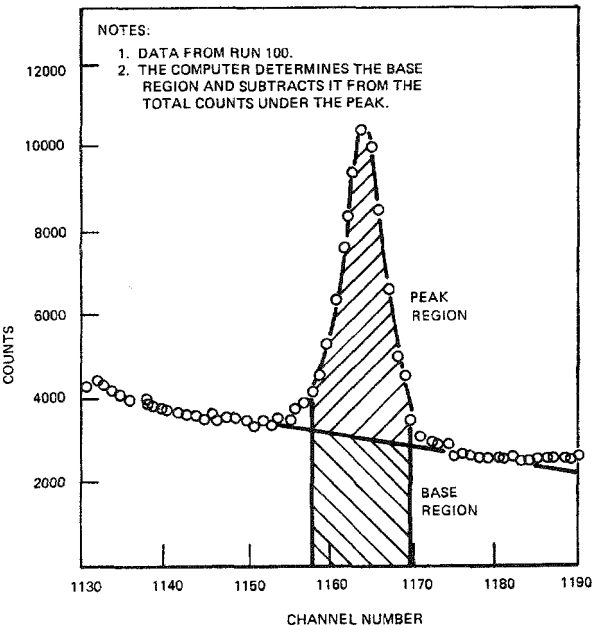

Figure 4–5. Detector 2 peak region sent to computer for analysis

The algorithm used considered all of these and approached the ideal minimum standard deviation caused by counting statistics. It proceeded as follows:

1) The peak channel was found.

2) Five consecutive channels at a predetermined distance from the peak channel were determined on each side of the peak. A linear curve was fit through the 10 total points by least squares. This was the base curve or background curve.

3) The background line was subtracted from all the points.

4) A least-squares parabolic curve was fit to a fixed number of points surrounding the peak channel.

5) The true peak was determined by differentiating this curve.

6) All channels in a predetermined distance about the true peak, including fractions of channels at the extremes of this range, were summed.

The computer routine used for these calculations made several checks for abnormal numbers and also calculated the background rate and the statistical standard deviation in the calculated rate.

First Collimator Set Calibration and Reduction

This section describes the procedures used to implement the equations derived earlier to the data taken with the first set of collimators. Sufficient information will be provided so that the reader will be able to repeat the calculations to convert the gamma count rates to void fraction.

Eq. 3-41 and 3-42 are the basic equations of the data reduction. Most of the parameters in these equations are determined directly; N_1^e, N_2^e, and N_3^e are the count rates of the three detectors during the experimental run. These values are listed in the Appendix B data tables for each run. N_1^r, N_2^r, and N_3^r are the count rates of the three detectors during the reference run. The densities ρ_{s2}^r and ρ_{s3}^r have the same value and are simply the fluid density during the reference run. These values are listed in Table 4-3 for each reference run. Each data entry of Appendix B for the first collimator set contains a reference run code number which refers back to the listing in Table 4-3.

Before proceeding with the description of the calibration, the following terms, which will be useful in the subsequent discussion, are defined:

$$\left.\begin{aligned} &C_1 = N_0 f_1 g_1 \varepsilon_1 \,, \quad C_2 = N_0 f_0 f_2 g_0 g_2 \varepsilon_2 \, C \,, \quad \text{and } C_3 = N_0 f_0 f_3 g_0 g_3 \varepsilon_3 \, C \\ &\sigma_1 = \mu_1 x_1 + \mu_1 x_0 \,, \quad \sigma_2 = \mu_1 x_0 + \mu_2 x_2 \,, \quad \text{and } \sigma_3 = \mu_1 x_0 + \mu_2 x_3 \\ &\bar{\rho}_1 = \frac{\mu_1 x_1 \rho_1 + \mu_1 x_0 \rho_0}{\mu_1 x_1 + \mu_1 x_0} \,, \quad \bar{\rho}_2 = \frac{\mu_1 x_0 \rho_0 + \mu_2 x_2 \rho_2}{\mu_1 x_0 + \mu_2 x_2} \,, \quad \text{and } \bar{\rho}_3 = \frac{\mu_1 x_0 \rho_0 + \mu_2 x_3 \rho_3}{\mu_1 x_0 + \mu_2 x_3} \end{aligned}\right\} \quad (4\text{-}3)$$

Table 4–3

COLLIMATOR SET 1 REFERENCE DATA

REF CODE	DENSITY	GAMMA RATE 1	GAMMA RATE 2	GAMMA RATE 3	ZERO DENSITY RATE 2	ZERO DENSITY RATE 3
1	718.1	264.84	156.94	126.93	23.40	28.84
2	717.2	262.73	155.88	127.03	23.70	28.84
3	703.4	264.04	154.66	125.88	23.70	28.84
4	806.2	245.32	162.44	131.48	23.70	28.84
5	697.0	255.31	154.42	124.13	23.70	28.84
6	0.0	0.00	0.00	0.00	22.18	27.47
7	709.4	261.09	153.71	122.51	22.18	27.47
8	757.7	259.46	158.69	125.89	22.18	27.47
9	771.6	259.78	156.79	126.51	22.18	27.47
10	793.9	253.29	157.61	128.03	22.18	27.47
11	863.3	238.86	160.60	131.40	22.18	27.47
12	724.4	263.52	152.32	124.17	22.18	27.47
13	798.8	250.51	158.35	129.38	22.18	27.47
14	845.4	242.98	161.82	130.14	22.18	27.47
15	849.8	244.58	161.74	132.72	22.18	27.47
16	883.8	238.57	164.92	132.37	22.18	27.47
17	817.2	244.24	158.67	129.94	22.18	27.47
18	800.7	197.43	999.99	117.97	25.08	22.06
19	800.7	197.43	999.99	117.98	25.08	22.06
20	779.0	202.48	999.99	116.02	25.08	22.06
21	848.6	239.83	167.26	140.45	23.70	28.84
22	828.6	252.75	167.82	146.13	23.70	28.84
23	720.0	264.76	157.92	127.61	23.70	28.84
24	718.1	264.84	156.94	126.93	23.70	28.84
25	809.5	246.83	157.57	129.17	22.18	27.47
26	778.3	257.14	157.28	126.33	22.18	27.47

DENSITY -------- Kg/M^3
GAMMA RATE ----- COUNTS/SEC.

The values of q_2 and q_3 are determined from the calibration runs described below. Their values are given in Table 4-4. The remaining parameters are the rod scatter contribution to the gamma detection rates. Their values are found from Eq. 3-39 and 3-40. Two of the terms in these equations, N_{mo2} and N_{mo3}, were measured by the calibration procedure (c) described later. These values were measured several times during the experimental program after alignment had been altered by safety inspections of the collimators. These empty vessel rod scatter rates are listed along with the reference values in Table 4-3. The values of ρ_{m2} and ρ_{m3} for the experimental runs are estimated from the average fluid density

determined from detector 1. Eq. 3-10 describes the response of the straight-through detector (1). Using the definitions of Eq. 4-3, this equation can be simplified to:

$$\frac{N_1^r}{N_1^e} = \exp\left[\sigma_1(\bar{\rho}_1^e - \bar{\rho}_1^r)\right] \tag{4-4}$$

and rearranging,

$$\bar{\rho}_1^e = \bar{\rho}_1^r + \frac{\log\,(N_1^r/N_1^e)}{\sigma_1} \tag{4-5}$$

The densities of ρ_{m2} and ρ_{m3} are assumed equal to the average fluid density, $\bar{\rho}_1^e$.

Table 4–4

COLLIMATOR SET 1 CALIBRATION SUMMARY
(Runs 69 - 492)

Constant	Value
σ_1	5.562×10^{-4} m^3/kg
σ_2	6.092×10^{-4} m^3/kg
σ_3	5.954×10^{-4} m^3/kg
σ_w	2.191×10^{-4} m^3/kg
σ_{m2}	3.901×10^{-4} m^3/kg
σ_{m3}	3.763×10^{-4} m^3/kg
q_2	1.087
q_3	1.063

To complete the determination of the rod scatter contribution, the values of σ_{m2} and σ_{m3} must be determined. The gammas that scatter off the rods pass through less water on the average than the gammas that scatter off the water. (See Figure 4-6.) The attenuation rates of gammas that scatter off the rods are

equal to the attenuation rates of gammas scattering off the water minus a term accounting for less distance traveled in water:

$$\sigma_{m2} = \sigma_2 - \sigma_w \tag{4-6}$$

$$\sigma_{m3} = \sigma_3 - \sigma_w \tag{4-7}$$

The term σ_w was determined from the rod bundle geometry. Its value is listed in Table 4-4.

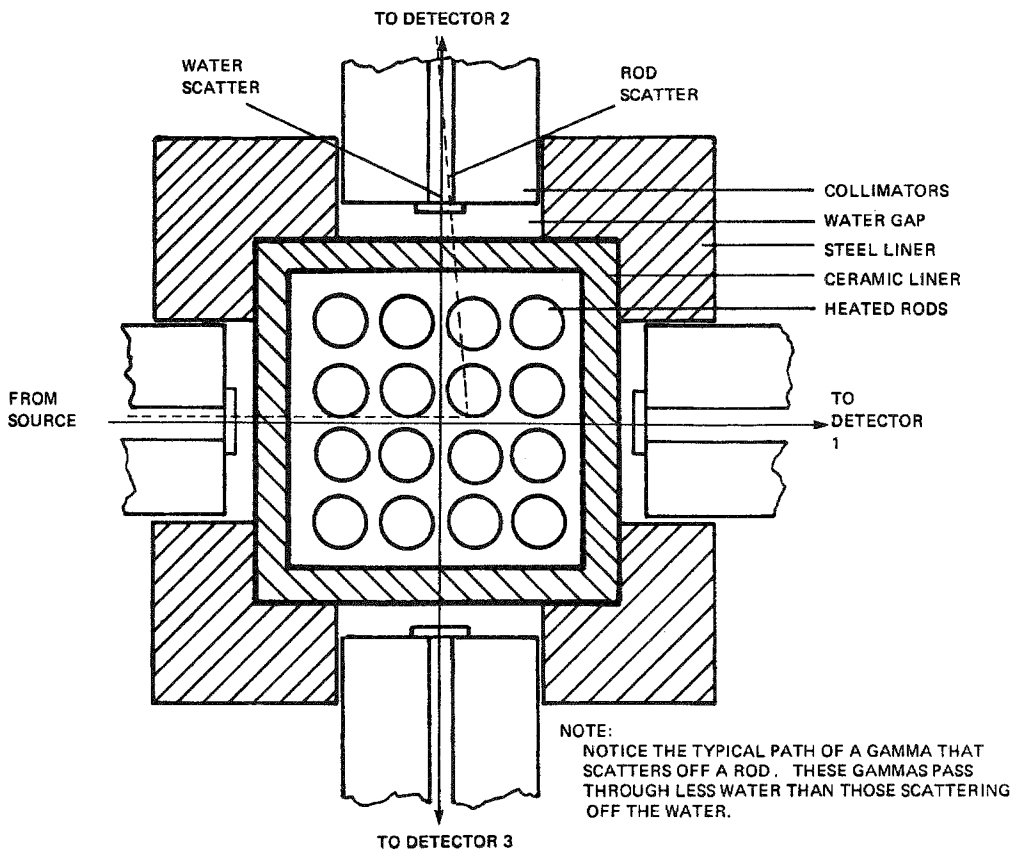

Figure 4–6. Gamma paths for collimator set 1

Several constants used in the data reduction were determined by taking 6000-second counts with known conditions in the rod bundle. The four calibration runs were taken at the following nominal conditions:

Designation	Material	Temperature	Pressure
a	Water	Ambient	Atmospheric
b	Nitrogen	Ambient	10.34 MPa
c	Air	Ambient	Atmospheric
d	Water	260° C	16.89 MPa

The empty vessel rod scatter rates N_{mo2} and N_{mo3} are determined directly from the count rates on detectors 2 and 3, respectively, during calibration (c). Although atmospheric air was present at the time of calibration, the assumption was made that the density was zero.

The value of σ_1, which represents the attenuation of the unscattered gammas through the bundle, was determined using calibrations (a) and (c), and Eq. 4-4 (repeated here):

$$\frac{N_1^a}{N_1^c} = \exp\left[\sigma_1 \left(\bar{\rho}_1^c - \bar{\rho}_1^a\right)\right]$$

The superscripts a and c, designating the calibration runs, replace the superscripts r and e, respectively, in the original equation. The values of N_1^a, N_1^c, $\bar{\rho}_1^a$, $\bar{\rho}_1^c$ were substituted into this equation and solved for σ_1.

The total side scatter detection rate is the sum of the water contribution and the rod contribution. The water contribution is given by Eq. 3-8, which can be simplified using the definitions of Eq. 4-3 to:

$$C_2 \rho_{s2} \exp\left(\sigma_2 \bar{\rho}_2\right)$$

The rod scatter rate is given by Eq. 3-39. Substituting the expression in Eq. 4-6, the following is obtained:

$$N_{mo2} \exp\left(\sigma_2 \rho_{m2} - \sigma_w \rho_{m2}\right)$$

Combining the preceding expressions results in an equation for the total side scatter detection rate:

$$N_2 = C_2\rho_{s2} \exp(\sigma_2\bar{\rho}_2) + N_{mo2} \exp(\sigma_2\rho_{m2} - \sigma_w\rho_{m2}) \quad (4\text{-}8)$$

The two unknowns C_2 and σ_2 were found using calibrations (a) and (b). The values determined in these runs were substituted into Eq. 4-8 for each run and the two equations were solved simultaneously. The densities were determined from the pressure and temperature of the fluid. N_{mo2} was determined using the procedure described above and σ_w is given in Table 4-4. The density of nitrogen found in calibration (b) was converted to the equivalent water density prior to insertion into the equations. This correction factor of 0.9 results from the different ratios of mass density to electron density between nitrogen and water. A parallel procedure was used to obtain the value of σ_3. These two values are listed in Table 4-4.

Finally, the values of q_2 and q_3 were determined using Eq. 3-41 and 3-42 with calibrations (a) and (b). After the equivalent water density of the nitrogen was calculated, all of the terms of these two equations, except q_2 and q_3, were known or calculated from known values. These equations were then solved for these unknowns. The values of q_2 and q_3 are also listed in Table 4-4. This completed the necessary calibrations for collimator set 1.

Second Collimator Set Calibration and Reduction

The second collimator set data were calibrated somewhat differently from the first set partly because the different geometry alters the estimating procedure for ρ_m. However, the principal reason for the different application resulted from problems encountered during calibration that caused the entire calibration set to be questioned. During calibrations (a), (c), and (d) described in the previous section, data were taken at an essentially zero density, a cold water density, and also at the density of hot water (about 260° C). The three count rates obtained from the straight-through detector should have fallen on a curve predicted by attenuation theory, given the geometry of the gamma path. This curve is a simple exponential-decay type curve through the zero density point which decreases asymptotically to zero as the density is increased. The cold water point fell on this line; however, the count rate at the 260° C density point was 20% higher than the predicted count rate.

Since the data obtained from this second set of collimators are very sensitive to alignment (the gamma beam is 30% as wide as that for the first set), small seating adjustments between the vessel collimators and the source shielding slit due to thermal expansion of the facility structure may have caused the count rate changes. The cause of the anomalous calibration results at 260° C was attributed to thermal expansion because, once at operating temperatures, the response of the detectors behaved generally as expected. This became clear as the detector response curves are derived and the experimental data are shown. On the basis of this observation, it was decided that the calibration could be based directly on the count rates taken during experimentation and on the nominal channel dimensions.

Figure 4-7 is a diagram of the test bundle and the gamma beams used in the model for the second collimator set data reduction. One of the things to note in this diagram is the region surrounding the ceramic liners. This region represents water that was outside the flow channel but was involved in the measurements. This exterior region was 4.65 mm wide and was located only where the beams enter the rod bundle (i.e., did not extend the length of the bundle as a flow path).

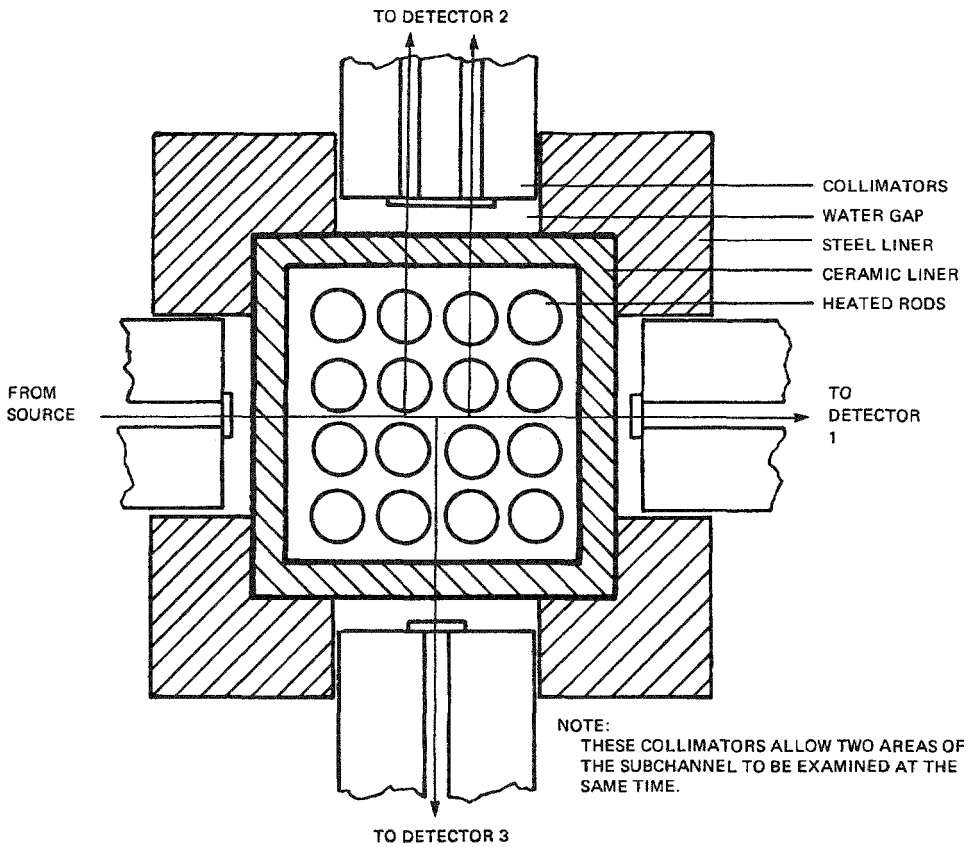

Figure 4–7. Gamma paths for collimator set 2

The exterior water region is required in this analysis because the gammas passed through this region and thus affected the response of the detectors. This region was not treated explicitly in the first collimator analysis since the region was located on all four sides and the assumption of symmetry was not violated. Symmetry is not assumed in the reduction of the second collimator set calibration data.

The equations governing the response of the three detectors are found by modifying Eq. 3-8 and 3-9, using the definitions of Eq. 4-3. The rod scatter rate contribution is added to the response of the side detectors. The water in the exterior water region is accounted for by adding its attenuation effect to the existing attenuation rate. These modifications lead to:

$$N_1 = C_1 \exp\left(-\sigma_1\bar{\rho}_1 - \sigma_{e1}\rho_e\right) \tag{4-9}$$

$$N_2 = C_2\,\rho_{s2} \exp\left(-\sigma_2\bar{\rho}_2 - \sigma_{e2}\rho_e\right) + N_{mo2} \exp\left(-\sigma_{m2}\rho_{m2} - \sigma_{e2}\rho_e\right) \tag{4-10}$$

The equation for detector 3 is similar to that for detector 2:

$$N_3 = C_3\,\rho_{s3} \exp\left(-\sigma_3\bar{\rho}_3 - \sigma_{e3}\rho_e\right) + N_{mo3} \exp\left(-\sigma_{m3}\rho_{m3} - \sigma_{e3}\rho_e\right) \tag{4-11}$$

The values σ_{e1}, σ_{e2}, and σ_{e3} have been introduced as the attenuation coefficients of the water in the exterior water region as they apply to detectors 1, 2, and 3, respectively. The density in the exterior water region, ρ_e, is assumed by symmetry to be the same for all four sides of the bundle.

The values of N_{mo2} and N_{mo3} were determined from the side detector count rates when the vessel was empty. The values are given in Table 4-5. The value of N_{mo3} was zero so this term drops out of Eq. 4-11.

Table 4–5

SUMMARY OF COLLIMATOR SET 2 REDUCTION COEFFICIENTS

Constant	Value
σ_1	4.881×10^{-4} m^3/kg
σ_2	3.546×10^{-4} m^3/kg
σ_3	5.857×10^{-4} m^3/kg
σ_{e1}	0.797×10^{-4} m^3/kg
σ_{e2}	0.957×10^{-4} m^3/kg
σ_{e3}	0.957×10^{-4} m^3/kg
σ_{m2}	3.546×10^{-4} m^3/kg
N_{mo2}	17.0 counts/sec
N_{mo3}	0.0 counts/sec

To determine the coefficients σ_1, σ_2, σ_3, and σ_{m2}, the following values are necessary:

Flow channel width (w)	--	5.695 cm
Flow channel height (h)	--	5.695 cm
Rod pitch (p)	--	1.273 cm
Rod diameter (d)	--	0.963 cm
Exterior water region width (s)	--	0.465 m
Source gamma attenuation coefficient (μ_1)	--	0.0857 cm^2/g
90° scattered gamma attenuation coefficient (μ_2)	--	0.1200 cm^2/g

The several values of σ are determined by summing for each segment of the applicable beam paths the product of the distance across the water by the attenuation coefficient. This leads to the following after examining the geometry in Figure 4-7.

$$\sigma_1 = w\mu_1$$

$$\sigma_2 = \left(\frac{w}{2} - \frac{p}{2}\right) + \left(\frac{w}{2} + \frac{p}{2}\right)\frac{\mu_1}{2} + \left(\frac{w}{2} - 2d\right)\mu_2$$

$$\sigma_3 = \left(\frac{w}{2}\right) \mu_1 + \left(\frac{w}{2}\right) \mu_2$$

$$\sigma_{e1} = (s + s) \mu_1$$

$$\sigma_{e2} = s\mu_1 + s\mu_2$$

$$\sigma_{e3} = s\mu_1 + s\mu_2$$

Since the rod scatter occurs at the same location as the water scatter for detector 2, $\sigma_{m2} = \sigma_2$. These have been calculated and their values are listed in Table 4-5. This same argument applies to the density so that $\rho_{m2} = \rho_2$.

During the experimentation, many of the experimental points were taken when the conditions at the point of measurement were single-phase. For these points, the fluid density could be determined from temperature and pressure and the ASME subcooled liquid tables. These points are plotted in Figures 4-8, 4-9, and 4-10 for each of the three detectors. Shown plotted are the count rates on the detector against the water density. These points are all of the single-phase points for the second collimator series which included Runs 512 through 608. The forms of Eq. 4-9, 4-10, and 4-11 have been fit to these data by adjusting the arbitrary coefficients, C_1, C_2 and C_3. Note that except for Runs 592, 593, and 608, all of the data for a given detector can be fit with a single curve. These three points are the single-phase points for two of the sets of thermal-hydraulic data. Runs 592 and 593 belong in one set; Run 608 in the other. These sets, the last two taken, occurred after the facility was shut down for a weekend. There is no completely satisfactory explanation for this abrupt change which had not been observed in all of the previous testing. Permanent alignment changes probably occurred during the facility down period. However, these questionable data that involves Runs 592 through 608 were included in this report. New response curves were determined for each of the two involved sets of data. These curves are also shown in Figures 4-8, 4-9, and 4-10.

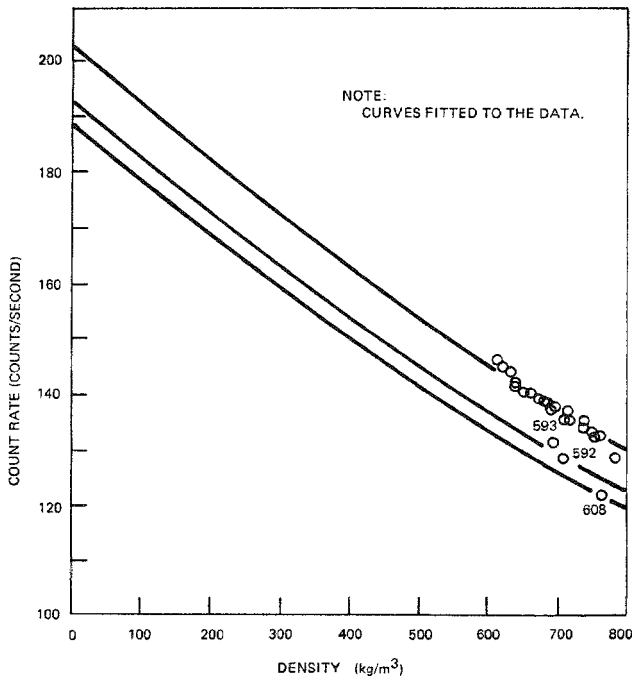

Figure 4–8. Single–phase count rate data for detector 1 – collimator set 2

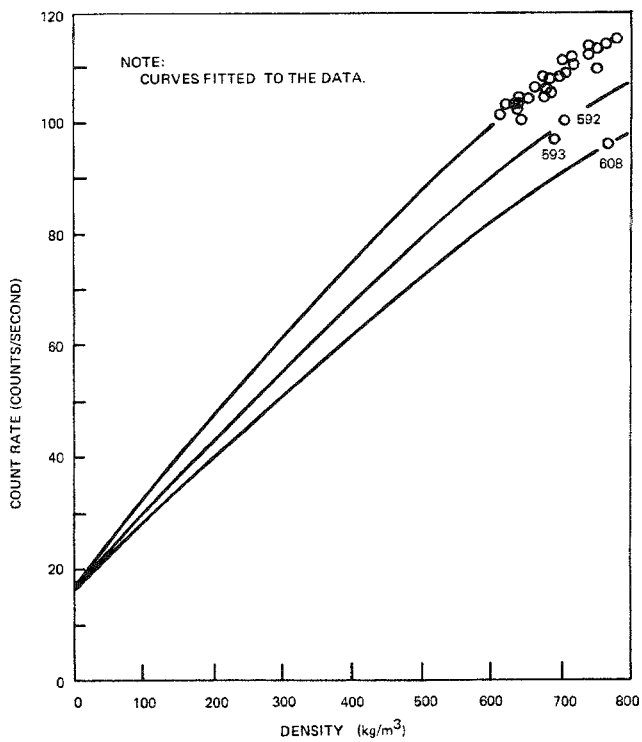

Figure 4–9. Single–phase count rate data for detector 2 – collimator set 2

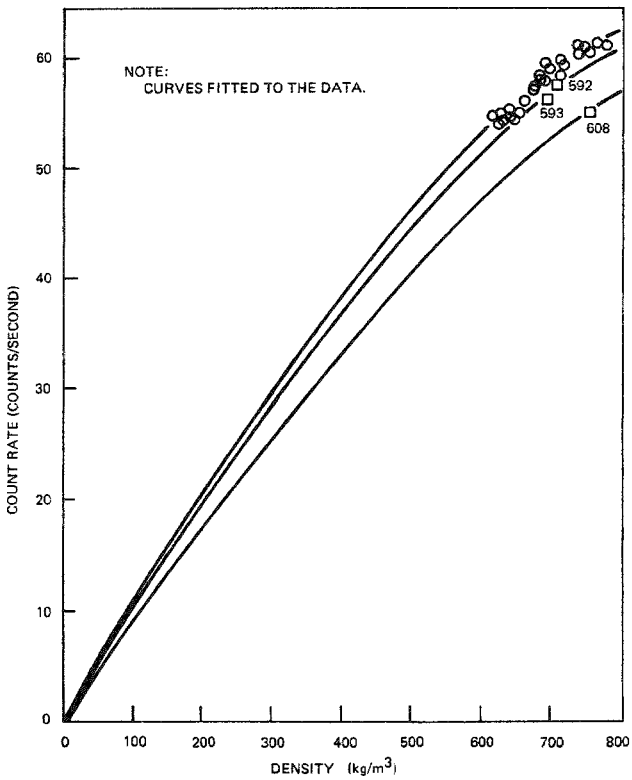

Figure 4—10. Single—phase count rate data for detector 3 — collimator set 2

The coefficients that fit the response curves to the data are as follows:

Run Numbers	C_1 Counts/sec	C_2 Counts - m^3/sec·kg	C_3 Counts - m^3/sec·kg
512 - 589	205.2	0.1880	0.1329
592 - 597	193.6	0.1696	0.1310
598 - 608	189.4	0.1541	0.1268

For the data reduction, it was assumed that $\bar{\rho}_3 = \bar{\rho}_1$. This follows from the symmetry of the bundle about the center of the center subchannel. It was also assumed that $\bar{\rho}_2 = \bar{\rho}_1$. This is not strictly true since the gammas leaving the scatter volume toward detector 2 generally pass through the gap region of the rods while those that continue on toward the straight-through detector pass through both central and gap regions of the subchannel. In other words, symmetry does not apply. The effect of this was examined in the preceding section (Section 3) and it was found to be less than 1% of the density measurement, which

was acceptable. The response curves, Eq. 4-9, 4-10, and 4-11, were then solved for $\bar{\rho}_1$, ρ_{s2}, and ρ_{s3}, respectively:

$$\bar{\rho}_1 = \frac{\log (c_1/N_1) - \sigma_{e1}\rho_e}{\sigma_1} \tag{4-12}$$

$$\rho_{s2} = \frac{N_2 \exp(\sigma_2\bar{\rho}_1 + \sigma_{e2}\rho_e) - N_{mo2}}{C_2} \tag{4-13}$$

$$\rho_{s3} = \frac{N_3 \exp(\sigma_2\bar{\rho}_1 + \sigma_{e3}\rho_e) - N_{mo3}}{C_2} \tag{4-14}$$

The relations determined earlier that $\rho_{m2} = \rho_2$ and $\sigma_{m2} = \sigma_2$ have been incorporated in these equations.

Prior to solving the equations, it was necessary to calculate the water density in the region outside the bundle (ρ_e). If the exit quality was less than zero, ρ_e was assumed the subcooled liquid density based on the exit temperature and pressure. If the exit quality was greater than zero, ρ_e was assumed the saturated liquid density based on the exit pressure.

Sufficient information has been provided in this section for the reader to repeat the calculations to obtain density from the count rates listed in the data tables in Appendix B.

Section 5

ANALYSIS OF VOID FRACTION DATA

REVIEW OF EXISTING VOID FRACTION MODELS

A review of the open literature has revealed that there are a wide variety of models available to predict void fraction in two-phase flow. Most of these models use the equations of continuity for each phase to develop an expression for void fraction in terms of the true or mass flow quality. The models which take this approach can be divided into two broad classes: Slip Models and Drift Flux Models. Both types of models take into account the fact that under most conditions the gas phase travels at a higher velocity than the liquid phase.

Derivation of Void - Quality Relation for Slip Models

The vapor void fraction, or more simply void fraction, of a gas/liquid flow is typically defined as the fractional area of the vapor phase across a plane perpendicular to the direction of flow. A more complete definition of void fraction is given by Lahey (5) as:

> The vapor (or holdup) void fraction represents the time-average volumetric fraction of vapor in a two-phase mixture. Mathematically,

$$\alpha \equiv \frac{\iiint_{V_g} dV}{\iiint_{V} dV} = \frac{V_g}{V_\ell + V_g} \qquad (5\text{-}1)$$

> where the subscripts ℓ and g denote the liquid phase and the vapor phase, respectively.

If the volume in question consists of the cross-sectional area of a flow tube times a differential length element, the void fraction can be considered as a time-averaged area fraction:

$$\alpha = \frac{\Delta Z \iint_{A_g} dA}{\Delta Z \iint_{A} dA} = \frac{A_g}{A_\ell + A_g} \tag{5-2}$$

The void fraction defined in Eq. 5-1 or 5-2 is deterministic. Actually, void fraction is a random variable in space and time. If we perform N statistically independent measurements of the instantaneous void fraction at location, r, for time, t, then the ensemble-averaged local void fraction is given as:

$$\alpha(r,t) = \frac{N_g\ (r,t)}{N} \tag{5-3}$$

where $N_g\ (r,t)$ is the number of experimental observations in which the location, r, was in vapor at time, t.

The link between Eq. 5-3 and 5-1 is the Ergodic Hypothesis, which essentially states that for a stationary random process, the ensemble average and the time average of a given member of the ensemble are identical. ... However, for our present purpose, it is important only to realize that the void fraction that is used in subsequent analyses is a time-averaged deterministic quantity.

Another important parameter in two-phase flow is the ratio of the steam mass flow rate to the total mass flow, or the true flow quality, X_t.

$$X_t \equiv \frac{\dot{m}_g}{\dot{m}_g + \dot{m}_\ell} \tag{5-4}$$

where:

$\dot{m}_g$ = mass flow rate of gas phase

$\dot{m}_\ell$ = mass flow rate of liquid phase

Under conditions of thermodynamic equilibrium, this flow quality is identical to the thermodynamic quality that would be obtained from a heat balance. However, in situations where subcooled boiling occurs, thermodynamic equilibrium does not exist and there can be significant amounts of vapor flow while the thermodynamic quality is negative. True flow quality has also been called the mass flow quality or mass dryness fraction. Conservation of mass requires that the following equations must be satisfied:

$$\dot{m}_g = \rho_g A_g V_g \tag{5-5}$$

$$\dot{m}_\ell = \rho_\ell A_\ell V_\ell \tag{5-6}$$

where:

ρ_ℓ = density of the liquid phase

ρ_g = density of the gaseous phase

V_g = cross-sectional average velocity of the gaseous phase

V_ℓ = cross-sectional average velocity of the liquid phase

These equations can be rearranged to give:

$$A_g = \frac{\dot{m}_g}{\rho_g V_g} \tag{5-7}$$

$$A_\ell = \frac{\dot{m}_\ell}{\rho_\ell V_\ell} \tag{5-8}$$

Substituting Eq. 5-7 and 5-8 into Eq. 5-2 and dividing through by $\dot{m}_g/\rho_g V_g$ gives:

$$\alpha = \frac{1}{1 + \frac{\dot{m}_\ell}{\rho_\ell V_\ell} \cdot \frac{\rho_g V_g}{\dot{m}_g}} \tag{5-9}$$

Dividing Eq. 5-4 through by $\dot{m}_g$ and solving for $\dot{m}_\ell/\dot{m}_g$ gives:

$$\frac{\dot{m}_\ell}{\dot{m}_g} = \frac{1 - X_t}{X_t} \tag{5-10}$$

Substituting $\dot{m}_\ell/\dot{m}_g$ into Eq. 5-9 and rearranging yields:

$$\alpha = \frac{1}{1 + \frac{V_g}{V_\ell}\frac{\rho_g}{\rho_\ell}\frac{1 - X_t}{X_t}} \tag{5-11}$$

The ratio of the gas phase velocity to liquid phase velocity is called the slip ratio, S, and is defined by the equation:

$$S \equiv \frac{V_g}{V_\ell} \tag{5-12}$$

Substituting Eq. 5-12 into Eq. 5-11 leads to the final result:

$$\alpha = \frac{1}{1 + S\frac{\rho_g}{\rho_\ell}\frac{1 - X_t}{X_t}} \tag{5-13}$$

This equation is the fundamental void - quality relationship used by all of the slip models to calculate void fraction. Although they do not all present their results in this form, they all may be reduced to an equation having this form. Since the density ratio and true flow quality are generally known, only the slip ratio must be specified to fix the void fraction. It is this information that the slip models provide. A list of some slip models available in the open literature is given in Table 5-1.

Table 5–1

SLIP MODELS

Author(s)	Slip Equation	Limitations
Marchaterre/Hoglund [Reference (6)]	Correlation Presented Graphically	Valid only beyond region of bulk boiling
Zivi [Reference (7)]	$S = \left(\frac{\rho_f}{\rho_g}\right)^{1/3}$	For idealized annular flow
Thom [Reference (8)]	S = f(P) presented in tabular form: well correlated by: $S = 15.58\ P^{-0.33}$ (Pressure, P, in psia)	
Ahmad [Reference (9)]	$S = \left(\frac{\rho_f}{\rho_g}\right)^{0.205} \left(\frac{GD_h}{\mu}\right)^{-0.016}$	Valid for: $P \geq 0.966$ MPa $G \geq 407$ kg/m^2·sec
Madsen [Reference (10)]	$S = \left(\frac{\rho_f}{\rho_g}\right)^{-L}$ $L = \frac{1}{2} - \frac{1/2 \log_{10}\left[X_t/(1-X_t)\right]}{\log_{10}\left[\alpha_o/(1-\alpha_o)\right] - \log_{10}\left[\rho_g/\rho_f\right]}$ $\alpha_o = 0.302$	Bulk boiling only

Derivation of Void - Quality Relation for Drift Flux Models

The development of the drift flux model is largely due to the work of Zuber and Findlay(11), who presented the void - quality relationship which is the starting point for all of the drift flux models. The derivation of this equation begins by defining the volumetric flux of each phase:

$$j_f \equiv \frac{Q_f}{A} = \text{volumetric flux of liquid phase} \qquad (5\text{-}14)$$

$$j_g \equiv \frac{Q_g}{A} = \text{volumetric flux of gas phase} \qquad (5\text{-}15)$$

where:

$$Q_f = \frac{\dot{m}_f}{\rho_f} = \text{volumetric flow rate of the liquid phase} \quad (5\text{-}16)$$

$$Q_g = \frac{\dot{m}_g}{\rho_g} = \text{volumetric flow rate of the gas phase} \quad (5\text{-}17)$$

A = total flow area

The total volumetric flux is then given by:

$$j = j_f + j_g = \frac{Q}{A} \quad (5\text{-}18)$$

The volumetric flux is sometimes also called the "superficial velocity". The continuity equations for each phase can be rewritten as:

$$\frac{\dot{m}_f}{\rho_f} = V_f A_f \quad (5\text{-}19)$$

$$\frac{\dot{m}_g}{\rho_g} = V_g A_g \quad (5\text{-}20)$$

Substituting Eq. 5-19 and 5-20 into Eq. 5-16 and 5-17 gives:

$$Q_f = V_f A_f \quad (5\text{-}21)$$

$$Q_g = V_g A_g \quad (5\text{-}22)$$

Substituting these two equations (5-21 and 5-22) into the definitions for the phasic volumetric flux yields:

$$j_f = V_f \frac{A_f}{A} \tag{5-23}$$

and

$$j_g = V_g \frac{A_g}{A} \tag{5-24}$$

These equations indicate that volumetric flux is a direct measure of velocity. Recalling the definition of void fraction, these two equations (5-23 and 5-24) may be written as:

$$V_f = j_f/(1 - \alpha) \tag{5-25}$$

$$V_g = j_g/\alpha \tag{5-26}$$

We now write the identity:

$$V_g = j + (V_g - j) \tag{5-27}$$

where the term $V_g - j$ is a measure of the drift velocity of the gaseous phase with respect to the mixture volumetric flux. Substituting Eq. 5-26 into Eq. 5-27 and multiplying through by α gives:

$$j_g = \alpha j + \alpha (V_g - j) \tag{5-28}$$

To obtain a cross-sectional average value for j_g, we must integrate this expression as follows:

$$\frac{1}{A} \iint_A j_g \, dA = \frac{1}{A} \iint_A \alpha j \, dA + \frac{1}{A} \iint_A \alpha (V_g - j) \, dA \tag{5-29}$$

This can be rewritten in Zuber's notation as:

$$\langle j_g \rangle = \langle \alpha j \rangle + \langle \alpha (V_g - j) \rangle \tag{5-30}$$

where the symbol $\langle \; \rangle$ indicates the cross-sectional average value of a variable.

We now define the following parameters:

$$C_o \equiv \langle \alpha j \rangle / (\langle \alpha \rangle \langle j \rangle) \tag{5-31}$$

$$\overline{V}_{gj} \equiv \langle \alpha (V_g - j) \rangle / \langle \alpha \rangle \tag{5-32}$$

Substituting these equations into Eq. 5-30 and solving for $\langle \alpha \rangle$ leads to the result:

$$\langle \alpha \rangle = \frac{\langle j_g \rangle}{C_o \langle j \rangle + \overline{V}_{gj}} \tag{5-33}$$

Since volumetric flux is not usually measured during an experiment, it is useful to express this equation in slightly different form. Eq. 5-17 can be substituted into Eq. 5-15 to give:

$$\langle j_g \rangle = \frac{\dot{m}_g}{A \rho_g} \tag{5-34}$$

Using the definition of flow quality, X_t, Eq. 5-34 can then be rewritten as:

$$\langle j_g \rangle = \frac{\dot{m}}{A} \frac{\langle X_t \rangle}{\rho_g} \tag{5-35}$$

The term $\dot{m}/A$, the mass flow rate per unit area, is called the mass flux and is given the symbol G. Thus:

$$\langle j_g \rangle = \frac{G \langle X_t \rangle}{\rho_g} \tag{5-36}$$

A similar development for $\langle j_f \rangle$ gives:

$$\langle j_f \rangle = \frac{G(1 - \langle X_t \rangle)}{\rho_f} \tag{5-37}$$

Since $\langle j \rangle = \langle j_g \rangle + \langle j_f \rangle$:

$$\langle j \rangle = G \left\{ \frac{\langle X_t \rangle}{\rho_g} + \frac{1 - \langle X_t \rangle}{\rho_f} \right\} \tag{5-38}$$

Substituting Eq. 5-36 and 5-38 into Eq. 5-33 leads to the final result:

$$\langle \alpha \rangle = \frac{\langle X_t \rangle}{C_o \left\{ \langle X_t \rangle + \frac{\rho_g}{\rho_f} (1 - \langle X_t \rangle) \right\} + \frac{\rho_g \overline{V}_{gj}}{G}} \tag{5-39}$$

This equation provides an expression for void fraction which is very similar to the expression used by the slip models. Setting the two equations equal and solving for the slip ratio leads to the result:

$$S = C_o + \frac{\langle X_t \rangle (C_o - 1) \rho_f}{\rho_g (1 - \langle X_t \rangle)} + \frac{\rho_g \overline{V}_{gj}}{G (1 - \langle X_t \rangle)} \tag{5-40}$$

The first two terms in this equation describe slip that results from averaging a nonuniform void fraction distribution in the presence of a nonuniform velocity distribution. This is sometimes called "global" or "integral" slip. The key variable in these terms is C_o, called the distribution parameter. It can be seen from the defining equation for C_o that, when either the void fraction or the total volumetric flux is constant across the flow channel, C_o has the value of unity. The distribution parameter takes into account two-dimensional effects that the slip models do not explicitly include. The last term in the above equation describes the local slip between the two phases. It contains the key parameter $\overline{V}_{gj}$, the weighted mean relative drift velocity, henceforth referred to as relative drift velocity. This parameter provides a direct measure of the difference in velocity between the two phases at a particular point in a flow channel (local slip). When the velocity of the two phases is the same at any given point in the flow channel, the total volumetric flux and the gas/liquid velocity have the same value, and the relative drift velocity is zero. Since G, X, ρ_f, and ρ_g are generally known, only the parameters C_o and $\overline{V}_{gj}$ must be specified in order to calculate void fraction from Eq. 5-39. A list of some models which present various methods of calculating these parameters is given in Table 5-2.

Table 5–2

DRIFT FLUX MODELS

Author(s)	Equation for Distribution Parameter	Equation for Relative Drift Velocity
Bankoff [Reference (12)]	$1/C_o = K_B = 0.71 + 0.0001\ P$ (Pressure, P, in psia)	$\bar{V}_{gj} = 0$ (No Local Slip)
Jones/Dight [Reference (13)]	$1/C_o = K_{BJ} = K_B + (1 - K_B)\ \alpha^{-r}$ $r = 3.448275 - (1.875 \times 10^{-4} - 5.85 \times 10^{-7}\ P)\ P$ (Pressure, P, in psia)	$\bar{V}_{gj} = 0$
Hughmark [Reference (14)]	Correlation for $1/C_o = K$ presented in tabular form; well correlated by: $Z < 1.3$ $\quad K = 0.142\ Z$ $1.3 \le Z \le 5.5$ $\quad K = 0.077 + 0.374\ \ln Z$ $Z > 5.5$ $\quad K = 0.59 + 0.08\ \ln Z$ $Z = Re^{1/6}\ Fr^{1/8} / Y^{1/4}$ $Y = \alpha_{homogeneous}$	$\bar{V}_{gj} = 0$
Zuber/Findlay [Reference (11)]	$C_o = 1.13$	For Slug Flow: $\bar{V}_{gj} = 0.35 \left(\frac{g\ \Delta\rho\ D_h}{\rho_f}\right)^{1/2}$ For Churn Turbulent Flow: $\bar{V}_{gj} = 1.53 \left(\frac{\sigma g\ \Delta\rho}{\rho_f^2}\right)^{1/4}$
Hancox/Nicoll [Reference (15)]	$C_o = \frac{1 - e^{-C_1 \alpha}}{1 - e^{-C_1}} (1 + C_2) - C_2\ \alpha$ $C_1 = 19.0;\ C_2 = 0.2$	Not Specified
Lellouche/Hancox/Nicoll [Reference (16)]	$C_o = \frac{1 - e^{-C_1 (\alpha - \alpha_o)}}{1 - e^{-C_1 (1 - \alpha_o)}} \left(1 + C_2 (1 - \alpha_o)\right) - C_2 (\alpha - \alpha_o)$ $\alpha_o = 0.03$	Not Specified
Lellouche [Reference (16)]	$1/C_o = K_L = K_{BJ} / L$ $L = \left\{ \frac{1 - e^{-C_1 (\alpha - \alpha_o)}}{1 - e^{-C_1 (1 - \alpha_o)}} \left[1 - \alpha K_{BJ} - \alpha_o (1 - K_B) (1 - \alpha^r)\right] - (\alpha - \alpha_o)\ (1 - K_B)\ (1 - \alpha^r) \right\} / (1 - \alpha)$ $C_1 = 4.4\ P_c^2 / \left(P\ (P_c - P)\right)$ (Pressure, P, in psia) P_c = critical pressure $\alpha_o = 0.03$	Not Specified
Dix [Reference (5)]	$C_o = \beta \left[1 + \left(\frac{1}{\beta} - 1\right)^b\right]$ $\beta = \alpha_{homogeneous}$ $b = \left(\frac{\rho_g}{\rho_f}\right)^{0.1}$	$\bar{V}_{gj} = 2.9 \left[\frac{(\rho_f - \rho_g)\ \sigma g\ g_c}{\rho_f^2}\right]^{1/4}$

Eq. 5-40 indicates that the drift flux models and the slip models are essentially equivalent. While the drift flux models provide greater insight into the nature of slip in two-phase flow, this insight is bought at the expense of having two unknown parameters to evaluate instead of one. The fundamental equations used by both types of models contain no assumptions about flow regime. While the parameters S, C_o, and $\overline{V}_{gj}$ are frequently assigned a single value over a wide range of void fractions, these parameters can be expected to depend on the flow regime.

Calculation of True Flow Quality

All of the void fraction models available in the open literature require that the true flow quality be known in order to calculate void fraction. Under conditions of bulk boiling, the true flow quality, X_t, and thermodynamic equilibrium quality, X_{eq}, are equal, and true flow quality can be calculated from:

$$X_t = X_{eq} = \frac{h - h_f}{h_{fg}} \tag{5-41}$$

where:

h = total enthalpy of the two-phase mixture

h_f = saturation enthalpy of the liquid phase

h_{fg} = latent heat of vaporization

However, during subcooled boiling significant vapor formation occurs even though the bulk enthalpy is below saturation. In many situations, the mass flow rate of the vapor phase is not known, so that Eq. 5-4 cannot be used to calculate X_t directly. One must then resort to some sort of model of the subcooled boiling process. This section discusses how subcooled boiling models were developed and how they are used to evaluate true flow quality.

The following diagram (Figure 5-1) is a representation of the boiling process along a heated tube with uniform heat flux. The experimental work of Griffith and others(10)(17) has shown that the boiling length can be divided into three distinct regions. In Region I, the fluid is highly subcooled. Vapor has only just formed and either remains attached to the walls or travels close to it. The amount of vapor generated in this region is small and is generally neglected in void fraction analysis.

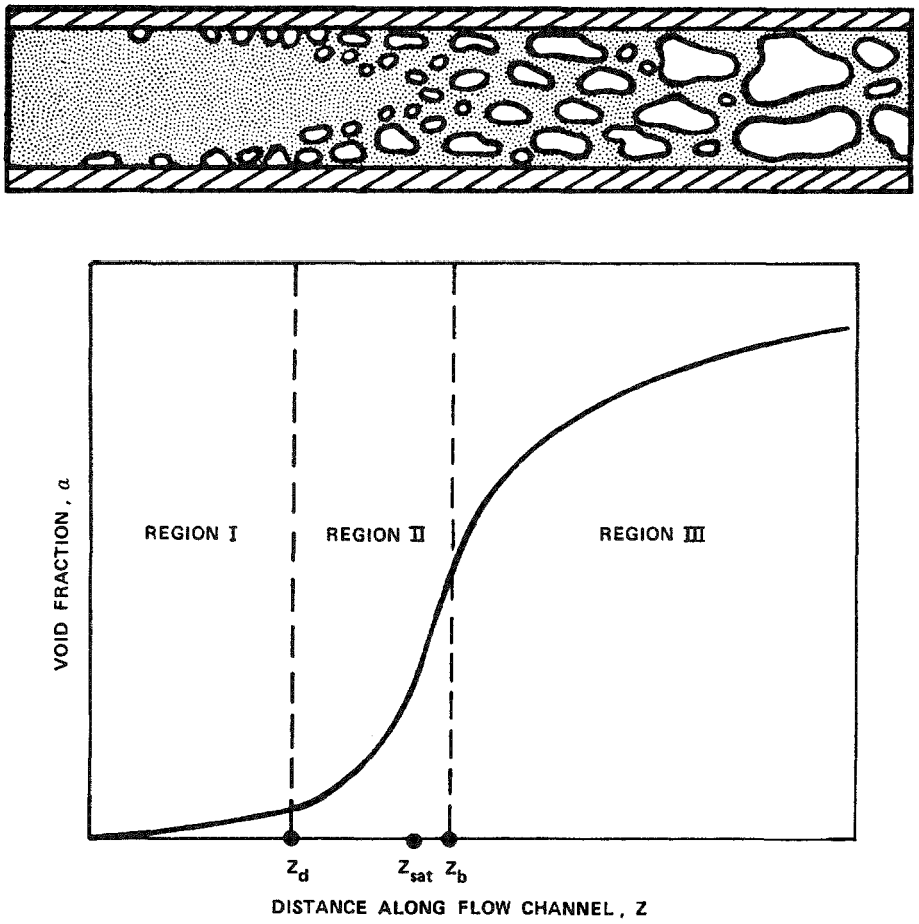

Figure 5–1. Boiling regions in two–phase flow

In Region II, subcooled nucleate boiling begins. Vapor generated at the wall travels well into the main stream and the void fraction rises rapidly. The beginning of Region II is called the point of bubble departure. This point has also been called the point of net vapor generation and the point of significant void formation. As the two-phase fluid travels along the tube, the bulk enthalpy continues to rise and eventually reaches the value of saturated liquid. However, the enthalpy of the liquid phase is still subcooled due to the presence of higher enthalpy vapor. Shortly downstream, the mean liquid enthalpy does reach saturation. Region II ends and Region III, the region of bulk boiling, begins. As stated before, true flow quality in Region III can be calculated from a simple heat balance. In Region I, no significant amount of vapor is formed and the true flow quality is assumed to be zero. The calculation of X_t in Region II centers on predicting the subcooling, or alternately the equilibrium quality, at the point of bubble departure at the beginning of Region II.

The first step in evaluating X_t in Region II is to assume a form for the liquid temperature profile in the direction of flow:

$$\frac{T_\ell (Z) - T_d}{T_{sat} - T_d} = f\left[\frac{Z - Z_d}{Z_{sat} - Z_d}\right] \qquad (5\text{-}42)$$

where:

Z = distance in the direction of flow

Z_d = location of point of bubble departure

Z_{sat} = point where the bulk temperature of mixture reaches saturation

T_ℓ = mean liquid temperature

T_d = bulk temperature at bubble departure

T_{sat} = saturation temperature

This function must satisfy the following boundary conditions:

when $Z - Z_d >> Z_{sat} - Z_d$, $T_\ell = T_{sat}$ and $f = 1.0$

when $Z = Z_d$, $T_\ell = T_d$ and $f = 0.0$

and when $Z = Z_d$, $\frac{dT_\ell (Z)}{dZ} = \frac{dT_b (Z)}{dZ}$, which implies that

when $Z = Z_d$, $\frac{df}{dZ} = \frac{\phi P_h}{\dot{m} C_p (T_{sat} - T_d)}$

where:

T_b = bulk fluid temperature

ϕ = heat flux

P_h = heated perimeter

$\dot{m}$ = total mass flow rate

C_p = specific heat at constant pressure

To see how this last boundary condition was obtained, we write down a heat balance up to the point $Z < Z_d$:

$$\dot{m}C_p \left(T_b(Z) - T_{in}\right) = \phi P_h Z \tag{5-43}$$

where:

T_{in} = inlet temperature

Then:

$$\frac{dT_b(Z)}{dZ} = \frac{\phi P_h}{\dot{m}C_p} \tag{5-44}$$

At $Z = Z_d$, $\dfrac{dT_\ell(Z)}{dZ} = \dfrac{dT_b(Z)}{dZ}$ and from Eq. 5-42 and 5-44 we obtain:

$$\left.\frac{df}{dZ}\right|_{Z = Z_d} = \frac{1}{T_{sat} - T_d} \left.\frac{dT_\ell(Z)}{dZ}\right|_{Z = Z_d} = \frac{\phi P_h}{\dot{m}C_p (T_{sat} - T_d)}$$

One of the simpler functions which satisfies the three boundary conditions given above is an exponential function of the form:

$$\frac{T_\ell(Z) - T_d}{T_{sat} - T_d} = 1 - \exp\left[\frac{Z - Z_d}{Z_{sat} - Z_d}\right] \tag{5-45}$$

The parameter Z_{sat} can be evaluated from Eq. 5-43 where $T_b\ (Z_{sat}) = T_{sat}$.

$$Z_{sat} = \frac{\dot{m}C_p\ (T_{sat} - T_{in})}{\phi P_h} \tag{5-46}$$

Similarly for Z_d:

$$Z_d = \frac{\dot{m}C_p\ (T_d - T_{in})}{\phi P_h} \tag{5-47}$$

From an energy balance on the two-phase fluid in Region II:

$$h_{tot}(Z) = \frac{\phi P_h\ Z}{\dot{m}} + h_{in} = X_t(Z)\ h_g + \Big(1 - X_t(Z)\Big)\ h_\ell(Z) \tag{5-48}$$

where:

h_{tot} = total mixture enthalpy

h_g = vapor saturation enthalpy

h_ℓ = mean liquid enthalpy

h_{in} = inlet enthalpy

But

$$h_\ell(Z) = C_p\ (T_\ell(Z) - T_{in}) + h_{in} \tag{5-49}$$

Substituting Eq. 5-45 and 5-49 into Eq. 5-48 and solving for X_t gives:

$$X_t = \frac{\frac{\phi P_h Z}{\dot{m}} - C_p (T_{sat} - T_{in}) + C_p (T_{sat} - T_d) \exp\left[\frac{Z - Z_d}{Z_{sat} - Z_d}\right]}{h_g - h_{in} - C_p(T_{sat} - T_{in}) + C_p(T_{sat} - T_d) \exp\left[\frac{Z - Z_d}{Z_{sat} - Z_d}\right]} \quad (5\text{-}50)$$

This equation can be simplified by dividing through by h_{fg} and recognizing that:

$$X_{eq} = \frac{1}{h_{fg}} \left(\frac{\phi P_h Z}{\dot{m}} - C_p(T_{sat} - T_{in}) \right) \quad (5\text{-}51)$$

and

$$h_g - h_{in} - C_p(T_{sat} - T_{in}) = h_{fg} \quad (5\text{-}52)$$

Eq. 5-50 then becomes:

$$X_t = \frac{X_{eq} - X_d \exp\left[\frac{Z - Z_d}{Z_{sat} - Z_d}\right]}{1 - X_d \exp\left[\frac{Z - Z_d}{Z_{sat} - Z_d}\right]} \quad (5\text{-}53)$$

where X_d is the equilibrium quality at bubble departure and is given by:

$$X_d = \frac{-C_p (T_{sat} - T_d)}{h_{fg}} \quad (5\text{-}54)$$

Using Eq. 5-46, 5-47, 5-50, and 5-54 to evaluate the argument of the exponential leads to the final result:

$$X_t = \frac{X_{eq} - X_d \exp\left[\frac{X_{eq}}{X_d} - 1\right]}{1 - X_d \exp\left[\frac{X_{eq}}{X_d} - 1\right]}$$

Thus the problem of calculating the true flow quality during subcooled boiling becomes one of determining either the equilibrium quality at bubble departure, X_d, or the subcooling at bubble departure, $(T_{sat} - T_d)$. Table 5-3 is a list of some of the subcooled boiling models available in the open literature.

Table 5–3

SUBCOOLED BOILING MODELS

Author(s)	Subcooled Boiling Equation
Bowring [Reference (5)] (Model given in English units)	$(T_{sat} - T_d) = n \frac{\phi}{G} \rho_f$ $n \equiv 0.94 + 0.00046\ P\ (psia)$ for $156 \leq P \leq 2000$ psia
Thom [Reference (8)]	$X_d = -0.15 \frac{h_f}{h_{fg}} \frac{\phi}{G}$
Levy [Reference (18)]	for $0 \leq Y_B^+ \leq 5$: $(T_{sat} - T_d) = \frac{\phi}{h_\ell} - Q\ Pr\ Y_B^+$ for $5 < Y_B^+ < 30$: $(T_{sat} - T_d) = \frac{\phi}{h_\ell} - 5Q\left\{Pr + \ln\left[1 + Pr\left(\frac{Y_B^+}{5} - 1\right)\right]\right\}$ for $Y_B^+ \geq 30$: $(T_{sat} - T_d) = \frac{\phi}{h_\ell} - 5Q\left\{Pr + \ln[1 + 5\ Pr] + \frac{1}{2}\ln\left[\frac{Y_B^+}{30}\right]\right\}$ where: $Y_B^+ = 0.010\ (\phi g_c D_h \rho_f)^{1/2} / \mu_f$ $Q = \phi / \left[\rho_f C_p \left(\frac{\tau_w g_c}{\rho_f}\right)^{1/2}\right]$
Saha/Zuber [Reference (17)]	for $Pe < 70{,}000$: $X_d = -0.0022 \frac{\phi}{h_{fg}} D_h \frac{C_{pf}}{k_f}$ for $Pe \geq 70{,}000$: $X_d = -154 \frac{\phi}{G\ h_{fg}}$
Sekoguchi, et al. [Reference (19)]	$X_d = -13.5 \left(\frac{\phi}{h_{fg}\ G}\right)^{0.65}$

DISCUSSION

As mentioned earlier, nearly all of the existing void fraction and subcooled boiling models must rely on experimental data to evaluate some key constant or parameter. Frequently, these parameters cannot be measured directly and are inferred from bulk void fraction data. The measurement of void fraction and other two-phase flow parameters in a heated rod array is an expensive and time-consuming task. As a result, the data base that makes up such an important part of the development of void fraction and subcooled boiling models is largely derived from experiments involving much simpler geometries such as rectangular channels or small diameter tubes. Subchannel thermal-hydraulic codes like COBRA extrapolate void fraction models based on simple geometry data to the more complex rod bundle geometry by considering that each individual subchannel behaves as a simple geometry flow channel. However, there are important implications that arise from the physical differences between the open, ventilated boundaries of subchannels and the impenetrable boundaries of simpler geometries.

In 1971, Lahey and other investigators conducted a bundle enthalpy distribution experiment at General Electric(20). In this experiment, two-phase fluid was withdrawn from representative subchannels in a 3 x 3 heated rod bundle and sent through a heat exchanger system to measure enthalpy and quality. This test showed that the quality was higher in the center subchannels and lower in the corner subchannels than the values predicted by the COBRA code. The preferential movement of the vapor phase towards the center of a flow channel is a well-established characteristic of two-phase flow in pipes. Lahey postulated that a similar lateral motion of the vapor phase (void drift) had taken place across the entire rod bundle, transporting vapor across the open subchannel boundaries from the outer subchannels to the inner channels.

The original goal in analyzing the void fraction data was to develop an improved void fraction model for use in the COBRA thermal-hydraulic code. However, the analysis of the void fraction data obtained in the present experiment supports the hypothesis that at higher void fractions, the vapor collects preferentially in the interior subchannels of a rod bundle. The most recent update of the COBRA code acknowledges that Lahey's test may indicate the occurrence of preferential lateral movement of vapor toward regions of higher velocity "which COBRA-IV does not model"(21). Rather than "force-fitting" a void fraction model to the data (which probably would not be applicable to all subchannels), the analysis of the data will show that further development of subchannel codes such as COBRA must center

on a more complete description of the interactions between subchannels -- a task beyond the scope of the present project. Nonetheless, the void fraction data obtained during the program and the analysis presented here are a significant contribution toward a better understanding of two-phase flow in heated rod bundles.

ANALYSIS OF DATA FROM COLLIMATOR SET 1

The measurement volume for collimator set 1 covered the largest portion of the subchannel possible while keeping the rod scatter contribution to the total count rate at acceptable levels. The location of this measurement area is shown in Figure 5-2.

SHOWN ARE THE CONSTANT WEIGHT LINES OF THE SCATTER VOLUME LOCATED IN THE CENTER SUBCHANNEL. THESE LINES ARE ANALOGOUS TO CONSTANT ELEVATION LINES ON A TOPOGRAPHIC MAP.

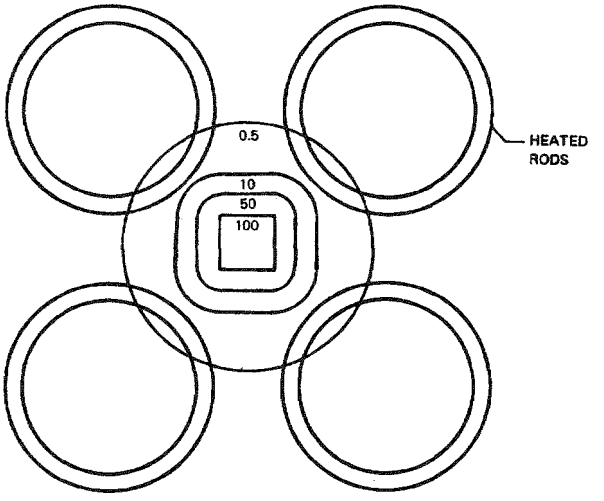

Figure 5–2. Scatter volume – collimator set 1

Existing void fraction and subcooled boiling models predict several general trends which have been observed in the plots of void fraction versus quality for collimator set 1. Existing void fraction models predict that when pressure is raised, the void fraction at a given quality decreases. The subcooled boiling models predict that the quality at bubble departure is a weak function of pressure with subcooled boiling beginning at slightly lower qualities for higher pressures. Figure 5-3 presents a family of data curves at various pressures for a constant heat flux and mass flux. This figure shows that the pressure trends observed in the void fraction data are consistent with the trends predicted by the models. The codes given in this and subsequent figures refer to given sets of thermal-hydraulic conditions as described in Appendix B.

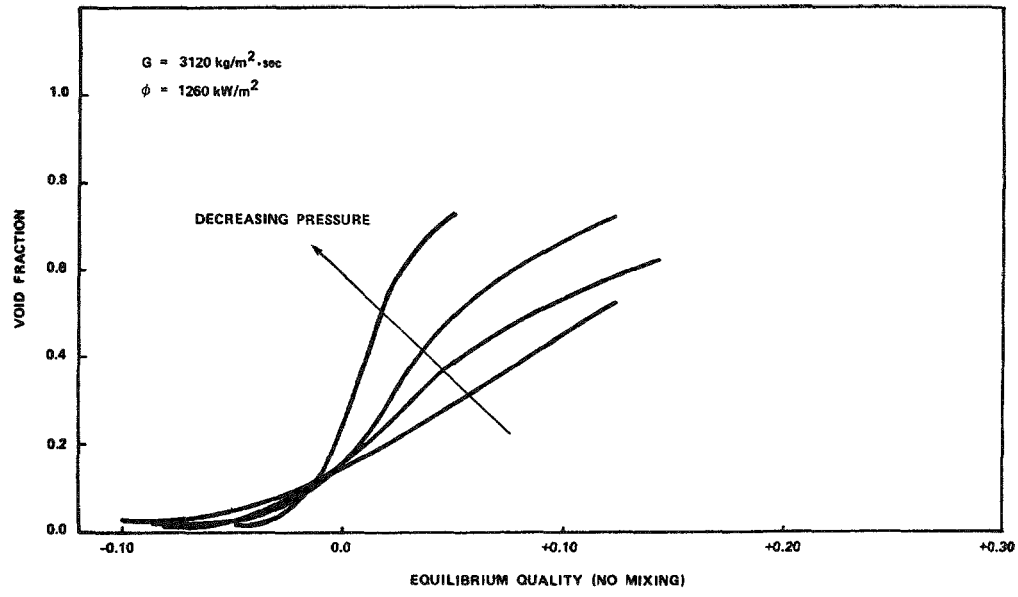

Figure 5–3. Void fraction versus quality (Collimator 1 – Codes 13, 15, 16, and 26)

All of the subcooled boiling models predict that the quality at bubble departure is proportional to the heat flux. Thus, in the subcooled boiling region as the heat flux is raised, subcooled boiling would begin at lower qualities and void fraction at a given quality would increase. Figure 5-4 is a family of data curves at various heat fluxes where the pressure and mass flux were held constant. The heat flux trends seen in this collimator set 1 data support the predictions of the subcooled boiling models. At higher qualities, the curves appear to merge providing an indication of how much the effects of subcooled boiling persist beyond the point of zero equilibrium quality.

All of the subcooled boiling models also predict that the quality at bubble departure is inversely proportional to the mass flux. Thus, lowering the mass flux would have an effect similar to that described above when the heat flux is raised. Figure 5-5 is a family of data curves at various mass fluxes where the pressure and heat flux were constant. Again, the data demonstrate the trends in mass flux described by the subcooling boiling models. As with the varying heat flux curves, the varying mass flux curves merge at higher qualities when bulk boiling begins.

Overall, Figures 5-3, 5-4, and 5-5 show that the data follow the general trends predicted by existing void fraction and subcooled boiling models. In the subcooled boiling region, heat and mass flux are the determining parameters for void fraction; in the bulk boiling region, pressure effects predominate.

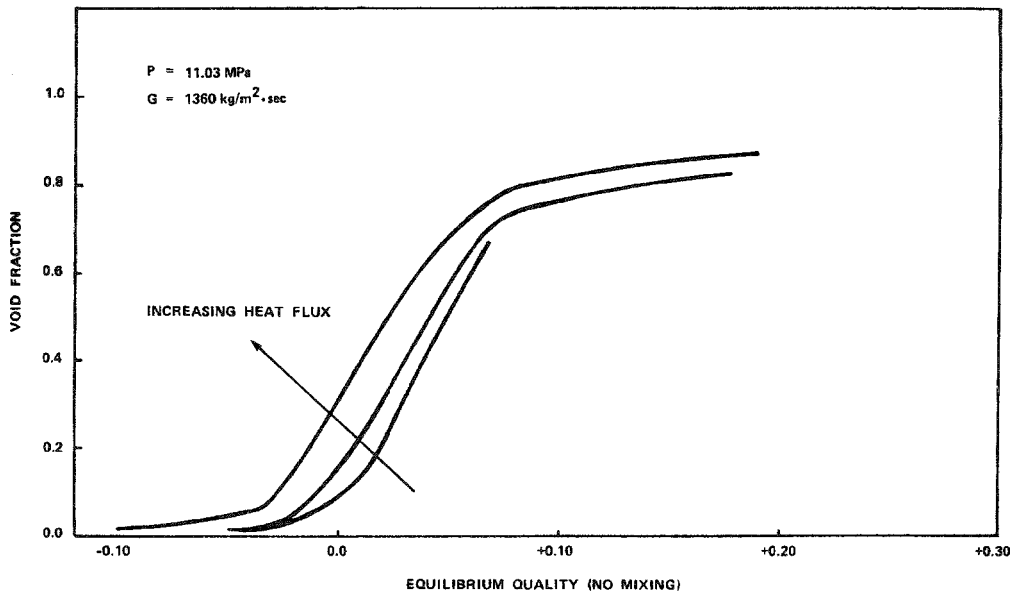

Figure 5–4. Void fraction versus quality (Collimator 1 – Codes 9, 18, and 20)

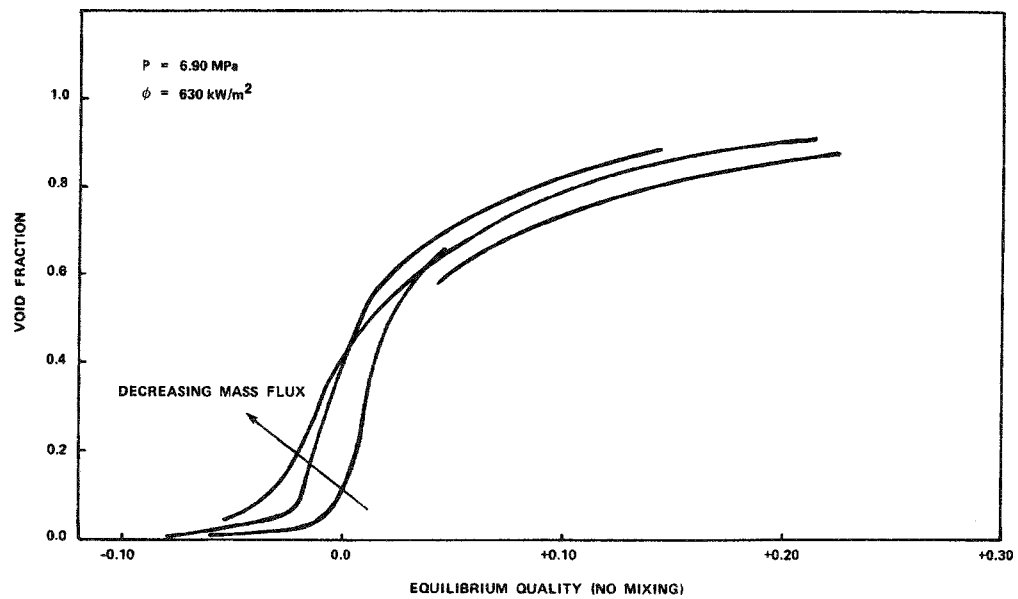

Figure 5–5. Void fraction versus quality (Collimator 1 – Codes 11, 12, 28, and 38)

The most striking feature about the collimator set 1 data is their relationship with existing models. At higher void fractions, all existing void fraction models predict void fractions which are considerably lower than the measured void fractions from this collimator set. Figures 5-6 through 5-10 are typical void-quality curves

for collimator set 1. The homogenous equilibrium model has been included for comparison since it serves as an upper limit for most void fraction models at higher void fractions. Except for the low flow cases, the collimator set 1 data lie well above and to the left of the homogeneous model.

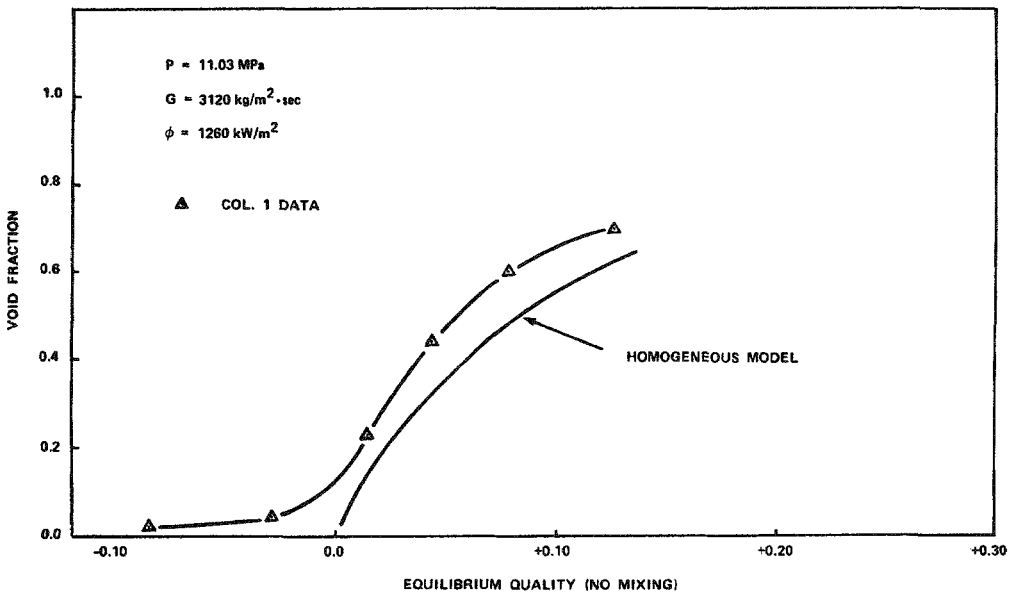

Figure 5–6. Void fraction versus quality (Collimator 1 – Code 15)

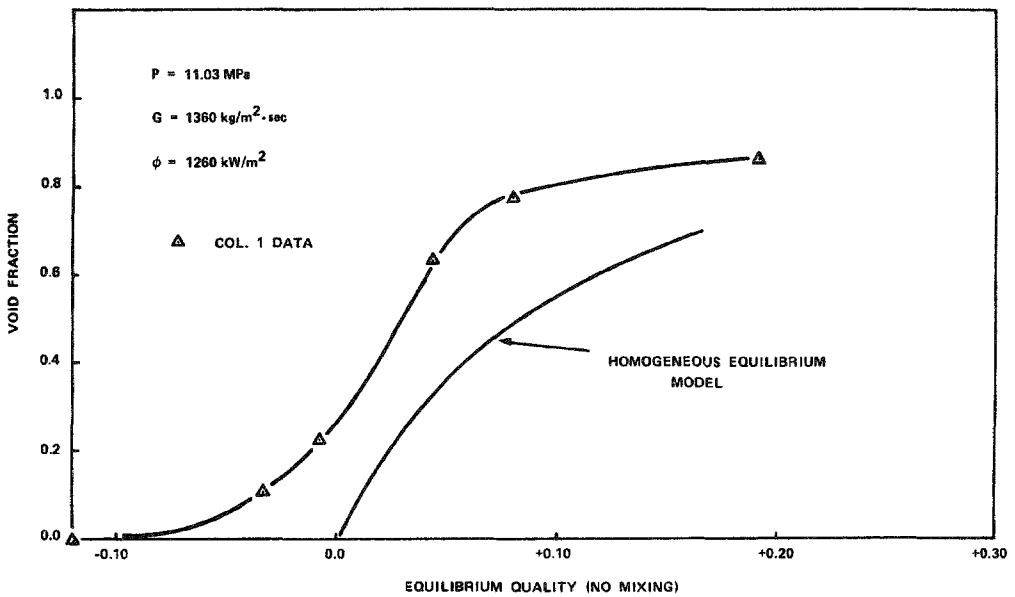

Figure 5–7. Void fraction versus quality (Collimator 1 – Code 20)

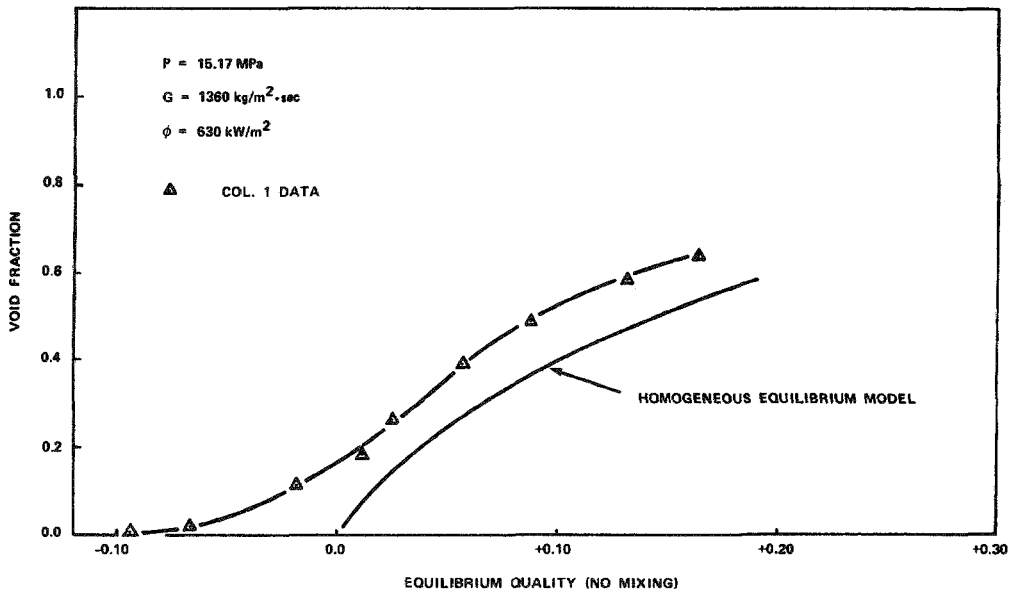

Figure 5–8. Void fraction versus quality (Collimator 1 – Code 5)

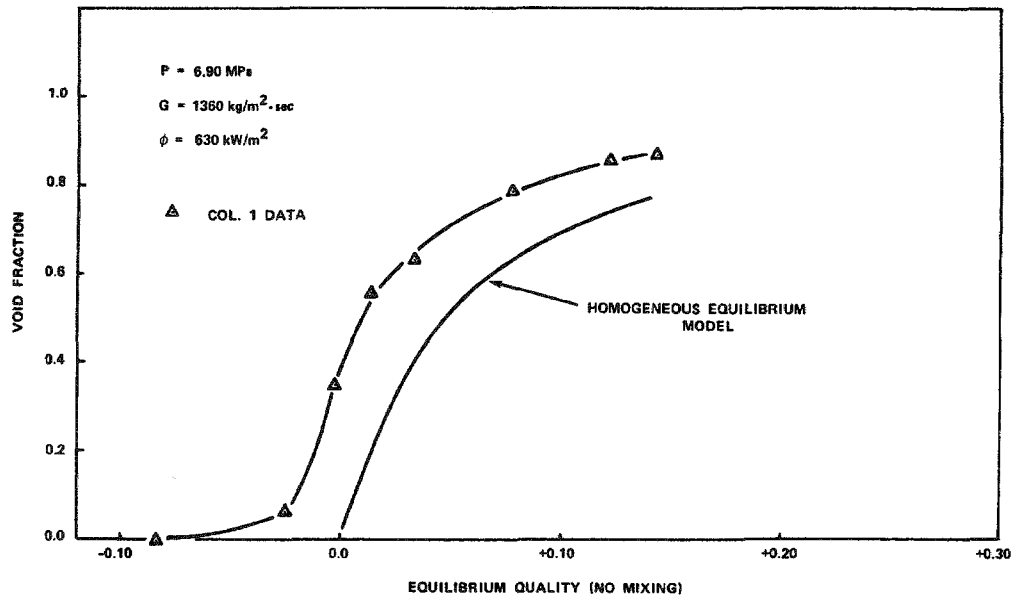

Figure 5–9. Void fraction versus quality (Collimator 1 – Code 12)

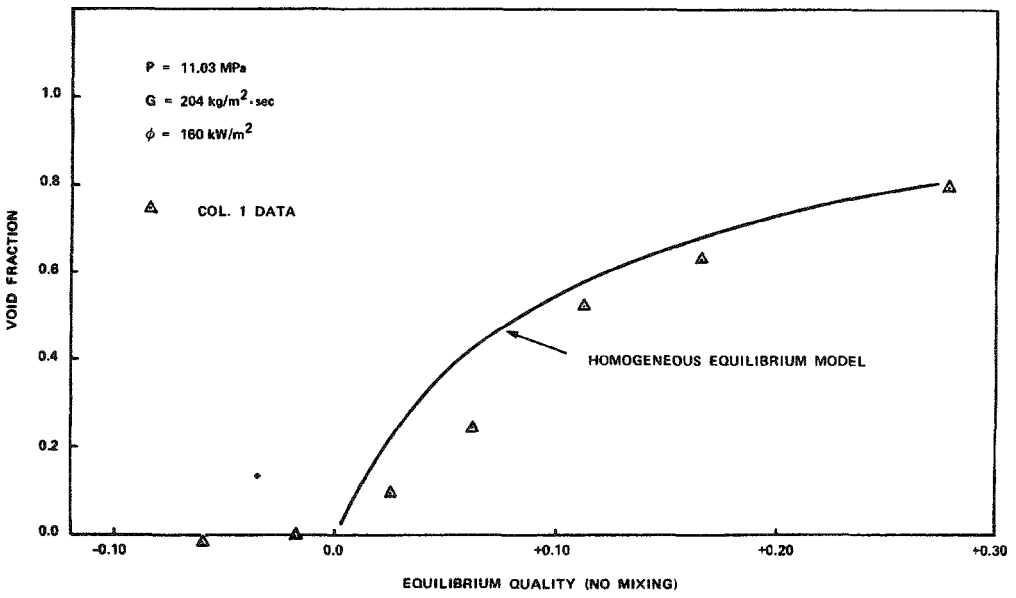

Figure 5–10. Void fraction versus quality (Collimator 1 – Code 35)

The heat balance error (discussed in Section 6 - Error Analysis) for the low flow data points ($G \leq 407$ kg/m^2·sec) was much larger than for other data points and was consistently in the positive direction. When a correction for the heat balance error is applied to the flow data, these void-quality curves fall close to or above the homogeneous model. An example is provided in Figure 5-11. The change in equilibrium quality was calculated from the equation:

$$\Delta X_{eq} = \frac{f_{nx} \ (HBE \ \phi/G)}{h_{fg}} \qquad (5\text{-}55)$$

where HBE is the heat balance error and f_{nx} is a geometry factor described in Section 6. For the conditions of Figure 5-11, the heat balance error was 5%. For the higher flow rate data, the heat balance errors were negligibly small and corrections were not applied to the data. Except for the low flow data, the quality used in these figures was calculated from Eq. 6-6 and assumed no mixing. The "no mixing" quality was used since it provides an upper limit on the quality as calculated by the COBRA code. Any mixing would affect the data by shifting the quality coordinate of each data point further to the left. Mixing effects are discussed in greater detail in Section 6.

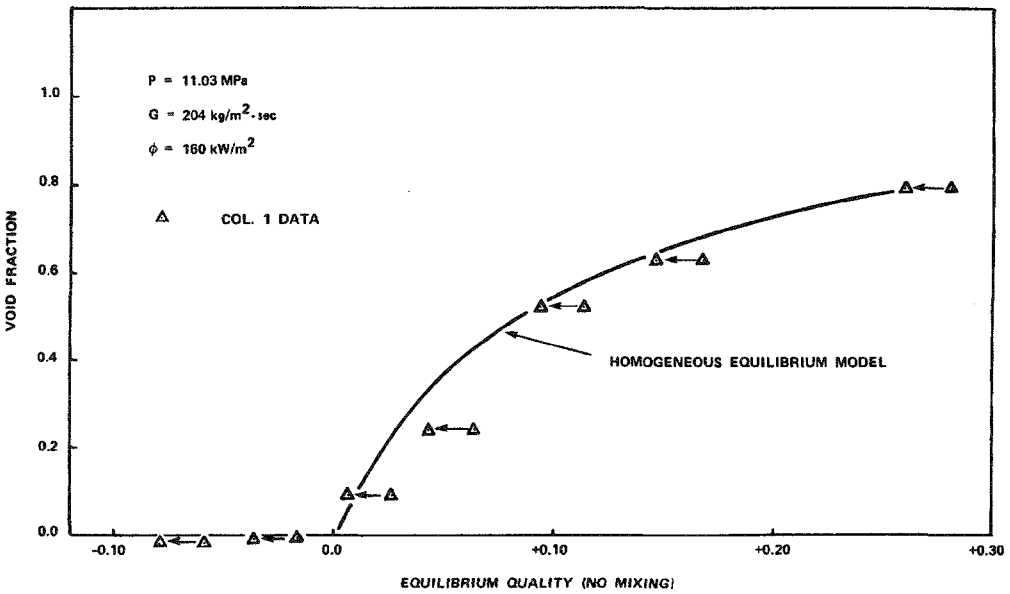

Figure 5—11. Low flow data corrected for heat balance error (Collimator 1 — Code 35)

A few general trends can be observed in the preceding figures (Figures 5-6 through 5-11). The data are farthest from the homogeneous model for low pressures and high heat flux to mass flux ratios. Although no subcooled boiling models have been included in the void-quality curves presented here, in the subcooled boiling region the data are adequately represented by several pairs of void fraction and subcooled boiling models.

In reviewing these curves for collimator set 1, one must keep in mind that this collimator set measured void fraction in the center of the subchannel. As discussed in the following section, the data from a second collimator series indicate that at high void fractions the void fraction in the center region of the subchannel can be significantly higher than the void fractions at the edge of the subchannel. Thus, the most useful comparison between the void fraction data and existing models at high void fractions involves the data from collimator set 2 as described later in this section.

ANALYSIS OF DATA FROM COLLIMATOR SET 2

Collimator set 2 was used to measure void fraction simultaneously in two regions of the center subchannel. As shown in Figure 5-12, one measurement area covered the center region of the subchannel while the second covered the region in the gap between the rods.

SHOWN ARE THE CONSTANT WEIGHT LINES OF EACH SCATTER VOLUME. SOLID LINES DEFINE THE SCATTER VOLUME SEEN BY DETECTOR 2. DASHED LINES DEFINE THE SCATTER VOLUME SEEN BY DETECTOR 3. THESE LINES ARE ANALOGOUS TO CONSTANT ELEVATION LINES ON A TOPOGRAPHIC MAP.

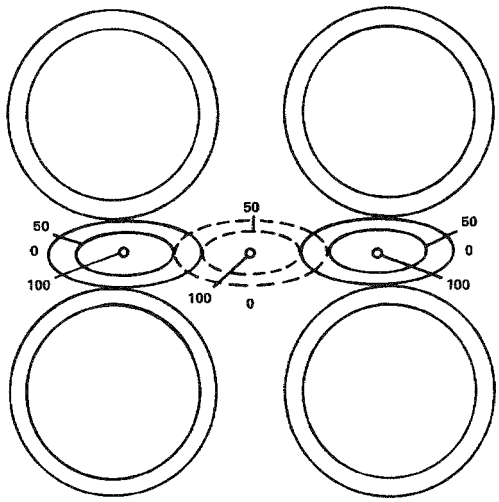

Figure 5—12. Scatter volumes — collimator set 2

The data from both regions of collimator set 2 exhibit the same general trends that were observed in the collimator set 1 data and were predicted by existing void fraction and subcooled boiling models. At higher heat fluxes and lower mass fluxes, subcooled boiling begins at lower, more negative values of equilibrium quality. In the bulk boiling region, pressure is the single most important parameter in determining the void fraction at a given quality.

Figures 5-13 through 5-18 present some typical void-quality plots for collimator set 2. These figures show that as boiling begins, the void fraction is higher in the gap between the rods than in the center of the subchannel. At some intermediate void fraction, a transition occurs and, at higher qualities, the void fraction becomes higher in the subchannel center. This behavior is entirely consistent with void fraction distributions observed in the transverse direction along the boiling length of a heated tube. Analysis of the data indicates that in general, the transition occurs at higher qualities and void fractions as the pressure is increased or the mass flux is decreased.

These figures also show that under certain conditions, a significant void fraction distribution can exist across the center subchannel. The magnitude of these

distribution effects appears to be a complex function of pressure and mass flux. In general, as the mass flux is raised, the void distribution effects become less pronounced, with the impact of mass flux being greatest at high pressures and least at low pressures. For pressures greater than about 13 MPa and mass fluxes greater than 680 $kg/m^2 \cdot sec$, void distribution effects are observed to be small.

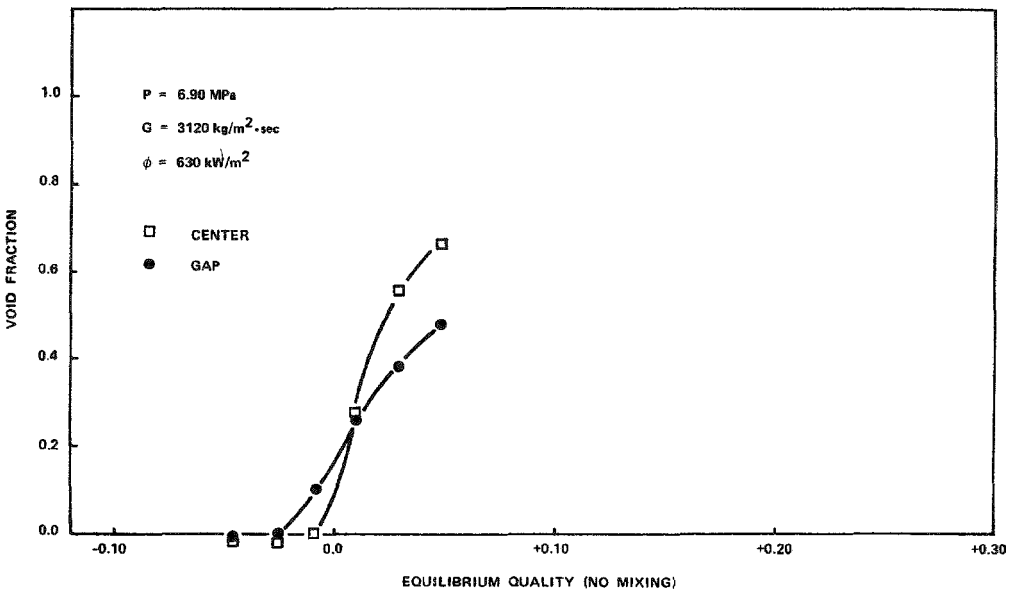

Figure 5–13. Void fraction versus quality (Collimator 2 – Code 42)

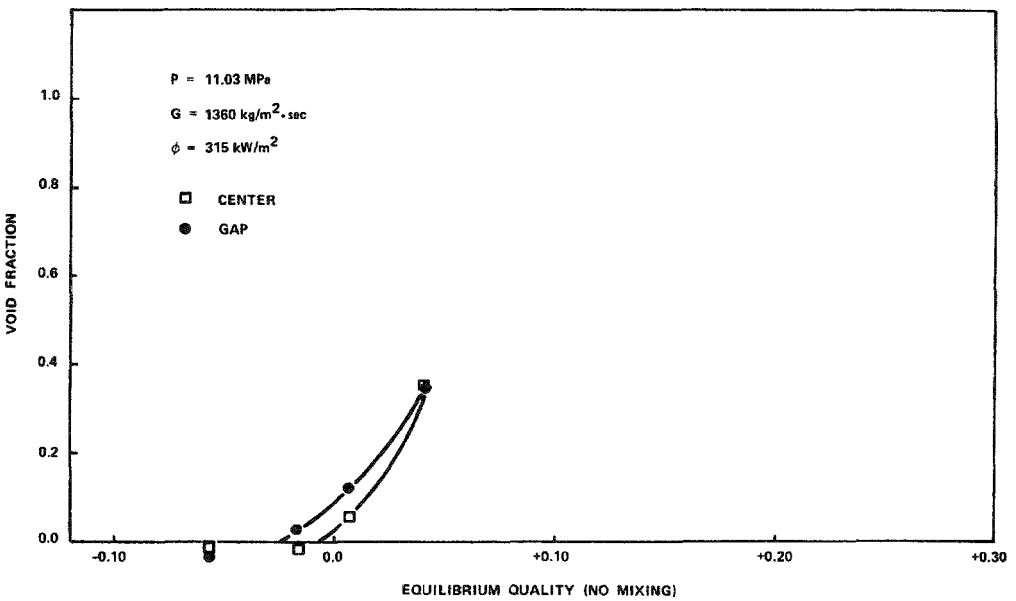

Figure 5–14. Void fraction versus quality (Collimator 2 – Code 43)

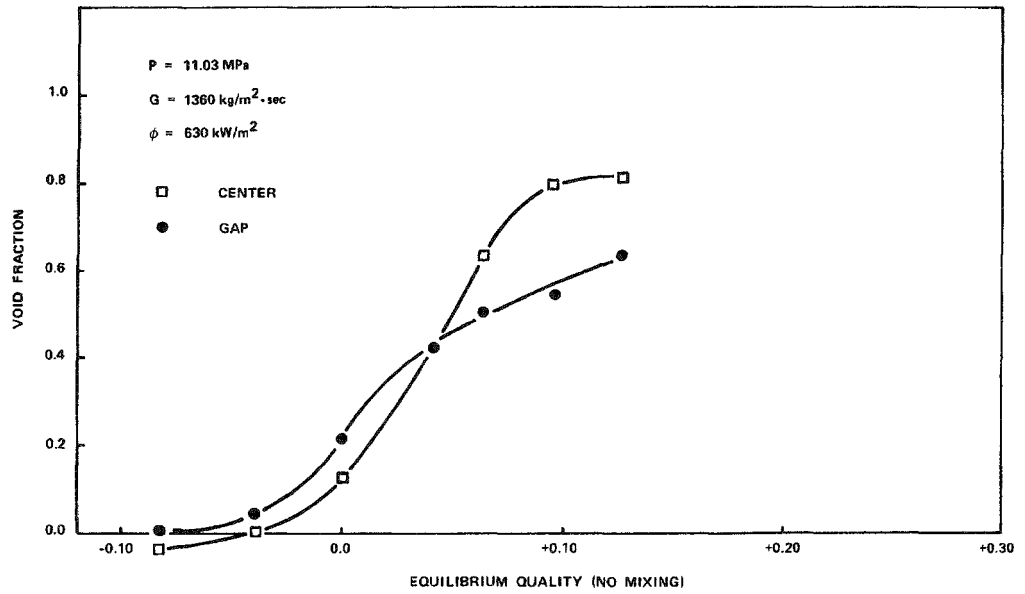

Figure 5–15. Void fraction versus quality (Collimator 2 – Code 45)

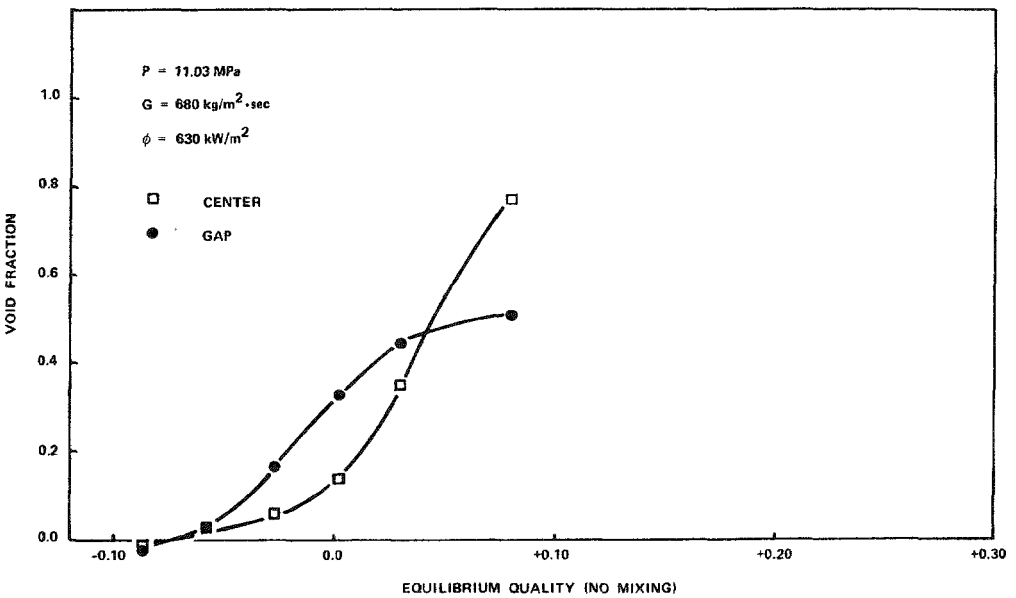

Figure 5–16. Void fraction versus quality (Collimator 2 – Code 52)

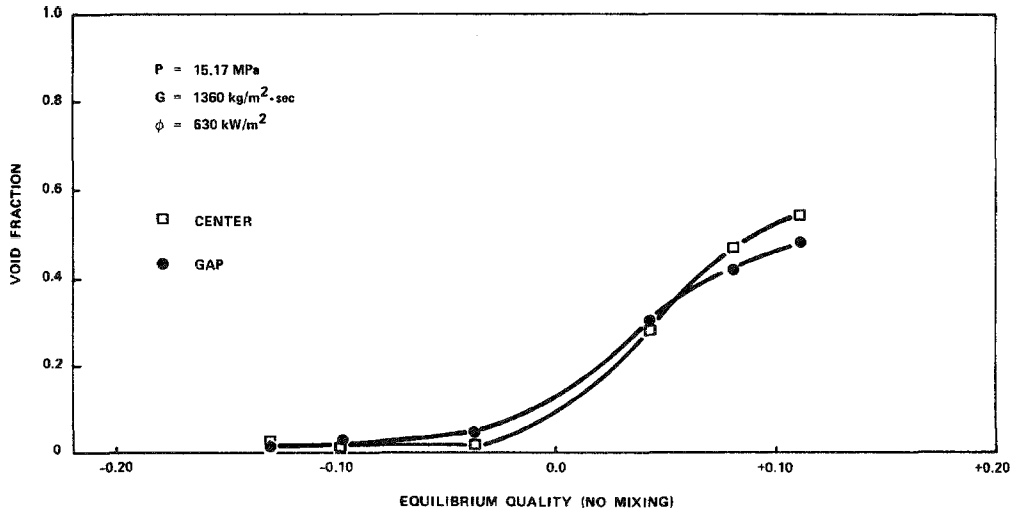

Figure 5–17. Void fraction versus quality (Collimator 2 – Code 49)

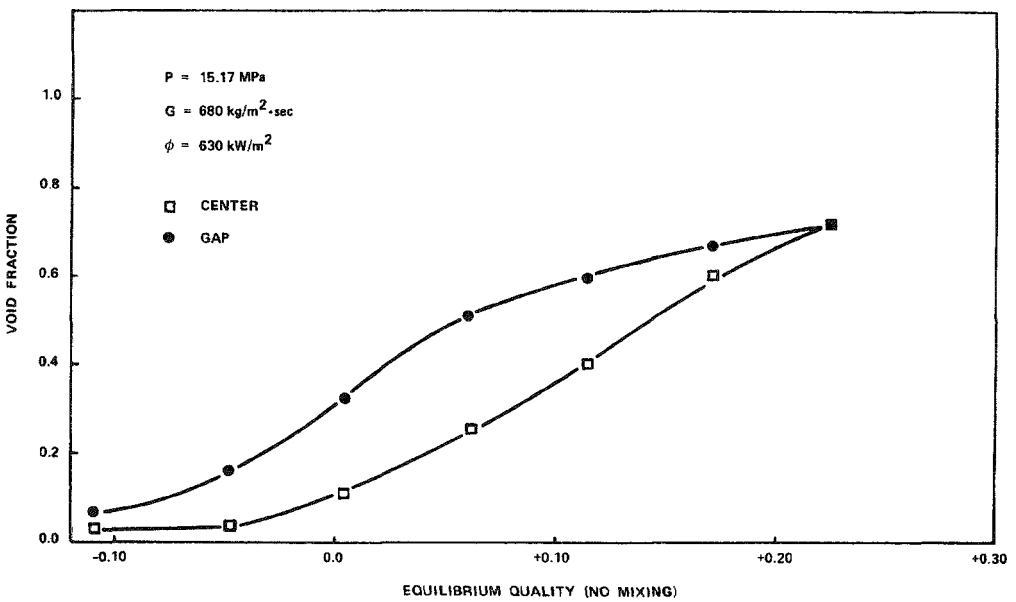

Figure 5–18. Void fraction versus quality (Collimator 2 – Code 47)

SUBCHANNEL AVERAGE VOID FRACTION

Subchannel codes like COBRA determine the thermal-hydraulic behavior of rod bundles using a technique called lumped subchannel analysis. In this technique, each subchannel is divided into a series of nodes along the flow path. The thermo-physical state of the fluid in each node is described by using suitably averaged values of properties like void fraction. The data from collimator set 2 have clearly shown that under a wide range of conditions, a significant void fraction distribution exists across the center subchannel. In light of this observation and in consideration of the local nature of the data, a method was developed to extend the collimator set 2 void fraction measurements to the entire subchannel so that a more valid comparison could be made with existing models as they are used in COBRA. Very briefly, in this method a void fraction distribution function was derived which describes the void fraction as a function of position within the center subchannel. Integration of this distribution function then yielded a subchannel average void fraction more suited for comparison with existing models. This section describes the development of the void distribution function, the calculation of subchannel average void fraction, and a comparison of the subchannel average void fraction with existing models.

Development of Void Distribution Function α (x,y)

The development of a void distribution function, α (x,y), to describe the void fraction as a function of position within the subchannel is outlined below. Let α (x,y) be represented by a power series expansion of the form:

$$\alpha\ (x,y) = \sum_{i=0}^{\infty} x^i \sum_{j=0}^{\infty} C_{ij} y^j \qquad (5\text{-}56)$$

The symmetric arrangement of the test section requires that α (x,y) = α (-x,y) and that α (x,y) = α (x, -y). Therefore, all the coefficients of the odd-powered terms in the expansion must be equal to 0.

Then:

$$\alpha\ (x,y) = \sum_{i=0,2,4\ldots}^{\infty} x^i \sum_{j=0,2,4\ldots}^{\infty} C_{ij} y^j \qquad (5\text{-}57)$$

Truncating all terms higher than fourth order leaves:

$$\alpha\ (x,y) \cong C_{00} + C_{02}\ y^2 + C_{04}\ y^4 + C_{20}\ x^2 + C_{40}\ x^4 + C_{22}\ x^2\ y^2 \qquad (5\text{-}58)$$

Again using symmetry arguments $\alpha\ (x,y) = \alpha\ (y,x)$, which leads to the result:

$$C_{02} = C_{20} \qquad (5\text{-}59)$$

$$C_{04} = C_{40} \qquad (5\text{-}60)$$

Eq. 5-58 becomes:

$$\alpha\ (x,y) = C_{00} + C_{02}\ (x^2 + y^2) + C_{04}\ (x^4 + y^4) + C_{22}\ x^2\ y^2 \qquad (5\text{-}61)$$

Applying the following boundary condition at the subchannel edge (P/2),

$$\text{when } x = \frac{P}{2}, \frac{\partial \alpha}{\partial x} = 0$$

leads to the result:

$$C_{02} = -C_{04} \frac{P^2}{2} \qquad (5\text{-}62)$$

$$C_{22} = 0 \qquad (5\text{-}63)$$

Substituting Eq. 5-62 and 5-63 into Eq. 5-61 and redefining the constants leads to the final form for the void distribution function:

$$\alpha\ (x,y) = a(x^4 + y^4) - a \frac{P^2}{2} (x^2 + y^2) + b \qquad (5\text{-}64)$$

where $a = C_{04}$ and $b = C_{00}$. The constants a and b must be evaluated using experimental data. In the above equation, the constant b is dimensionless and represents the void fraction at the very center of the subchannel. The sign of the constant a determines whether the void fraction is higher at the center or the edge of the subchannel. If a is positive, the void fraction is highest in the center of the subchannel. If a is negative, the void fraction is highest at the subchannel edge. The larger the magnitude of a is, the more peaked the void fraction profile.

The constant a has units of length to the -4th power. Note that this function is indeed symmetric in x and y.

Using constants found from some typical collimator set 2 conditions, Figure 5-19 shows the development of the void fraction profile across the centerline of the center subchannel as the quality is raised.

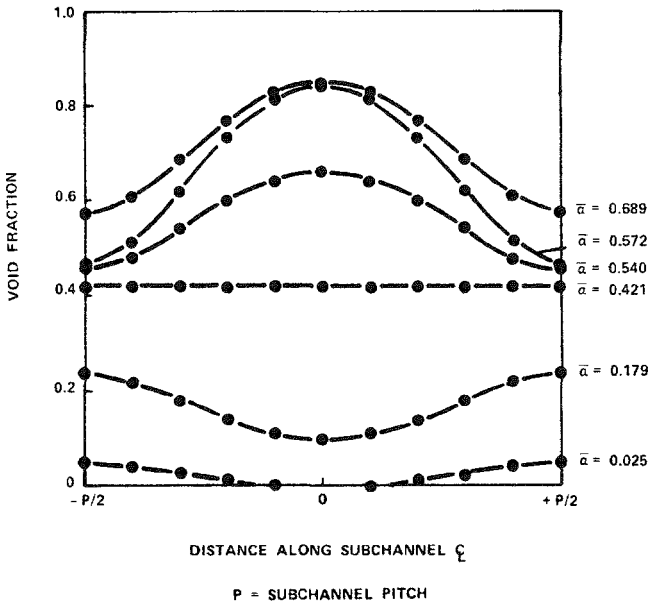

Figure 5—19. Typical subchannel void fraction profile from void distribution function α (x, y)

Figure 5-20 shows curves of constant void fraction for the general form of the void distribution function. In the inner region the curves are nearly circular, then begin to spread toward the edges of the subchannel.

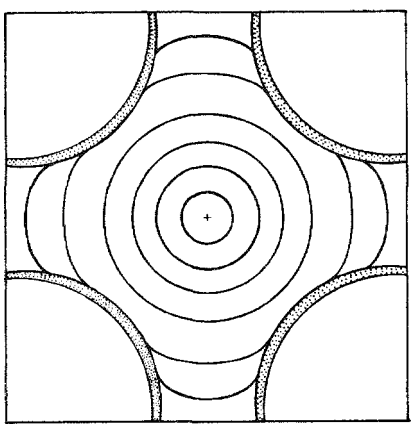

Figure 5—20. Lines of constant void fraction from void distribution model

Calculation of $\bar{\alpha}_{sc}$ Subchannel Average Void Fraction

The average subchannel void fraction, $\bar{\alpha}_{sc}$, is found by integrating the void distribution function across the subchannel. Taking advantage of quarter symmetry:

$$\bar{\alpha}_{sc} = \frac{\frac{1}{4}\iint_{sc} \alpha\,(x,y)\,dx\,dy}{\frac{1}{4}\iint_{sc} dx\,dy} \tag{5-65}$$

After a few pages of integration and algebra, we obtain the final result:

$$\bar{\alpha}_{sc} = \frac{b + \frac{aP^4}{120}\left\{-7 + 256\left(\frac{R}{P}\right)^5 - 30\,\pi\left(\frac{R}{P}\right)^6 - 60\,\pi\left(\frac{R}{P}\right)^4 + 16\,\pi\left(\frac{R}{P}\right)^2\right\}}{1 - \pi\left(\frac{R}{P}\right)^2} \tag{5-66}$$

where:

P = subchannel pitch

R = rod radius

For our test geometry, R/P = 0.3782 and P = 1.27 cm. Substituting this information into Eq. 5-66 gives:

$$\bar{\alpha}_{sc} = b - 0.0957\ cm^4\ a \tag{5-67}$$

As will be shown, the constants a and b are evaluated using experimental data from collimator set 2.

Evaluation of Constants from Experimental Data

The same equation used to calculate the subchannel average void fraction can be written in a more general form in order to calculate an average void fraction, $\bar{\alpha}_i$, over some region i within the subchannel:

$$\bar{\alpha}_i = \frac{\iint_{\text{region } i} \alpha\,(x,y)\,dx\,dy}{\iint_{\text{region } i} dx\,dy} \qquad (5\text{-}68)$$

In a reverse situation, if the average void fraction is known in two given regions within the subchannel, this equation can be used to solve for the constants a and b in the void distribution function. In principle, this is how the constants a and b were found using experimental data from collimator set 2. In actual practice, these calculations were complicated by the fact that the measurement scatter volume boundaries were not sharp.

Figure 5-21 shows that as the gamma beam extends from the source to the scatter volume and arrives at the side detector, there are a number of paths within the beam that an individual gamma ray may take. This exaggerated figure shows that various gamma rays leaving the source will travel through different amounts of collimator material and through varying thicknesses of metal, air and water/steam. As a result of the different attenuation paths, the intensity of the gamma beam arriving at the center of the rod bundle will vary across the center subchannel -- even with a uniform density mixture within the bundle. Ultimately, this means that small elements within the subchannel do not contribute equally to the total count rate observed by the side detector. This "contribution distribution" is accentuated by similar attenuation effects as the beam leaves the subchannel and arrives at the side detector.

To calculate an average void fraction applicable to the void fraction measurements, the above integral (Eq. 5-68) must be modified to include weighting functions which describe the relative contribution of points within the scatter volume to the total count rate. The formula for the weighted average void fraction in a region i is then:

$$\bar{\alpha}_i = \frac{\iint_{\text{region } i} W_i\,(x,y)\,\alpha(x,y)\,dx\,dy}{\iint_{\text{region } i} W_i\,(x,y)\,dx\,dy} \qquad (5\text{-}69)$$

Note that when W_i or α is constant, this equation is equivalent to Eq. 5-68. Thus, if either the void fraction or the weighting function does not vary greatly over the region i, the weighted subchannel average void fraction will be very close to the unweighted subchannel average void fraction.

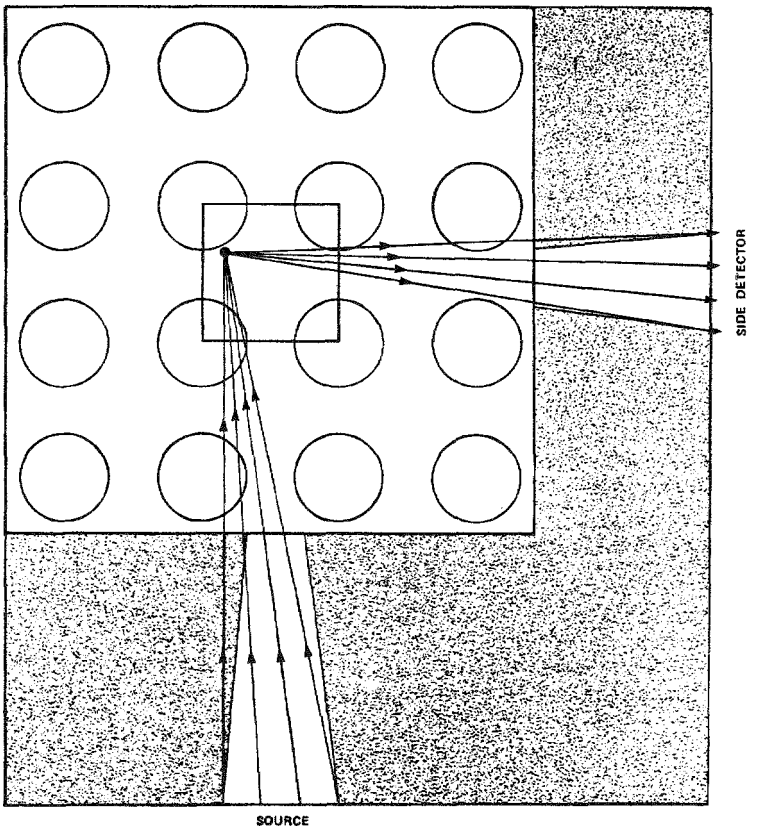

Figure 5–21. Attenuation paths for incoming and scattered gamma beams

The appropriate weighting functions were determined using a computer simulation of the gamma scattering technique. The program calculated incoming and outgoing attenuation factors for a large number of rays (250,000) leaving the source, then scattering at various positions within the center subchannel, and finally arriving at the side detector. From the model output, basic equations were developed for each collimator series for use as weighting functions. These equations provide good approximations to the true spatial contribution to the total count rate.

The weighting functions used to represent the collimator set 2 center and gap measurements were:

$$W_{2\text{-}c}(x,y) = (1 - C|x|)(1 - D|y|) \qquad \text{for } |x| < 1/C \text{ and } |y| < 1/D \qquad (5\text{-}70)$$

$$W_{2\text{-}c}(x,y) = 0 \qquad \text{for } |x| > 1/C \text{ or } |y| > 1/D \qquad (5\text{-}71)$$

$$W_{2\text{-}g}(x,y) = (1 - C|x - x_0|)(1 - D|y|) \qquad \text{for } |x - x_0| < 1/C \text{ and } |y| < 1/D \qquad (5\text{-}72)$$

$$W_{2\text{-}g}(x,y) = 0 \qquad \text{for } |x - x_0| > 1/C \text{ or } |y| > 1/D \qquad (5\text{-}73)$$

where:

$C = 2.56\ cm^{-1}$

$D = 5.25\ cm^{-1}$

$x_0 = 0.528\ cm$

This x-axis is defined by the nominal path of the incoming gamma beam. Note that, except for the fact that the gap weighting function is offset toward the subchannel edge by an amount x_0, these two weighting functions are identical.

When Eq. 5-69 is applied to the gap and center measurement regions, the only unknowns in these two equations are the constants a and b. Solving for a and b:

$$a = -9.49\ cm^{-4}\ \left[\ \bar{\alpha}_{2\text{-}g}(\text{measured}) - \bar{\alpha}_{2\text{-}c}(\text{measured})\right] \qquad (5\text{-}74)$$

$$b = 1.227\ \bar{\alpha}_{2\text{-}c}(\text{measured}) + 0.227\ \bar{\alpha}_{2\text{-}g}(\text{measured}) \qquad (5\text{-}75)$$

Substituting these values for a and b into Eq. 5-67 gives:

$$\bar{\alpha}_{sc} = 0.682\ \bar{\alpha}_{2\text{-}g}(\text{measured}) + 0.318\ \bar{\alpha}_{2\text{-}c}(\text{measured}) \qquad (5\text{-}76)$$

Eq. 5-76 shows that the subchannel average void fraction is weighted more towards the gap void fraction than the center void fraction. This is consistent with the larger area covered by the gap measurement. This equation also shows that when

the measured void fraction is the same in both the gap and center regions of the subchannel, the average subchannel void fraction has that same value. This equation also indicates that on a plot of void fraction versus quality, $\bar{\alpha}_{sc}$ will fall between the gap and center void fractions. Figures 5-22 and 5-23 demonstrate that this is indeed the case.

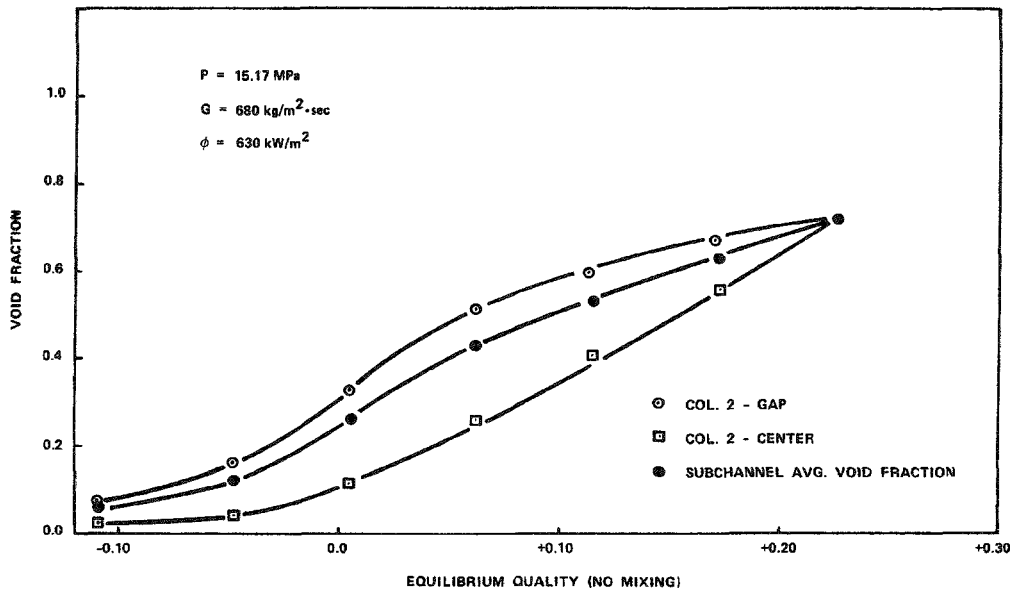

Figure 5–22. Subchannel average void fraction versus quality (Code 47)

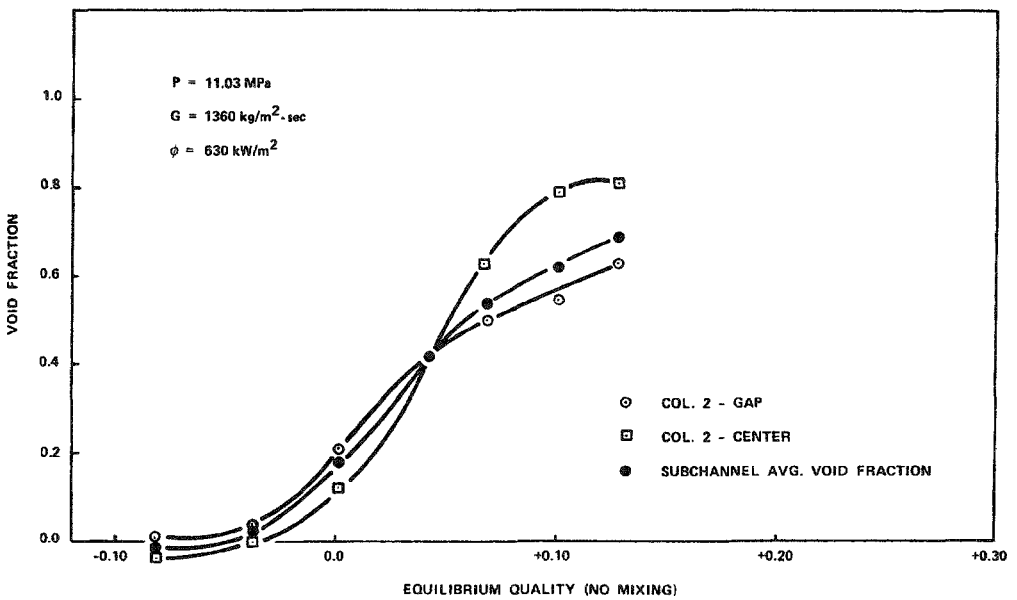

Figure 5–23. Subchannel average void fraction versus quality (Code 45)

Comparison of Subchannel Average Void Fraction $\bar{\alpha}_{sc}$ with Existing Models

Eq. 5-76 provides void fractions which can be directly compared with existing models. The comparison with the models was achieved by calculating the residual sum of squares (RSS) for each of the 17 void fraction models listed in Table 5-4 as they were paired with each of the six subcooled boiling models listed in Table 5-5. The RSS was calculated from:

$$RSS = \sum\left(\bar{\alpha}_{sc} - \hat{\alpha}\right)^2 \qquad (5\text{-}77)$$

where $\hat{\alpha}$ is the value of void fraction predicted by the combined void fraction/subcooled boiling model, and where the summation extended over all the subchannel average void fractions calculated from the collimator set 2 data. The 10 void fraction/subcooled boiling models which gave the lowest RSS are listed in Table 5-6. This comparison with existing models indicates that over the entire range of data, the homogeneous model gives the best fit to the data. Figures 5-24 through 5-29 indicate that this is due to the fact that at higher void fractions, the subchannel average void fraction is higher than the homogeneous model and, by implication, even higher than other existing models. Since the homogeneous model provides the highest void fractions in this range, it could be expected to fall closest to the higher void fraction points. This is not to suggest, however, that the homogeneous model provides an accurate representation of two-phase flow in rod bundles. Rather, this apparent agreement is likely due to competing processes canceling one another. As slip tends to lower the measured void fraction, lateral motion of the vapor phase tends to increase the void fraction in the center measurement subchannel.

It is likely that any vapor concentration effect would not be a significant factor in the subcooled boiling region. The RSS was recalculated for each of the model pairs using only those subchannel void fractions below 30%. This comparison shows, as expected, that for low void fractions the subcooled boiling model plays a much bigger role in determining the void fraction than the specific void fraction model. As Table 5-7 indicates, at lower void fractions there are several void fraction models which do a better job of predicting the data than the homogeneous model.

Table 5–4

VOID FRACTION MODELS
COMPARED WITH
WEIGHTED SUBCHANNEL VOID FRACTIONS

Model/Author(s)	Reference
Homogeneous	(21)
Modified Armand	(21)
Bankoff	(12)
Bankoff/Jones/Dight	(13)
Thom	(8)
Ahmad	(9)
Hancox/Nicoll	(15)
Modified Hancox/Nicoll	(16)
Lellouche	(16)
Zuber and Findlay	(11)
Zivi	(7)
Madsen	(10)
Smith	(22)
Martinelli/Nelson	(5)
Hughmark	(14)
Dix	(5)
Levy	(23)

Table 5–5

SUBCOOLED BOILING MODELS
COMPARED WITH
WEIGHTED SUBCHANNEL VOID FRACTIONS

Model/Author(s)	Reference
Bowring	(5)
Thom	(8)
Levy	(18)
Ahmad	(9)
Saha and Zuber	(17)
Sekoguchi, et al.	(19)

Table 5–6

TOP TEN VOID/SUBCOOLED BOILING COMBINED MODELS
FOR ALL WEIGHTED VOID FRACTIONS

Void Model	Subcooled Boiling Model	$\sum(\bar{\alpha}_i - \hat{\alpha})^2$
Homogeneous	Saha and Zuber	0.110
Homogeneous	Levy	0.128
Homogeneous	Ahmad	0.152
Homogeneous	Bowring	0.163
Homogeneous	Thom	0.205
Homogeneous	Sekoguchi, et al.	0.232
Modified Hancox/Nicoll	Ahmad	0.257
Modified Hancox/Nicoll	Saha and Zuber	0.275
Hancox/Nicoll	Saha and Zuber	0.278
Hancox/Nicoll	Ahmad	0.280

Table 5–7

TOP TEN VOID/SUBCOOLED BOILING COMBINED MODELS
FOR WEIGHTED VOID FRACTIONS LESS THAN 0.30

Void Model	Subcooled Boiling Model	$\sum(\bar{\alpha}_i - \hat{\alpha})^2$
Bankoff	Saha and Zuber	0.032
Smith	Saha and Zuber	0.036
Zuber/Findlay	Saha and Zuber	0.037
Modified Hancox/Nicoll	Saha and Zuber	0.038
Homogeneous	Levy	0.038
Homogeneous	Saha and Zuber	0.039
Modified Armand	Saha and Zuber	0.040
Ahmad	Saha and Zuber	0.041
Hughmark	Saha and Zuber	0.041
Dix	Bowring	0.041

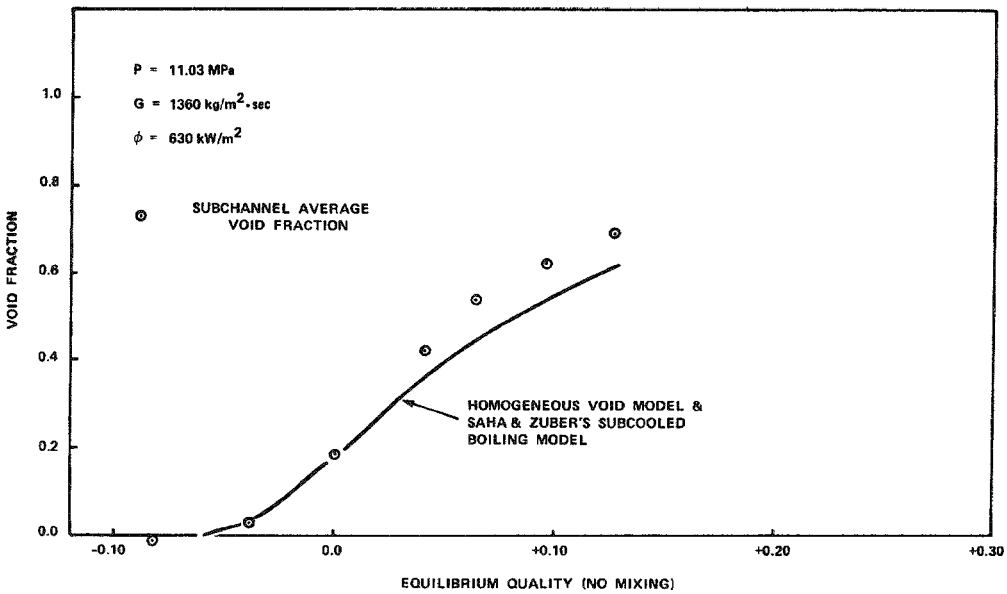

Figure 5–24. Subchannel average void fraction versus quality (Code 45)

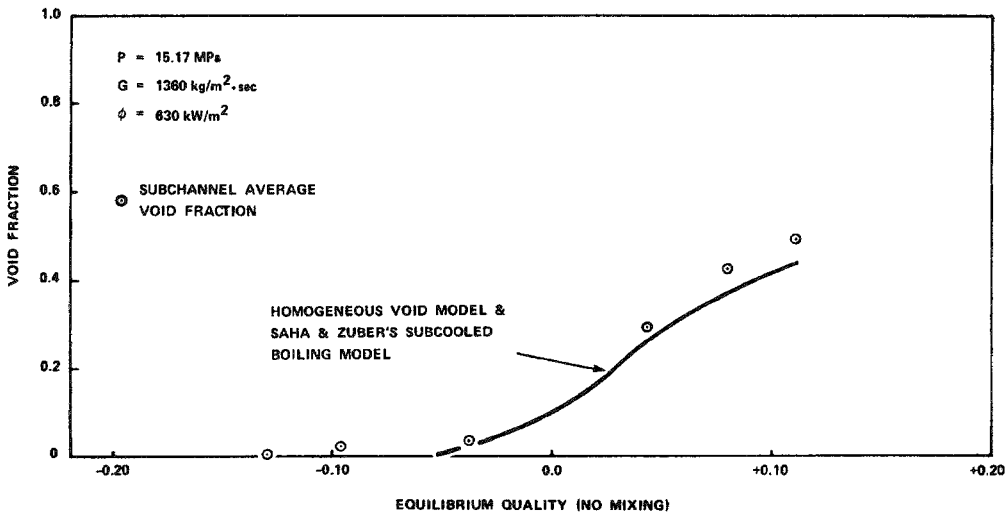

Figure 5–25. Subchannel average void fraction versus quality (Code 49)

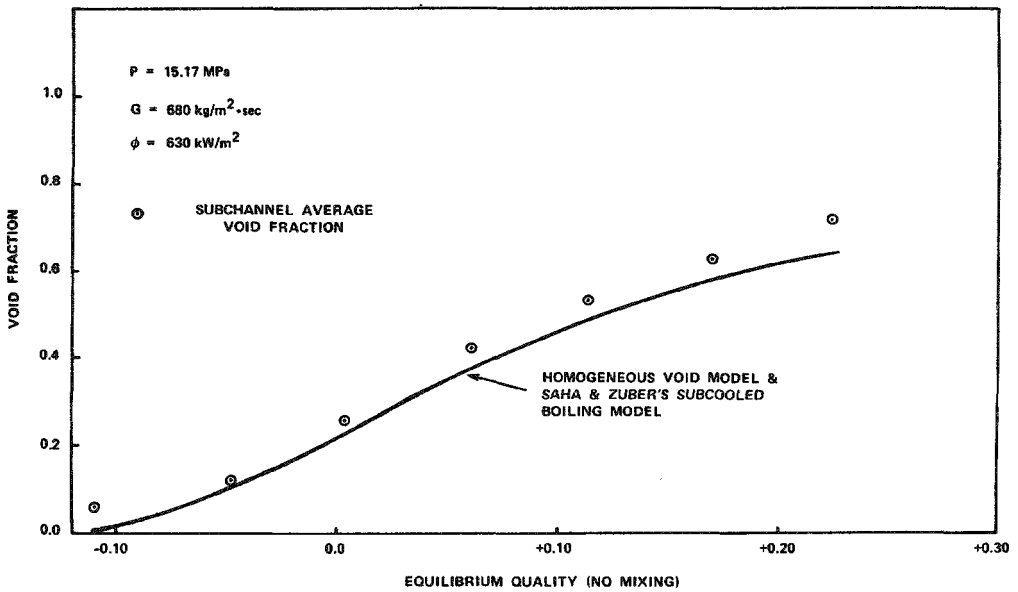

Figure 5–26 Subchannel average void fraction versus quality (Code 47)

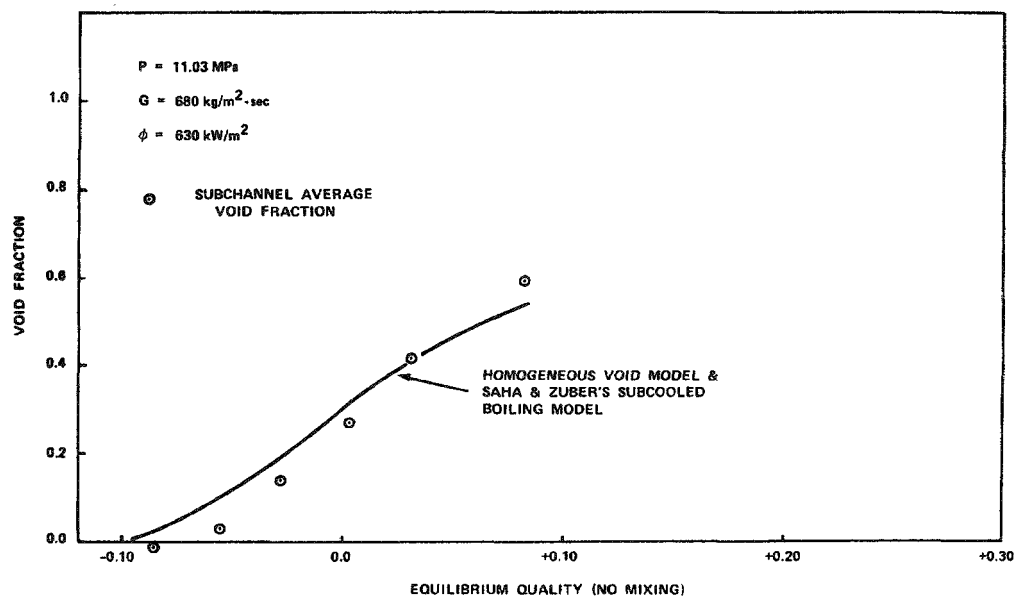

Figure 5–27. Subchannel average void fraction versus quality (Code 52)

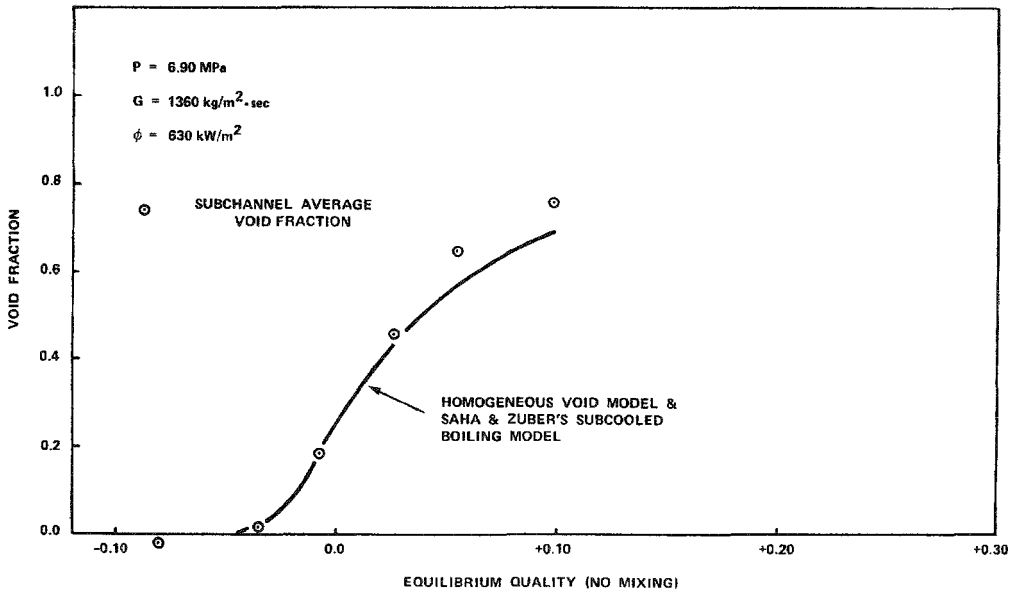

Figure 5–28. Subchannel average void fraction versus quality (Code 41)

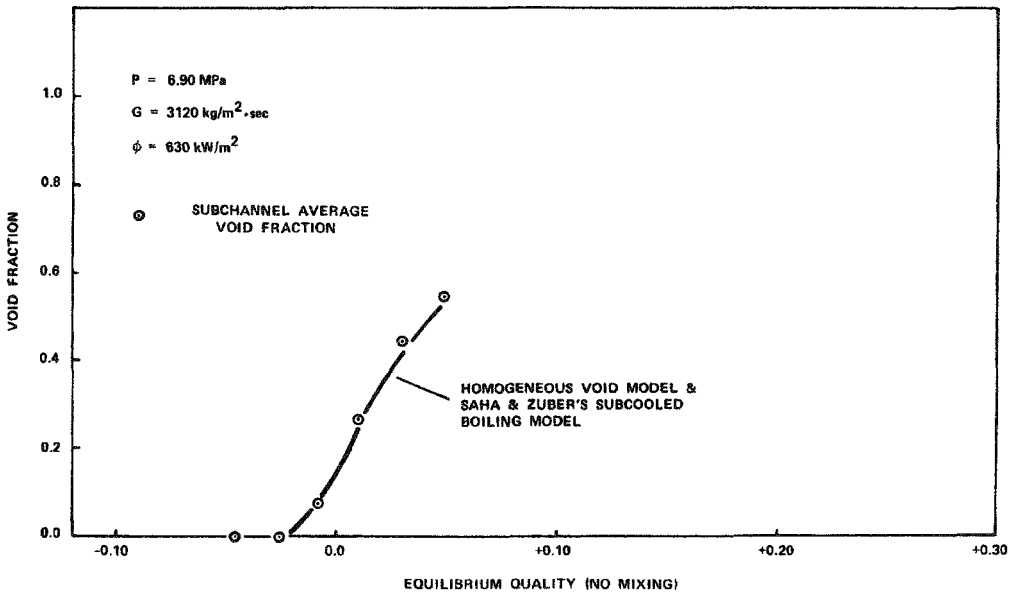

Figure 5–29. Subchannel average void fraction versus quality (Code 42)

Comparison of Collimator Set 1 Data and Collimator Set 2 Data

The scattering model described in this section entitled "Evaluation of Constants from Experimental Data" was also used to develop a weighting function W_1 (x, y) to represent collimator set 1. Applying Eq. 5-69 to collimator set 1:

$$\alpha_1(\text{measured}) = \frac{\frac{1}{4}\iint_{SC} W_1\,(x,y)\ \alpha\,(x,y)\,dx\,dy}{\frac{1}{4}\iint_{SC} W_1\,(x,y)\,dx\,dy} \qquad (5\text{-}78)$$

Since the data for collimator set 2 are implicitly contained in α (x,y) through the constants a and b, this equation provides a means of comparing the data for collimator sets 1 and 2, and also provide a check on the void distribution model. The weighting function for collimator set 1 is given by:

$W_1\,(x,y) = 1.0$ for $|x|$ and $|y| < F$

$W_1\,(x,y) = 1.0 - E(|x| - F)$ for $|x| > F$ and $|y| < F$

$W_1\,(x,y) = 1.0 - E(|y| - F)$ for $|y| > F$ and $|x| < F$

$W_1\,(x,y) = \left[1 - E(|x| - F)\right]\left[1 - E(|y| - F)\right]$ for $F < |x|$ and $|y| < G$

$W_1\,(x,y) = 0$ for $|x|$ or $|y| > G$

where:

$E = 4.972\ cm^{-1}$

$F = 0.104$ cm

$G = 1/E + F$

Integration of Eq. 5-78 then gives:

$$\alpha_1(\text{measured}) = -2.673 \times 10^{-2}\ cm^4\ a + b \qquad (5\text{-}79)$$

Using the previously determined values for constants a and b (Eq. 5-74 and 5-75):

$$a = -9.49\ cm^4 \left[\bar{\alpha}_{2\text{-}g}(\text{measured}) - \bar{\alpha}_{2\text{-}c}(\text{measured})\right]$$

$$b = 1.227\ \bar{\alpha}_{2\text{-}c}(\text{measured}) - 0.227\ \bar{\alpha}_{2\text{-}g}(\text{measured})$$

and substituting these values for a and b into Eq. 5-79 gives:

$$\alpha_1(\text{measured}) = 0.027\ \bar{\alpha}_{2\text{-}g}(\text{measured}) + 0.973\ \bar{\alpha}_{2\text{-}c}(\text{measured}) \qquad (5\text{-}80)$$

Eq. 5-80 indicates that the void-quality curves for collimator set 1 and the collimator set 2 center should be nearly the same. Figures 5-30 and 5-31 show that these two curves are generally in good agreement.

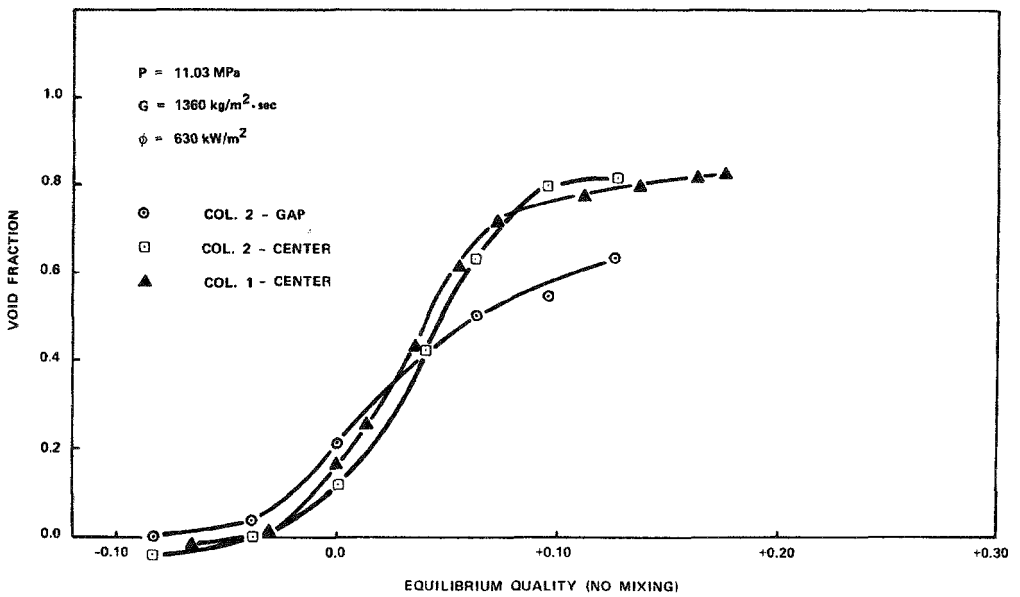

Figure 5–30. Void fraction versus quality (Collimator 1 – Code 9 and Collimator 2 – Code 45)

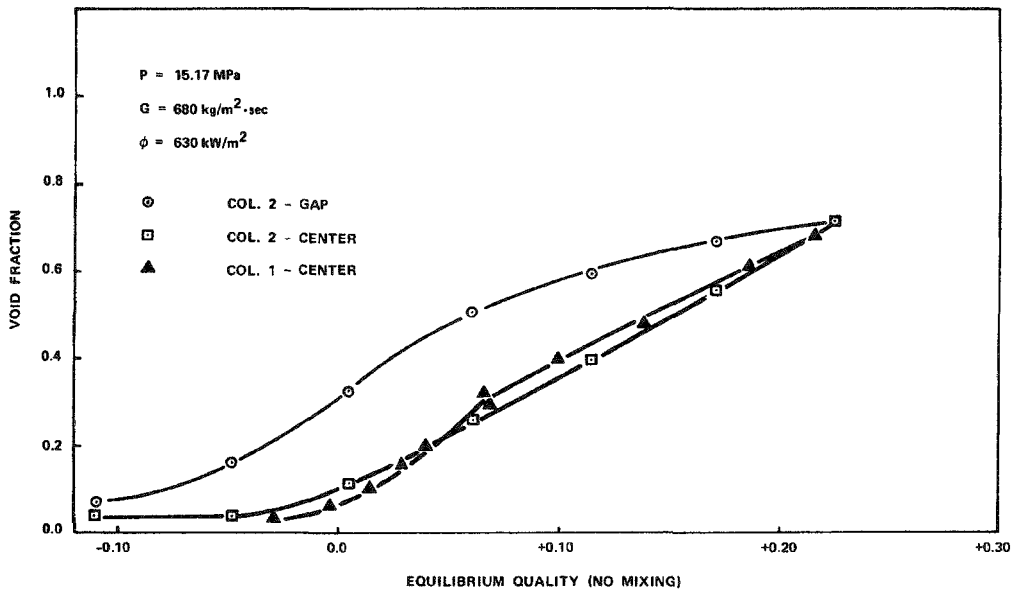

Figure 5-31. Void fraction versus quality (Collimator 1 – Code 24 and Collimator 2 – Code 47)

Eq. 5-80 applies only for measurements made at the same equilibrium quality. Thus, it was necessary to curve-fit the collimator set 1 data in terms of quality in order to make a direct comparison between the sets of data using this equation. The collimator set 1 measurements, which had corresponding collimator set 2 measurements, were correlated in terms of the no mixing equilibrium quality for constant pressure, heat flux and mass flux using the general equation:

$$\alpha_1(X_{eq}) = C_1 e^{-C_2 e^{-C_3 X_{eq}}} \quad \text{(No Mixing)} \tag{5-81}$$

The correlation coefficients and regression coefficient are given in Table 5-8. The regression coefficients ranged from 0.989 to 0.998. A form suggested by the drift flux and subcooled boiling models:

$$\alpha(X_{eq}) = \frac{C_1}{1 + C_2 \left(\frac{1}{X_{eq} - C_3 \exp\left(\frac{X_{eq}}{C_3} - 1\right)} - 1 \right)} \tag{5-82}$$

did not give acceptable regression coefficients.

Table 5–8

CORRELATION AND REGRESSION COEFFICIENTS
FOR MISCELLANEOUS COLLIMATOR SET 1 DATA

Thermal-Hydraulic Code	C_1	C_2	C_3	R^2
12 (41)*	0.854	0.813	38.62	0.989
28 (42)	0.698	1.546	71.37	0.998
18 (43)	0.946	2.677	29.27	0.997
21 (44)	0.734	3.000	38.09	0.994
9 (45)	0.821	1.799	31.43	0.996
8 (46)	0.557	1.970	43.89	0.998
24 (47)	0.858	2.277	10.70	0.993
29 (48)	0.647	2.007	20.39	0.998
5 (49)	0.730	1.548	15.25	0.997
4 (50)	0.657	2.162	20.83	0.997
17 (51)	0.647	2.220	22.98	0.996
10 (52)	0.842	2.263	25.72	0.992
11 (40 & 53)	0.885	0.832	21.59	0.993

*Number in parentheses is the thermal-hydraulic code for corresponding collimator 2 data.

Eq. 5-81 was used to compare the collimator set 1 data with specific collimator set 2 data points. This analysis showed that 80% of the calculated collimator set 1 void fractions fell within ±0.05 (in void fraction) of the collimator set 2-center data.

Section 6

ERROR ANALYSIS

This section discusses potential source of error in the experimental measurements and in the techniques used to analyze the data. The error analysis has been divided into four parts. The first part deals with the uncertainty in the thermal-hydraulic data. The second section discusses the calculation of equilibrium quality. The third part examines the uncertainty in the measured void fractions. The fourth and final part presents an analysis of the effects of annular flow on the calculated subchannel average void fractions and on their comparison with existing void models.

UNCERTAINTY IN THE THERMAL-HYDRAULIC DATA

Steady-State Conditions

An inability to hold conditions exactly steady during a run actually adds negligible error to the data. As long as the variation is small and the value reported is the average of this variation, then the secondary quantities calculated from this primary quantity vary linearly and their averages are approximately the reported average secondary quantities. For example, the pressure was found to vary at most by 0.108 MPa from the average reported value. Under equilibrium conditions, this variation affects the void fraction by 0.0001%. This comes from the slight non-linearity in the relations between pressure and the saturated liquid and vapor densities.

A small sampling error is introduced from the fact that a finite number of data scans (about 36) are made during the run. The uncertainty in the average of these 36 scans can be statistically related to the true average. Four quantities were calculated for each measurement listed in Table 6-1. The first is the variation from the mean value of the quantity averaged for all the runs. The second value is simply the maximum of these variations seen during any of the runs. The last two terms represent the size of the uncertainties introduced into the reported average value by the variation during the run. The first is the average uncertainty for all the runs; the last is the maximum uncertainty. These four values show

that the error introduced in the average data point is very small, and only rarely do the errors approach the size of other sources to be discussed in the following paragraphs.

Table 6–1

SUMMARY OF ERRORS
INTRODUCED BY
VARIATION FROM STEADY–STATE

Measurement	Variation Averaged Over All Runs	Maximum Variation	Uncertainty Averaged Over All Runs	Maximum Uncertainty
Outlet Pressure	0.025 MPa	0.108 Mpa	0.004 MPa	0.18 MPa
Outlet Temperature	0.23°C	1.2°C	0.04°C	0.2°C
Inlet Temperature	0.33°C	2.2°C	0.06°C	0.4°C
Flow Rate	0.23%	1.02%	0.04%	0.17%
Heat Flux	0.36%	0.81%	0.06%	0.14%

Duplicate Measurements

Several measurements were made with duplicate instruments so that a comparison between them would be possible. This was quantified by calculating the differences in the readings for all the runs and determining the standard deviation between the readings:

Duplicate Measurements	Standard Deviation
Outlet Pressure	0.0066 MPa
Inlet Temperature	0.16°C
Outlet Temperature	0.35°C
Test Section Voltage (used to determine rod heat flux)	0.024%

These values illustrate the high degree of accuracy achieved by the thermal-hydraulic instruments.

Temperature Versus Pressure Comparisons

A comparison was made between the outlet pressure and the pressure calculated from temperature $\left[P_{sat} - P(T_{sat})\right]$ for all two-phase points which had saturated conditions at the outlet. This was also done for the reverse situation where outlet temperature was calculated from pressure. The temperature measurement chosen for the comparison was the RTD located on the south side at the outlet.

Comparison	Average Value
$T_{sat} - T(P_{sat})$	-0.11°C
$P_{sat} - P(T_{sat})$	0.017 MPa

These values are significant in that two totally separate measurements were made and compared for their absolute values. This comparison assures the accuracy of the pressure and temperature measurements.

To compare the other temperature measurements against the instrument used in the pressure comparison, a measurement was made at zero power. The temperature was raised to about 260°C at a high flow rate to minimize the effect of any heat loss between the inlet and outlet of the vessel. The water temperature measured by the other three vessel RTDs was compared against the south outlet RTD with the following results:

Comparison	Average Value
North Outlet - South Outlet	0.02°C
North Inlet - South Outlet	0.023°C
South Inlet - South Outlet	0.08°C

Using these comparisons with the one above, the largest difference between the temperature measurements and a reference temperature based on converting the saturation pressure is 0.12°C.

Heat Balance - Heat Loss

An overall determination of the accuracy of the several thermal-hydraulic calibrations can be achieved by performing an energy balance on the test section. A quantity defined as the heat balance was calculated for all experimental runs where single-phase conditions existed at the outlet of the test section. This heat balance represents the percent difference between the power going into the test section (determined from voltage and current) and the power leaving the test section (determined from the enthalpy rise of the water and heat lost through the sides of the vessel).

The heat loss was determined by a low-flow, zero power experiment at about 290°C. The rate of heat loss is proportional to the difference between this temperature and ambient. However, since the loss was small, corrections for an average temperature different from 290°C was not made. The heat loss determined from flow and temperature measurements of the water was 2100 watts.

In addition to heat loss, other factors affecting heat balance are:

1) Current shunt calibration
2) AC component ripple factor
3) Calibrations of the voltage dividers
4) Voltmeter and analog to digital converter accuracy
5) Flow nozzle calibration
6) Differential pressure transducer calibrations
7) RTD temperature measurements

Every important thermal-hydraulic parameter except pressure is directly involved in this comparison so that heat balance is indeed a good check on the accuracy of the measurements.

For almost all of the coded conditions presented in the data tables (Appendix B), the average heat balance of the points in single-phase was calculated. The coded conditions for which heat balance was not calculated had no single-phase outlet conditions. The heat balance was found to depend on the thermal-hydraulic conditions and varied only slightly from run to run within a given set of conditions. Table 6-2 summarizes the heat balance results.

Table 6–2

SUMMARY OF HEAT BALANCE MEASUREMENTS

Thermal-Hydraulic Code	Heat Balance (%)	Thermal-Hydraulic Code	Heat Balance (%)
1	-0.1	28	-1.0
2	-0.2	29	1.3
3	0.6	30	3.2
4	0.8	31	3.6
5	-0.3	32	4.1
6	0.0	33	2.6
7	0.5	34	*
8	0.6	35	5.0
9	-0.4	36	2.0
10	0.8	37	5.4
11	-0.1	38	*
12	-0.6	39	3.1
13	0.3	40	0.6
14	-0.8	41	-0.4
15	0.2	42	0.0
16	-0.1	43	-0.3
17	-1.6	44	-0.2
18	-1.7	45	-0.2
19	0.1	46	0.6
20	0.6	47	0.1
21	0.5	48	-1.2
22	-1.1	49	-0.9
23	-0.9	50	0.1
24	0.3	51	-0.6
25	0.0	52	-0.2
26	-0.2	53	0.0
27	0.2		

*No single-phase data were taken at these points.

Summary of Thermal-Hydraulic Uncertainty

Based on the preceding analysis, the thermal-hydraulic data have been assigned the following uncertainties:

Pressure	±0.35 MPa
Heat Flux	±1%
Flow Rate	±1%
Inlet Temperature	±0.5°C

UNCERTAINTY IN EQUILIBRIUM QUALITY

The equilibrium quality is calculated from the equation:

$$X_{eq} = \frac{h_{in} - h_f + f\frac{\phi}{G}}{h_{fg}} \tag{6-1}$$

where:

h_{in} = inlet enthalpy

h_f = liquid saturation enthalpy

h_{fg} = latent heat of vaporization

and f = 611 is a geometry/mixing factor which is to be discussed shortly. The overriding uncertainty in this calculation comes from the uncertainties in the heat flux and the mass flux. Thus:

$$\sigma_{X_{eq}} = \frac{f}{h_{fg}} \sigma_{\phi/G} \tag{6-2}$$

where:

$\sigma_{X_{eq}}$ = uncertainty in the calculated equilibrium quality

$\sigma_{\phi/G}$ = uncertainty in the heat flux to mass flux ratio

But:

$$\sigma_{\phi/G} = \frac{\phi}{G}\sqrt{\left(\frac{\sigma_\phi}{\phi}\right)^2 + \left(\frac{\sigma_G}{G}\right)^2} \tag{6-3}$$

From the previously determined thermal-hydraulic uncertainties, $\sigma_\phi = 0.01\phi$ and $\sigma_G = 0.01G$. Then $\sigma_{\phi/G} = 0.0141\phi/G$. Substituting this result into Eq. 6-3 gives the uncertainty in equilibrium quality:

$$\sigma_{X_{eq}} = \frac{f}{h_{fg}}\ 0.0141\ \frac{\phi}{G} = \frac{9\ \phi/G}{h_{fg}} \tag{6-4}$$

In the rod bundle geometry of this test, the uncertainty in equilibrium quality in the center subchannel goes beyond that resulting from uncertainties in the measured primary variables of pressure, inlet temperature, heat flux, and mass flux. In a heated pipe or tube, the quality can easily be calculated from a heat balance up to the point Z. If each subchannel did not interact with its neighboring subchannels, the quality for each subchannel could be calculated from a similar heat balance. However, the subchannels within a rod bundle do interact across the gap between rods, mixing fluid and exchanging energy from one subchannel to the next. The rod bundle with heated shroud used in this test was designed to develop a nearly uniform quality/enthalpy profile across the bundle. However, to avoid critical heat flux on the heated walls of the bundle, the heat flux on the shroud for the collimator set 1 data was slightly lower than the heat flux on the rods. As a result, if there was little or no mixing between subchannels, qualities in individual subchannels could vary significantly from the bundle average quality. For a given heat flux and mass flux, the limiting cases of complete and no mixing can be calculated for any subchannel by using appropriate heat balances. A heat balance on the center subchannel gives:

$$X_{eq}(\text{no mixing}) = \frac{h_{in} - h_f + \dfrac{\phi_{rod} P_{h,cs} Z}{G A_{cs}}}{h_{fg}} \qquad (6\text{-}5)$$

where:

ϕ_{rod} = heat flux on the rods

$P_{h,cs}$ = heated perimeter of center subchannel = 3.024 cm

Z = measurement elevation = 180 cm

G = bundle average mass flux

A_{cs} = flow area of center subchannel = 0.892 cm^2

Substituting in values gives:

$$X_{eq}(\text{no mixing}) = \frac{h_{in} - h_f + f_{nx} \frac{\phi_{rod}}{G}}{h_{fg}} \qquad (6\text{-}6)$$

where:

$$f_{nx} = \frac{P_{h,cs}\, Z}{A_{cs}} = 611$$

For complete mixing, the quality is the same in all of the subchannels and is calculated from a heat balance on the entire rod bundle:

$$X_{eq}(\text{complete mixing}) = \frac{h_{in} - h_f + \phi_{rods}\left(P_{h,rods} + \frac{\phi_{shroud}}{\phi_{rods}} P_{h,shroud} \right) Z}{G\, A_{f,tot}} \Bigg/ h_{fg} \qquad (6\text{-}7)$$

where:

$P_{h,rods}$ = heated perimeter of all rods = 48.39 cm

$P_{h,shroud}$ = heated perimeter of shroud = 18.97 cm

$A_{f,tot}$ = total bundle flow area = 20.78 cm^2

For data taken with collimator/shroud 1, $\phi_{shroud}/\phi_{rods} = 0.795$ and:

$$X_{eq}(\text{complete mixing collimator/shroud 1}) = \frac{h_{in} - h_f + f_{axl} \frac{\phi_{rod}}{G}}{h_{fg}} \qquad (6\text{-}8)$$

where:

$$f_{axl} = P_{h,rods} + \frac{\phi_{shroud\ 1}}{\phi_{rods}} P_{h,shroud} = 550$$

As testing began with collimator set 2, severe electrolysis at the bottom of the test section forced the replacement of the heated shroud. The new shroud material was thicker and gave a higher relative heat flux than the original shroud.

For collimator/shroud 2, $\phi_{shroud}/\phi_{rods} = 1$ and:

$$X_{eq}(\text{complete mixing collimator/shroud 2}) = \frac{h_{in} - h_f + f_{ax2}\,\frac{\phi_{rod}}{G}}{h_{fg}} \qquad (6\text{-}9)$$

where:

$$f_{ax2} = P_{h,rods} + \frac{\phi_{shroud\ 2}}{\phi_{rods}}\,P_{h,shroud} = 584$$

Thus, the bundle design for collimator set 2 was less sensitive to mixing effects than collimator set 1.

The equation given above for no mixing quality (Eq. 6-6) contains the tacit assumption that the average mass flux in the center subchannel is the same as the bundle average mass flux. As Figure 6-1 suggests, this assumption is a good one in the high and intermediate mass flux range of the data. In this range, qualities calculated from Eq. 6-6 are in good agreement with the qualities found using the COBRA code. However, in the lower mass flux range of the data, calculations with the COBRA code showed that the mass flux in the center subchannel was significantly higher than the bundle average mass flux. As a result, the actual quality under conditions of no mixing was significantly lower than the no mixing qualities found from Eq. 6-6. In analyzing the low flow data, the no mixing qualities were determined using COBRA rather than Eq. 6-6 and are given in Tables 6-3, 6-4, and 6-5.

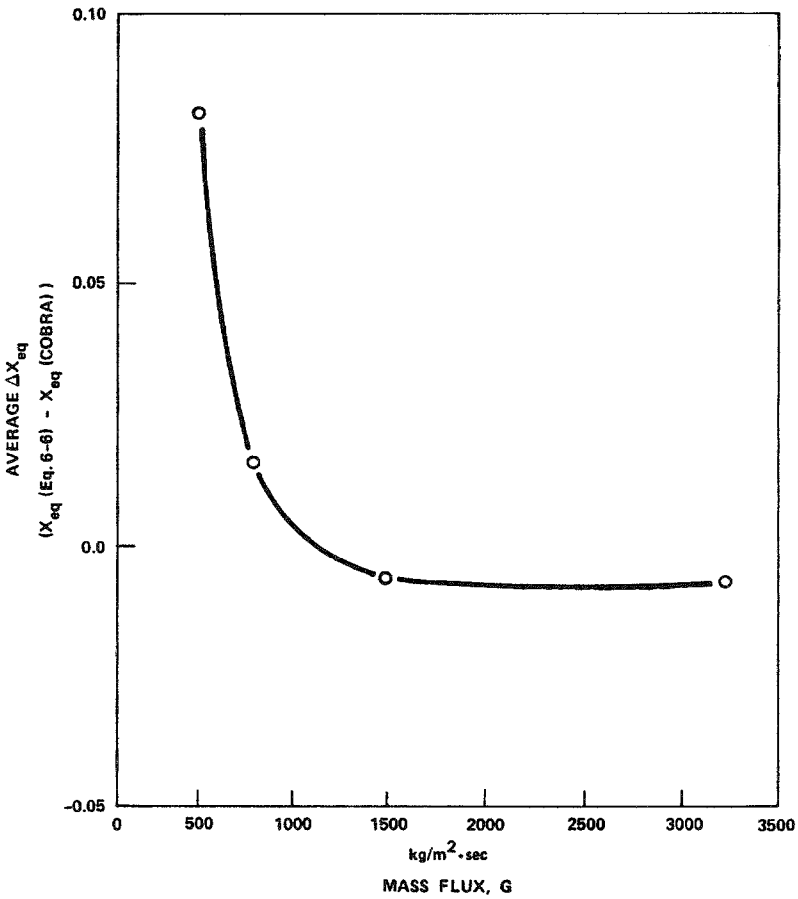

Figure 6–1. Average difference between no mixing qualities from COBRA and Eq. 6–6 versus mass flux

Table 6–3

NO MIXING QUALITIES FROM COBRA
(Codes 30, 31, and 32)

Code Number	Run Number	X_{eq} (Eq. 6-6)	X_{eq} (COBRA - No Mixing)
30	403	-0.258	-0.284
	404	-0.196	-0.224
	405	-0.045	-0.071
	411	0.015	-0.017
	406	0.050	0.020
	407	0.118	0.085
	408	0.197	0.168
	409	0.278	0.253
	410	0.312	0.292
31	412	-0.111	-0.141
	413	-0.043	-0.077
	414	0.021	-0.012
	415	0.064	0.032
	416	0.117	0.084
	417	0.186	0.156
	418	0.234	0.205
	419	0.272	0.243
	420	0.339	0.319
32	486	-0.182	-0.214
	487	-0.096	-0.123
	488	-0.018	-0.048
	489	0.095	0.059
	490	0.119	0.088
	491	0.188	0.158
	492	0.288	0.268
	421	0.310	0.290
	422	0.361	0.338

Table 6–4

NO MIXING QUALITIES FROM COBRA
(Codes 33, 34, and 35)

Code Number	Run Number	X_{eq} (Eq. 6-6)	X_{eq} (COBRA - No Mixing)
33	431	-0.051	-0.072
	430	-0.018	-0.041
	429	0.020	-0.007
	428	0.053	0.014
	427	0.081	0.052
	426	0.156	0.118
	425	0.201	0.170
	423	0.262	0.236
	424	0.304	0.284
34	465	0.107	0.040
	464	0.161	--
	463	0.218	--
	436	0.289	0.232
	435	0.335	0.285
	462	0.387	0.343
	434	0.365	0.321
	433	0.443	--
	432	0.491	--
35	439	-0.079	-0.114
	440	-0.020	-0.060
	441	0.016	-0.019
	442	0.068	0.025
	444	0.101	0.062
	443	0.151	0.113
	445	0.198	0.166
	446	0.300	0.269

Table 6–5

NO MIXING QUALITIES FROM COBRA
(Codes 36, 37, 38, and 39)

Code Number	Run Number	X_{eq} (Eq. 6-6)	X_{eq} (COBRA - No Mixing)
36	455	-0.032	-0.082
	454	0.001	-0.042
	453	0.071	0.028
	450	0.161	0.116
	447	0.231	0.189
	449	0.284	0.249
	448	0.358	0.329
37	457	-0.117	-0.165
	459	0.117	0.072
	460	0.184	0.143
38	468	0.087	0.036
	470	0.156	0.097
	469	0.179	0.119
	471	0.162	0.107
	472	0.200	0.150
	473	0.225	0.175
	474	0.272	0.225
	475	0.336	0.297
39	480	-0.107	-0.182
	479	-0.081	-0.158
	481	0.007	-0.080
	478	0.058	-0.025
	477	0.057	-0.026
	476	0.095	0.012
	482	0.149	0.059
	483	0.189	0.099
	484	0.228	0.147

UNCERTAINTY IN MEASURED VOID FRACTIONS

Measured void fraction was calculated from measured density using the equation:

$$\alpha = \frac{\rho_\ell - \rho}{\rho_\ell - \rho_v} \qquad (6\text{-}10)$$

where:

ρ_ℓ = density of the liquid phase

ρ = measured density

ρ_v = density of the gas phase

In this calculation, ρ_v was taken to be the density of saturated vapor at the measured pressure. This is a good assumption since the vapor phase would not have been superheated in the quality range covered by the data. On the other hand, the quality range did cover the subcooled boiling region where the density of the subcooled liquid could be significantly different from that of saturated liquid.

Eq. 6-10 shows then that the two main sources of uncertainty in the measured void fractions come from uncertainties in the liquid density and from a combination of random and non-random uncertainties in the measured density.

Uncertainty in Liquid Density

As discussed earlier, the subcooled liquid density was found using an iterative technique which determined values of ρ_ℓ and the corresponding liquid enthalpy. These values were required to satisfy the following equation:

$$\frac{\rho_\ell - \rho}{\rho_\ell - \rho_g} = \frac{1}{1 + \frac{\rho_\ell}{\rho_g}\frac{1 - X_t}{X_t}}$$

where:

$$X_t = \frac{h - h_\ell}{h_g - h_\ell}$$

If the calculated liquid enthalpy was greater than the saturation value, the liquid density was assigned the saturation value, ρ_f.

This method requires that the total subchannel enthalpy be known. Thus, the major uncertainty in liquid density is due to uncertainty in mixing. During subcooled boiling, much of the heated length is single-phase. Rogers and Todreas(24) have suggested that the single-phase mixing coefficient, β, has the form:

$$\beta = 0.0062 \left(\frac{D_h}{Z_{ij}} \right) Re^{-0.1} \qquad (6\text{-}11)$$

where:

D_h = hydraulic diameter

Z_{ij} = clearance space between rods

Re = Reynolds number

For the conditions tested, this equation gives β a value of approximately 0.007. This in turn gives values for enthalpy closest to the no mixing enthalpy. Thus, the no mixing enthalpy was used in the calculation of liquid density for data included in the data analysis. The limits on the subchannel enthalpy can be found assuming complete mixing and no mixing. A comparison between the assumptions of complete mixing and no mixing as it effects measured void fractions is given in Table 6-6. In the region of greatest interest -- the high void fractions -- the assumptions on mixing have little effect.

An analysis of the effect of uncertainty in enthalpy on the measured void fraction indicates that a 10 Btu/lb error in enthalpy has about a 0.01 effect on void fraction. In the bulk boiling region, the liquid density equals the saturated liquid density and the only source of error in measured void fraction is due to uncertainties in measured density.

Table 6–6

EFFECT OF MIXING ON REDUCTION
OF DENSITY TO VOID FRACTION

Run Number	α (Complete Mixing)	α (No Mixing)
191	0.012	0.000
192	0.010	-0.003
193	0.071	0.057
195	0.359	0.349
194	0.566	0.559
196	0.640	0.634
197	0.793	0.789
198	0.865	0.863
199	0.877	0.875

Random and Non-Random Errors in Measured Density

A complete error analysis which carries along the gamma counting statistics as they are involved in calibrations and experimentation is unnecessary. For the majority of data runs, two separate measurements were made of the center subchannel density by gamma detectors located on either side of the test bundle. A statistical analysis of these two measurements indicates the precision of the density measuring technique.

First, the data was divided into groups according to density with each group being 80 kg/m^3 wide. The differences between the two detectors were used to calculate two statistical quantities. The first is the average difference between the two detectors; the second is the precision of a single measurement. The precision listed in Table 6-7 is the size of the band within which 95% of the readings would fall if the measurements were repeated. The majority of the precision band is due simply to the gamma counting statistics which are approximately 11 kg/m^3.

Table 6–7

SUMMARY OF THE STATISTICAL ANALYSIS
OF THE TWO DENSITY MEASUREMENTS

Range kg/m^3	Number of Runs	Average Difference kg/m^3	Single Measurement Precision (95%) kg/m^3
80-160	14	- 1.0	13
160-240	27	2.6	10
240-320	31	0.8	14
320-400	24	7.8	13
400-480	32	9.3	11
480-560	41	10.3	14
560-640	54	5.3	15
640-720	44	6.1	13
720-800	37	3.5	13
Total	304	5.4	14

Based on this analysis, the measured density has been assigned an uncertainty due to random sources of error of ± 16.01 kg/m^3.

In Section 3 (Gamma Model Development), the size of non-random errors (E) in measured density was examined. The results of these examinations are summarized as:

Imperfect collimation	--	No significant effect
Density asymmetry		
Collimator set 1	--	No significant effect
Collimator set 2	--	$0 > E > -0.9\%$
Dynamic bias	--	$0 > E > -1.25\%$ (In slug-flow regime)
Finite scatter volume	--	No significant effect
Gamma counting statistics	--	No non-random errors
Non-exponential attenuation	--	$0 < E < 0.1\%$
Magnetic attraction and rod temperature	--	$0 < E < 1\%$

If the dynamic bias is considered as a special case because of its limited applicability, the bias errors can be roughly estimated as being ±1% of the density. The average density seen in the measurements is about 480 kg/m^3, so that the size of this error is approximately 4.8 kg/m^3. If this non-random uncertainty in measured density (4.8 kg/m^3) is simply added to the random uncertainty (16 kg/m^3), the total uncertainty in measured void fraction is given by:

$$\sigma_\alpha = \frac{\sigma_{\rho_m}}{\rho_f - \rho_g} = \frac{20.8}{\rho_f - \rho_g} \qquad (6\text{-}12)$$

This equation (Eq. 6-12) indicates that the uncertainty in measured void fraction will range from 0.029 at 6.90 MPa to 0.046 at 16.90 MPa.

EFFECT OF ANNULAR FLOW ON CALCULATED SUBCHANNEL AVERAGE VOID FRACTION

The void fraction measurements made during this test program did not completely cover all points within the subchannel. The density of the rods at the corners of the subchannel was several times greater than even single-phase water. If the void fraction measurements had been made too close to the rods, gamma rays scattering off the rods would have effectively masked any changes in the density of the fluid within the subchannel. The measured void fractions covered as much of the center subchannel as was possible while limiting the rod scatter to acceptable levels. In a bubbly-type flow regime where the void distribution was fairly uniform, this would not present any special problems. However, it was possible that at higher void fractions an annular-type flow regime had existed in the rod bundle. In such a situation, significant amounts of water would travel up against the rods where the void measurement technique was relatively insensitive to changes in density.

This section presents an analysis made to estimate the effects of annular flow on the calculated subchannel average void fraction. This analysis involved using a simplified two region model for annular-type flow. The void distribution for annular-type flow was approximated by rings of water centered about the rods. The terms α_1 and α_2 were designated as the void fractions outside and inside the annular region about the rods, and the liquid film thickness was represented by the symbol δ.

From Section 5, Eq. 5-69 implies that for any known void fraction distribution such as the one described above, a weighted void fraction can be calculated for each of the collimator set 2 measurement areas, i.e.,

$$\bar{\alpha}_{2\text{-}c} = \frac{\int_0^{1/D}\int_0^{1/C}\left[W_{2\text{-}c}(x,y)\,\alpha(x,y)\right]dx\,dy}{\int_0^{1/D}\int_0^{1/C} W_{2\text{-}c}(x,y)\,dx\,dy} \qquad (6\text{-}13)$$

$$\bar{\alpha}_{2\text{-}g} = \frac{\int_0^{1/D}\int_{x_0-1/C}^{x_0+1/C}\left[W_{2\text{-}g}(x,y)\,\alpha(x,y)\right]dx\,dy}{\int_0^{1/D}\int_{x_0-1/C}^{x_0+1/C} W_{2\text{-}g}(x,y)\,dx\,dy} \qquad (6\text{-}14)$$

These weighted void fractions can be used to provide an estimate of the void fractions that would be measured by the gap and center detectors for the assumed annular flow void distribution. The weighted void fractions can then be used in Eq. 5-76 (from Section 5; repeated here for convenience) to calculate a subchannel average void fraction as if they were experimental values:

$$\bar{\alpha}_{sc}(\text{calculated}) = 0.682\,\bar{\alpha}_{2\text{-}g} + 0.318\,\bar{\alpha}_{2\text{-}c} \qquad (5\text{-}76)$$

Since the void fraction distribution is known, the true average void fraction can be calculated from:

$$\bar{\alpha}_{sc}(\text{true}) = \frac{\alpha_1\pi\left[(R_{rod}+\delta)^2 - R_{rod}^{\,2}\right] + \alpha_2\left[P^2 - \pi\,(R_{rod}+\delta)^2\right]}{P^2 - \pi\,R_{rod}^{\,2}} \qquad (6\text{-}15)$$

Once the integrals described by Eq. 6-13 and 6-14 had been evaluated, only values for the void fractions in the two-region annular flow model and the size of the liquid film thicknesses were needed in order to estimate the subchannel average void fraction that would have been calculated from the data if annular flow had occurred. A brief review of the literature provided little if any guidance in selecting values for α_1, α_2, and δ.

In working with the annular flow model, it became obvious that for reasonable values of film thickness, the weighted center void fraction, $\alpha_{2\text{-}c}$ (weighted), was independent of the liquid film thickness. Based on this observation, the liquid film thickness was found as follows: For specific pairs of gap/center data from collimator set 2, the void fraction in the region outside the annulus (α_1) was set equal to the void fraction measured in the center of the subchannel. Iterations on $\alpha_{2\text{-}g}$ (weighted) and δ were made until $\alpha_{2\text{-}g}$ (weighted), calculated from Eq. 6-14, gave the same value as the void fraction that had actually been measured in the gap region. This calculation was made for values of α_2, the void fraction of the annulus, ranging from 0 to 20%.

Calculations of liquid film thickness were made for all of the collimator set 2 data where the void fraction measured in the center was higher than the void fraction measured in the gap. It was felt that the state of the art of determining flow regimes was not far enough advanced to allow sufficient accuracy in identifying data points in annular flow. Applying the annular flow analysis to all the data points which met the above criterion would ensure that no points where annular flow might have occurred would be excluded from the analysis.

Once values for liquid film thickness were available, it was possible to evaluate Eq. 6-13 and 6-14 to determine an estimate of the subchannel average void fraction that would have been calculated from experimental data under conditions of annular flow.

The difference between these two void fractions provided an indication of any possible bias in the subchannel average void fractions calculated from Eq. 5-76. This difference was calculated for all the collimator set 2 data where the void fraction was higher in the gap than in the center using the following equation:

$$\Delta\alpha = \bar{\alpha}_{sc} \text{ (Eq. 5-76)} - \bar{\alpha}_{sc} \text{ (Eq. 6-15)} \qquad (6\text{-}16)$$

An analysis of these differences showed, as expected, that $\Delta\alpha$ was largest for data points where the difference between the gap and center measured void fractions was largest. For no voids in the liquid film ($\alpha_2 = 0$), $\Delta\alpha$ ranged from 0 to 0.119. The liquid film thickness, δ, ranged from 0 to 0.097 cm. Table 6-8 shows the results for a few of the data points from collimator set 2. While these results are generally typical, they do include the two runs which had the largest values of $\Delta\alpha$.

Table 6–8

DIFFERENCE BETWEEN CALCULATED AND TRUE SUBCHANNEL AVERAGE VOID FRACTION DURING SIMULATED ANNULAR FLOW

Run Number	$\alpha_{2\text{-}g}$ (measured)	$\alpha_{2\text{-}c}$ (measured)	δ cm			$\Delta\alpha$		
			$\alpha_2 = 0$	$\alpha_2 = 0.10$	$\alpha_2 = 0.20$	$\alpha_2 = 0$	$\alpha_2 = 0.10$	$\alpha_2 = 0.20$
549	0.421	0.422	0.003	0.003	0.003	0.002	0.002	0.002
550	0.498	0.629	0.079	0.086	0.097	0.090	0.078	0.065
551	0.545	0.790	0.097	0.104	0.114	0.119	0.104	0.087
552	0.632	0.811	0.081	0.086	0.094	0.117	0.105	0.092

Conditions:

Code 45

P = 11.03 MPa

G = 1360 kg/m^2.sec

ϕ = 630 kW/m^2

$\alpha_{2\text{-}g} < \alpha_{2\text{-}c}$

Notes:

δ = liquid film thickness

α_2 = void fraction in the liquid film

$\Delta\alpha = \bar{\alpha}_{sc}$ (Eq. 5-75) - $\bar{\alpha}_{sc}$ (Eq. 6-15)

For each of the subchannel void fractions where the void fraction was higher in the center than in the gap, Eq. 6-16 was used to estimate the uncertainty in the subchannel average void fraction due to potential annular flow effects. This uncertainty was combined with both the random and non-random experimental measurement uncertainties to give an uncertainty band on the subchannel average void-quality plots.

As an example of how the measurement uncertainty was combined with the uncertainty in the calculated subchannel average void fraction, consider the highest void fraction point in Figure 6-2 (Run 552):

Measurement uncertainty	=	$\pm$ 0.034
Subchannel averaging uncertainty	=	- 0.117
Total uncertainty in subchannel average void fraction	=	+ 0.034 - 0.151

Some typical uncertainty bands are shown in Figures 6-2 and 6.3. The Hancox/Nicoll model is included on these plots since it is the highest of the non-homogeneous models. These figures show that even when the error bars are extended to allow for possible annular flow effects, much of the data still remains higher than the predictions of the non-homogeneous models -- in spite of the conservative approach used in the annular flow analysis. As an additional conservatism, it is worth noting that the bundle contained spacer grids which would tend to disperse an annular-type flow.

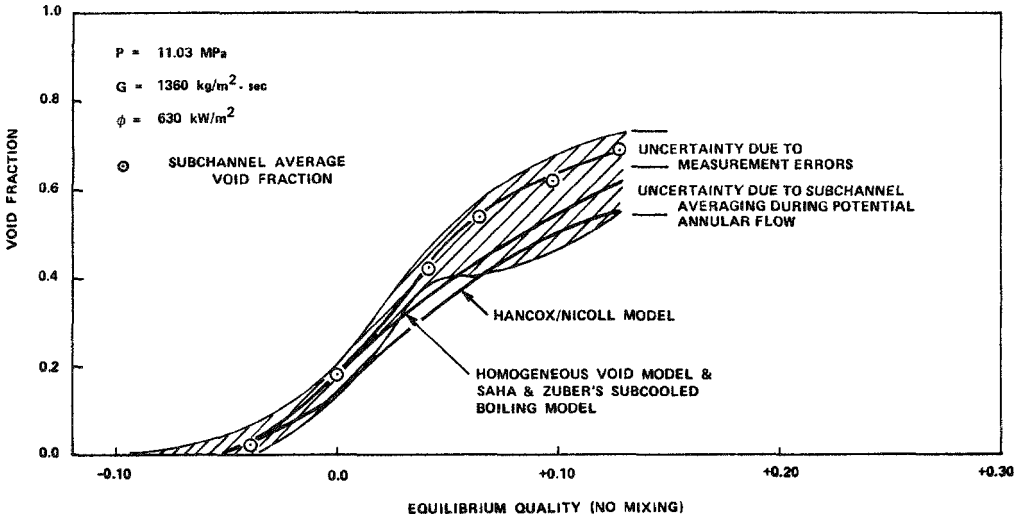

Figure 6–2. Uncertainty band for comparison with existing models (Code 45)

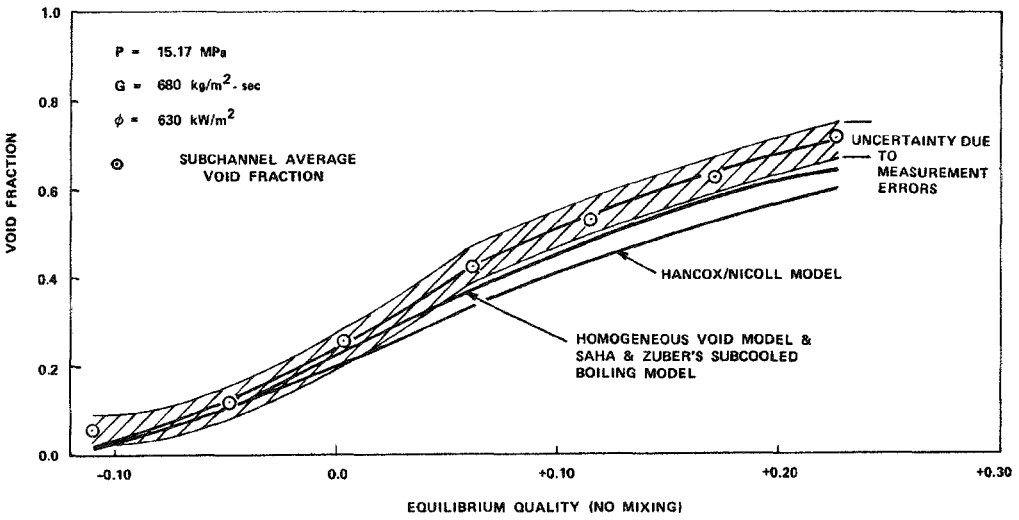

Figure 6–3. Uncertainty band for comparison with existing models (Code 47)

Section 7

RESULTS

- Over 300 void fraction data points were obtained with thermal-hydraulic conditions covering the following ranges:

  Pressure - 6.90 to 16.90 MPa

  Heat Flux - 158 to 1260 kW/m^2

  Mass Flux - 204 to 3122 $kg/m^2 \cdot sec$

- Measurement times were about five minutes -- a significant improvement over previous gamma scattering experiments.

- Analysis of the collimator set 1 and collimator set 2 data has shown that the void fraction versus quality curves demonstrate several general trends predicted by existing void fraction and subcooled boiling models. In the subcooled boiling region, the data show that the void fraction at a given quality is highest for high heat flux to mass flux ratios. In the bulk boiling region, the void fraction at a given quality is highest for the lowest pressure.

- The data from collimator set 2 demonstrate that as boiling begins the void fraction in the gap between the rods is higher than in the center of the subchannel. As the quality is raised, a transition occurs and the void fraction becomes highest in the center of the subchannel. In general, this transition occurs at higher qualities as the pressure increases or the mass flux decreases.

- The data from collimator set 2 also show that under certain conditions steep void fraction profiles exist across a subchannel. The magnitude of these distribution effects appear to be strongly related to the mass flux and, to a lesser extent, also related to pressure. The void distribution effects were seen to be small at pressures greater than about 13 MPa and at mass fluxes greater than 680 $kg/m^2 \cdot sec$.

- A void distribution model has been developed which describes the void fraction in the center subchannel as a function of position. The data from collimator set 2 were used to evaluate constants in the model. Integration of the void distribution function has provided a subchannel average void fraction which can be compared with the predictions of existing models.

- In the bulk boiling region, the observed subchannel average void fractions are higher than existing models, including the homogeneous model, predict. Slip effects would tend to give void fractions lower than the homogeneous model.

- A worst case analysis showed that under conditions of idealized annular flow, the calculated subchannel average void fraction could be higher than the actual subchannel average by as much as $\sim$0.10 in void fraction. However, when this additional uncertainty was taken into consideration, even the highest non-homogeneous model still did not fall completely within the error bands for much of the data.

- In the subcooled boiling region, there are several models which provide a good fit to the data.

- A lack of knowledge about void fractions in neighboring subchannels and the uncertainty in equilibrium quality prevented precise quantification of the effects of lateral vapor motion.

Section 8

CONCLUSIONS

- The gamma scattering technique was successfully applied to the measurement of regional void fractions within the 4 x 4 rod bundle operating at reactor-like conditions.

- In general, the technique cannot be applied to fast transients. However, under specific conditions of a relaxed accuracy requirement, a large scatter volume, and a very active gamma source, measurement times could be reduced to the point where slow transient void fractions are measurable.

- Application of the technique required considerable front-end engineering, preparation, control, and calibration. The amount of effort is dependent on the application. Effort was particularly acute in this experiment because gamma scattering off the heated rods interfered with the simple fluid scattering measurement. In applications where interference scatter is negligible, implementation of the technique is considerably simplified.

- The analysis of the void fraction data obtained in this program demonstrates that significant void distributions can exist across a subchannel. At higher qualities and void fractions, the vapor phase can be seen to concentrate in the center of the center subchannel.

- The relationship of the data with respect to existing models indicates that this vapor concentration effect may also occur on a bundle-wide basis.

Section 9

RECOMMENDATIONS

- The gamma scattering technique is recommended as a laboratory tool for nonintrusive, steady-state, regional measurements of density in complex geometries where test conditions justify the expense and effort involved in implementing the technique.

- Several techniques are recommended to simplify the implementation of the gamma scattering technique:

  -- Tungsten collimators should be used to minimize the uncertainty in defining the scatter volume caused by gamma penetration of the collimators.

  -- A high energy gamma source should be used to minimize attenuation. Cesium is a good choice because of its cost and availability.

  -- A high activity source is recommended to minimize measurement times required to obtain a specified accuracy.

  -- Considerable attention to fixing the source-detector-test geometry is recommended to minimize misalignment problems.

  -- Shielded detectors are recommended to minimize interference from large magnetic fields that accompany electrically-heated test sections.

  -- The avoidance of scatter off of fixed objects that interfere with the detection rate of gammas scattering off the fluid is recommended.

- The data obtained in this program should not be used to develop a new void - quality model for thermal-hydraulic codes such as COBRA because these codes do not now include a preferential liquid/vapor exchange mechanism that may be necessary to describe two-phase flow in rod bundles.

- The potential for lateral vapor motion between subchannels suggests that further development of subchannel codes must center on a more complete description of the interactions across subchannel boundaries.

- Two fluid models, which use separate sets of conservation equations for each phase, are currently being developed for accident analysis. In order to further improve the prediction of steady-state thermal-hydraulic conditions in rod bundles, these models should be investigated for their ability to properly incorporate a net liquid/vapor exchange process.

Section 10

REFERENCES

1. N. N. Kondic, "Density Field Determination by an External Stationary Source Using a Kernal Technique", Measurements in Polyphase Flows - Winter Annual ASME Heat Transfer Meeting; December 1968

2. N. N. Kondic and G. D. Lassahn, "Nonintrusive Density Distribution Measurement in Dynamic High Temperature Systems", Proc. of the 24th International Instrumentation Symposium; May 1978

3. N. M. Schaeffer, "Reactor Shielding for Nuclear Engineers", TID-25951; May 1973

4. D. S. Rowe, "COBRA IIIC - A Digital Computer Program for Steady-State and Transient Thermal-Hydraulic Analysis of Rod Bundle Nuclear Fuel Elements", BNWL-1965; March 1973

5. T. R. Lahey, Jr. and F. J. Moody, "The Thermal-Hydraulics of a Boiling Water Nuclear Reactor", ANS Monograph; 1977, pp. 207-209

6. J. F. Marchaterre and B. M. Hoglund, "Correlation for Two-Phase Flow", Nucleonics; August 1962, p. 142

7. S. M. Zivi, "Estimation of Steady-State Steam Void-Fraction by Means of the Principle of Minimum Entropy Production", Trans. ASME, Journal of Heat Transfer; May 1964, p. 247

8. J. R. S. Thom, "Prediction of Pressure Drop During Forced Circulation of Boiling Water", Int. Journal of Heat & Mass Transfer, Vol 17; 1964, p. 709

9. S. Y. Ahmad, "Axial Distribution of Bulk Temperature and Void Fraction in a Heated Channel with Inlet Subcooling", Trans. ASME, Journal of Heat Transfer; November 1970, p. 595

10. N. Madsen, "A Void Fraction Correlation for Vertical and Horizontal Bulk-Boiling of Water", Proc. Fifth Int. Heat Transfer Conf; 1975, Vol IV, p. 185

11. N. Zuber and J. A. Findlay, "Average Volumetric Concentration in Two-Phase Flow Systems", Trans. ASME, Journal of Heat Transfer; November 1976, p. 453

12. S. G. Bankoff, "A Variable Density Single-Fluid Model for Two-Phase Flow", Trans. ASME, Journal of Heat Transfer, Vol 82; November 1960, p. 265

13. C. C. St. Pierre and S. G. Bankoff, "Vapor Volume Profiles in Developing Two-Phase Flow", Int. Journal of Heat & Mass Transfer, Vol 10; 1967, p. 237

14. G. A. Hughmark, "Holdup in Gas-Liquid Flow", Chem. Eng. Prog., Vol 58, No. 4; 1962, p. 62

15. W. T. Hancox and W. B. Nicoll, "A General Technique for the Prediction of Void Distributions in Non-Steady Two-Phase Forced Convection", Int. Journal of Heat & Mass Transfer, Vol 14; 1971, p. 1377

16. G. S. Lellouche, "A Model for Predicting Two-Phase Flow", BNL 18628/RP-1032; February 1974

17. P. Saha and N. Zuber, "Point of Net Vapor Generation and Vapor Void Fraction in Subcooled Boiling", Proc. Fifth Int. Heat Transfer Conf., Vol IV; 1974, p. 175

18. S. Levy, "Forced Convection Subcooled Boiling - Prediction of Vapor Volumetric Fraction", Int. Journal of Heat Transfer, Vol 10; p. 953

19. Sekoguchi, et al., "Flow Boiling in Subcooled and Low Quality Regions - Heat Transfer and Local Void Fraction", Proc. Fifth Int. Heat Transfer Conf., Vol IV; 1974, p. 180

20. R. T. Lahey, Jr., et al., "Mass Flux and Enthalpy Distribution in a Rod Bundle for Single- and Two-Phase Conditions:, Trans. ASME, Journal of Heat Transfer; May 1971, p. 197

21. C. W. Stewart, et al., "COBRA-IV : The Model and the Method", BNWL-2214, NRC-4; 1977, pp. 97, 98, and 122

22. S. L. Smith, "Void Fraction in Two-Phase Flow: A Correlation Based Upon an Equal Velocity Head Model", Proc. Instn. Mech. Engrs., 1969-1970, Vol 184, Part 1, No. 36; p. 647

23. S. Levy, "Steam Slip-Theoretical Prediction from Momentum Model", Trans. ASME, Journal of Heat Transfer; May 1960, p. 113

24. J. T. Rogers and N. E. Todreas, "Coolant Interchange Mixing in Reactor Fuel Rod Bundles Single-Phase Coolants", Heat Transfer in Rod Bundles, Winter Annual ASME Heat Transfer Meeting; December 1968, p. 1

Appendix A

DYNAMIC EFFECTS IN VOID MEASUREMENTS BY RADIATION SCATTERING

Appendix A

DYNAMIC EFFECTS IN VOID MEASUREMENTS BY RADIATION SCATTERING

INTRODUCTION

In 1971, Harms and Forest investigated the error due to the time variation of voids that is introduced when radiation attenuation is used to measure the voids. The dynamic error in this case is due to the nonlinearity of the exponential attenuation curve that typifies the signal response. Because of this nonlinearity, the average of the response to the fluctuating voids is not the response to the average of the voids.

An additional mechanism is introduced using radiation scattering that is independent of the nonlinearity of the radiation attenuation curve. Typically, the signal response is a product of two terms: one related to the local volume where scattering occurs; the other related to the radiation paths through the fluid channel to and from the local scatter volume. The error is introduced because, in general, the average of a product is not equal to the product of the averages. The analysis presented here shows that the size of the dynamic error in radiation scattering is the same order of magnitude as in radiation attenuation given similar assumptions regarding the flow patterns. In addition, a method is developed to estimate the dynamic error in more generalized flow situations.

Detector Response

The following equations describe the response of the straight-through and a side detector, respectively, to the densities in the rod bundle:

$$N_1 = N_0 f_1 g_1 \varepsilon_1 \exp\left(-\mu_1 \rho_0 x - \mu_1 \rho_0 x_0\right) \tag{A-1}$$

$$N_2 = N_0 f_0 f_2 g_0 g_2 \varepsilon_2 \rho_{s2} C \exp\left(-\mu_1 \rho_0 x_0 - \mu_2 \rho_2 x_2\right) \tag{A-2}$$

To simplify the equations, the following definitions are used:

$$
\left.
\begin{aligned}
C_1 &= N_0 f_1 g_1 \varepsilon_1 \\
C_2 &= N_0 f_0 f_2 g_0 g_2 \varepsilon_2\ C \\
\sigma_1 &= \mu_1 x_1 + \mu_1 x_0 \\
\bar{\rho}_1 &= \frac{\mu_1 x_1 \rho_1 + \mu_1 x_0 \rho_0}{\mu_1 x_1 + \mu_1 x_0} \\
\sigma_2 &= \mu_1 x_0 + \mu_2 x_2 \\
\bar{\rho}_2 &= \frac{\mu_1 x_0 \rho_0 + \mu_2 x_2 \rho_2}{\mu_1 x_0 + \mu_2 x_2}
\end{aligned}
\right\} \quad \text{(A-3)}
$$

Substituting these definitions into Eq. A-1 and A-2 yields:

$$N_1 = C_1 \exp\ (-\sigma_1\ \bar{\rho}_1) \qquad \text{(A-4)}$$

$$N_2 = C_2\ \bar{\rho}_{s2}\ \exp\ (-\sigma_2\ \bar{\rho}_2) \qquad \text{(A-5)}$$

To further simplify the analysis, these equations will be altered to eliminate density in favor of void fraction. It will be assumed that attenuation and scatter in the void are negligible. This is not true in the case of high pressure steam-water mixtures, but the assumption is conservative. Finally, since this is an analysis of time variations, time must enter the equations as a variable.

Let $\alpha_{sv,a}$ and $\alpha_{bp,a}$ be the true instantaneous void fractions in the scatter volume and along the beam path respectively. The subscript (a) is used to denote the actual values as opposed to the calculated values introduced below. The averages of these void fractions over a time interval, τ, in which the measurement is made are found from:

$$\bar{\alpha}_{sv,a} = \frac{1}{\tau}\int_0^{\tau} \alpha_{sv,a}\,(t)\,dt \qquad \text{(A-6)}$$

$$\bar{\alpha}_{bp,a} = \frac{1}{\tau}\int_0^{\tau} \alpha_{bp,a}\,(t)\,dt \qquad \text{(A-7)}$$

The density terms of Eq. A-4 and A-5 are related to the void fraction as follows:

$$\bar{\rho}_2 = \rho_f\,(1 - \alpha_{bp,a}) \qquad \text{(A-8)}$$

$$\bar{\rho}_1 = \rho_f\,(1 - \alpha_{bp,a}) \qquad \text{(A-9)}$$

$$\bar{\rho}_{s2} = \rho_f\,(1 - \alpha_{sv,a}) \qquad \text{(A-10)}$$

where ρ_f is the density of the liquid phase.

These terms can be entered into Eq. A-4 and A-5 to obtain:

$$N_1(t) = C_1 \exp\,(\sigma_1\,\rho_f) \exp\,\left[-\sigma_1\,\rho_f\,\alpha_{bp,a}(t)\right] \qquad \text{(A-11)}$$

$$N_2(t) = C_2 \exp\,(\sigma_2\,\rho_f)\,\left[1 - \alpha_{sv,a}(t)\right] \exp\,\left[-\sigma_2\,\rho_f\,\alpha_{bp,a}(t)\right] \qquad \text{(A-12)}$$

Then, these can be simplified to:

$$N_1(t) = C_1' \exp\left[\lambda_1\,\alpha_{bp,a}(t)\right] \qquad \text{(A-13)}$$

$$N_2(t) = C_2'\left[1 - \alpha_{sv,a}(t)\right] \exp\,\left[-\lambda_2\,\alpha_{bp,a}(t)\right] \qquad \text{(A-14)}$$

By defining:

$$C_1' = C_1 \exp(\sigma_1 \rho_f) \tag{A-15}$$

$$C_2' = C_2 \rho_f \exp(\sigma_2 \rho_f) \tag{A-16}$$

$$\lambda_1 = \sigma_1 \rho_f \tag{A-17}$$

$$\lambda_2 = \sigma_2 \rho_f \tag{A-18}$$

Finally, we define the transmittance as:

$$T_1(t) = N_1(t)/C_1'$$

$$T_2(t) = N_2(t)/C_2'$$

so that:

$$T_1(t) = \exp\left[-\lambda_1 \alpha_{bp,a}(t)\right] \tag{A-19}$$

$$T_2(t) = \left[1 - \alpha_{sv,a}(t)\right] \exp\left[-\lambda_2 \alpha_{bp,a}(t)\right] \tag{A-20}$$

The average transmittance is obtained by integrating the instantaneous transmittance over the time interval, τ, of the measurement and then dividing by this interval.

$$\bar{T}_1 = \frac{1}{\tau}\int_0^{\tau} T_1(t)\ dt \tag{A-21}$$

$$\bar{T}_2 = \frac{1}{\tau}\int_0^{\tau} T_2(t)\ dt \tag{A-22}$$

Eq. A-23 reduces the detector response to density:

$$\rho_{s2}^{e} = \rho_{s2}^{r} \left(\frac{N_2^{e}}{N_2^{r}} \right) \left(\frac{N_1^{r}}{N_1^{e}} \right)^{q_2} \tag{A-23}$$

Eq. A-23 can be simplified for this analysis by realizing that the reference values are obtained with zero void fraction. The transmittances for both detectors for the reference case are therefore both unity. In terms of transmittance, Eq. A-23 can then be written as:

$$\rho_{s2}^{e} = \rho_f \ \overline{T}_2 \ (\overline{T}_1)^{q_2} \tag{A-24}$$

From Eq. A-3, A-17, and A-18, we determined that $q_2 = \lambda_2/\lambda_1$. The calculated void fraction in the scatter volume $\overline{\alpha}_{sv,c}$ is related to the scatter volume density by:

$$\rho_{s2}^{e} = \rho_f \ (1 - \overline{\alpha}_{sv,c}) \tag{A-25}$$

Substituting Eq. A-25 into Eq. A-24 and rearranging yields:

$$\overline{\alpha}_{sv,c} = 1 - \overline{T}_2 \ (\overline{T}_1)^{q_2} \tag{A-26}$$

METHOD OF ANALYSIS

The dynamic error, E, is defined as the difference between the actual average scatter volume void fraction and the calculated average scatter volume void fraction as follows:

$$E = \overline{\alpha}_{sv,c} - \overline{\alpha}_{sv,a} \tag{A-27}$$

To calculate the dynamic error, it is necessary to assume a flow pattern. The instantaneous transmittance will be calculated from Eq. A-19 and A-20 which will be used to determine the average transmittance according to Eq. A-21 and A-22. These values will then be used in Eq. A-24 to calculate the scatter volume void fraction. It should be noted that this value will be in error because of the

assumption of a constant void fraction. This value will then be compared to the true value determined directly from the flow pattern in Eq. A-27. Two flow patterns will be assumed: the first is a conservative worst case pattern; the second is a generalized flow pattern in which better estimates of the error and sensitivity to the parameters can be determined.

Worst Case Flow Pattern

A worst case flow pattern was first investigated by Harms and Forest in their paper on attenuation errors. They proposed this model since it gave the largest possible errors in attenuation measurements. In radiation scattering, the worst case is not the one proposed by Harms and Forest but is rather a pattern where the voids in the scatter volume are varying 180° out of phase with the rest of the flow channel. Since this is an improbable pattern, the one proposed by Harms and Forest is analyzed as a "worst case".

The pattern can be physically thought of as a series of liquid slugs traveling down the flow channel separated from each other by gas. Each fluid slug fills the entire cross-section. Both the beam path and the scatter volume are either entirely liquid or entirely gas at the same time. It is assumed that the time duration of each slug is much less than the time interval of the measurement. The individual slugs can be combined mathematically into one large slug for easy analysis leading to:

$$\alpha_{sv,a}(t) = \alpha_{bp,a}(t) = \left\{ \begin{array}{l} 1,\ 0 \le t \le \tau\bar{\alpha}_{sv,a} \\ 0,\ \tau\bar{\alpha}_{sv,a} \le t \le \tau \end{array} \right\} \qquad \text{(A-28)}$$

This expression is consistent with the definition of $\alpha_{sv,a}$ and $\alpha_{bp,a}$ given in Eq. A-6 and A-7, respectively. Following the procedure outlined above we get:

$$\bar{T}_1 = \frac{\tau\,\bar{\alpha}_{sv,a}\ \exp(0) + (\tau - \tau\,\bar{\alpha}_{sv,a})\ \exp(-\lambda_1)}{\tau} \qquad \text{(A-29)}$$

$$\bar{T}_1 = \bar{\alpha}_{sv,a} + (1 - \bar{\alpha}_{sv,a})\ \exp(-\lambda_1)$$

and

$$\overline{T}_2 = 0 + (\tau - \tau\,\overline{\alpha}_{sv,a}) \quad (1 - 0) \exp\left(-\lambda_2(1 - 0)\right) \tag{A-30}$$

$$\overline{T}_2 = (1 - \overline{\alpha}_{sv,a}) \exp\ (-\lambda_2)$$

Then from Eq. A-26:

$$\overline{\alpha}_{sv,c} = 1 - \frac{(1 - \overline{\alpha}_{sv,a})}{\left(\overline{\alpha}_{sv,a} \exp\ (\lambda_1) + 1 - \overline{\alpha}_{sv,a}\right)^{\lambda_2/\lambda_1}} \tag{A-31}$$

where we have used $q_2 = \lambda_2/\lambda_1$. Finally, from Eq. A-27:

$$E = (1 - \overline{\alpha}_{sv,a}) \left[1 - \frac{1}{\left(\overline{\alpha}_{sv,a} \exp\ (\lambda_1) + 1 - \alpha_{sv,a}\right)^{\lambda_2/\lambda_1}}\right] \tag{A-32}$$

For λ_2 and λ_1 less than 1, which is applicable to this test, this expression can be simplified to:

$$E = \alpha_{sv,a} (1 - \alpha_{sv,a}) \quad \lambda_2 \tag{A-33}$$

with a negligible error introduced. This error is maximized for a void fraction equal to 0.5. The value of λ_2 where the entire flow channel is involved in slugging is about 0.48. This leads to a maximum error of 0.12, so that if the actual void fraction is 0.50, the measured void fraction is 0.62.

Generalized Flow Pattern

A more general approach to the estimate of dynamic errors incorporates information about the diameter of the voids. Assume each subchannel is independent of the others and contains either all liquid or all void at any given time. The average void fraction in each subchannel is $\overline{\alpha}_{k,a}$, where k denotes the kth subchannel. Over a given interval of time, the fraction of the time the subchannel contains void is $\overline{\alpha}_{k,a}$. The scatter volume is assumed to be contained completely within one subchannel.

It is also assumed that the average void fraction in each subchannel is the same, since the dynamic error is not highly dependent on the distribution of the void fraction among the subchannels but rather on the average void fraction over all the subchannels. This simplifies the analysis and allows the subscript k to be dropped. In a given instant of time, the probability that the scatter volume contains liquid and is causing scattering is $1 - \bar{\alpha}_a$. The probability that the other n-1 subchannels contain k voids -- in other words, the probability that the instantaneous beam path void fraction is k/n given that the scatter volume contains liquid -- is found from the binomial distribution as:

$$P(k) = \frac{(n-1)!}{k!\,(n-1-k)!}\,\bar{\alpha}_a^{\,k}\,(1 - \bar{\alpha}_a)^{n-1-k} \qquad \text{(A-34)}$$

The total probability that there are k voids and a liquid scatter volume is:

$$P(k)_{liquid} = (1 - \bar{\alpha}_a)\,\frac{(n-1)!}{k!\,(n-1-k)!}\,\bar{\alpha}_a^{\,k}\,(1 - \bar{\alpha}_a)^{n-1-k} \qquad \text{(A-35)}$$

The instantaneous transmittance given k voids and a liquid scatter volume is:

$$T_2(k)_{liquid} = 1 * \exp\left[-\lambda_2\,(1 - k/n)\right] \qquad \text{(A-36)}$$

The instantaneous transmittance given a voided scatter volume is zero so that the average transmittance is found by summing the product $P_{k,liquid}$ and $T_{k,liquid}$ over all k from 0 to n-1.

$$\bar{T}_2 = \sum_{k=0}^{n-1} (1 - \bar{\alpha}_a)\,\frac{(n-1)!}{k!\,(n-1-k)!}\,\bar{\alpha}_a^{\,k}\,(1 - \bar{\alpha}_a)^{n-1-k}\,\exp\left[-\lambda_2\,(1 - k/n)\right] \qquad \text{(A-37)}$$

$$\bar{T}_2 = (1 - \bar{\alpha}_a)\,e^{-\lambda_2} \sum_{k=0}^{n-1} \frac{(n-1)!}{k!\,(n-1-k)!}\left[\bar{\alpha}_a \exp(\lambda_2/n)\right]^k (1 - \bar{\alpha}_a)^{n-1-k}$$

Recognizing the summation as a binomial expansion leads to a more compact expression:

$$\bar{T}_2 = (1 - \bar{\alpha}_a)\, e^{-\lambda_2} \left[\bar{\alpha}_a \exp(\lambda_2/n) + 1 + \bar{\alpha} \right]^{n-1} \tag{A-38}$$

The same type of analysis can be done for the straight-through detector. This leads to:

$$\bar{T}_1 = e^{-\lambda_1} \left[\bar{\alpha}_a \exp(\lambda_1/n) + 1 - \bar{\alpha} \right]^{n} \tag{A-39}$$

In general, the number of slugs encountered by the scattered and unscattered gammas are different. Therefore, in combining Eq. A-38 and A-39 into Eq. A-26, the number of slugs must be differentiated as follows:

$$\bar{\alpha}_c = 1 - (1 - \bar{\alpha}_a) \frac{\left[\bar{\alpha}_a \exp(\lambda_2/n_2) + 1 - \bar{\alpha}_a \right]^{n_2 - 1}}{\left[\bar{\alpha}_a \exp(\lambda_1/n_1) + 1 - \bar{\alpha}_a \right]^{n_1 \lambda_2/\lambda_1}} \tag{A-40}$$

Finally, from Eq. A-27:

$$E = (1 - \bar{\alpha}_a) \left[1 - \frac{\left(\bar{\alpha}_a \exp(\lambda_2/n_2) + 1 - \bar{\alpha}_a \right)^{n_2 - 1}}{\left(\bar{\alpha}_a \exp(\lambda_1/n_1) + 1 - \bar{\alpha}_a \right)^{n_1 \lambda_2/\lambda_1}} \right] \tag{A-41}$$

For values of λ_1 and λ_2 that are less than one, this expression can be simplified with negligible loss of accuracy to:

$$E = \frac{\bar{\alpha}_a (1 - \bar{\alpha}_a)\ \lambda_2}{n_2} \tag{A-42}$$

For this experiment, λ_1 and λ_2 are both less than one so this simplification applies. The absolute value of E reaches a maximum at a void fraction of 0.5. We can therefore write:

$$E_{max} = \frac{\lambda_2}{4n_2} \tag{A-43}$$

To estimate the possible maximum dynamic bias error for the present experiment, slugging is assumed to be occurring in each subchannel. A gamma path in and out of the bundle crosses five subchannels so that $n_2 = 5$. The slugs are assumed to occupy the entire inscribed circular region between the four rods that define the subchannel. To maintain conservatism, the density of the liquid slugs is assumed the saturated value and the density of the vapor is assumed zero. With these assumptions, the value of λ_2 is found to be 0.249 so that:

$$E_{max} = \frac{0.249}{(4)(5)} \tag{A-44}$$

$$E_{max} = 0.0125$$

Since slugging is expected to occur over only a small portion of the test conditions, if at all, and since its true effect is expected to be somewhat less than that given in Eq. A-44, the dyanmic bias error was decided to be negligible.

Appendix B

DATA

Appendix B

DATA

This appendix contains the output data listings. The data are presented in both SI units and English units. Further, the data are grouped in sections according to the nominal thermal-hydraulic conditions specified by the data matrix (see Section 4 of the main body of this report). These nominal conditions are displayed above each data listing. The CODE value is an arbitrary number assigned to a thermal-hydraulic grouping to aid in specifying the group.

Within each group, the data are listed in order of increasing inlet temperature. There are 14 columns of information listed for each data point. They are:

RUN	-	Each data point has a unique run number assigned at the time the data were taken.
REF CODE	-	The reference code assigns the specific reduction constants (listed in Table 4-3 - Section 4) to the data point. These constants are used in the first collimator set data reduction. Since a different reduction technique was used for collimator set 2 data points, no reference codes are listed for them.
PRESSURE	-	This absolute pressure is measured near the exit of the test bundle.
HEAT FLUX	-	This is the average bundle heat flux. Conversion to individual subchannel heat flux is provided by Table 4-2 - Section 4.
FLOW RATE	-	This is the average mass flux in the bundle.
INLET TEMP	-	This represents the temperature of the water entering the test vessel.
GAMMA RATE (1)(2)(3) (3 Columns)	-	These numbers, produced by the multichannel analyzer reduction algorithm, represent the average number of gammas counted per second. The specifiers -- 1, 2, and 3 -- refer to the straight-through detector and the two side detectors, respectively.

QUALITY - This is the average bundle quality at the plane of the void measurements.

DENSITY (SIDE 2/3) (GAP/CENTER) (2 Columns) - The density values given in the tables are calculated by the reduction routines outlined in Section 4. The two values result from the two gamma detectors used in each measurement. The scatter volume seen by each detector was nominally identical in Runs 69 through 492, although the second side detector malfunctioned in Runs 468 through 492. After Run 511, the first density was measured in the gap region of the subchannel and the second density was measured in the center region.

VOID (SIDE 2/3) (GAP/CENTER) (2 Columns) - The void fraction values are calculated from the procedures given in Section 4. Each value corresponds to the same region of the subchannel as the density values described above.

UNIT OF MEASUREMENT
CROSS-REFERENCE

SI Units	Parameter	English Units
MPa	PRESSURE	psia
$kg/m^2 \cdot sec$	FLOW RATE	$Mlb/hr \cdot ft^2$
kW/m^2	HEAT FLUX	$MBtu/hr \cdot ft^2$
°C	TEMPERATURE	°F
Counts/sec	GAMMA RATE	Counts/sec
kg/m^3	DENSITY	lbm/ft^3
%	VOID FRACTION	%

SI UNITS

FINAL DATA (SI UNITS)

PRESSURE ------- 16.90 MPa
FLOW RATE ------ 1357. Kg/M^2-Sec
HEAT FLUX ------ 315. Kw/M^2
CODE ---------- 1

RUN	REF CODE	PRESURE	HEAT FLUX	FLOW RATE	INLET TEMP	GAMMA RATE 1	GAMMA RATE 2	GAMMA RATE 3	QUALITY	DENSITY (SIDE 2)	DENSITY (SIDE 3)	VOID (SIDE 2)	VOID (SIDE 3)
76	1	16.90	297.1	1357.	305.7	271.58	150.29	121.14	-0.2206	664.9	658.1	-1.43	0.07
77	1	16.89	296.8	1353.	311.4	275.44	147.20	120.45	-0.1821	638.6	642.3	1.06	0.20
78	1	16.89	294.9	1372.	316.2	276.16	145.77	120.07	-0.1535	629.6	637.9	0.43	-1.52
79	1	16.91	296.1	1359.	322.9	279.63	147.21	116.81	-0.1061	627.3	607.1	-4.30	0.79
80	1	16.90	292.4	1366.	327.5	283.16	140.79	114.75	-0.0749	587.2	584.7	2.27	2.93
81	1	16.90	292.7	1364.	333.1	288.20	137.44	112.95	-0.0316	559.2	560.9	4.57	4.10
82	1	16.88	294.6	1365.	338.9	298.58	123.68	101.93	0.0183	473.5	470.4	23.11	24.10
83	1	16.90	293.6	1357.	342.4	306.04	119.49	95.44	0.0485	441.0	417.7	29.43	36.31

PRESSURE ------- 16.90 MPa
FLOW RATE ------ 1357. Kg/M^2-Sec
HEAT FLUX ------ 631. Kw/M^2
CODE ---------- 2

RUN	REF CODE	PRESURE	HEAT FLUX	FLOW RATE	INLET TEMP	GAMMA RATE 1	GAMMA RATE 2	GAMMA RATE 3	QUALITY	DENSITY (SIDE 2)	DENSITY (SIDE 3)	VOID (SIDE 2)	VOID (SIDE 3)
90	2	16.87	594.8	1367.	279.4	269.53	148.61	122.22	-0.2325	659.2	663.5	-0.38	-1.33
91	2	16.88	596.1	1361.	280.3	269.78	147.90	121.06	-0.2265	654.8	655.1	-0.01	-0.06
92	2	16.88	596.1	1358.	286.1	273.14	146.78	121.47	-0.1912	639.7	647.9	0.18	-1.70
93	2	16.88	597.0	1356.	291.8	275.01	145.60	121.31	-0.1569	628.7	641.6	-0.65	-3.74
94	2	16.88	596.4	1357.	298.1	280.19	142.10	117.79	-0.1187	597.9	604.6	2.83	1.11
95	2	16.88	597.0	1377.	302.8	282.95	140.25	114.17	-0.0936	582.1	574.6	3.97	6.06
96	2	16.85	598.0	1360.	305.8	283.81	136.39	112.09	-0.0682	561.6	559.3	6.62	7.22
97	2	16.88	598.6	1373.	308.1	287.17	137.09	110.17	-0.0574	557.0	539.3	6.36	11.26
98	2	16.87	598.0	1360.	312.1	292.71	130.24	106.66	-0.0291	512.7	505.2	15.36	17.39
99	2	16.85	598.9	1359.	314.8	295.66	124.91	101.86	-0.0094	482.1	470.0	21.97	25.35
100	2	16.89	598.3	1365.	320.2	302.58	114.60	95.86	0.0244	422.8	421.1	35.53	36.02
101	2	16.83	598.6	1343.	323.4	310.60	108.39	89.14	0.0549	382.4	368.7	44.71	48.72

PRESSURE ------- 16.90 MPa
FLOW RATE ------ 3122. Kg/M^2-Sec
HEAT FLUX ------ 631. Kw/M^2
CODE ---------- 3

RUN	REF CODE	PRESURE	HEAT FLUX	FLOW RATE	INLET TEMP	GAMMA RATE 1	GAMMA RATE 2	GAMMA RATE 3	QUALITY	DENSITY (SIDE 2)	DENSITY (SIDE 3)	VOID (SIDE 2)	VOID (SIDE 3)
102	2	16.96	598.0	2957.	309.5	270.63	151.14	123.66	-0.2110	668.7	669.8	-3.36	-3.59
103	2	16.95	596.7	2892.	313.8	273.19	148.65	121.83	-0.1791	648.9	650.2	-1.81	-2.11
104	2	16.94	598.0	2867.	317.8	275.40	146.33	119.57	-0.1501	631.3	629.1	-0.54	-0.02
105	2	16.94	597.0	2878.	323.3	279.17	145.38	117.89	-0.1123	616.5	607.9	-0.96	1.18
106	2	16.95	595.1	2875.	328.9	282.26	140.90	115.51	-0.0716	587.0	584.8	1.73	2.30
107	2	16.96	595.1	2878.	334.6	286.75	138.51	111.84	-0.0277	564.7	550.6	2.30	6.24
108	2	16.95	595.1	2869.	338.0	292.86	129.90	106.33	0.0014	510.8	502.9	14.06	16.32
109	2	16.96	595.1	2837.	340.7	297.70	124.17	104.00	0.0254	474.7	478.7	21.76	20.60

FINAL DATA (SI UNITS)

PRESSURE ------- 15.17 MPa
FLOW RATE ------ 3122. Kg/M^2-Sec
HEAT FLUX ------ 631. Kw/M^2
CODE ---------- 4

RUN	REF CODE	PRESURE	HEAT FLUX	FLOW RATE	INLET TEMP	GAMMA RATE 1	GAMMA RATE 2	GAMMA RATE 3	QUALITY	DENSITY (SIDE 2)	DENSITY (SIDE 3)	VOID (SIDE 2)	VOID (SIDE 3)
117	2	15.13	595.8	2857.	317.8	277.14	147.08	119.94	-0.0539	630.2	626.7	-1.85	-1.05
115	2	15.13	616.9	2856.	320.9	280.16	142.28	114.91	-0.0307	598.9	586.3	2.69	5.66
116	2	15.13	607.7	2814.	323.5	285.67	141.09	112.57	-0.0139	579.5	557.8	5.30	10.45
114	2	15.14	613.4	2841.	324.6	285.53	138.02	111.45	-0.0067	565.2	551.1	7.84	11.22
113	2	15.15	612.2	2852.	327.9	292.44	130.02	105.73	0.0132	512.2	500.1	18.46	21.40
112	2	15.15	610.9	2848.	329.3	295.00	124.36	103.35	0.0229	480.9	480.3	25.13	25.27
111	2	15.14	602.1	2893.	331.6	298.32	121.78	99.13	0.0355	462.7	448.3	28.48	32.10
110	2	15.15	599.9	2846.	335.3	308.01	112.26	91.80	0.0631	403.3	388.1	40.96	44.71

PRESSURE ------- 15.17 MPa
FLOW RATE ------ 1357. Kg/M^2-Sec
HEAT FLUX ------ 631. Kw/M^2
CODE ---------- 5

RUN	REF CODE	PRESURE	HEAT FLUX	FLOW RATE	INLET TEMP	GAMMA RATE 1	GAMMA RATE 2	GAMMA RATE 3	QUALITY	DENSITY (SIDE 2)	DENSITY (SIDE 3)	VOID (SIDE 2)	VOID (SIDE 3)
127	3	15.16	594.2	1367.	280.9	270.12	147.69	120.42	-0.1263	649.7	648.1	-0.06	0.28
126	3	15.15	598.0	1368.	286.1	273.11	144.44	118.81	-0.0980	625.1	629.0	2.42	1.59
125	3	15.12	596.4	1354.	294.6	282.22	136.85	112.70	-0.0494	564.8	565.6	11.05	10.87
119	3	15.12	598.9	1363.	300.3	287.64	131.38	107.33	-0.0194	526.4	519.2	17.05	18.71
120	3	15.12	598.0	1368.	303.0	291.01	124.01	101.61	-0.0059	485.0	476.7	25.53	27.46
121	3	15.07	595.8	1363.	308.5	298.20	113.18	92.89	0.0273	421.9	410.2	37.98	40.86
122	3	15.16	594.8	1370.	314.4	304.72	104.35	86.13	0.0567	371.9	359.5	48.16	51.21
123	3	15.14	594.2	1362.	321.1	315.84	96.40	81.06	0.0999	321.9	314.2	58.06	59.97
124	3	15.17	594.5	1366.	326.4	321.53	92.30	76.84	0.1322	297.5	283.5	62.61	66.18

PRESSURE ------- 13.79 MPa
FLOW RATE ------ 1357. Kg/M^2-Sec
HEAT FLUX ------ 631. Kw/M^2
CODE ---------- 6

RUN	REF CODE	PRESURE	HEAT FLUX	FLOW RATE	INLET TEMP	GAMMA RATE 1	GAMMA RATE 2	GAMMA RATE 3	QUALITY	DENSITY (SIDE 2)	DENSITY (SIDE 3)	VOID (SIDE 2)	VOID (SIDE 3)
128	3	13.78	593.5	1356.	235.8	252.63	157.93	127.27	-0.2654	758.6	751.7	-3.54	-2.37
129	3	13.77	593.9	1365.	245.1	256.88	156.63	126.52	-0.2262	737.0	731.6	-2.65	-1.71
130	3	13.78	596.4	1361.	263.1	261.74	152.35	123.83	-0.1455	698.7	696.8	-2.52	-2.17
131	3	13.78	592.0	1364.	286.7	279.90	139.74	114.37	-0.0381	584.4	582.0	10.06	10.54
132	3	13.78	592.6	1364.	294.9	289.93	122.96	98.34	0.0025	482.3	458.8	28.15	33.11
133	3	13.78	594.8	1371.	303.8	305.40	105.57	86.86	0.0472	376.2	362.6	48.10	51.16
134	3	13.81	592.3	1371.	309.9	311.48	97.24	81.21	0.0777	331.2	321.1	56.52	58.79
135	3	13.81	593.2	1365.	315.1	320.98	90.93	77.13	0.1072	292.5	285.7	63.87	65.41
136	3	13.85	593.5	1349.	319.0	322.82	84.46	72.55	0.1312	263.6	258.4	69.52	70.69

FINAL DATA (SI UNITS)

PRESSURE ------- 13.79 MPa
FLOW RATE ------ 3122. Kg/M^2-Sec
HEAT FLUX ------ 631. Kw/M^2
CODE ---------- 7

RUN	REF CODE	PRESURE	HEAT FLUX	FLOW RATE	INLET TEMP	GAMMA RATE 1	GAMMA RATE 2	GAMMA RATE 3	QUALITY	DENSITY (SIDE 2)	DENSITY (SIDE 3)	VOID (SIDE 2)	VOID (SIDE 3)
144	3	13.76	590.4	3115.	285.2	262.59	155.00	125.81	-0.1759	709.7	707.6	-0.68	-0.30
143	3	13.85	590.4	3130.	289.6	263.54	155.18	125.43	-0.1594	707.6	701.9	-1.93	-0.90
142	3	13.84	590.7	3094.	294.4	265.00	151.83	122.96	-0.1338	685.8	680.5	-0.05	0.93
141	3	13.86	592.6	3086.	300.2	267.91	150.59	121.83	-0.1053	670.8	664.1	0.20	1.48
140	3	13.86	591.7	3120.	305.5	270.38	150.80	121.35	-0.0786	664.6	653.5	-1.10	1.09
139	3	13.86	591.7	3120.	311.3	274.16	147.26	119.41	-0.0476	636.2	629.9	1.37	2.64
137	3	13.89	592.6	3113.	316.4	277.22	145.86	116.88	-0.0201	621.0	605.2	1.55	4.94
138	3	13.85	592.0	3113.	318.7	281.24	139.16	114.17	-0.0055	578.3	577.4	9.25	9.45

PRESSURE ------- 11.03 MPa
FLOW RATE ------ 3122. Kg/M^2-Sec
HEAT FLUX ------ 631. Kw/M^2
CODE ---------- 8

RUN	REF CODE	PRESURE	HEAT FLUX	FLOW RATE	INLET TEMP	GAMMA RATE 1	GAMMA RATE 2	GAMMA RATE 3	QUALITY	DENSITY (SIDE 2)	DENSITY (SIDE 3)	VOID (SIDE 2)	VOID (SIDE 3)
145	3	11.01	587.2	3118.	247.3	248.88	160.33	131.65	-0.2128	785.2	796.9	-1.98	-3.73
146	3	10.96	589.8	3124.	260.1	254.99	157.72	127.64	-0.1616	749.2	745.9	0.13	0.65
147	3	10.99	593.5	3135.	280.2	261.54	157.09	128.84	-0.0825	723.9	731.8	-2.07	-3.37
148	3	11.01	593.9	3117.	288.1	265.66	152.24	125.41	-0.0495	685.9	695.0	1.33	-0.22
154	3	11.02	597.0	3109.	293.8	268.48	151.00	121.91	-0.0249	671.1	662.9	1.74	3.19
149	3	11.01	592.9	3098.	297.5	272.60	145.79	116.22	-0.0084	633.2	613.4	6.87	10.42
153	3	11.04	596.1	3098.	302.9	285.15	125.08	102.52	0.0150	502.2	494.8	28.59	30.01
150	3	10.97	590.7	3105.	304.5	292.24	120.93	99.42	0.0236	468.2	460.8	34.37	35.71
151	3	11.04	595.8	3114.	308.0	298.46	109.80	91.13	0.0384	406.2	399.3	44.76	46.04
152	3	11.08	596.4	3080.	309.4	300.95	107.72	90.48	0.0447	392.8	391.1	46.88	47.18

PRESSURE ------- 11.03 MPa
FLOW RATE ------ 1357. Kg/M^2-Sec
HEAT FLUX ------ 631. Kw/M^2
CODE ---------- 9

RUN	REF CODE	PRESURE	HEAT FLUX	FLOW RATE	INLET TEMP	GAMMA RATE 1	GAMMA RATE 2	GAMMA RATE 3	QUALITY	DENSITY (SIDE 2)	DENSITY (SIDE 3)	VOID (SIDE 2)	VOID (SIDE 3)
165	3	11.03	592.9	1365.	249.6	259.11	155.58	125.33	-0.0910	724.0	715.7	-2.56	-1.18
164	3	11.03	600.5	1361.	257.8	265.61	151.62	123.27	-0.0561	682.9	680.7	1.26	1.62
163	3	11.03	600.5	1357.	265.6	275.52	136.52	113.71	-0.0251	579.7	589.2	16.77	15.08
160	3	11.05	597.3	1364.	269.7	281.74	129.77	106.05	-0.0114	532.0	524.7	24.23	25.55
161	3	11.08	594.2	1360.	275.7	291.09	110.37	91.84	0.0108	421.6	416.8	42.71	43.59
162	3	11.04	597.6	1357.	279.6	302.12	90.00	78.34	0.0297	312.1	317.8	61.80	60.77
159	3	11.00	595.8	1362.	283.8	307.98	78.90	69.23	0.0471	256.2	257.1	71.32	71.15
158	3	11.01	598.0	1362.	293.1	321.94	73.96	64.62	0.0869	221.0	215.8	76.72	77.64
157	3	11.04	597.3	1362.	299.1	325.99	72.35	62.63	0.1123	210.6	201.1	78.09	79.85
156	3	11.04	595.8	1362.	305.0	330.78	69.80	61.27	0.1386	196.2	189.4	80.25	81.53
155	3	11.04	596.1	1357.	307.6	331.27	67.54	59.77	0.1515	186.7	180.9	81.79	82.87

FINAL DATA (SI UNITS)

PRESSURE ------- 11.03 MPa
FLOW RATE ------ 679. Kg/M^2-Sec
HEAT FLUX ------ 631. Kw/M^2
CODE ---------- 10

RUN	REF CODE	PRESURE	HEAT FLUX	FLOW RATE	INLET TEMP	GAMMA RATE 1	GAMMA RATE 2	GAMMA RATE 3	QUALITY	DENSITY (SIDE 2)	DENSITY (SIDE 3)	VOID (SIDE 2)	VOID (SIDE 3)
171	4	11.05	594.2	688.	192.1	261.80	152.92	122.07	-0.1010	697.7	681.6	0.78	3.51
170	4	11.06	594.2	686.	200.8	267.68	147.19	118.05	-0.0694	650.6	636.6	6.03	8.48
169	4	11.05	594.5	689.	206.5	273.15	141.56	115.23	-0.0505	607.3	602.6	12.12	12.96
172	4	11.05	595.8	688.	209.1	277.11	136.77	109.14	-0.0397	573.7	552.9	17.23	20.95
173	4	11.06	595.8	688.	212.9	281.17	129.78	103.03	-0.0262	530.3	504.3	23.91	28.70
174	4	11.04	595.1	689.	215.4	284.36	121.15	99.81	-0.0178	482.3	477.0	32.15	33.11
176	4	11.04	595.4	684.	218.6	289.65	108.62	92.04	-0.0032	413.5	418.3	43.78	42.90
175	4	11.06	594.8	685.	221.1	292.17	102.17	85.07	0.0042	379.4	371.2	49.63	51.12
177	4	11.06	594.2	685.	224.8	297.65	89.83	77.34	0.0177	315.2	316.2	60.88	60.69
178	4	11.06	595.1	687.	227.2	299.50	83.69	73.85	0.0256	285.2	292.8	66.09	64.69
179	4	11.04	590.7	682.	232.2	306.83	75.80	66.90	0.0447	241.9	243.0	73.40	73.21
180	4	11.06	589.4	682.	235.9	310.58	75.21	67.07	0.0567	235.5	239.7	74.30	73.53
181	4	11.07	589.8	684.	238.2	311.62	72.24	65.01	0.0638	221.7	226.8	76.66	75.72
182	4	11.07	589.1	685.	246.3	321.24	74.59	65.08	0.0937	222.4	217.1	75.84	76.83

PRESSURE ------- 6.90 MPa
FLOW RATE ------ 679. Kg/M^2-Sec
HEAT FLUX ------ 631. Kw/M^2
CODE ---------- 11

RUN	REF CODE	PRESURE	HEAT FLUX	FLOW RATE	INLET TEMP	GAMMA RATE 1	GAMMA RATE 2	GAMMA RATE 3	QUALITY	DENSITY (SIDE 2)	DENSITY (SIDE 3)	VOID (SIDE 2)	VOID (SIDE 3)
190	4	6.90	597.3	683.	142.4	251.13	156.19	125.24	-0.0978	750.5	739.4	3.38	4.94
189	4	6.93	594.2	684.	158.0	266.86	125.24	103.54	-0.0566	541.7	541.9	30.55	30.53
188	4	6.91	593.9	686.	167.2	280.09	100.87	85.20	-0.0311	393.8	393.4	50.96	51.00
187	4	6.91	593.5	685.	180.4	295.61	85.10	72.60	0.0073	296.5	290.7	64.14	65.01
186	4	6.88	594.2	686.	190.2	310.94	71.12	61.95	0.0369	217.6	210.2	75.37	76.49
185	4	6.88	582.2	686.	206.4	324.49	59.75	57.69	0.0777	158.5	173.7	83.78	81.41
184	4	6.89	593.2	687.	217.7	331.19	55.17	53.19	0.1171	135.5	144.2	86.88	85.51
183	4	6.89	594.5	685.	232.9	340.23	51.35	48.67	0.1655	115.1	114.2	89.62	89.76

PRESSURE ------- 6.90 MPa
FLOW RATE ------ 1357. Kg/M^2-Sec
HEAT FLUX ------ 631. Kw/M^2
CODE ---------- 12

RUN	REF CODE	PRESURE	HEAT FLUX	FLOW RATE	INLET TEMP	GAMMA RATE 1	GAMMA RATE 2	GAMMA RATE 3	QUALITY	DENSITY (SIDE 2)	DENSITY (SIDE 3)	VOID (SIDE 2)	VOID (SIDE 3)
191	4	6.90	593.2	1365.	191.5	246.91	163.88	129.90	-0.1266	808.0	788.5	-1.21	1.44
192	4	6.90	592.9	1370.	199.2	247.84	161.60	130.21	-0.1047	792.0	787.2	-0.49	0.16
193	4	6.90	593.9	1358.	218.0	258.17	155.80	124.40	-0.0470	724.4	709.3	4.85	7.01
195	4	6.90	594.5	1358.	225.3	270.32	119.69	99.59	-0.0245	505.6	507.2	35.13	34.91
194	4	6.90	593.2	1361.	230.9	281.82	92.82	81.11	-0.0078	352.3	364.4	56.88	55.10
196	4	6.89	595.8	1361.	237.1	297.57	87.80	74.71	0.0122	306.1	300.6	63.09	63.91
197	4	6.94	595.4	1360.	251.4	318.58	66.52	60.92	0.0559	191.2	196.8	79.41	78.56
198	4	6.90	596.4	1357.	264.8	331.93	58.50	51.44	0.1014	148.4	134.3	85.28	87.43
199	4	6.92	595.4	1358.	271.2	338.14	56.35	51.35	0.1216	135.9	129.5	87.00	87.98

FINAL DATA (SI UNITS)

PRESSURE ------- 16.90 MPa
FLOW RATE ------ 3122. Kg/M^2-Sec
HEAT FLUX ------ 1262. Kw/M^2
CODE ---------- 13

RUN	REF CODE	PRESURE	HEAT FLUX	FLOW RATE	INLET TEMP	GAMMA RATE 1	GAMMA RATE 2	GAMMA RATE 3	QUALITY	DENSITY (SIDE 2)	DENSITY (SIDE 3)	VOID (SIDE 2)	VOID (SIDE 3)
228	7	16.90	1195.0	3100.	293.0	273.61	145.50	116.34	-0.1876	630.9	629.3	2.11	2.48
229	7	16.87	1191.2	3109.	300.4	275.96	145.10	114.47	-0.1418	622.7	610.5	-0.26	2.69
234	7	16.90	1195.3	3109.	309.0	279.89	139.53	112.25	-0.0874	585.5	585.6	2.70	2.68
230	7	16.86	1187.4	3108.	318.5	288.56	130.25	102.41	-0.0232	521.5	502.2	12.79	18.10
231	7	16.90	1193.7	3118.	323.3	294.79	121.11	98.42	0.0085	466.8	464.4	24.79	25.46
232	7	16.85	1195.3	3085.	327.4	303.96	112.86	91.93	0.0437	413.5	408.1	36.85	38.49
233	7	16.91	1193.7	2963.	332.8	314.03	101.93	83.81	0.0931	350.9	344.5	51.35	53.31

PRESSURE ------- 11.03 MPa
FLOW RATE ------ 3122. Kg/M^2-Sec
HEAT FLUX ------ 315. Kw/M^2
CODE ---------- 14

RUN	REF CODE	PRESURE	HEAT FLUX	FLOW RATE	INLET TEMP	GAMMA RATE 1	GAMMA RATE 2	GAMMA RATE 3	QUALITY	DENSITY (SIDE 2)	DENSITY (SIDE 3)	VOID (SIDE 2)	VOID (SIDE 3)
244	9	11.09	293.6	3113.	277.7	263.93	155.71	125.34	-0.1409	751.5	748.7	-1.73	-1.29
245	9	11.09	293.0	3112.	288.6	267.42	153.85	122.66	-0.0954	730.1	718.1	-1.88	0.10
246	9	11.07	294.9	3100.	300.6	271.18	148.86	121.21	-0.0416	692.1	696.0	-0.16	-0.84
247	9	11.10	295.8	3100.	304.6	273.12	149.91	121.45	-0.0244	691.8	691.7	-1.71	-1.70
248	9	11.10	297.1	3101.	307.0	277.30	147.75	117.93	-0.0127	668.5	655.2	1.19	3.56
249	9	11.01	297.1	3124.	309.2	282.79	141.57	118.14	0.0000	622.2	641.2	8.52	5.09
250	9	11.01	298.7	3117.	312.1	291.69	127.39	106.14	0.0147	531.0	540.3	23.79	22.10

PRESSURE ------- 11.03 MPa
FLOW RATE ------ 3122. Kg/M^2-Sec
HEAT FLUX ------ 1262. Kw/M^2
CODE ---------- 15

RUN	REF CODE	PRESURE	HEAT FLUX	FLOW RATE	INLET TEMP	GAMMA RATE 1	GAMMA RATE 2	GAMMA RATE 3	QUALITY	DENSITY (SIDE 2)	DENSITY (SIDE 3)	VOID (SIDE 2)	VOID (SIDE 3)
252	25	11.04	1191.5	3099.	232.8	258.57	155.27	124.99	-0.1771	754.2	736.4	-0.48	2.30
253	25	11.02	1195.6	3117.	251.6	264.26	149.77	124.19	-0.1063	706.0	711.9	1.99	1.02
254	25	11.04	1195.3	3107.	266.2	271.46	146.82	120.13	-0.0499	668.7	661.9	3.40	4.57
255	25	11.04	1196.6	3107.	276.8	286.97	129.43	106.48	-0.0076	541.6	532.3	22.44	24.11
256	25	11.01	1198.4	3100.	283.7	300.47	108.15	91.53	0.0230	414.2	412.4	43.62	43.93
257	25	11.02	1196.2	3116.	292.3	315.07	93.12	78.08	0.0577	324.6	310.7	58.49	61.11
258	25	11.06	1192.8	3069.	302.8	328.74	80.04	71.28	0.1053	252.7	255.9	70.42	69.80

FINAL DATA (SI UNITS)

PRESSURE ------- 13.79 MPa
FLOW RATE ------ 3122. Kg/M^2-Sec
HEAT FLUX ------ 1262. Kw/M^2
CODE ---------- 16

RUN	REF CODE	PRESURE	HEAT FLUX	FLOW RATE	INLET TEMP	GAMMA RATE 1	GAMMA RATE 2	GAMMA RATE 3	QUALITY	DENSITY (SIDE 2)	DENSITY (SIDE 3)	VOID (SIDE 2)	VOID (SIDE 3)
263	25	13.82	1191.5	3115.	280.3	272.65	146.68	120.31	-0.0978	664.5	659.6	-0.21	0.76
262	25	13.82	1196.6	3112.	288.5	278.94	142.04	118.09	-0.0576	623.6	627.1	3.91	3.20
261	25	13.80	1194.0	3115.	298.8	291.20	127.08	103.32	-0.0067	521.0	502.9	20.74	24.64
259	25	13.79	1190.2	3121.	310.0	309.24	106.56	88.92	0.0514	392.6	382.1	44.47	46.76
260	25	13.78	1197.8	2987.	320.4	326.52	90.55	78.12	0.1208	299.3	296.1	61.72	62.49

PRESSURE ------- 13.79 MPa
FLOW RATE ------ 1357. Kg/M^2-Sec
HEAT FLUX ------ 315. Kw/M^2
CODE ---------- 17

RUN	REF CODE	PRESURE	HEAT FLUX	FLOW RATE	INLET TEMP	GAMMA RATE 1	GAMMA RATE 2	GAMMA RATE 3	QUALITY	DENSITY (SIDE 2)	DENSITY (SIDE 3)	VOID (SIDE 2)	VOID (SIDE 3)
267	26	13.83	295.8	1363.	258.7	259.15	156.30	122.89	-0.2871	765.9	746.0	-2.54	0.72
268	26	13.88	293.9	1357.	268.8	262.77	153.56	124.60	-0.2440	738.8	746.0	-1.10	-2.32
269	26	13.82	293.3	1357.	280.9	266.77	152.06	121.64	-0.1850	717.8	711.7	-1.74	-0.65
270	26	13.87	294.6	1354.	292.3	270.22	149.34	118.63	-0.1313	692.8	679.7	-1.83	0.64
271	26	13.84	295.2	1350.	301.4	275.63	146.32	116.24	-0.0836	661.4	647.2	-0.09	2.69
272	26	13.84	293.9	1359.	308.6	278.89	142.51	115.80	-0.0471	633.0	635.1	1.92	1.48
273	26	13.82	295.2	1362.	314.8	288.49	135.64	113.23	-0.0117	574.6	592.7	10.64	6.77
274	26	13.78	294.9	1358.	320.7	299.90	123.29	99.24	0.0237	490.9	477.7	25.51	28.41
275	26	13.83	294.6	1361.	326.2	310.88	110.65	89.34	0.0543	413.1	396.9	40.27	43.89

PRESSURE ------- 11.03 MPa
FLOW RATE ------ 1357. Kg/M^2-Sec
HEAT FLUX ------ 315. Kw/M^2
CODE ---------- 18

RUN	REF CODE	PRESURE	HEAT FLUX	FLOW RATE	INLET TEMP	GAMMA RATE 1	GAMMA RATE 2	GAMMA RATE 3	QUALITY	DENSITY (SIDE 2)	DENSITY (SIDE 3)	VOID (SIDE 2)	VOID (SIDE 3)
278	10	11.04	293.9	1367.	252.6	259.39	153.15	125.00	-0.1815	747.8	750.0	1.44	1.10
289	10	11.00	292.7	1358.	256.6	259.51	152.22	124.91	-0.1643	742.3	748.9	1.21	0.18
290	10	11.02	293.0	1358.	262.6	260.65	152.10	124.31	-0.1418	737.8	740.6	0.26	-0.20
291	10	11.05	297.1	1359.	282.8	267.79	151.36	118.21	-0.0602	710.8	674.7	-2.13	4.04
292	10	11.04	297.7	1370.	287.6	272.17	147.40	118.90	-0.0404	676.8	666.2	1.94	3.77
293	10	11.08	295.5	1368.	296.0	282.67	140.90	112.53	-0.0062	614.8	594.5	9.68	13.36
294	10	11.09	295.5	1365.	301.4	298.15	121.38	98.71	0.0179	485.2	471.1	31.34	33.98
296	10	11.04	293.9	1357.	304.0	305.15	105.64	85.96	0.0315	399.5	380.3	46.27	49.77
295	10	11.06	293.9	1366.	308.1	314.43	87.52	76.05	0.0495	304.5	307.5	62.89	62.35

FINAL DATA (SI UNITS)

PRESSURE ------- 15.17 MPa
FLOW RATE ------ 3122. Kg/M^2-Sec
HEAT FLUX ------ 1262. Kw/M^2
CODE ---------- 19

RUN	REF CODE	PRESURE	HEAT FLUX	FLOW RATE	INLET TEMP	GAMMA RATE 1	GAMMA RATE 2	GAMMA RATE 3	QUALITY	DENSITY (SIDE 2)	DENSITY (SIDE 3)	VOID (SIDE 2)	VOID (SIDE 3)
264	25	15.12	1191.8	3107.	280.8	272.37	146.11	119.92	-0.1552	662.4	657.8	0.62	1.55
265	25	15.18	1194.0	3106.	295.4	278.82	140.24	116.54	-0.0807	614.9	617.4	3.10	2.56
335	12	15.18	1195.9	3113.	299.6	282.31	140.66	113.87	-0.0583	610.2	599.6	1.68	4.19
336	12	15.19	1195.6	3112.	304.8	286.41	134.79	108.40	-0.0296	571.2	554.0	7.58	11.71
337	12	15.15	1198.4	3121.	310.3	295.62	122.36	100.42	0.0034	491.4	483.1	23.38	25.45
341	12	15.17	1197.8	3110.	310.3	298.48	121.81	99.51	0.0037	483.2	471.7	25.38	28.00
338	12	15.18	1197.5	3109.	315.9	306.36	113.44	92.99	0.0365	430.2	417.4	35.40	38.56
340	12	15.16	1190.6	3103.	316.5	307.05	112.54	92.61	0.0398	424.9	413.9	36.46	39.14
339	12	15.20	1193.1	3074.	319.3	310.54	105.91	89.46	0.0580	389.4	389.4	43.82	43.84

PRESSURE ------- 11.03 MPa
FLOW RATE ------ 1357. Kg/M^2-Sec
HEAT FLUX ------ 1262. Kw/M^2
CODE ---------- 20

RUN	REF CODE	PRESURE	HEAT FLUX	FLOW RATE	INLET TEMP	GAMMA RATE 1	GAMMA RATE 2	GAMMA RATE 3	QUALITY	DENSITY (SIDE 2)	DENSITY (SIDE 3)	VOID (SIDE 2)	VOID (SIDE 3)
298	11	11.06	1192.5	1357.	146.8	252.12	154.70	127.06	-0.2503	777.4	778.0	-0.82	-0.91
299	11	11.03	1192.8	1367.	171.5	257.17	148.88	123.66	-0.1675	727.6	735.4	1.23	-0.02
300	11	10.98	1193.1	1358.	194.7	273.70	138.74	116.61	-0.0825	623.9	635.1	11.92	10.00
304	11	11.06	1182.7	1358.	203.8	282.56	128.26	106.69	-0.0563	548.6	546.6	22.82	23.17
301	11	11.04	1195.9	1357.	216.8	302.53	81.58	75.15	-0.0046	290.1	312.2	66.12	62.20
302	11	11.04	1189.6	1364.	227.9	313.25	66.84	61.58	0.0317	211.7	218.9	79.02	77.77
303	11	11.08	1207.6	1366.	256.6	340.88	58.74	55.29	0.1436	155.6	159.3	87.31	86.65

PRESSURE ------- 11.03 MPa
FLOW RATE ------ 679. Kg/M^2-Sec
HEAT FLUX ------ 315. Kw/M^2
CODE ---------- 21

RUN	REF CODE	PRESURE	HEAT FLUX	FLOW RATE	INLET TEMP	GAMMA RATE 1	GAMMA RATE 2	GAMMA RATE 3	QUALITY	DENSITY (SIDE 2)	DENSITY (SIDE 3)	VOID (SIDE 2)	VOID (SIDE 3)
305	10	11.03	295.8	686.	231.7	259.60	153.56	124.57	-0.1586	749.3	746.1	-1.17	-0.68
306	10	11.01	297.4	683.	243.4	266.03	153.29	122.84	-0.1129	726.6	712.4	-1.07	1.25
307	10	11.03	294.2	685.	253.5	270.13	150.98	121.85	-0.0779	701.6	692.6	0.12	1.64
308	10	11.02	295.5	686.	260.0	273.43	146.74	119.64	-0.0523	669.7	667.5	3.27	3.65
309	10	10.98	295.8	682.	271.7	289.07	127.63	102.42	-0.0032	534.1	513.6	23.30	27.10
310	10	11.05	296.5	687.	276.9	298.10	112.26	91.70	0.0141	442.4	427.7	38.80	41.48
311	10	11.04	297.1	688.	282.7	312.33	88.71	76.81	0.0390	312.5	314.8	61.41	60.99
312	10	11.04	298.0	686.	287.8	320.28	83.74	71.78	0.0612	281.0	275.3	66.42	67.47
313	10	10.99	298.0	691.	295.4	330.95	79.38	69.81	0.0939	250.9	252.0	70.98	70.79

FINAL DATA (SI UNITS)

PRESSURE ------- 6.90 MPa
FLOW RATE ------ 679. Kg/M^2-Sec
HEAT FLUX ------ 315. Kw/M^2
CODE ----------- 22

RUN	REF CODE	PRESURE	HEAT FLUX	FLOW RATE	INLET TEMP	GAMMA RATE 1	GAMMA RATE 2	GAMMA RATE 3	QUALITY	DENSITY (SIDE 2)	DENSITY (SIDE 3)	VOID (SIDE 2)	VOID (SIDE 3)
322	10	6.93	295.5	686.	203.9	255.11	156.46	124.28	-0.0927	780.9	759.8	0.14	3.07
321	10	6.94	294.9	687.	209.9	254.98	152.93	126.29	-0.0758	761.7	774.9	1.51	-0.35
320	10	6.95	293.6	687.	216.5	259.29	153.20	124.21	-0.0570	748.3	744.6	2.06	2.60
319	10	6.90	293.0	683.	221.4	266.89	144.91	116.82	-0.0398	679.4	667.7	10.85	12.57
318	10	6.99	293.6	684.	228.8	280.69	112.36	94.01	-0.0201	476.6	477.2	39.08	38.99
317	10	6.92	293.6	683.	236.0	294.77	100.18	81.76	0.0046	391.0	371.5	50.71	53.62
316	10	6.94	294.2	685.	250.9	322.96	74.59	65.79	0.0507	238.5	238.0	72.31	72.38
315	10	6.92	294.2	686.	262.7	338.32	66.75	60.23	0.0896	191.9	192.2	78.70	78.65
314	10	6.87	294.9	687.	272.6	345.46	60.52	53.96	0.1243	161.5	152.8	82.88	84.26

PRESSURE ------- 6.90 MPa
FLOW RATE ------ 3122. Kg/M^2-Sec
HEAT FLUX ------ 315. Kw/M^2
CODE ----------- 23

RUN	REF CODE	PRESURE	HEAT FLUX	FLOW RATE	INLET TEMP	GAMMA RATE 1	GAMMA RATE 2	GAMMA RATE 3	QUALITY	DENSITY (SIDE 2)	DENSITY (SIDE 3)	VOID (SIDE 2)	VOID (SIDE 3)
323	10	6.93	293.9	3108.	230.3	250.15	161.03	128.94	-0.1429	825.1	812.6	-1.58	0.08
324	10	6.87	293.9	3106.	246.8	254.31	156.32	126.98	-0.0893	783.0	782.5	0.74	0.81
325	10	6.90	293.3	3112.	255.5	256.10	157.06	127.11	-0.0626	780.7	776.9	-0.96	-0.43
326	10	6.90	293.6	3118.	266.6	259.58	155.94	124.90	-0.0263	762.4	748.6	-1.06	0.93
327	10	6.89	292.7	3113.	271.6	263.54	154.08	124.81	-0.0092	738.9	734.5	1.05	1.70
328	10	6.90	293.0	3102.	274.6	273.57	140.63	113.86	0.0010	637.7	627.8	15.14	16.60
329	10	6.93	294.2	3109.	276.9	282.17	123.87	101.69	0.0081	531.1	524.5	30.41	31.38

PRESSURE ------- 15.17 MPa
FLOW RATE ------ 679. Kg/M^2-Sec
HEAT FLUX ------ 631. Kw/M^2
CODE ----------- 24

RUN	REF CODE	PRESURE	HEAT FLUX	FLOW RATE	INLET TEMP	GAMMA RATE 1	GAMMA RATE 2	GAMMA RATE 3	QUALITY	DENSITY (SIDE 2)	DENSITY (SIDE 3)	VOID (SIDE 2)	VOID (SIDE 3)
395	13	15.18	591.0	685.	235.7	281.26	140.03	113.91	-0.0954	606.7	595.4	3.18	5.75
396	13	15.17	591.3	686.	241.3	285.03	137.46	111.36	-0.0694	584.6	569.4	5.56	9.12
350	13	15.16	591.0	685.	244.6	287.59	133.88	108.26	-0.0530	561.1	543.6	9.23	13.39
397	13	15.17	594.2	686.	247.4	290.89	128.89	104.66	-0.0380	529.7	513.5	15.05	18.97
349	13	15.17	592.9	687.	250.2	294.53	126.00	102.38	-0.0264	508.2	491.5	19.08	23.16
398	13	15.16	597.6	687.	254.8	303.22	116.70	95.76	0.0002	448.2	434.2	31.33	34.85
348	13	15.16	594.8	683.	255.0	299.67	119.00	95.56	0.0018	465.3	439.6	26.98	33.33
347	13	15.18	595.8	683.	261.4	307.80	110.18	89.57	0.0328	410.8	389.6	37.93	43.43
346	13	15.16	594.2	687.	270.2	316.02	102.62	85.00	0.0723	364.6	350.2	47.02	50.73
345	13	15.19	594.8	687.	279.4	323.40	91.35	75.65	0.1182	306.2	287.5	59.54	64.54
344	13	15.19	596.1	688.	285.5	329.32	84.06	72.83	0.1494	268.8	264.9	67.99	69.04
343	13	15.20	597.3	687.	291.7	334.47	75.66	69.03	0.1841	228.9	238.6	77.11	74.57

FINAL DATA (SI UNITS)

PRESSURE ------- 13.79 MPa
FLOW RATE ------ 679. Kg/M^2-Sec
HEAT FLUX ------ 631. Kw/M^2
CODE ---------- 25

RUN	REF CODE	PRESURE	HEAT FLUX	FLOW RATE	INLET TEMP	GAMMA RATE 1	GAMMA RATE 2	GAMMA RATE 3	QUALITY	DENSITY (SIDE 2)	DENSITY (SIDE 3)	VOID (SIDE 2)	VOID (SIDE 3)
391	13	13.77	592.6	700.	218.8	274.34	144.79	117.37	-0.1161	649.2	636.8	2.10	4.53
392	13	13.77	592.0	693.	226.3	278.24	141.79	114.55	-0.0808	623.4	607.5	3.71	6.93
352	13	13.83	599.2	687.	232.8	287.21	133.22	105.71	-0.0454	558.8	528.3	13.43	19.98
394	13	13.77	588.8	683.	233.8	287.18	132.83	108.18	-0.0447	557.0	544.1	13.99	16.84
393	13	13.77	588.8	684.	236.7	290.29	128.12	101.49	-0.0329	527.3	495.0	19.24	26.22
351	13	13.86	595.4	683.	239.4	295.04	123.40	99.83	-0.0189	494.9	474.7	24.77	29.26
353	13	13.81	596.1	684.	245.3	300.18	115.30	94.54	0.0082	447.2	432.5	33.14	36.46
354	13	13.80	594.8	686.	251.9	308.32	107.04	88.30	0.0351	395.8	381.3	42.81	46.14
355	13	13.78	594.8	685.	265.7	324.16	84.28	73.45	0.0979	275.3	274.3	67.07	67.31
356	13	13.80	593.9	688.	274.9	332.61	74.06	65.25	0.1368	224.0	220.1	77.37	78.23
357	13	13.80	594.2	682.	286.0	339.45	65.84	55.94	0.1933	184.8	164.2	84.71	88.90
358	13	13.82	592.3	689.	291.2	343.96	64.12	56.88	0.2117	174.5	165.7	86.64	88.45

PRESSURE ------- 6.90 MPa
FLOW RATE ------ 3122. Kg/M^2-Sec
HEAT FLUX ------ 1262. Kw/M^2
CODE ---------- 26

RUN	REF CODE	PRESURE	HEAT FLUX	FLOW RATE	INLET TEMP	GAMMA RATE 1	GAMMA RATE 2	GAMMA RATE 3	QUALITY	DENSITY (SIDE 2)	DENSITY (SIDE 3)	VOID (SIDE 2)	VOID (SIDE 3)
366	12	6.89	1195.0	3109.	173.5	241.22	160.08	131.72	-0.1980	849.0	863.3	-2.05	-3.89
367	12	6.89	1193.7	3107.	212.7	250.41	155.28	127.26	-0.0831	785.8	792.9	-1.08	-2.08
368	12	6.89	1192.5	3115.	228.1	261.28	150.54	121.73	-0.0367	722.1	714.5	4.65	5.73
372	12	6.94	1193.7	3112.	234.5	272.76	131.22	107.29	-0.0186	587.0	580.8	22.97	23.89
369	12	6.89	1194.0	3102.	239.0	283.24	102.97	87.52	-0.0023	421.7	426.0	46.54	45.91
370	12	6.89	1194.7	3103.	246.2	304.72	77.38	69.69	0.0201	268.5	280.2	68.53	66.79
371	12	6.94	1193.1	3109.	251.6	312.37	72.42	64.89	0.0353	237.9	242.6	72.77	72.07

PRESSURE ------- 6.90 MPa
FLOW RATE ------ 1357. Kg/M^2-Sec
HEAT FLUX ------ 1262. Kw/M^2
CODE ---------- 27

RUN	REF CODE	PRESURE	HEAT FLUX	FLOW RATE	INLET TEMP	GAMMA RATE 1	GAMMA RATE 2	GAMMA RATE 3	QUALITY	DENSITY (SIDE 2)	DENSITY (SIDE 3)	VOID (SIDE 2)	VOID (SIDE 3)
381	12	6.92	1201.6	1366.	137.4	252.12	153.46	127.50	-0.1105	769.3	788.3	1.66	-0.98
380	12	6.88	1195.6	1363.	141.4	256.85	151.06	122.76	-0.0989	739.5	736.8	5.02	5.40
379	12	6.92	1197.2	1358.	145.2	263.11	140.93	118.67	-0.0880	664.8	687.1	14.74	11.59
378	12	6.92	1196.9	1361.	152.0	272.97	115.59	97.58	-0.0695	506.2	514.6	36.27	35.06
382	12	6.93	1198.4	1355.	156.1	282.11	97.99	85.25	-0.0562	399.1	413.3	51.07	49.02
377	12	6.93	1202.2	1357.	166.2	293.54	74.07	69.08	-0.0264	266.2	291.4	69.50	65.82
376	12	6.92	1192.1	1351.	176.4	307.65	70.23	62.94	0.0018	232.9	236.4	73.79	73.28
375	12	6.90	1195.9	1362.	194.1	324.42	55.65	53.47	0.0522	154.7	165.4	84.68	83.08
374	12	6.92	1193.4	1364.	214.7	339.24	47.34	48.30	0.1115	111.1	125.9	90.71	88.45
373	12	6.93	1195.6	1360.	233.3	346.22	44.26	42.40	0.1698	95.3	90.5	92.73	92.30

FINAL DATA (SI UNITS)

PRESSURE ------- 6.90 MPa
FLOW RATE ------ 3122. Kg/M^2-Sec
HEAT FLUX ------ 631. Kw/M^2
CODE ---------- 28

RUN	REF CODE	PRESURE	HEAT FLUX	FLOW RATE	INLET TEMP	GAMMA RATE 1	GAMMA RATE 2	GAMMA RATE 3	QUALITY	DENSITY (SIDE 2)	DENSITY (SIDE 3)	VOID (SIDE 2)	VOID (SIDE 3)
383	13	6.91	597.6	3095.	227.4	250.36	159.13	128.77	-0.1128	803.8	794.9	-0.88	0.32
384	13	6.90	600.2	3104.	240.9	254.69	157.13	127.55	-0.0708	776.8	770.1	-0.14	0.80
385	13	6.94	594.2	3106.	252.9	259.60	155.12	126.31	-0.0347	748.7	744.0	1.14	1.92
390	13	6.86	592.9	3108.	258.1	263.56	150.34	122.07	-0.0153	710.2	701.1	5.47	6.79
386	13	6.90	594.5	3104.	263.8	281.38	121.71	100.02	0.0021	515.6	505.1	32.84	34.39
387	13	6.91	595.1	3111.	267.8	295.36	96.90	81.34	0.0151	369.7	360.4	53.87	55.26
388	13	6.92	594.2	3113.	270.5	300.77	89.99	78.89	0.0234	329.5	337.0	59.57	58.45
389	13	6.90	593.9	3101.	274.5	312.32	82.75	72.47	0.0380	282.1	283.1	66.25	66.10

PRESSURE ------- 15.17 MPa
FLOW RATE ------ 1357. Kg/M^2-Sec
HEAT FLUX ------ 315. Kw/M^2
CODE ---------- 29

RUN	REF CODE	PRESURE	HEAT FLUX	FLOW RATE	INLET TEMP	GAMMA RATE 1	GAMMA RATE 2	GAMMA RATE 3	QUALITY	DENSITY (SIDE 2)	DENSITY (SIDE 3)	VOID (SIDE 2)	VOID (SIDE 3)
73	1	15.12	293.9	1382.	309.7	275.04	149.43	121.16	-0.0993	650.8	648.2	-1.39	-0.83
72	1	15.11	293.6	1371.	313.8	276.98	148.10	118.04	-0.0738	638.8	622.3	-1.42	2.21
71	1	15.12	293.0	1370.	319.0	281.96	144.09	116.95	-0.0427	606.1	601.9	2.42	3.37
74	1	15.12	295.8	1368.	322.6	285.76	139.10	112.69	-0.0190	572.8	565.1	7.51	9.31
70	1	15.13	294.6	1427.	324.9	289.34	137.14	112.35	-0.0103	555.1	554.4	10.75	10.93
75	1	15.12	298.0	1376.	327.3	293.55	127.30	105.64	0.0115	500.1	503.3	21.62	20.85
69	1	15.13	296.8	1348.	331.1	305.14	120.04	96.36	0.0391	445.1	424.7	32.47	37.40

PRESSURE ------- 13.79 MPa
FLOW RATE ------ 407. Kg/M^2-Sec
HEAT FLUX ------ 315. Kw/M^2
CODE ---------- 30

RUN	REF CODE	PRESURE	HEAT FLUX	FLOW RATE	INLET TEMP	GAMMA RATE 1	GAMMA RATE 2	GAMMA RATE 3	QUALITY	DENSITY (SIDE 2)	DENSITY (SIDE 3)	VOID (SIDE 2)	VOID (SIDE 3)
403	15	13.87	293.3	390.	186.8	257.62	158.44	128.38	-0.3031	781.7	768.1	-6.38	-4.11
404	15	13.86	294.6	392.	202.0	262.94	156.06	127.65	-0.2416	750.4	744.5	-5.61	-4.57
405	15	13.87	294.2	389.	237.1	274.89	150.91	120.57	-0.0916	685.9	658.8	-7.77	-2.18
411	15	13.74	293.6	392.	250.8	283.58	145.40	117.52	-0.0308	633.8	614.8	-1.43	2.09
406	15	13.84	293.6	390.	259.0	290.46	136.15	110.13	0.0036	571.3	550.6	9.81	13.67
407	15	13.81	294.2	392.	274.1	309.33	116.64	96.20	0.0720	441.8	427.5	33.91	36.57
408	15	13.80	293.6	392.	290.9	329.16	90.89	77.83	0.1509	300.8	293.7	60.06	61.38
409	15	13.81	293.0	386.	305.5	342.91	71.73	63.70	0.2303	208.1	203.2	78.67	79.85
410	15	13.82	293.9	393.	313.2	357.03	74.71	65.28	0.2661	208.4	199.2	77.40	79.84

FINAL DATA (SI UNITS)

PRESSURE ------- 15.17 MPa
FLOW RATE ------ 407. Kg/M^2-Sec
HEAT FLUX ------ 315. Kw/M^2
CODE ---------- 31

RUN	REF CODE	PRESURE	HEAT FLUX	FLOW RATE	INLET TEMP	GAMMA RATE 1	GAMMA RATE 2	GAMMA RATE 3	QUALITY	DENSITY (SIDE 2)	DENSITY (SIDE 3)	VOID (SIDE 2)	VOID (SIDE 3)
412	15	15.19	293.0	390.	235.7	273.93	150.11	122.75	-0.1611	684.6	676.2	-6.12	-4.24
413	15	15.15	294.9	389.	248.9	278.38	146.38	119.45	-0.0934	652.9	641.4	-6.60	-4.07
414	15	15.19	294.9	389.	262.5	286.89	144.39	116.39	-0.0295	620.2	598.9	-3.97	0.28
415	15	15.17	293.9	388.	271.5	296.54	136.47	109.09	0.0144	558.9	530.3	8.32	14.01
416	15	15.17	294.2	389.	281.6	305.83	119.95	100.21	0.0661	463.1	457.6	27.39	28.49
417	15	15.17	296.5	389.	294.0	322.67	107.65	87.91	0.1348	380.8	358.4	43.79	48.25
418	15	15.16	293.9	389.	303.4	335.29	98.18	81.84	0.1828	323.9	307.9	55.13	58.30
419	15	15.20	295.2	389.	310.0	340.78	83.95	73.10	0.2210	259.5	254.9	67.95	69.86
420	15	15.16	296.1	390.	320.9	352.63	70.09	61.00	0.2878	193.8	181.1	83.40	86.61

PRESSURE ------- 16.90 MPa
FLOW RATE ------ 407. Kg/M^2-Sec
HEAT FLUX ------ 315. Kw/M^2
CODE ---------- 32

RUN	REF CODE	PRESURE	HEAT FLUX	FLOW RATE	INLET TEMP	GAMMA RATE 1	GAMMA RATE 2	GAMMA RATE 3	QUALITY	DENSITY (SIDE 2)	DENSITY (SIDE 3)	VOID (SIDE 2)	VOID (SIDE 3)
486	20	16.90	293.0	407.	242.5	214.96	0.00	109.16	-0.2480	0.0	675.7	0.00	-4.68
487	20	16.98	294.2	405.	258.1	219.61	0.00	106.65	-0.1632	0.0	640.7	0.00	-5.88
488	20	16.97	295.8	394.	268.6	224.97	0.00	103.69	-0.0872	0.0	601.8	0.00	-5.67
489	20	16.96	295.5	377.	283.8	235.49	0.00	95.78	0.0230	0.0	516.8	0.00	11.13
490	20	16.86	298.7	405.	293.2	241.54	0.00	87.65	0.0522	0.0	448.3	0.00	26.69
491	20	16.87	299.6	404.	303.7	249.37	0.00	81.10	0.1202	0.0	389.7	0.00	39.65
492	20	16.99	301.5	405.	319.1	258.93	0.00	70.96	0.2189	0.0	310.4	0.00	57.21
421	15	16.88	295.5	390.	321.9	339.11	94.36	77.33	0.2515	303.7	279.3	58.75	64.17
422	15	16.90	294.9	386.	328.2	345.38	82.64	70.50	0.3012	249.7	236.6	70.75	74.24

PRESSURE ------- 11.03 MPa
FLOW RATE ------ 407. Kg/M^2-Sec
HEAT FLUX ------ 315. Kw/M^2
CODE ---------- 33

RUN	REF CODE	PRESURE	HEAT FLUX	FLOW RATE	INLET TEMP	GAMMA RATE 1	GAMMA RATE 2	GAMMA RATE 3	QUALITY	DENSITY (SIDE 2)	DENSITY (SIDE 3)	VOID (SIDE 2)	VOID (SIDE 3)
431	15	11.12	296.5	393.	209.9	266.93	152.59	124.39	-0.0908	718.9	708.8	-3.48	-1.76
430	15	11.09	296.1	395.	219.5	272.81	152.07	124.03	-0.0580	698.1	688.1	-2.80	-1.04
429	15	11.04	296.8	392.	228.4	280.18	145.90	118.07	-0.0203	645.5	627.5	4.32	7.27
428	15	11.06	295.5	388.	236.8	288.67	132.99	111.10	0.0122	560.2	561.0	18.27	18.14
427	15	11.10	296.5	397.	246.6	305.50	114.68	94.21	0.0410	439.6	422.5	38.04	40.86
426	15	11.06	295.2	388.	263.8	331.65	86.07	74.90	0.1148	277.7	274.7	64.70	65.20
425	15	11.04	294.9	388.	275.0	341.83	77.30	68.54	0.1598	231.5	229.8	72.29	72.58
423	15	11.02	297.4	389.	289.2	358.45	68.81	61.81	0.2209	184.6	180.6	80.32	81.15
424	15	11.03	296.5	389.	299.2	366.25	61.70	58.63	0.2631	152.4	159.0	86.26	84.89

FINAL DATA (SI UNITS)

PRESSURE ------- 6.90 MPa
FLOW RATE ------ 204. Kg/M^2-Sec
HEAT FLUX ------ 315. Kw/M^2
CODE ---------- 34

RUN	REF CODE	PRESURE	HEAT FLUX	FLOW RATE	INLET TEMP	GAMMA RATE 1	GAMMA RATE 2	GAMMA RATE 3	QUALITY	DENSITY (SIDE 2)	DENSITY (SIDE 3)	VOID (SIDE 2)	VOID (SIDE 3)
465	17	6.89	296.5	198.	106.0	292.15	112.88	94.43	0.0422	446.3	440.9	41.94	42.71
464	17	6.90	296.1	197.	125.0	314.13	90.73	78.87	0.0960	311.7	313.0	60.97	60.79
463	17	6.90	295.5	197.	145.6	336.05	72.36	64.60	0.1530	211.4	209.7	75.16	75.41
436	15	6.93	296.5	198.	170.4	366.47	59.90	53.91	0.2233	145.5	135.7	84.51	85.89
435	15	6.98	296.8	198.	187.2	372.80	52.14	49.92	0.2694	113.3	112.6	89.09	89.19
462	17	6.90	296.5	197.	203.1	374.58	46.07	44.76	0.3214	87.5	84.0	92.71	93.20
434	15	7.00	294.9	205.	206.1	378.50	48.68	46.14	0.3021	98.1	91.6	91.27	92.19
433	15	7.05	292.7	198.	226.6	384.46	41.85	40.63	0.3783	71.2	63.1	95.47	96.27
432	15	7.04	293.9	198.	240.8	386.05	38.31	37.36	0.4265	58.1	47.3	97.50	98.51

PRESSURE ------- 11.03 MPa
FLOW RATE ------ 204. Kg/M^2-Sec
HEAT FLUX ------ 158. Kw/M^2
CODE ---------- 35

RUN	REF CODE	PRESURE	HEAT FLUX	FLOW RATE	INLET TEMP	GAMMA RATE 1	GAMMA RATE 2	GAMMA RATE 3	QUALITY	DENSITY (SIDE 2)	DENSITY (SIDE 3)	VOID (SIDE 2)	VOID (SIDE 3)
439	16	11.06	146.0	197.	202.3	263.64	157.03	126.36	-0.1220	744.8	742.6	-4.78	-4.42
440	16	11.04	145.4	196.	218.6	267.71	153.63	124.65	-0.0625	713.8	717.2	-4.96	-5.55
441	16	11.04	146.0	196.	227.8	272.19	151.99	123.02	-0.0278	691.6	692.0	-3.28	-3.33
442	16	11.01	147.3	196.	241.0	282.48	143.32	115.74	0.0245	619.3	613.9	8.69	9.57
444	16	11.05	147.9	196.	249.7	298.38	131.22	107.57	0.0576	524.1	523.5	24.22	24.32
443	16	11.05	147.6	195.	262.2	319.00	101.34	84.73	0.1073	354.5	349.9	52.09	52.84
445	16	11.03	146.0	195.	275.0	341.80	91.21	79.46	0.1546	284.4	290.8	63.60	62.56
446	16	11.05	147.9	196.	298.1	363.20	71.76	64.90	0.2549	190.0	194.3	79.11	78.41

PRESSURE ------- 15.17 MPa
FLOW RATE ------ 204. Kg/M^2-Sec
HEAT FLUX ------ 158. Kw/M^2
CODE ---------- 36

RUN	REF CODE	PRESURE	HEAT FLUX	FLOW RATE	INLET TEMP	GAMMA RATE 1	GAMMA RATE 2	GAMMA RATE 3	QUALITY	DENSITY (SIDE 2)	DENSITY (SIDE 3)	VOID (SIDE 2)	VOID (SIDE 3)
455	16	15.22	147.9	195.	250.7	281.77	148.06	120.65	-0.0867	644.5	648.1	-5.83	-6.62
454	16	15.23	146.0	197.	260.3	284.81	144.78	117.96	-0.0522	620.4	622.2	-4.14	-4.50
453	16	15.16	146.0	196.	273.6	294.61	138.63	113.47	0.0177	567.0	568.8	6.75	6.38
450	16	15.17	147.0	194.	288.9	312.35	120.04	97.48	0.1056	446.6	434.9	30.70	33.01
447	16	15.19	147.6	195.	302.2	340.15	105.04	87.99	0.1753	341.9	338.7	51.52	52.16
449	16	15.18	146.7	194.	311.5	348.41	89.75	77.82	0.2281	271.8	274.6	65.50	64.93
448	16	15.18	146.0	196.	324.4	358.40	82.53	72.34	0.3024	234.5	236.1	72.92	72.60

FINAL DATA (SI UNITS)

PRESSURE ------- 16.90 MPa
FLOW RATE ------ 204. Kg/M^2-Sec
HEAT FLUX ------ 158. Kw/M^2
CODE ---------- 37

RUN	REF CODE	PRESURE	HEAT FLUX	FLOW RATE	INLET TEMP	GAMMA RATE 1	GAMMA RATE 2	GAMMA RATE 3	QUALITY	DENSITY (SIDE 2)	DENSITY (SIDE 3)	VOID (SIDE 2)	VOID (SIDE 3)
457	16	16.93	146.0	196.	252.5	276.66	147.53	119.19	-0.1799	656.0	652.8	-7.55	-6.77
458	16	16.95	145.7	198.	277.4	287.08	142.00	115.19	-0.0453	601.1	598.3	-7.66	-7.03
459	16	16.86	145.7	195.	292.5	299.79	132.24	108.99	0.0548	525.8	529.2	9.49	8.74
460	16	17.01	144.4	194.	304.5	309.87	121.16	99.11	0.1202	455.9	449.1	24.58	26.11

PRESSURE ------- 6.90 MPa
FLOW RATE ------ 407. Kg/M^2-Sec
HEAT FLUX ------ 631. Kw/M^2
CODE ---------- 38

RUN	REF CODE	PRESURE	HEAT FLUX	FLOW RATE	INLET TEMP	GAMMA RATE 1	GAMMA RATE 2	GAMMA RATE 3	QUALITY	DENSITY (SIDE 2)	DENSITY (SIDE 3)	VOID (SIDE 2)	VOID (SIDE 3)
468	18	6.93	591.0	415.	109.0	236.54	0.00	70.90	0.0204	0.0	340.9	0.00	56.82
470	18	6.93	587.2	385.	117.8	254.04	0.00	58.38	0.0843	0.0	235.1	0.00	71.81
469	18	6.94	586.3	383.	126.1	262.08	0.00	54.53	0.1079	0.0	202.6	0.00	76.42
471	18	6.89	589.8	410.	133.4	257.17	0.00	53.51	0.0952	0.0	202.1	0.00	76.48
472	18	6.89	590.4	406.	144.6	263.41	0.00	48.49	0.1324	0.0	166.1	0.00	81.58
473	18	6.91	592.3	410.	154.9	268.50	0.00	46.20	0.1572	0.0	148.3	0.00	84.11
474	18	6.91	593.9	405.	168.0	274.72	0.00	42.47	0.2033	0.0	122.3	0.00	87.78
475	18	6.90	594.2	411.	193.0	281.21	0.00	36.30	0.2680	0.0	84.2	0.00	93.18

PRESSURE ------- 15.17 MPa
FLOW RATE ------ 407. Kg/M^2-Sec
HEAT FLUX ------ 631. Kw/M^2
CODE ---------- 39

RUN	REF CODE	PRESURE	HEAT FLUX	FLOW RATE	INLET TEMP	GAMMA RATE 1	GAMMA RATE 2	GAMMA RATE 3	QUALITY	DENSITY (SIDE 2)	DENSITY (SIDE 3)	VOID (SIDE 2)	VOID (SIDE 3)
480	18	15.19	589.1	412.	134.6	210.46	0.00	114.60	-0.2083	0.0	717.9	0.00	-12.82
479	18	15.18	592.3	409.	137.9	211.40	0.00	110.34	-0.1838	0.0	682.9	0.00	-8.16
481	19	15.11	599.2	407.	154.2	220.24	0.00	108.38	-0.0968	0.0	636.7	0.00	-6.91
478	18	15.17	593.2	403.	166.1	224.60	0.00	104.61	-0.0475	0.0	596.1	0.00	0.91
477	18	15.18	592.9	409.	169.4	225.01	0.00	104.96	-0.0466	0.0	597.2	0.00	0.66
476	18	15.20	593.2	408.	177.4	229.45	0.00	101.25	-0.0095	0.0	558.4	0.00	8.34
482	19	15.13	595.8	408.	188.7	239.71	0.00	91.67	0.0450	0.0	468.2	0.00	26.47
483	19	15.16	596.1	409.	197.9	244.26	0.00	84.88	0.0847	0.0	414.7	0.00	37.05
484	19	15.14	597.0	407.	205.3	247.70	0.00	79.97	0.1231	0.0	377.1	0.00	44.56

FINAL DATA (SI UNITS)

PRESSURE ------- 6.90 MPa
FLOW RATE ------ 679. Kg/M^2-Sec
HEAT FLUX ------ 631. Kw/M^2
CODE ---------- 40

RUN	REF CODE	PRESURE	HEAT FLUX	FLOW RATE	INLET TEMP	GAMMA RATE 1	GAMMA RATE 2	GAMMA RATE 3	QUALITY	DENSITY (GAP)	DENSITY (CENTER)	VOID (GAP)	VOID (CENTER)
513	-	6.88	598.6	685.	134.0	125.53	114.00	61.01	-0.1210	803.3	828.5	-0.70	-4.12
512	-	6.87	596.1	684.	141.5	127.61	110.74	61.46	-0.1002	767.2	818.2	2.86	-4.16
514	-	6.89	594.2	684.	155.2	133.99	96.69	61.40	-0.0632	631.7	770.9	19.31	-0.36
515	-	6.85	599.9	688.	170.6	150.38	87.17	34.33	-0.0163	507.6	375.3	34.63	53.91
516	-	6.88	598.0	682.	184.5	162.33	67.36	26.57	0.0246	346.6	265.0	56.73	68.96
517	-	6.92	596.4	686.	193.9	166.77	59.71	22.44	0.0478	289.4	216.6	64.65	75.73
518	-	6.86	598.3	685.	204.9	173.97	49.51	16.27	0.0832	215.0	149.3	75.22	85.36

PRESSURE ------- 6.90 MPa
FLOW RATE ------ 1357. Kg/M^2-Sec
HEAT FLUX ------ 631. Kw/M^2
CODE ---------- 41

RUN	REF CODE	PRESURE	HEAT FLUX	FLOW RATE	INLET TEMP	GAMMA RATE 1	GAMMA RATE 2	GAMMA RATE 3	QUALITY	DENSITY (GAP)	DENSITY (CENTER)	VOID (GAP)	VOID (CENTER)
519	-	6.94	596.7	1355.	203.3	128.74	115.26	61.17	-0.0909	796.2	805.8	-1.40	-2.72
520	-	6.94	596.4	1344.	218.1	132.74	109.99	61.02	-0.0455	736.3	774.8	3.70	-1.80
521	-	6.91	595.1	1350.	227.3	140.67	97.06	54.56	-0.0173	608.6	646.2	20.32	14.84
522	-	6.90	595.4	1349.	238.2	156.76	85.11	28.76	0.0165	475.9	299.0	37.99	64.31
523	-	6.91	596.4	1345.	247.2	165.10	63.14	24.04	0.0455	314.2	234.9	61.19	73.18
524	-	6.92	597.3	1344.	260.6	175.35	53.49	15.92	0.0887	237.7	144.7	71.77	86.12

PRESSURE ------- 6.90 MPa
FLOW RATE ------ 3122. Kg/M^2-Sec
HEAT FLUX ------ 631. Kw/M^2
CODE ---------- 42

RUN	REF CODE	PRESURE	HEAT FLUX	FLOW RATE	INLET TEMP	GAMMA RATE 1	GAMMA RATE 2	GAMMA RATE 3	QUALITY	DENSITY (GAP)	DENSITY (CENTER)	VOID (GAP)	VOID (CENTER)
525	-	6.90	599.5	2911.	246.0	132.88	114.83	61.36	-0.0500	772.2	778.2	-0.66	-1.52
526	-	6.89	600.2	2876.	252.0	133.53	113.79	61.37	-0.0296	761.0	773.8	-0.57	-2.40
531	-	6.89	606.8	2872.	256.9	136.74	104.52	61.06	-0.0124	677.9	748.2	10.21	-0.03
527	-	6.90	602.7	2925.	263.4	146.08	93.62	48.67	0.0064	565.3	550.9	25.49	27.63
529	-	6.91	604.3	2890.	269.1	157.13	84.74	34.40	0.0262	472.5	356.7	38.20	55.61
530	-	6.94	604.9	2904.	274.9	163.06	76.25	28.43	0.0447	402.6	282.0	48.07	66.21

FINAL DATA (SI UNITS)

PRESSURE ------- 11.03 MPa
FLOW RATE ------ 1357. Kg/M^2-Sec
HEAT FLUX ------ 315. Kw/M^2
CODE ---------- 43

RUN	REF CODE	PRESURE	HEAT FLUX	FLOW RATE	INLET TEMP	GAMMA RATE 1	GAMMA RATE 2	GAMMA RATE 3	QUALITY	DENSITY (GAP)	DENSITY (CENTER)	VOID (GAP)	VOID (CENTER)
533	-	11.03	295.8	1347.	271.6	135.68	112.02	59.59	-0.1050	737.0	737.1	-2.04	-2.04
534	-	11.04	294.9	1348.	281.6	138.05	112.04	58.96	-0.0649	726.2	714.2	-3.69	-1.67
535	-	11.04	295.8	1352.	291.1	139.74	105.00	57.76	-0.0247	667.5	689.5	2.73	-1.10
536	-	11.02	296.5	1349.	296.2	143.14	97.93	55.01	-0.0017	603.9	638.0	11.94	5.81
537	-	11.06	295.8	1344.	304.1	154.10	82.43	43.55	0.0330	463.5	462.3	34.79	34.99

PRESSURE ------- 11.03 MPa
FLOW RATE ------ 679. Kg/M^2-Sec
HEAT FLUX ------ 315. Kw/M^2
CODE ---------- 44

RUN	REF CODE	PRESURE	HEAT FLUX	FLOW RATE	INLET TEMP	GAMMA RATE 1	GAMMA RATE 2	GAMMA RATE 3	QUALITY	DENSITY (GAP)	DENSITY (CENTER)	VOID (GAP)	VOID (CENTER)
544	-	11.02	294.9	687.	255.7	137.13	108.14	59.72	-0.0697	701.7	729.2	0.50	-4.13
543	-	11.04	295.2	687.	262.5	139.05	106.58	58.42	-0.0437	682.0	701.6	1.44	-1.93
542	-	11.05	295.2	685.	267.8	141.57	98.00	57.88	-0.0223	610.3	680.2	12.16	-0.13
541	-	11.05	294.6	685.	272.6	145.86	87.83	56.62	-0.0035	523.9	642.0	26.05	4.86
540	-	11.03	295.2	684.	275.6	149.49	83.48	53.68	0.0100	483.0	590.9	32.49	13.29
539	-	11.03	295.8	685.	281.2	155.92	77.31	40.65	0.0327	424.6	425.4	41.73	41.58
538	-	11.03	295.2	684.	287.5	163.12	78.69	27.35	0.0589	416.9	271.2	41.85	68.68

PRESSURE ------- 11.03 MPa
FLOW RATE ------ 1357. Kg/M^2-Sec
HEAT FLUX ------ 631. Kw/M^2
CODE ---------- 45

RUN	REF CODE	PRESURE	HEAT FLUX	FLOW RATE	INLET TEMP	GAMMA RATE 1	GAMMA RATE 2	GAMMA RATE 3	QUALITY	DENSITY (GAP)	DENSITY (CENTER)	VOID (GAP)	VOID (CENTER)
546	-	11.06	592.6	1350.	248.2	135.56	109.28	59.94	-0.0951	717.2	742.2	-0.06	-4.18
547	-	11.01	597.0	1346.	258.7	139.61	105.65	57.98	-0.0510	673.2	692.9	3.62	0.25
548	-	11.03	592.6	1347.	269.2	145.61	92.30	53.36	-0.0123	556.0	606.3	20.96	12.08
549	-	11.03	594.5	1344.	279.0	155.79	76.99	40.35	0.0287	422.8	422.7	42.26	42.28
550	-	11.04	598.3	1343.	284.2	160.93	71.42	30.15	0.0515	374.6	303.8	49.93	62.99
551	-	11.06	601.4	1347.	292.1	167.46	68.20	21.87	0.0845	341.0	210.1	54.62	79.01
552	-	11.06	599.2	1347.	299.0	171.05	61.03	20.85	0.1142	289.7	195.2	63.29	81.12

FINAL DATA (SI UNITS)

PRESSURE ------- 11.03 MPa
FLOW RATE ------ 3122. Kg/M^2-Sec
HEAT FLUX ------ 631. Kw/M^2
CODE ---------- 46

RUN	REF CODE	PRESURE	HEAT FLUX	FLOW RATE	INLET TEMP	GAMMA RATE 1	GAMMA RATE 2	GAMMA RATE 3	QUALITY	DENSITY (GAP)	DENSITY (CENTER)	VOID (GAP)	VOID (CENTER)
557	-	11.05	604.0	3110.	276.5	137.52	111.11	58.51	-0.0973	722.2	712.0	-0.23	1.44
556	-	11.03	600.8	3103.	287.8	139.49	108.73	57.98	-0.0501	695.9	693.6	0.09	0.48
555	-	11.05	599.9	3112.	292.9	139.50	107.56	57.34	-0.0297	687.1	685.9	-0.20	-0.01
554	-	11.00	601.7	3106.	298.9	144.47	98.61	53.85	-0.0010	604.0	617.7	11.97	9.52
553	-	11.01	601.4	3095.	308.2	156.18	80.76	40.06	0.0417	447.0	418.5	37.34	42.66

PRESSURE ------- 15.17 MPa
FLOW RATE ------ 679. Kg/M^2-Sec
HEAT FLUX ------ 631. Kw/M^2
CODE ---------- 47

RUN	REF CODE	PRESURE	HEAT FLUX	FLOW RATE	INLET TEMP	GAMMA RATE 1	GAMMA RATE 2	GAMMA RATE 3	QUALITY	DENSITY (GAP)	DENSITY (CENTER)	VOID (GAP)	VOID (CENTER)
558	-	15.18	596.7	690.	225.2	142.18	100.20	54.71	-0.1428	623.4	639.7	7.36	4.02
559	-	15.18	595.1	687.	238.3	146.01	92.54	53.88	-0.0814	555.5	610.2	16.36	4.37
560	-	15.17	597.3	688.	249.1	150.26	80.92	50.57	-0.0287	462.2	553.4	32.96	11.92
561	-	15.18	595.4	686.	260.8	156.30	69.11	45.19	0.0274	368.0	471.6	51.10	25.97
562	-	15.18	597.0	685.	271.1	162.62	63.53	40.29	0.0804	319.0	401.0	60.01	39.76
563	-	15.18	597.3	685.	282.4	168.29	58.89	34.08	0.1375	279.8	325.4	67.08	55.13
564	-	15.18	595.4	685.	293.1	172.36	55.27	27.11	0.1918	251.0	251.6	72.24	72.09

PRESSURE ------- 15.17 MPa
FLOW RATE ------ 1357. Kg/M^2-Sec
HEAT FLUX ------ 315. Kw/M^2
CODE ---------- 48

RUN	REF CODE	PRESURE	HEAT FLUX	FLOW RATE	INLET TEMP	GAMMA RATE 1	GAMMA RATE 2	GAMMA RATE 3	QUALITY	DENSITY (GAP)	DENSITY (CENTER)	VOID (GAP)	VOID (CENTER)
565	-	15.23	298.0	1388.	310.0	141.46	105.14	55.42	-0.1015	660.8	652.0	-2.96	-1.07
566	-	15.17	297.4	1389.	313.8	142.83	103.33	54.99	-0.0768	642.4	639.5	-1.32	-0.68
567	-	15.19	297.7	1390.	320.9	145.07	101.36	52.82	-0.0340	619.8	602.9	-1.01	2.81
568	-	15.17	296.8	1384.	323.9	146.54	97.59	52.72	-0.0133	588.1	594.5	4.00	2.49
569	-	15.13	295.8	1389.	326.8	148.45	92.12	49.71	0.0059	543.9	551.9	12.48	10.55
570	-	15.14	294.9	1388.	329.8	152.82	88.85	45.01	0.0257	508.6	482.6	18.89	25.24

FINAL DATA (SI UNITS)

PRESSURE ------- 15.17 MPa
FLOW RATE ------ 1357. Kg/M^2-Sec
HEAT FLUX ------ 631. Kw/M^2
CODE ---------- 49

RUN	REF CODE	PRESURE	HEAT FLUX	FLOW RATE	INLET TEMP	GAMMA RATE 1	GAMMA RATE 2	GAMMA RATE 3	QUALITY	DENSITY (GAP)	DENSITY (CENTER)	VOID (GAP)	VOID (CENTER)
571	-	15.18	601.7	1387.	277.7	140.42	104.59	55.16	-0.1448	661.5	654.7	0.77	2.15
572	-	15.20	596.4	1390.	284.8	142.27	102.13	54.69	-0.1115	636.4	638.9	2.73	2.20
573	-	15.18	593.9	1391.	296.2	144.35	97.84	53.24	-0.0518	597.8	611.3	5.30	2.26
574	-	15.19	592.6	1388.	302.1	144.35	97.84	53.24	-0.0198	597.4	611.3	1.75	-1.57
575	-	15.15	594.8	1388.	310.0	154.96	81.98	44.37	0.0283	456.8	467.9	30.75	28.02
576	-	15.15	596.4	1388.	316.2	160.92	75.45	37.62	0.0657	399.6	379.1	41.81	46.87
577	-	15.20	598.9	1390.	321.3	164.24	71.19	34.92	0.0959	365.1	343.4	48.36	53.83

PRESSURE ------- 15.17 MPa
FLOW RATE ------ 3122. Kg/M^2-Sec
HEAT FLUX ------ 631. Kw/M^2
CODE ---------- 50

RUN	REF CODE	PRESURE	HEAT FLUX	FLOW RATE	INLET TEMP	GAMMA RATE 1	GAMMA RATE 2	GAMMA RATE 3	QUALITY	DENSITY (GAP)	DENSITY (CENTER)	VOID (GAP)	VOID (CENTER)
578	-	15.18	597.0	3072.	314.6	144.03	103.67	54.56	-0.0840	640.5	628.1	-0.11	2.56
579	-	15.19	596.1	3049.	318.6	145.32	103.90	54.19	-0.0591	637.0	617.2	-2.05	2.36
580	-	15.19	598.3	3045.	321.3	146.29	101.98	54.79	-0.0419	619.9	619.0	-0.22	-0.01
581	-	15.19	599.2	3042.	326.3	149.04	98.33	52.53	-0.0090	584.9	580.4	4.24	5.30
582	-	15.18	601.1	2891.	333.1	157.36	84.14	43.38	0.0442	464.9	449.1	27.78	31.70

PRESSURE ------- 13.79 MPa
FLOW RATE ------ 1357. Kg/M^2-Sec
HEAT FLUX ------ 315. Kw/M^2
CODE ---------- 51

RUN	REF CODE	PRESURE	HEAT FLUX	FLOW RATE	INLET TEMP	GAMMA RATE 1	GAMMA RATE 2	GAMMA RATE 3	QUALITY	DENSITY (GAP)	DENSITY (CENTER)	VOID (GAP)	VOID (CENTER)
583	-	13.79	299.9	1391.	289.0	138.90	108.97	57.26	-0.1452	700.0	688.5	-1.03	1.06
584	-	13.81	296.1	1389.	293.9	139.53	108.92	57.07	-0.1233	696.8	682.6	-2.39	0.27
585	-	13.81	293.6	1387.	299.2	140.40	106.49	55.94	-0.0972	675.4	664.0	-0.69	1.49
586	-	13.80	293.9	1386.	307.8	142.01	104.44	54.87	-0.0519	653.8	642.5	-0.82	1.45
587	-	13.80	293.6	1390.	316.8	145.23	96.45	51.89	-0.0031	585.1	591.4	8.36	6.99
589	-	13.80	294.6	1387.	320.9	149.52	91.22	46.87	0.0213	535.0	515.9	16.67	20.89
588	-	13.79	294.6	1375.	326.1	157.04	79.91	39.33	0.0538	438.3	408.1	35.28	41.92

FINAL DATA (SI UNITS)

PRESSURE ------- 11.03 MPa
FLOW RATE ------ 679. Kg/M^2-Sec
HEAT FLUX ------ 631. Kw/M^2
CODE ---------- 52

RUN	REF CODE	PRESURE	HEAT FLUX	FLOW RATE	INLET TEMP	GAMMA RATE 1	GAMMA RATE 2	GAMMA RATE 3	QUALITY	DENSITY (GAP)	DENSITY (CENTER)	VOID (GAP)	VOID (CENTER)
592	-	11.05	598.0	686.	187.9	128.21	101.01	57.73	-0.1120	726.0	722.8	-0.88	-0.36
593	-	11.05	599.2	687.	196.2	131.21	97.39	56.12	-0.0827	682.7	683.5	3.90	3.76
594	-	11.05	598.3	688.	204.5	134.74	87.45	55.39	-0.0542	589.0	653.4	17.61	6.42
595	-	11.03	598.3	686.	212.5	139.90	76.57	52.47	-0.0235	486.5	591.6	33.38	14.81
596	-	11.04	597.0	687.	220.8	146.18	68.94	43.61	0.0047	411.2	466.6	45.17	35.19
597	-	11.04	598.6	685.	234.1	158.24	66.14	22.87	0.0553	363.0	222.4	51.47	77.20

PRESSURE ------- 6.90 MPa
FLOW RATE ------ 679. Kg/M^2-Sec
HEAT FLUX ------ 631. Kw/M^2
CODE ---------- 53

RUN	REF CODE	PRESURE	HEAT FLUX	FLOW RATE	INLET TEMP	GAMMA RATE 1	GAMMA RATE 2	GAMMA RATE 3	QUALITY	DENSITY (GAP)	DENSITY (CENTER)	VOID (GAP)	VOID (CENTER)
608	-	6.92	598.6	686.	149.1	122.32	95.72	57.68	-0.0805	769.3	768.9	0.99	1.05
606	-	6.88	596.7	684.	155.3	128.00	87.22	54.78	-0.0613	664.8	691.4	14.52	10.76
605	-	6.93	596.7	683.	160.1	131.64	87.00	48.88	-0.0484	647.1	596.6	16.15	23.38
607	-	6.87	597.3	683.	164.1	136.01	85.63	37.81	-0.0348	617.5	443.8	19.69	44.70
604	-	6.89	600.8	681.	167.3	139.54	85.41	33.25	-0.0237	602.1	378.3	21.19	53.70
603	-	6.90	599.2	682.	174.9	144.40	76.14	30.19	-0.0036	508.9	329.7	33.71	60.14
602	-	6.91	597.3	684.	185.5	153.07	63.36	25.01	0.0248	383.5	254.6	51.14	70.50
601	-	6.87	598.3	683.	194.9	159.71	54.88	18.63	0.0544	304.4	180.3	62.14	81.08
599	-	6.90	597.0	686.	199.2	160.22	52.71	18.10	0.0641	266.6	173.5	67.70	81.99
598	-	6.90	596.4	685.	204.5	163.63	50.27	15.35	0.0799	244.3	143.4	70.75	86.32

ENGLISH UNITS

FINAL DATA (ENGLISH UNITS)

PRESSURE ------- 2450 PSIA
FLOW RATE ------ 1.00E+6 LBM/SQFT-HR
HEAT FLUX ------ 0.10E+6 BTU/SQFT-HR
CODE ----------- 1

RUN	REF CODE	PRESURE	HEAT FLUX	FLOW RATE	INLET TEMP	GAMMA RATE 1	GAMMA RATE 2	GAMMA RATE 3	QUALITY	DENSITY (SIDE 2)	DENSITY (SIDE 3)	VOID (SIDE 2)	VOID (SIDE 3)
76	1	2450.	0.0942	1.000	582.2	271.58	150.29	121.14	-0.2206	41.47	41.05	-1.43	0.07
77	1	2449.	0.0941	0.997	592.6	275.44	147.20	120.45	-0.1821	39.83	40.06	1.06	0.20
78	1	2450.	0.0935	1.011	601.2	276.16	145.77	120.07	-0.1535	39.27	39.78	0.43	-1.52
79	1	2452.	0.0939	1.002	613.2	279.63	147.21	116.81	-0.1061	39.13	37.87	-4.30	0.79
80	1	2451.	0.0927	1.006	621.4	283.16	140.79	114.75	-0.0749	36.63	36.47	2.27	2.93
81	1	2451.	0.0928	1.005	631.5	288.20	137.44	112.95	-0.0316	34.88	34.98	4.57	4.10
82	1	2448.	0.0934	1.005	642.0	298.58	123.68	101.93	0.0183	29.54	29.34	23.11	24.10
83	1	2450.	0.0931	1.000	648.3	306.04	119.49	95.44	0.0485	27.51	26.05	29.43	36.31

PRESSURE ------- 2450 PSIA
FLOW RATE ------ 1.00E+6 LBM/SQFT-HR
HEAT FLUX ------ 0.20E+6 BTU/SQFT-HR
CODE ----------- 2

RUN	REF CODE	PRESURE	HEAT FLUX	FLOW RATE	INLET TEMP	GAMMA RATE 1	GAMMA RATE 2	GAMMA RATE 3	QUALITY	DENSITY (SIDE 2)	DENSITY (SIDE 3)	VOID (SIDE 2)	VOID (SIDE 3)
90	2	2447.	0.1886	1.007	535.0	269.53	148.61	122.22	-0.2325	41.11	41.38	-0.38	-1.33
91	2	2448.	0.1890	1.003	536.5	269.78	147.90	121.06	-0.2265	40.84	40.86	-0.01	-0.06
92	2	2447.	0.1890	1.000	547.0	273.14	146.78	121.47	-0.1912	39.90	40.41	0.18	-1.70
93	2	2448.	0.1893	0.999	557.2	275.01	145.60	121.31	-0.1569	39.21	40.02	-0.65	-3.74
94	2	2448.	0.1891	1.000	568.7	280.19	142.10	117.79	-0.1187	37.29	37.71	2.83	1.11
95	2	2448.	0.1893	1.015	577.0	282.95	140.25	114.17	-0.0936	36.31	35.84	3.97	6.06
96	2	2443.	0.1896	1.002	582.5	283.81	136.39	112.09	-0.0682	35.03	34.89	6.62	7.22
97	2	2447.	0.1898	1.011	586.6	287.17	137.09	110.17	-0.0574	34.74	33.64	6.36	11.26
98	2	2447.	0.1896	1.002	593.7	292.71	130.24	106.66	-0.0291	31.98	31.51	15.36	17.39
99	2	2444.	0.1899	1.002	598.5	295.66	124.91	101.86	-0.0094	30.07	29.31	21.97	25.35
100	2	2449.	0.1897	1.005	608.3	302.58	114.60	95.86	0.0244	26.37	26.26	35.53	36.02
101	2	2441.	0.1898	0.990	614.2	310.60	108.39	89.14	0.0549	23.85	22.99	44.71	48.72

PRESSURE ------- 2450 PSIA
FLOW RATE ------ 2.30E+6 LBM/SQFT-HR
HEAT FLUX ------ 0.20E+6 BTU/SQFT-HR
CODE ----------- 3

RUN	REF CODE	PRESURE	HEAT FLUX	FLOW RATE	INLET TEMP	GAMMA RATE 1	GAMMA RATE 2	GAMMA RATE 3	QUALITY	DENSITY (SIDE 2)	DENSITY (SIDE 3)	VOID (SIDE 2)	VOID (SIDE 3)
102	2	2459.	0.1896	2.179	589.2	270.63	151.14	123.66	-0.2110	41.71	41.77	-3.36	-3.59
103	2	2457.	0.1892	2.131	596.8	273.19	148.65	121.83	-0.1791	40.47	40.55	-1.81	-2.11
104	2	2457.	0.1896	2.112	604.0	275.40	146.33	119.57	-0.1501	39.37	39.24	-0.54	-0.02
105	2	2456.	0.1893	2.120	613.8	279.17	145.38	117.89	-0.1123	38.45	37.92	-0.96	1.18
106	2	2458.	0.1887	2.118	624.1	282.26	140.90	115.51	-0.0716	36.61	36.47	1.73	2.30
107	2	2459.	0.1887	2.120	634.3	286.75	138.51	111.84	-0.0277	35.22	34.34	2.30	6.24
108	2	2457.	0.1887	2.114	640.4	292.86	129.90	106.33	0.0014	31.86	31.37	14.06	16.32
109	2	2460.	0.1887	2.090	645.3	297.70	124.17	104.00	0.0254	29.61	29.86	21.76	20.60

FINAL DATA (ENGLISH UNITS)

PRESSURE ------- 2200 PSIA
FLOW RATE ------ 2.30E+6 LBM/SQFT-HR
HEAT FLUX ------ 0.20E+6 BTU/SQFT-HR
CODE ----------- 4

RUN	REF CODE	PRESURE	HEAT FLUX	FLOW RATE	INLET TEMP	GAMMA RATE 1	GAMMA RATE 2	GAMMA RATE 3	QUALITY	DENSITY (SIDE 2)	DENSITY (SIDE 3)	VOID (SIDE 2)	VOID (SIDE 3)
117	2	2193.	0.1889	2.104	604.0	277.14	147.08	119.94	-0.0539	39.31	39.09	-1.85	-1.05
115	2	2194.	0.1956	2.104	609.5	280.16	142.28	114.91	-0.0307	37.35	36.57	2.69	5.66
116	2	2194.	0.1927	2.073	614.2	285.67	141.09	112.57	-0.0139	36.14	34.79	5.30	10.45
114	2	2195.	0.1945	2.093	616.4	285.53	138.02	111.45	-0.0067	35.25	34.37	7.84	11.22
113	2	2196.	0.1941	2.101	622.1	292.44	130.02	105.73	0.0132	31.95	31.19	18.46	21.40
112	2	2197.	0.1937	2.098	624.8	295.00	124.36	103.35	0.0229	29.99	29.96	25.13	25.27
111	2	2195.	0.1909	2.132	628.9	298.32	121.78	99.13	0.0355	28.86	27.96	28.48	32.10
110	2	2197.	0.1902	2.097	635.5	308.01	112.26	91.80	0.0631	25.15	24.20	40.96	44.71

PRESSURE ------- 2200 PSIA
FLOW RATE ------ 1.00E+6 LBM/SQFT-HR
HEAT FLUX ------ 0.20E+6 BTU/SQFT-HR
CODE ----------- 5

RUN	REF CODE	PRESURE	HEAT FLUX	FLOW RATE	INLET TEMP	GAMMA RATE 1	GAMMA RATE 2	GAMMA RATE 3	QUALITY	DENSITY (SIDE 2)	DENSITY (SIDE 3)	VOID (SIDE 2)	VOID (SIDE 3)
127	3	2198.	0.1884	1.007	537.7	270.12	147.69	120.42	-0.1263	40.52	40.42	-0.06	0.28
126	3	2197.	0.1896	1.008	546.9	273.11	144.44	118.81	-0.0980	38.99	39.23	2.42	1.59
125	3	2192.	0.1891	0.997	562.3	282.22	136.85	112.70	-0.0494	35.23	35.28	11.05	10.87
119	3	2192.	0.1899	1.004	572.5	287.64	131.38	107.33	-0.0194	32.83	32.38	17.05	18.71
120	3	2193.	0.1896	1.008	577.3	291.01	124.01	101.61	-0.0059	30.25	29.73	25.53	27.46
121	3	2186.	0.1889	1.004	587.3	298.20	113.18	92.89	0.0273	26.32	25.58	37.98	40.86
122	3	2198.	0.1886	1.009	597.8	304.72	104.35	86.13	0.0567	23.19	22.42	48.16	51.21
123	3	2195.	0.1884	1.003	610.0	315.84	96.40	81.06	0.0999	20.07	19.60	58.06	59.97
124	3	2199.	0.1885	1.007	619.4	321.53	92.30	76.84	0.1322	18.56	17.68	62.61	66.18

PRESSURE ------- 2000 PSIA
FLOW RATE ------ 1.00E+6 LBM/SQFT-HR
HEAT FLUX ------ 0.20E+6 BTU/SQFT-HR
CODE ----------- 6

RUN	REF CODE	PRESURE	HEAT FLUX	FLOW RATE	INLET TEMP	GAMMA RATE 1	GAMMA RATE 2	GAMMA RATE 3	QUALITY	DENSITY (SIDE 2)	DENSITY (SIDE 3)	VOID (SIDE 2)	VOID (SIDE 3)
128	3	1999.	0.1882	0.999	456.4	252.63	157.93	127.27	-0.2654	47.32	46.88	-3.54	-2.37
129	3	1997.	0.1883	1.006	473.1	256.88	156.63	126.52	-0.2262	45.97	45.63	-2.65	-1.71
130	3	1999.	0.1891	1.003	505.6	261.74	152.35	123.83	-0.1455	43.58	43.46	-2.52	-2.17
131	3	1998.	0.1877	1.005	548.0	279.90	139.74	114.37	-0.0381	36.45	36.30	10.06	10.54
132	3	1998.	0.1879	1.005	562.8	289.93	122.96	98.34	0.0025	30.08	28.62	28.15	33.11
133	3	1998.	0.1886	1.010	578.8	305.40	105.57	86.86	0.0472	23.47	22.62	48.10	51.16
134	3	2003.	0.1878	1.010	589.9	311.48	97.24	81.21	0.0777	20.66	20.03	56.52	58.79
135	3	2003.	0.1881	1.005	599.1	320.98	90.93	77.13	0.1072	18.24	17.82	63.87	65.41
136	3	2009.	0.1882	0.994	606.2	322.82	84.46	72.55	0.1312	16.44	16.12	69.52	70.69

FINAL DATA (ENGLISH UNITS)

PRESSURE ------- 2000 PSIA
FLOW RATE ------ 2.30E+6 LBM/SQFT-HR
HEAT FLUX ------ 0.20E+6 BTU/SQFT-HR
CODE ----------- 7

RUN	REF CODE	PRESURE	HEAT FLUX	FLOW RATE	INLET TEMP	GAMMA RATE 1	GAMMA RATE 2	GAMMA RATE 3	QUALITY	DENSITY (SIDE 2)	DENSITY (SIDE 3)	VOID (SIDE 2)	VOID (SIDE 3)
144	3	1995.	0.1872	2.295	545.4	262.59	155.00	125.81	-0.1759	44.27	44.13	-0.68	-0.30
143	3	2008.	0.1872	2.306	553.2	263.54	155.18	125.43	-0.1594	44.13	43.78	-1.93	-0.90
142	3	2007.	0.1873	2.280	562.0	265.00	151.83	122.96	-0.1338	42.78	42.45	-0.05	0.93
141	3	2010.	0.1879	2.273	572.3	267.91	150.59	121.83	-0.1053	41.84	41.42	0.20	1.48
140	3	2010.	0.1876	2.298	581.9	270.38	150.80	121.35	-0.0786	41.45	40.76	-1.10	1.09
139	3	2010.	0.1876	2.298	592.4	274.16	147.26	119.41	-0.0476	39.68	39.29	1.37	2.64
137	3	2014.	0.1879	2.293	601.5	277.22	145.86	116.88	-0.0201	38.74	37.74	1.55	4.94
138	3	2009.	0.1877	2.293	605.7	281.24	139.16	114.17	-0.0055	36.07	36.01	9.25	9.45

PRESSURE ------- 1600 PSIA
FLOW RATE ------ 2.30E+6 LBM/SQFT-HR
HEAT FLUX ------ 0.20E+6 BTU/SQFT-HR
CODE ----------- 8

RUN	REF CODE	PRESURE	HEAT FLUX	FLOW RATE	INLET TEMP	GAMMA RATE 1	GAMMA RATE 2	GAMMA RATE 3	QUALITY	DENSITY (SIDE 2)	DENSITY (SIDE 3)	VOID (SIDE 2)	VOID (SIDE 3)
145	3	1596.	0.1862	2.297	477.2	248.88	160.33	131.65	-0.2128	48.97	49.70	-1.98	-3.73
146	3	1590.	0.1870	2.302	500.3	254.99	157.72	127.64	-0.1616	46.73	46.52	0.13	0.65
147	3	1594.	0.1882	2.310	536.4	261.54	157.09	128.84	-0.0825	45.15	45.64	-2.07	-3.37
148	3	1596.	0.1883	2.296	550.6	265.66	152.24	125.41	-0.0495	42.78	43.35	1.33	-0.22
154	3	1598.	0.1893	2.291	560.8	268.48	151.00	121.91	-0.0249	41.86	41.35	1.74	3.19
149	3	1596.	0.1880	2.282	567.6	272.60	145.79	116.22	-0.0084	39.50	38.26	6.87	10.42
153	3	1601.	0.1890	2.283	577.2	285.15	125.08	102.52	0.0150	31.32	30.86	28.59	30.01
150	3	1591.	0.1873	2.288	580.1	292.24	120.93	99.42	0.0236	29.20	28.74	34.37	35.71
151	3	1601.	0.1889	2.294	586.4	298.46	109.80	91.13	0.0384	25.34	24.90	44.76	46.04
152	3	1607.	0.1891	2.269	589.0	300.95	107.72	90.48	0.0447	24.50	24.39	46.88	47.18

PRESSURE ------- 1600 PSIA
FLOW RATE ------ 1.00E+6 LBM/SQFT-HR
HEAT FLUX ------ 0.20E+6 BTU/SQFT-HR
CODE ----------- 9

RUN	REF CODE	PRESURE	HEAT FLUX	FLOW RATE	INLET TEMP	GAMMA RATE 1	GAMMA RATE 2	GAMMA RATE 3	QUALITY	DENSITY (SIDE 2)	DENSITY (SIDE 3)	VOID (SIDE 2)	VOID (SIDE 3)
165	3	1600.	0.1880	1.006	481.3	259.11	155.58	125.33	-0.0910	45.16	44.64	-2.56	-1.18
164	3	1599.	0.1904	1.003	496.0	265.61	151.62	123.27	-0.0561	42.59	42.46	1.26	1.62
163	3	1600.	0.1904	1.000	510.1	275.52	136.52	113.71	-0.0251	36.16	36.75	16.77	15.08
160	3	1602.	0.1894	1.005	517.5	281.74	129.77	106.05	-0.0114	33.18	32.73	24.23	25.55
161	3	1607.	0.1884	1.002	528.2	291.09	110.37	91.84	0.0108	26.30	26.00	42.71	43.59
162	3	1601.	0.1895	0.999	535.2	302.12	90.00	78.34	0.0297	19.47	19.82	61.80	60.77
159	3	1596.	0.1889	1.004	542.9	307.98	78.90	69.23	0.0471	15.98	16.04	71.32	71.15
158	3	1597.	0.1896	1.003	559.5	321.94	73.96	64.62	0.0869	13.78	13.46	76.72	77.64
157	3	1601.	0.1894	1.004	570.4	325.99	72.35	62.63	0.1123	13.14	12.54	78.09	79.85
156	3	1601.	0.1889	1.004	581.0	330.78	69.80	61.27	0.1386	12.24	11.81	80.25	81.53
155	3	1601.	0.1890	0.999	585.6	331.27	67.54	59.77	0.1515	11.65	11.29	81.79	82.87

FINAL DATA (ENGLISH UNITS)

PRESSURE ------- 1600 PSIA
FLOW RATE ------ 0.50E+6 LBM/SQFT-HR
HEAT FLUX ------ 0.20E+6 BTU/SQFT-HR
CODE ---------- 10

RUN	REF CODE	PRESURE	HEAT FLUX	FLOW RATE	INLET TEMP	GAMMA RATE 1	GAMMA RATE 2	GAMMA RATE 3	QUALITY	DENSITY (SIDE 2)	DENSITY (SIDE 3)	VOID (SIDE 2)	VOID (SIDE 3)
171	4	1602.	0.1884	0.507	377.7	261.80	152.92	122.07	-0.1010	43.52	42.51	0.78	3.51
170	4	1603.	0.1884	0.505	393.4	267.68	147.19	118.05	-0.0694	40.58	39.70	6.03	8.48
169	4	1602.	0.1885	0.508	403.6	273.15	141.56	115.23	-0.0505	37.88	37.58	12.12	12.96
172	4	1602.	0.1889	0.507	408.5	277.11	136.77	109.14	-0.0397	35.78	34.48	17.23	20.95
173	4	1603.	0.1889	0.507	415.2	281.17	129.78	103.03	-0.0262	33.08	31.45	23.91	28.70
174	4	1601.	0.1887	0.508	419.7	284.36	121.15	99.81	-0.0178	30.08	29.75	32.15	33.11
176	4	1601.	0.1888	0.504	425.5	289.65	108.62	92.04	-0.0032	25.79	26.09	43.78	42.90
175	4	1603.	0.1886	0.505	430.0	292.17	102.17	85.07	0.0042	23.66	23.15	49.63	51.12
177	4	1604.	0.1884	0.504	436.7	297.65	89.83	77.34	0.0177	19.66	19.72	60.88	60.69
178	4	1604.	0.1887	0.506	441.0	299.50	83.69	73.85	0.0256	17.79	18.26	66.09	64.69
179	4	1601.	0.1873	0.502	450.0	306.83	75.80	66.90	0.0447	15.09	15.15	73.40	73.21
180	4	1604.	0.1869	0.502	456.5	310.58	75.21	67.07	0.0567	14.69	14.95	74.30	73.53
181	4	1605.	0.1870	0.504	460.7	311.62	72.24	65.01	0.0638	13.83	14.15	76.66	75.72
182	4	1605.	0.1868	0.504	475.4	321.24	74.59	65.08	0.0937	13.87	13.54	75.84	76.83

PRESSURE ------- 1000 PSIA
FLOW RATE ------ 0.50E+6 LBM/SQFT-HR
HEAT FLUX ------ 0.20E+6 BTU/SQFT-HR
CODE ---------- 11

RUN	REF CODE	PRESURE	HEAT FLUX	FLOW RATE	INLET TEMP	GAMMA RATE 1	GAMMA RATE 2	GAMMA RATE 3	QUALITY	DENSITY (SIDE 2)	DENSITY (SIDE 3)	VOID (SIDE 2)	VOID (SIDE 3)
190	4	1001.	0.1894	0.503	288.4	251.13	156.19	125.24	-0.0978	46.81	46.12	3.38	4.94
189	4	1005.	0.1884	0.504	316.4	266.86	125.24	103.54	-0.0566	33.79	33.80	30.55	30.53
188	4	1002.	0.1883	0.506	333.0	280.09	100.87	85.20	-0.0311	24.56	24.54	50.96	51.00
187	4	1003.	0.1882	0.505	356.7	295.61	85.10	72.60	0.0073	18.49	18.13	64.14	65.01
186	4	997.	0.1884	0.505	374.3	310.94	71.12	61.95	0.0369	13.57	13.11	75.37	76.49
185	4	997.	0.1846	0.506	403.5	324.49	59.75	57.69	0.0777	9.89	10.83	83.78	81.41
184	4	999.	0.1881	0.506	423.8	331.19	55.17	53.19	0.1171	8.45	8.99	86.88	85.51
183	4	999.	0.1885	0.504	451.3	340.23	51.35	48.67	0.1655	7.18	7.13	89.62	89.76

PRESSURE ------- 1000 PSIA
FLOW RATE ------ 1.00E+6 LBM/SQFT-HR
HEAT FLUX ------ 0.20E+6 BTU/SQFT-HR
CODE ---------- 12

RUN	REF CODE	PRESURE	HEAT FLUX	FLOW RATE	INLET TEMP	GAMMA RATE 1	GAMMA RATE 2	GAMMA RATE 3	QUALITY	DENSITY (SIDE 2)	DENSITY (SIDE 3)	VOID (SIDE 2)	VOID (SIDE 3)
191	4	1000.	0.1881	1.006	376.7	246.91	163.88	129.90	-0.1266	50.40	49.18	-1.21	1.44
192	4	1000.	0.1880	1.009	390.5	247.84	161.60	130.21	-0.1047	49.40	49.10	-0.49	0.16
193	4	1001.	0.1883	1.000	424.4	258.17	155.80	124.40	-0.0470	45.18	44.24	4.85	7.01
195	4	1000.	0.1885	1.001	437.5	270.32	119.69	99.59	-0.0245	31.54	31.63	35.13	34.91
194	4	1000.	0.1881	1.003	447.7	281.82	92.82	81.11	-0.0078	21.97	22.73	56.88	55.10
196	4	999.	0.1889	1.002	458.8	297.57	87.80	74.71	0.0122	19.09	18.75	63.09	63.91
197	4	1006.	0.1888	1.002	484.6	318.58	66.52	60.92	0.0559	11.93	12.27	79.41	78.56
198	4	1000.	0.1891	1.000	508.7	331.93	58.50	51.44	0.1014	9.25	8.37	85.28	87.43
199	4	1003.	0.1888	1.001	520.1	338.14	56.35	51.35	0.1216	8.47	8.08	87.00	87.98

FINAL DATA (ENGLISH UNITS)

PRESSURE ------- 2450 PSIA
FLOW RATE ------ 2.30E+6 LBM/SQFT-HR
HEAT FLUX ------ 0.40E+6 BTU/SQFT-HR
CODE ----------- 13

RUN	REF CODE	PRESURE	HEAT FLUX	FLOW RATE	INLET TEMP	GAMMA RATE 1	GAMMA RATE 2	GAMMA RATE 3	QUALITY	DENSITY (SIDE 2)	DENSITY (SIDE 3)	VOID (SIDE 2)	VOID (SIDE 3)
228	7	2451.	0.3789	2.284	559.4	273.61	145.50	116.34	-0.1876	39.35	39.25	2.11	2.48
229	7	2446.	0.3777	2.290	572.6	275.96	145.10	114.47	-0.1418	38.84	38.08	-0.26	2.69
234	7	2451.	0.3790	2.290	588.3	279.89	139.53	112.25	-0.0874	36.52	36.53	2.70	2.68
230	7	2444.	0.3765	2.290	605.4	288.56	130.25	102.41	-0.0232	32.53	31.32	12.79	18.10
231	7	2451.	0.3785	2.297	613.9	294.79	121.11	98.42	0.0085	29.11	28.96	24.79	25.46
232	7	2444.	0.3790	2.273	621.3	303.96	112.86	91.93	0.0437	25.79	25.45	36.85	38.49
233	7	2451.	0.3785	2.183	631.1	314.03	101.93	83.81	0.0931	21.89	21.49	51.35	53.31

PRESSURE ------- 1600 PSIA
FLOW RATE ------ 2.30E+6 LBM/SQFT-HR
HEAT FLUX ------ 0.10E+6 BTU/SQFT-HR
CODE ----------- 14

RUN	REF CODE	PRESURE	HEAT FLUX	FLOW RATE	INLET TEMP	GAMMA RATE 1	GAMMA RATE 2	GAMMA RATE 3	QUALITY	DENSITY (SIDE 2)	DENSITY (SIDE 3)	VOID (SIDE 2)	VOID (SIDE 3)
244	9	1608.	0.0931	2.293	531.9	263.93	155.71	125.34	-0.1409	46.87	46.70	-1.73	-1.29
245	9	1608.	0.0929	2.293	551.5	267.42	153.85	122.66	-0.0954	45.54	44.79	-1.88	0.10
246	9	1606.	0.0935	2.284	573.1	271.18	148.86	121.21	-0.0416	43.17	43.41	-0.16	-0.84
247	9	1609.	0.0938	2.284	580.2	273.12	149.91	121.45	-0.0244	43.15	43.14	-1.71	-1.70
248	9	1609.	0.0942	2.284	584.7	277.30	147.75	117.93	-0.0127	41.69	40.87	1.19	3.56
249	9	1597.	0.0942	2.301	588.5	282.79	141.57	118.14	0.0000	38.81	39.99	8.52	5.09
250	9	1596.	0.0947	2.296	593.8	291.69	127.39	106.14	0.0147	33.12	33.70	23.79	22.10

PRESSURE ------- 1600 PSIA
FLOW RATE ------ 2.30E+6 LBM/SQFT-HR
HEAT FLUX ------ 0.40E+6 BTU/SQFT-HR
CODE ----------- 15

RUN	REF CODE	PRESURE	HEAT FLUX	FLOW RATE	INLET TEMP	GAMMA RATE 1	GAMMA RATE 2	GAMMA RATE 3	QUALITY	DENSITY (SIDE 2)	DENSITY (SIDE 3)	VOID (SIDE 2)	VOID (SIDE 3)
252	25	1601.	0.3778	2.283	451.1	258.57	155.27	124.99	-0.1771	47.04	45.93	-0.48	2.30
253	25	1598.	0.3791	2.296	484.8	264.26	149.77	124.19	-0.1063	44.03	44.40	1.99	1.02
254	25	1601.	0.3790	2.289	511.1	271.46	146.82	120.13	-0.0499	41.71	41.28	3.40	4.57
255	25	1602.	0.3794	2.289	530.2	286.97	129.43	106.48	-0.0076	33.78	33.20	22.44	24.11
256	25	1596.	0.3800	2.284	542.7	300.47	108.15	91.53	0.0230	25.83	25.72	43.62	43.93
257	25	1598.	0.3793	2.296	558.2	315.07	93.12	78.08	0.0577	20.24	19.38	58.49	61.11
258	25	1604.	0.3782	2.261	577.1	328.74	80.04	71.28	0.1053	15.76	15.96	70.42	69.80

FINAL DATA (ENGLISH UNITS)

PRESSURE ------- 2000 PSIA
FLOW RATE ------ 2.30E+6 LBM/SQFT-HR
HEAT FLUX ------ 0.40E+6 BTU/SQFT-HR
CODE ----------- 16

RUN	REF CODE	PRESURE	HEAT FLUX	FLOW RATE	INLET TEMP	GAMMA RATE 1	GAMMA RATE 2	GAMMA RATE 3	QUALITY	DENSITY (SIDE 2)	DENSITY (SIDE 3)	VOID (SIDE 2)	VOID (SIDE 3)
263	25	2004.	0.3778	2.295	536.6	272.65	146.68	120.31	-0.0978	41.45	41.14	-0.21	0.76
262	25	2004.	0.3794	2.293	551.3	278.94	142.04	118.09	-0.0576	38.90	39.12	3.91	3.20
261	25	2001.	0.3786	2.295	569.8	291.20	127.08	103.32	-0.0067	32.49	31.37	20.74	24.64
259	25	2000.	0.3774	2.299	590.0	309.24	106.56	88.92	0.0514	24.48	23.83	44.47	46.76
260	25	1997.	0.3798	2.201	608.8	326.52	90.55	78.12	0.1208	18.67	18.47	61.72	62.49

PRESSURE ------- 2000 PSIA
FLOW RATE ------ 1.00E+6 LBM/SQFT-HR
HEAT FLUX ------ 0.10E+6 BTU/SQFT-HR
CODE ----------- 17

RUN	REF CODE	PRESURE	HEAT FLUX	FLOW RATE	INLET TEMP	GAMMA RATE 1	GAMMA RATE 2	GAMMA RATE 3	QUALITY	DENSITY (SIDE 2)	DENSITY (SIDE 3)	VOID (SIDE 2)	VOID (SIDE 3)
267	26	2006.	0.0938	1.004	497.6	259.15	156.30	122.89	-0.2871	47.77	46.53	-2.54	0.72
268	26	2013.	0.0932	1.000	515.9	262.77	153.56	124.60	-0.2440	46.08	46.53	-1.10	-2.32
269	26	2004.	0.0930	0.999	537.6	266.77	152.06	121.64	-0.1850	44.77	44.39	-1.74	-0.65
270	26	2011.	0.0934	0.998	558.2	270.22	149.34	118.63	-0.1313	43.21	42.40	-1.83	0.64
271	26	2007.	0.0936	0.995	574.5	275.63	146.32	116.24	-0.0836	41.25	40.37	-0.09	2.69
272	26	2007.	0.0932	1.001	587.4	278.89	142.51	115.80	-0.0471	39.48	39.61	1.92	1.48
273	26	2003.	0.0936	1.003	598.7	288.49	135.64	113.23	-0.0117	35.84	36.97	10.64	6.77
274	26	1998.	0.0935	1.001	609.3	299.90	123.29	99.24	0.0237	30.62	29.79	25.51	28.41
275	26	2006.	0.0934	1.003	619.2	310.88	110.65	89.34	0.0543	25.77	24.76	40.27	43.89

PRESSURE ------- 1600 PSIA
FLOW RATE ------ 1.00E+6 LBM/SQFT-HR
HEAT FLUX ------ 0.10E+6 BTU/SQFT-HR
CODE ----------- 18

RUN	REF CODE	PRESURE	HEAT FLUX	FLOW RATE	INLET TEMP	GAMMA RATE 1	GAMMA RATE 2	GAMMA RATE 3	QUALITY	DENSITY (SIDE 2)	DENSITY (SIDE 3)	VOID (SIDE 2)	VOID (SIDE 3)
278	10	1601.	0.0932	1.007	486.7	259.39	153.15	125.00	-0.1815	46.64	46.78	1.44	1.10
289	10	1595.	0.0928	1.001	494.0	259.51	152.22	124.91	-0.1643	46.30	46.71	1.21	0.18
290	10	1597.	0.0929	1.001	504.6	260.65	152.10	124.31	-0.1418	46.02	46.20	0.26	-0.20
291	10	1602.	0.0942	1.001	541.0	267.79	151.36	118.21	-0.0602	44.33	42.08	-2.13	4.04
292	10	1600.	0.0944	1.010	549.7	272.17	147.40	118.90	-0.0404	42.21	41.55	1.94	3.77
293	10	1606.	0.0937	1.008	564.8	282.67	140.90	112.53	-0.0062	38.35	37.08	9.68	13.36
294	10	1608.	0.0937	1.005	574.5	298.15	121.38	98.71	0.0179	30.26	29.38	31.34	33.98
296	10	1601.	0.0932	1.000	579.2	305.15	105.64	85.96	0.0315	24.92	23.72	46.27	49.77
295	10	1604.	0.0932	1.006	586.7	314.43	87.52	76.05	0.0495	18.99	19.18	62.89	62.35

FINAL DATA (ENGLISH UNITS)

PRESSURE ------- 2200 PSIA
FLOW RATE ------ 2.30E+6 LBM/SQFT-HR
HEAT FLUX ------ 0.40E+6 BTU/SQFT-HR
CODE ----------- 19

RUN	REF CODE	PRESURE	HEAT FLUX	FLOW RATE	INLET TEMP	GAMMA RATE 1	GAMMA RATE 2	GAMMA RATE 3	QUALITY	DENSITY (SIDE 2)	DENSITY (SIDE 3)	VOID (SIDE 2)	VOID (SIDE 3)
264	25	2192.	0.3779	2.289	537.4	272.37	146.11	119.92	-0.1552	41.32	41.03	0.62	1.55
265	25	2201.	0.3786	2.288	563.8	278.82	140.24	116.54	-0.0807	38.35	38.51	3.10	2.56
335	12	2201.	0.3792	2.294	571.2	282.31	140.66	113.87	-0.0583	38.06	37.40	1.68	4.19
336	12	2202.	0.3791	2.293	580.6	286.41	134.79	108.40	-0.0296	35.63	34.55	7.58	11.71
337	12	2197.	0.3800	2.300	590.5	295.62	122.36	100.42	0.0034	30.65	30.13	23.38	25.45
341	12	2199.	0.3798	2.291	590.6	298.48	121.81	99.51	0.0037	30.13	29.42	25.38	28.00
338	12	2201.	0.3797	2.290	600.7	306.36	113.44	92.99	0.0365	26.83	26.03	35.40	38.56
340	12	2199.	0.3775	2.286	601.8	307.05	112.54	92.61	0.0398	26.50	25.82	36.46	39.14
339	12	2205.	0.3783	2.265	606.7	310.54	105.91	89.46	0.0580	24.29	24.29	43.82	43.84

PRESSURE ------- 1600 PSIA
FLOW RATE ------ 1.00E+6 LBM/SQFT-HR
HEAT FLUX ------ 0.40E+6 BTU/SQFT-HR
CODE ----------- 20

RUN	REF CODE	PRESURE	HEAT FLUX	FLOW RATE	INLET TEMP	GAMMA RATE 1	GAMMA RATE 2	GAMMA RATE 3	QUALITY	DENSITY (SIDE 2)	DENSITY (SIDE 3)	VOID (SIDE 2)	VOID (SIDE 3)
298	11	1603.	0.3781	1.000	296.3	252.12	154.70	127.06	-0.2503	48.49	48.52	-0.82	-0.91
299	11	1599.	0.3782	1.007	340.7	257.17	148.88	123.66	-0.1675	45.38	45.87	1.23	-0.02
300	11	1592.	0.3783	1.001	382.4	273.70	138.74	116.61	-0.0825	38.91	39.61	11.92	10.00
304	11	1604.	0.3750	1.000	398.9	282.56	128.26	106.69	-0.0563	34.22	34.09	22.82	23.17
301	11	1601.	0.3792	1.000	422.2	302.53	81.58	75.15	-0.0046	18.09	19.47	66.12	62.20
302	11	1601.	0.3772	1.005	442.3	313.25	66.84	61.58	0.0317	13.21	13.65	79.02	77.77
303	11	1607.	0.3829	1.006	493.8	340.88	58.74	55.29	0.1436	9.71	9.94	87.31	86.65

PRESSURE ------- 1600 PSIA
FLOW RATE ------ 0.50E+6 LBM/SQFT-HR
HEAT FLUX ------ 0.10E+6 BTU/SQFT-HR
CODE ----------- 21

RUN	REF CODE	PRESURE	HEAT FLUX	FLOW RATE	INLET TEMP	GAMMA RATE 1	GAMMA RATE 2	GAMMA RATE 3	QUALITY	DENSITY (SIDE 2)	DENSITY (SIDE 3)	VOID (SIDE 2)	VOID (SIDE 3)
305	10	1599.	0.0938	0.505	449.1	259.60	153.56	124.57	-0.1586	46.73	46.54	-1.17	-0.68
306	10	1597.	0.0943	0.503	470.1	266.03	153.29	122.84	-0.1129	45.32	44.44	-1.07	1.25
307	10	1599.	0.0933	0.505	488.3	270.13	150.98	121.85	-0.0779	43.76	43.20	0.12	1.64
308	10	1598.	0.0937	0.506	499.9	273.43	146.74	119.64	-0.0523	41.77	41.63	3.27	3.65
309	10	1593.	0.0938	0.502	521.1	289.07	127.63	102.42	-0.0032	33.31	32.03	23.30	27.10
310	10	1602.	0.0940	0.506	530.3	298.10	112.26	91.70	0.0141	27.59	26.67	38.80	41.48
311	10	1601.	0.0942	0.507	540.9	312.33	88.71	76.81	0.0390	19.49	19.63	61.41	60.99
312	10	1601.	0.0945	0.505	550.0	320.28	83.74	71.78	0.0612	17.52	17.17	66.42	67.47
313	10	1594.	0.0945	0.509	563.6	330.95	79.38	69.81	0.0939	15.65	15.71	70.98	70.79

FINAL DATA (ENGLISH UNITS)

PRESSURE ------- 1000 PSIA
FLOW RATE ------ 0.50E+6 LBM/SQFT-HR
HEAT FLUX ------ 0.10E+6 BTU/SQFT-HR
CODE ----------- 22

RUN	REF CODE	PRESURE	HEAT FLUX	FLOW RATE	INLET TEMP	GAMMA RATE 1	GAMMA RATE 2	GAMMA RATE 3	QUALITY	DENSITY (SIDE 2)	DENSITY (SIDE 3)	VOID (SIDE 2)	VOID (SIDE 3)
322	10	1004.	0.0937	0.506	399.0	255.11	156.46	124.28	-0.0927	48.71	47.39	0.14	3.07
321	10	1007.	0.0935	0.506	409.8	254.98	152.93	126.29	-0.0758	47.51	48.33	1.51	-0.35
320	10	1008.	0.0931	0.506	421.7	259.29	153.20	124.21	-0.0570	46.67	46.44	2.06	2.60
319	10	1001.	0.0929	0.503	430.6	266.89	144.91	116.82	-0.0398	42.38	41.64	10.85	12.57
318	10	1013.	0.0931	0.504	443.9	280.69	112.36	94.01	-0.0201	29.73	29.76	39.08	38.99
317	10	1004.	0.0931	0.503	456.8	294.77	100.18	81.76	0.0046	24.39	23.17	50.71	53.62
316	10	1007.	0.0933	0.504	483.6	322.96	74.59	65.79	0.0507	14.87	14.84	72.31	72.38
315	10	1004.	0.0933	0.505	504.9	338.32	66.75	60.23	0.0896	11.97	11.99	78.70	78.65
314	10	997.	0.0935	0.506	522.7	345.46	60.52	53.96	0.1243	10.07	9.53	82.88	84.26

PRESSURE ------- 1000 PSIA
FLOW RATE ------ 2.30E+6 LBM/SQFT-HR
HEAT FLUX ------ 0.10E+6 BTU/SQFT-HR
CODE ----------- 23

RUN	REF CODE	PRESURE	HEAT FLUX	FLOW RATE	INLET TEMP	GAMMA RATE 1	GAMMA RATE 2	GAMMA RATE 3	QUALITY	DENSITY (SIDE 2)	DENSITY (SIDE 3)	VOID (SIDE 2)	VOID (SIDE 3)
323	10	1005.	0.0932	2.290	446.6	250.15	161.03	128.94	-0.1429	51.46	50.68	-1.58	0.08
324	10	997.	0.0932	2.288	476.2	254.31	156.32	126.98	-0.0893	48.84	48.80	0.74	0.81
325	10	1000.	0.0930	2.292	491.8	256.10	157.06	127.11	-0.0626	48.69	48.46	-0.96	-0.43
326	10	1001.	0.0931	2.297	511.9	259.58	155.94	124.90	-0.0263	47.55	46.69	-1.06	0.93
327	10	999.	0.0928	2.293	520.8	263.54	154.08	124.81	-0.0092	46.09	45.81	1.05	1.70
328	10	1000.	0.0929	2.286	526.2	273.57	140.63	113.86	0.0010	39.78	39.16	15.14	16.60
329	10	1004.	0.0933	2.290	530.5	282.17	123.87	101.69	0.0081	33.12	32.72	30.41	31.38

PRESSURE ------- 2200 PSIA
FLOW RATE ------ 0.50E+6 LBM/SQFT-HR
HEAT FLUX ------ 0.20E+6 BTU/SQFT-HR
CODE ----------- 24

RUN	REF CODE	PRESURE	HEAT FLUX	FLOW RATE	INLET TEMP	GAMMA RATE 1	GAMMA RATE 2	GAMMA RATE 3	QUALITY	DENSITY (SIDE 2)	DENSITY (SIDE 3)	VOID (SIDE 2)	VOID (SIDE 3)
395	13	2201.	0.1874	0.504	456.2	281.26	140.03	113.91	-0.0954	37.84	37.13	3.18	5.75
396	13	2200.	0.1875	0.506	466.3	285.03	137.46	111.36	-0.0694	36.46	35.52	5.56	9.12
350	13	2198.	0.1874	0.505	472.2	287.59	133.88	108.26	-0.0530	35.00	33.90	9.23	13.39
397	13	2200.	0.1884	0.505	477.4	290.89	128.89	104.66	-0.0380	33.04	32.03	15.05	18.97
349	13	2200.	0.1880	0.506	482.4	294.53	126.00	102.38	-0.0264	31.70	30.66	19.08	23.16
398	13	2199.	0.1895	0.506	490.7	303.22	116.70	95.76	0.0002	27.95	27.08	31.33	34.85
348	13	2198.	0.1886	0.503	491.1	299.67	119.00	95.56	0.0018	29.02	27.42	26.98	33.33
347	13	2201.	0.1889	0.503	502.5	307.80	110.18	89.57	0.0328	25.62	24.30	37.93	43.43
346	13	2199.	0.1884	0.506	518.4	316.02	102.62	85.00	0.0723	22.74	21.85	47.02	50.73
345	13	2202.	0.1886	0.506	535.0	323.40	91.35	75.65	0.1182	19.10	17.93	59.54	64.54
344	13	2203.	0.1890	0.507	545.8	329.32	84.06	72.83	0.1494	16.76	16.52	67.99	69.04
343	13	2204.	0.1894	0.506	557.0	334.47	75.66	69.03	0.1841	14.28	14.88	77.11	74.57

FINAL DATA (ENGLISH UNITS)

PRESSURE ------- 2000 PSIA
FLOW RATE ------ 0.50E+6 LBM/SQFT-HR
HEAT FLUX ------ 0.20E+6 BTU/SQFT-HR
CODE ----------- 25

RUN	REF CODE	PRESURE	HEAT FLUX	FLOW RATE	INLET TEMP	GAMMA RATE 1	GAMMA RATE 2	GAMMA RATE 3	QUALITY	DENSITY (SIDE 2)	DENSITY (SIDE 3)	VOID (SIDE 2)	VOID (SIDE 3)
391	13	1996.	0.1879	0.516	425.8	274.34	144.79	117.37	-0.1161	40.49	39.72	2.10	4.53
392	13	1996.	0.1877	0.511	439.3	278.24	141.79	114.55	-0.0808	38.88	37.89	3.71	6.93
352	13	2005.	0.1900	0.506	451.1	287.21	133.22	105.71	-0.0454	34.85	32.95	13.43	19.98
394	13	1996.	0.1867	0.503	452.9	287.18	132.83	108.18	-0.0447	34.74	33.93	13.99	16.84
393	13	1996.	0.1867	0.504	458.0	290.29	128.12	101.49	-0.0329	32.89	30.87	19.24	26.22
351	13	2009.	0.1888	0.503	463.0	295.04	123.40	99.83	-0.0189	30.86	29.61	24.77	29.26
353	13	2002.	0.1890	0.504	473.5	300.18	115.30	94.54	0.0082	27.89	26.98	33.14	36.46
354	13	2001.	0.1886	0.506	485.5	308.32	107.04	88.30	0.0351	24.69	23.78	42.81	46.14
355	13	1998.	0.1886	0.504	510.2	324.16	84.28	73.45	0.0979	17.17	17.11	67.07	67.31
356	13	2001.	0.1883	0.507	526.8	332.61	74.06	65.25	0.1368	13.97	13.73	77.37	78.23
357	13	2001.	0.1884	0.502	546.7	339.45	65.84	55.94	0.1933	11.53	10.24	84.71	88.90
358	13	2004.	0.1878	0.508	556.2	343.96	64.12	56.88	0.2117	10.89	10.33	86.64	88.45

PRESSURE ------- 1000 PSIA
FLOW RATE ------ 2.30E+6 LBM/SQFT-HR
HEAT FLUX ------ 0.40E+6 BTU/SQFT-HR
CODE ----------- 26

RUN	REF CODE	PRESURE	HEAT FLUX	FLOW RATE	INLET TEMP	GAMMA RATE 1	GAMMA RATE 2	GAMMA RATE 3	QUALITY	DENSITY (SIDE 2)	DENSITY (SIDE 3)	VOID (SIDE 2)	VOID (SIDE 3)
366	12	999.	0.3789	2.290	344.2	241.22	160.08	131.72	-0.1980	52.96	53.84	-2.05	-3.89
367	12	999.	0.3785	2.289	414.8	250.41	155.28	127.26	-0.0831	49.01	49.45	-1.08	-2.08
368	12	999.	0.3781	2.295	442.6	261.28	150.54	121.73	-0.0367	45.04	44.57	4.65	5.73
372	12	1006.	0.3785	2.293	454.1	272.76	131.22	107.29	-0.0186	36.61	36.22	22.97	23.89
369	12	998.	0.3786	2.285	462.1	283.24	102.97	87.52	-0.0023	26.30	26.57	46.54	45.91
370	12	999.	0.3788	2.286	475.1	304.72	77.38	69.69	0.0201	16.75	17.48	68.53	66.79
371	12	1006.	0.3783	2.291	484.8	312.37	72.42	64.89	0.0353	14.84	15.13	72.77	72.07

PRESSURE ------- 1000 PSIA
FLOW RATE ------ 1.00E+6 LBM/SQFT-HR
HEAT FLUX ------ 0.40E+6 BTU/SQFT-HR
CODE ----------- 27

RUN	REF CODE	PRESURE	HEAT FLUX	FLOW RATE	INLET TEMP	GAMMA RATE 1	GAMMA RATE 2	GAMMA RATE 3	QUALITY	DENSITY (SIDE 2)	DENSITY (SIDE 3)	VOID (SIDE 2)	VOID (SIDE 3)
381	12	1004.	0.3810	1.006	279.4	252.12	153.46	127.50	-0.1105	47.98	49.17	1.66	-0.98
380	12	998.	0.3791	1.004	286.4	256.85	151.06	122.76	-0.0989	46.13	45.96	5.02	5.40
379	12	1004.	0.3796	1.001	293.3	263.11	140.93	118.67	-0.0880	41.46	42.86	14.74	11.59
378	12	1004.	0.3795	1.003	305.5	272.97	115.59	97.58	-0.0695	31.57	32.10	36.27	35.06
382	12	1005.	0.3800	0.998	312.9	282.11	97.99	85.25	-0.0562	24.89	25.78	51.07	49.02
377	12	1005.	0.3812	0.999	331.2	293.54	74.07	69.08	-0.0264	16.60	18.17	69.50	65.82
376	12	1003.	0.3780	0.995	349.5	307.65	70.23	62.94	0.0018	14.53	14.74	73.79	73.28
375	12	1001.	0.3792	1.003	381.4	324.42	55.65	53.47	0.0522	9.65	10.31	84.68	83.08
374	12	1004.	0.3784	1.005	418.5	339.24	47.34	48.30	0.1115	6.93	7.86	90.71	88.45
373	12	1005.	0.3791	1.002	452.0	346.22	44.26	42.40	0.1698	5.95	5.64	92.73	92.30

FINAL DATA (ENGLISH UNITS)

PRESSURE ------- 1000 PSIA
FLOW RATE ------ 2.30E+6 LBM/SQFT-HR
HEAT FLUX ------ 0.20E+6 BTU/SQFT-HR
CODE ----------- 28

RUN	REF CODE	PRESURE	HEAT FLUX	FLOW RATE	INLET TEMP	GAMMA RATE 1	GAMMA RATE 2	GAMMA RATE 3	QUALITY	DENSITY (SIDE 2)	DENSITY (SIDE 3)	VOID (SIDE 2)	VOID (SIDE 3)
383	13	1002.	0.1895	2.280	441.4	250.36	159.13	128.77	-0.1128	50.13	49.58	-0.88	0.32
384	13	1001.	0.1903	2.287	465.6	254.69	157.13	127.55	-0.0708	48.45	48.03	-0.14	0.80
385	13	1006.	0.1884	2.288	487.3	259.60	155.12	126.31	-0.0347	46.70	46.40	1.14	1.92
390	13	995.	0.1880	2.290	496.6	263.56	150.34	122.07	-0.0153	44.29	43.73	5.47	6.79
386	13	1000.	0.1885	2.287	506.8	281.38	121.71	100.02	0.0021	32.16	31.51	32.84	34.39
387	13	1002.	0.1887	2.292	514.1	295.36	96.90	81.34	0.0151	23.06	22.48	53.87	55.26
388	13	1003.	0.1884	2.293	518.8	300.77	89.99	78.89	0.0234	20.55	21.02	59.57	58.45
389	13	1001.	0.1883	2.285	526.1	312.32	82.75	72.47	0.0380	17.60	17.66	66.25	66.10

PRESSURE ------- 2200 PSIA
FLOW RATE ------ 1.00E+6 LBM/SQFT-HR
HEAT FLUX ------ 0.10E+6 BTU/SQFT-HR
CODE ----------- 29

RUN	REF CODE	PRESURE	HEAT FLUX	FLOW RATE	INLET TEMP	GAMMA RATE 1	GAMMA RATE 2	GAMMA RATE 3	QUALITY	DENSITY (SIDE 2)	DENSITY (SIDE 3)	VOID (SIDE 2)	VOID (SIDE 3)
73	1	2193.	0.0932	1.018	589.5	275.04	149.43	121.16	-0.0993	40.59	40.43	-1.39	-0.83
72	1	2191.	0.0931	1.010	596.8	276.98	148.10	118.04	-0.0738	39.84	38.81	-1.42	2.21
71	1	2192.	0.0929	1.009	606.2	281.96	144.09	116.95	-0.0427	37.80	37.54	2.42	3.37
74	1	2192.	0.0938	1.008	612.7	285.76	139.10	112.69	-0.0190	35.73	35.25	7.51	9.31
70	1	2194.	0.0934	1.051	616.8	289.34	137.14	112.35	-0.0103	34.62	34.58	10.75	10.93
75	1	2192.	0.0945	1.014	621.1	293.55	127.30	105.64	0.0115	31.19	31.39	21.62	20.85
69	1	2194.	0.0941	0.993	627.9	305.14	120.04	96.36	0.0391	27.76	26.49	32.47	37.40

PRESSURE ------- 2000 PSIA
FLOW RATE ------ 0.30E+6 LBM/SQFT-HR
HEAT FLUX ------ 0.10E+6 BTU/SQFT-HR
CODE ----------- 30

RUN	REF CODE	PRESURE	HEAT FLUX	FLOW RATE	INLET TEMP	GAMMA RATE 1	GAMMA RATE 2	GAMMA RATE 3	QUALITY	DENSITY (SIDE 2)	DENSITY (SIDE 3)	VOID (SIDE 2)	VOID (SIDE 3)
403	15	2011.	0.0930	0.287	368.2	257.62	158.44	128.38	-0.3031	48.76	47.91	-6.38	-4.11
404	15	2010.	0.0934	0.289	395.7	262.94	156.06	127.65	-0.2416	46.81	46.44	-5.61	-4.57
405	15	2012.	0.0933	0.286	458.8	274.89	150.91	120.57	-0.0916	42.78	41.09	-7.77	-2.18
411	15	1992.	0.0931	0.289	483.5	283.58	145.40	117.52	-0.0308	39.53	38.34	-1.43	2.09
406	15	2008.	0.0931	0.287	498.3	290.46	136.15	110.13	0.0036	35.64	34.34	9.81	13.67
407	15	2003.	0.0933	0.289	525.3	309.33	116.64	96.20	0.0720	27.56	26.66	33.91	36.57
408	15	2001.	0.0931	0.289	555.6	329.16	90.89	77.83	0.1509	18.76	18.32	60.06	61.38
409	15	2002.	0.0929	0.285	581.9	342.91	71.73	63.70	0.2303	12.98	12.67	78.67	79.85
410	15	2004.	0.0932	0.289	595.8	357.03	74.71	65.28	0.2661	13.00	12.42	77.40	79.84

FINAL DATA (ENGLISH UNITS)

PRESSURE ------- 2200 PSIA
FLOW RATE ------ 0.30E+6 LBM/SQFT-HR
HEAT FLUX ------ 0.10E+6 BTU/SQFT-HR
CODE ----------- 31

RUN	REF CODE	PRESURE	HEAT FLUX	FLOW RATE	INLET TEMP	GAMMA RATE 1	GAMMA RATE 2	GAMMA RATE 3	QUALITY	DENSITY (SIDE 2)	DENSITY (SIDE 3)	VOID (SIDE 2)	VOID (SIDE 3)
412	15	2202.	0.0929	0.287	456.3	273.93	150.11	122.75	-0.1611	42.70	42.18	-6.12	-4.24
413	15	2197.	0.0935	0.287	480.0	278.38	146.38	119.45	-0.0934	40.72	40.01	-6.60	-4.07
414	15	2203.	0.0935	0.287	504.6	286.89	144.39	116.39	-0.0295	38.68	37.36	-3.97	0.28
415	15	2200.	0.0932	0.286	520.6	296.54	136.47	109.09	0.0144	34.86	33.08	8.32	14.01
416	15	2200.	0.0933	0.286	538.9	305.83	119.95	100.21	0.0661	28.88	28.54	27.39	28.49
417	15	2200.	0.0940	0.286	561.2	322.67	107.65	87.91	0.1348	23.75	22.35	43.79	48.25
418	15	2198.	0.0932	0.286	578.1	335.29	98.18	81.84	0.1828	20.20	19.21	55.13	58.30
419	15	2204.	0.0936	0.287	590.0	340.78	83.95	73.10	0.2210	16.18	15.90	67.95	68.86
420	15	2199.	0.0939	0.287	609.5	352.63	70.09	61.00	0.2878	12.09	11.29	83.40	86.61

PRESSURE ------- 2450 PSIA
FLOW RATE ------ 0.30E+6 LBM/SQFT-HR
HEAT FLUX ------ 0.10E+6 BTU/SQFT-HR
CODE ----------- 32

RUN	REF CODE	PRESURE	HEAT FLUX	FLOW RATE	INLET TEMP	GAMMA RATE 1	GAMMA RATE 2	GAMMA RATE 3	QUALITY	DENSITY (SIDE 2)	DENSITY (SIDE 3)	VOID (SIDE 2)	VOID (SIDE 3)
486	20	2450.	0.0929	0.300	468.5	214.96	0.00	109.16	-0.2480	0.00	42.14	0.00	-4.68
487	20	2461.	0.0933	0.298	496.6	219.61	0.00	106.65	-0.1632	0.00	39.96	0.00	-5.88
488	20	2461.	0.0938	0.290	515.5	224.97	0.00	103.69	-0.0872	0.00	37.53	0.00	-5.67
489	20	2459.	0.0937	0.278	542.8	235.49	0.00	95.78	0.0230	0.00	32.23	0.00	11.13
490	20	2444.	0.0947	0.299	559.7	241.54	0.00	87.65	0.0522	0.00	27.96	0.00	26.69
491	20	2446.	0.0950	0.298	578.7	249.37	0.00	81.10	0.1202	0.00	24.31	0.00	39.65
492	20	2463.	0.0956	0.299	606.3	258.93	0.00	70.96	0.2189	0.00	19.36	0.00	57.21
421	15	2448.	0.0937	0.287	611.3	339.11	94.36	77.33	0.2515	18.94	17.42	58.75	64.17
422	15	2450.	0.0935	0.284	622.7	345.38	82.64	70.50	0.3012	15.57	14.76	70.75	74.24

PRESSURE ------- 1600 PSIA
FLOW RATE ------ 0.30E+6 LBM/SQFT-HR
HEAT FLUX ------ 0.10E+6 BTU/SQFT-HR
CODE ----------- 33

RUN	REF CODE	PRESURE	HEAT FLUX	FLOW RATE	INLET TEMP	GAMMA RATE 1	GAMMA RATE 2	GAMMA RATE 3	QUALITY	DENSITY (SIDE 2)	DENSITY (SIDE 3)	VOID (SIDE 2)	VOID (SIDE 3)
431	15	1612.	0.0940	0.289	409.9	266.93	152.59	124.39	-0.0908	44.84	44.21	-3.48	-1.76
430	15	1608.	0.0939	0.291	427.0	272.81	152.07	124.03	-0.0580	43.54	42.91	-2.80	-1.04
429	15	1600.	0.0941	0.289	443.1	280.18	145.90	118.07	-0.0203	40.26	39.14	4.32	7.27
428	15	1604.	0.0937	0.286	458.3	288.67	132.99	111.10	0.0122	34.94	34.99	18.27	18.14
427	15	1609.	0.0940	0.293	475.9	305.50	114.68	94.21	0.0410	27.42	26.35	38.04	40.86
426	15	1603.	0.0936	0.286	506.9	331.65	86.07	74.90	0.1148	17.32	17.13	64.70	65.20
425	15	1601.	0.0935	0.286	527.0	341.83	77.30	68.54	0.1598	14.44	14.33	72.29	72.58
423	15	1599.	0.0943	0.287	552.5	358.45	68.81	61.81	0.2209	11.51	11.26	80.32	81.15
424	15	1600.	0.0940	0.287	570.5	366.25	61.70	58.63	0.2631	9.51	9.92	86.26	84.85

FINAL DATA (ENGLISH UNITS)

PRESSURE ------- 1000 PSIA
FLOW RATE ------ 0.15E+6 LBM/SQFT-HR
HEAT FLUX ------ 0.10E+6 BTU/SQFT-HR
CODE ----------- 34

RUN	REF CODE	PRESURE	HEAT FLUX	FLOW RATE	INLET TEMP	GAMMA RATE 1	GAMMA RATE 2	GAMMA RATE 3	QUALITY	DENSITY (SIDE 2)	DENSITY (SIDE 3)	VOID (SIDE 2)	VOID (SIDE 3)
465	17	999.	0.0940	0.146	222.7	292.15	112.88	94.43	0.0422	27.84	27.50	41.94	42.71
464	17	1001.	0.0939	0.145	257.1	314.13	90.73	78.87	0.0960	19.44	19.52	60.97	60.79
463	17	1000.	0.0937	0.145	294.0	336.05	72.36	64.60	0.1530	13.19	13.08	75.16	75.41
436	15	1005.	0.0940	0.146	338.7	366.47	59.90	53.91	0.2233	9.08	8.47	84.51	85.89
435	15	1013.	0.0941	0.146	369.0	372.80	52.14	49.92	0.2694	7.07	7.02	89.09	89.19
462	17	1001.	0.0940	0.145	397.6	374.58	46.07	44.76	0.3214	5.46	5.24	92.71	93.20
434	15	1016.	0.0935	0.151	403.0	378.50	48.68	46.14	0.3021	6.12	5.71	91.27	92.19
433	15	1023.	0.0928	0.146	439.8	384.46	41.85	40.63	0.3783	4.44	3.93	95.47	96.27
432	15	1021.	0.0932	0.146	465.5	386.05	38.31	37.36	0.4265	3.62	2.95	97.50	98.51

PRESSURE ------- 1600 PSIA
FLOW RATE ------ 0.15E+6 LBM/SQFT-HR
HEAT FLUX ------ 0.05E+6 BTU/SQFT-HR
CODE ----------- 35

RUN	REF CODE	PRESURE	HEAT FLUX	FLOW RATE	INLET TEMP	GAMMA RATE 1	GAMMA RATE 2	GAMMA RATE 3	QUALITY	DENSITY (SIDE 2)	DENSITY (SIDE 3)	VOID (SIDE 2)	VOID (SIDE 3)
439	16	1604.	0.0463	0.145	396.2	263.64	157.03	126.36	-0.1220	46.46	46.32	-4.78	-4.42
440	16	1601.	0.0461	0.144	425.5	267.71	153.63	124.65	-0.0625	44.52	44.74	-4.96	-5.55
441	16	1601.	0.0463	0.144	442.1	272.19	151.99	123.02	-0.0278	43.14	43.16	-3.28	-3.33
442	16	1596.	0.0467	0.145	465.9	282.48	143.32	115.74	0.0245	38.62	38.29	8.69	9.57
444	16	1603.	0.0469	0.144	481.4	298.38	131.22	107.57	0.0576	32.69	32.65	24.22	24.32
443	16	1602.	0.0468	0.144	503.9	319.00	101.34	84.73	0.1073	22.11	21.83	52.09	52.84
445	16	1599.	0.0463	0.144	527.0	341.80	91.21	79.46	0.1546	17.74	18.14	63.60	62.56
446	16	1602.	0.0469	0.144	568.7	363.20	71.76	64.90	0.2549	11.85	12.12	79.11	78.41

PRESSURE ------- 2200 PSIA
FLOW RATE ------ 0.15E+6 LBM/SQFT-HR
HEAT FLUX ------ 0.05E+6 BTU/SQFT-HR
CODE ----------- 36

RUN	REF CODE	PRESURE	HEAT FLUX	FLOW RATE	INLET TEMP	GAMMA RATE 1	GAMMA RATE 2	GAMMA RATE 3	QUALITY	DENSITY (SIDE 2)	DENSITY (SIDE 3)	VOID (SIDE 2)	VOID (SIDE 3)
455	16	2207.	0.0469	0.143	483.3	281.77	148.06	120.65	-0.0867	40.20	40.42	-5.83	-6.62
454	16	2208.	0.0463	0.145	500.5	284.81	144.78	117.96	-0.0522	38.70	38.81	-4.14	-4.50
453	16	2198.	0.0463	0.145	524.4	294.61	138.63	113.47	0.0177	35.36	35.48	6.75	6.38
450	16	2199.	0.0466	0.143	552.0	312.35	120.04	97.48	0.1056	27.85	27.13	30.70	33.01
447	16	2203.	0.0468	0.144	575.9	340.15	105.04	87.99	0.1753	21.32	21.12	51.52	52.16
449	16	2201.	0.0465	0.143	592.7	348.41	89.75	77.82	0.2281	16.95	17.13	65.50	64.93
448	16	2201.	0.0463	0.144	616.0	358.40	82.53	72.34	0.3024	14.65	14.73	72.92	72.60

FINAL DATA (ENGLISH UNITS)

PRESSURE ------- 2450 PSIA
FLOW RATE ------ 0.15E+6 LBM/SQFT-HR
HEAT FLUX ------ 0.05E+6 BTU/SQFT-HR
CODE ----------- 37

RUN	REF CODE	PRESURE	HEAT FLUX	FLOW RATE	INLET TEMP	GAMMA RATE 1	GAMMA RATE 2	GAMMA RATE 3	QUALITY	DENSITY (SIDE 2)	DENSITY (SIDE 3)	VOID (SIDE 2)	VOID (SIDE 3)
457	16	2455.	0.0463	0.145	486.5	276.66	147.53	119.19	-0.1799	40.92	40.72	-7.55	-6.77
458	16	2457.	0.0462	0.146	531.4	287.08	142.00	115.19	-0.0453	37.49	37.32	-7.66	-7.03
459	16	2444.	0.0462	0.144	558.5	299.79	132.24	108.99	0.0548	32.80	33.01	9.49	8.74
460	16	2466.	0.0458	0.143	580.1	309.87	121.16	99.11	0.1202	28.44	28.01	24.58	26.11

PRESSURE ------- 1000 PSIA
FLOW RATE ------ 0.30E+6 LBM/SQFT-HR
HEAT FLUX ------ 0.20E+6 BTU/SQFT-HR
CODE ----------- 38

RUN	REF CODE	PRESURE	HEAT FLUX	FLOW RATE	INLET TEMP	GAMMA RATE 1	GAMMA RATE 2	GAMMA RATE 3	QUALITY	DENSITY (SIDE 2)	DENSITY (SIDE 3)	VOID (SIDE 2)	VOID (SIDE 3)
468	18	1005.	0.1874	0.306	228.3	236.54	0.00	70.90	0.0204	0.00	21.26	0.00	56.82
470	18	1005.	0.1862	0.283	244.0	254.04	0.00	58.38	0.0843	0.00	14.66	0.00	71.81
469	18	1007.	0.1859	0.282	258.9	262.08	0.00	54.53	0.1079	0.00	12.64	0.00	76.42
471	18	999.	0.1870	0.302	272.1	257.17	0.00	53.51	0.0952	0.00	12.61	0.00	76.48
472	18	999.	0.1872	0.299	292.4	263.41	0.00	48.49	0.1324	0.00	10.36	0.00	81.58
473	18	1003.	0.1878	0.302	310.9	268.50	0.00	46.20	0.1572	0.00	9.25	0.00	84.11
474	18	1002.	0.1883	0.299	334.4	274.72	0.00	42.47	0.2033	0.00	7.63	0.00	87.78
475	18	1001.	0.1884	0.303	379.3	281.21	0.00	36.30	0.2680	0.00	5.25	0.00	93.18

PRESSURE ------- 2200 PSIA
FLOW RATE ------ 0.30E+6 LBM/SQFT-HR
HEAT FLUX ------ 0.20E+6 BTU/SQFT-HR
CODE ----------- 39

RUN	REF CODE	PRESURE	HEAT FLUX	FLOW RATE	INLET TEMP	GAMMA RATE 1	GAMMA RATE 2	GAMMA RATE 3	QUALITY	DENSITY (SIDE 2)	DENSITY (SIDE 3)	VOID (SIDE 2)	VOID (SIDE 3)
480	18	2203.	0.1868	0.303	274.3	210.46	0.00	114.60	-0.2083	0.00	44.78	0.00	-12.82
479	18	2202.	0.1878	0.301	280.2	211.40	0.00	110.34	-0.1838	0.00	42.60	0.00	-8.16
481	19	2190.	0.1900	0.300	309.6	220.24	0.00	108.38	-0.0968	0.00	39.71	0.00	-6.91
478	18	2200.	0.1881	0.297	331.0	224.60	0.00	104.61	-0.0475	0.00	37.18	0.00	0.91
477	18	2201.	0.1880	0.301	336.9	225.01	0.00	104.96	-0.0466	0.00	37.25	0.00	0.66
476	18	2203.	0.1881	0.300	351.4	229.45	0.00	101.25	-0.0095	0.00	34.83	0.00	8.34
482	19	2194.	0.1889	0.301	371.6	239.71	0.00	91.67	0.0450	0.00	29.20	0.00	26.47
483	19	2198.	0.1890	0.301	388.2	244.26	0.00	84.88	0.0847	0.00	25.87	0.00	37.05
484	19	2195.	0.1893	0.300	401.6	247.70	0.00	79.97	0.1231	0.00	23.52	0.00	44.56

FINAL DATA (ENGLISH UNITS)

PRESSURE ------- 1000 PSIA
FLOW RATE ------ 0.50E+6 LBM/SQFT-HR
HEAT FLUX ------ 0.20E+6 BTU/SQFT-HR
CODE ----------- 40

RUN	REF CODE	PRESURE	HEAT FLUX	FLOW RATE	INLET TEMP	GAMMA RATE 1	GAMMA RATE 2	GAMMA RATE 3	QUALITY	DENSITY (GAP)	DENSITY (CENTER)	VOID (GAP)	VOID (CENTER)
513	-	997.	0.1898	0.505	273.2	125.53	114.00	61.01	-0.1210	50.10	51.67	-0.70	-4.12
512	-	997.	0.1890	0.504	286.6	127.61	110.74	61.46	-0.1002	47.85	51.03	2.86	-4.16
514	-	999.	0.1884	0.504	311.4	133.99	96.69	61.40	-0.0632	39.40	48.08	19.31	-0.36
515	-	993.	0.1902	0.507	339.1	150.38	87.17	34.33	-0.0163	31.66	23.41	34.63	53.91
516	-	997.	0.1896	0.502	364.2	162.33	67.36	26.57	0.0246	21.62	16.53	56.73	68.96
517	-	1003.	0.1891	0.505	381.0	166.77	59.71	22.44	0.0478	18.05	13.51	64.65	75.73
518	-	995.	0.1897	0.505	400.8	173.97	49.51	16.27	0.0832	13.41	9.31	75.22	85.36

PRESSURE ------- 1000 PSIA
FLOW RATE ------ 1.00E+6 LBM/SQFT-HR
HEAT FLUX ------ 0.20E+6 BTU/SQFT-HR
CODE ----------- 41

RUN	REF CODE	PRESURE	HEAT FLUX	FLOW RATE	INLET TEMP	GAMMA RATE 1	GAMMA RATE 2	GAMMA RATE 3	QUALITY	DENSITY (GAP)	DENSITY (CENTER)	VOID (GAP)	VOID (CENTER)
519	-	1006.	0.1892	0.998	398.0	128.74	115.26	61.17	-0.0909	49.66	50.26	-1.40	-2.72
520	-	1007.	0.1891	0.990	424.7	132.74	109.99	61.02	-0.0455	45.93	48.33	3.70	-1.80
521	-	1002.	0.1887	0.994	441.2	140.67	97.06	54.56	-0.0173	37.96	40.30	20.32	14.84
522	-	1001.	0.1888	0.994	460.7	156.76	85.11	28.76	0.0165	29.68	18.65	37.99	64.31
523	-	1002.	0.1891	0.991	477.0	165.10	63.14	24.04	0.0455	19.59	14.65	61.19	73.18
524	-	1003.	0.1894	0.990	501.0	175.35	53.49	15.92	0.0887	14.82	9.03	71.77	86.12

PRESSURE ------- 1000 PSIA
FLOW RATE ------ 2.30E+6 LBM/SQFT-HR
HEAT FLUX ------ 0.20E+6 BTU/SQFT-HR
CODE ----------- 42

RUN	REF CODE	PRESURE	HEAT FLUX	FLOW RATE	INLET TEMP	GAMMA RATE 1	GAMMA RATE 2	GAMMA RATE 3	QUALITY	DENSITY (GAP)	DENSITY (CENTER)	VOID (GAP)	VOID (CENTER)
525	-	1001.	0.1901	2.145	474.8	132.88	114.83	61.36	-0.0500	48.16	48.54	-0.66	-1.52
526	-	1000.	0.1903	2.119	485.5	133.53	113.79	61.37	-0.0296	47.47	48.26	-0.57	-2.40
531	-	999.	0.1924	2.116	494.4	136.74	104.52	61.06	-0.0124	42.28	46.67	10.21	-0.03
527	-	1001.	0.1911	2.155	506.1	146.08	93.62	48.67	0.0064	35.26	34.36	25.49	27.63
529	-	1002.	0.1916	2.129	516.4	157.13	84.74	34.40	0.0262	29.47	22.25	38.20	55.61
530	-	1006.	0.1918	2.139	526.8	163.06	76.25	28.43	0.0447	25.11	17.59	48.07	66.21

FINAL DATA (ENGLISH UNITS)

PRESSURE ------- 1600 PSIA
FLOW RATE ------ 1.00E+6 LBM/SQFT-HR
HEAT FLUX ------ 0.10E+6 BTU/SQFT-HR
CODE ----------- 43

RUN	REF CODE	PRESURE	HEAT FLUX	FLOW RATE	INLET TEMP	GAMMA RATE 1	GAMMA RATE 2	GAMMA RATE 3	QUALITY	DENSITY (GAP)	DENSITY (CENTER)	VOID (GAP)	VOID (CENTER)
533	-	1600.	0.0938	0.992	520.9	135.68	112.02	59.59	-0.1050	45.97	45.97	-2.04	-2.04
534	-	1600.	0.0935	0.993	538.9	138.05	112.04	58.96	-0.0649	45.29	44.54	-3.69	-1.67
535	-	1601.	0.0938	0.996	556.0	139.74	105.00	57.76	-0.0247	41.64	43.00	2.73	-1.10
536	-	1599.	0.0940	0.993	565.2	143.14	97.93	55.01	-0.0017	37.67	39.79	11.94	5.81
537	-	1603.	0.0938	0.990	579.4	154.10	82.43	43.55	0.0330	28.91	28.84	34.79	34.99

PRESSURE ------- 1600 PSIA
FLOW RATE ------ 0.50E+6 LBM/SQFT-HR
HEAT FLUX ------ 0.10E+6 BTU/SQFT-HR
CODE ----------- 44

RUN	REF CODE	PRESURE	HEAT FLUX	FLOW RATE	INLET TEMP	GAMMA RATE 1	GAMMA RATE 2	GAMMA RATE 3	QUALITY	DENSITY (GAP)	DENSITY (CENTER)	VOID (GAP)	VOID (CENTER)
544	-	1598.	0.0935	0.506	492.2	137.13	108.14	59.72	-0.0697	43.77	45.48	0.50	-4.13
543	-	1601.	0.0936	0.506	504.5	139.05	106.58	58.42	-0.0437	42.54	43.76	1.44	-1.93
542	-	1602.	0.0936	0.505	514.1	141.57	98.00	57.88	-0.0223	38.07	42.43	12.16	-0.13
541	-	1602.	0.0934	0.504	522.7	145.86	87.83	56.62	-0.0035	32.67	40.04	26.05	4.86
540	-	1599.	0.0936	0.504	528.1	149.49	83.48	53.68	0.0100	30.13	36.86	32.49	13.29
539	-	1600.	0.0938	0.505	538.2	155.92	77.31	40.65	0.0327	26.48	26.54	41.73	41.58
538	-	1600.	0.0936	0.504	549.5	163.12	78.69	27.35	0.0589	26.00	16.91	41.85	68.68

PRESSURE ------- 1600 PSIA
FLOW RATE ------ 1.00E+6 LBM/SQFT-HR
HEAT FLUX ------ 0.20E+6 BTU/SQFT-HR
CODE ----------- 45

RUN	REF CODE	PRESURE	HEAT FLUX	FLOW RATE	INLET TEMP	GAMMA RATE 1	GAMMA RATE 2	GAMMA RATE 3	QUALITY	DENSITY (GAP)	DENSITY (CENTER)	VOID (GAP)	VOID (CENTER)
546	-	1604.	0.1879	0.995	478.7	135.56	109.28	59.94	-0.0951	44.73	46.29	-0.06	-4.18
547	-	1597.	0.1893	0.991	497.6	139.61	105.65	57.98	-0.0510	41.99	43.22	3.62	0.25
548	-	1600.	0.1879	0.992	516.5	145.61	92.30	53.36	-0.0123	34.68	37.81	20.96	12.08
549	-	1599.	0.1885	0.990	534.3	155.79	76.99	40.35	0.0287	26.37	26.37	42.26	42.28
550	-	1601.	0.1897	0.989	543.6	160.93	71.42	30.15	0.0515	23.36	18.95	49.93	62.99
551	-	1604.	0.1907	0.993	557.7	167.46	68.20	21.87	0.0845	21.27	13.10	54.62	79.01
552	-	1603.	0.1900	0.992	570.1	171.05	61.03	20.85	0.1142	18.07	12.18	63.29	81.12

FINAL DATA (ENGLISH UNITS)

PRESSURE ------- 1600 PSIA
FLOW RATE ------ 2.30E+6 LBM/SQFT-HR
HEAT FLUX ------ 0.20E+6 BTU/SQFT-HR
CODE ----------- 46

RUN	REF CODE	PRESURE	HEAT FLUX	FLOW RATE	INLET TEMP	GAMMA RATE 1	GAMMA RATE 2	GAMMA RATE 3	QUALITY	DENSITY (GAP)	DENSITY (CENTER)	VOID (GAP)	VOID (CENTER)
557	-	1602.	0.1915	2.292	529.8	137.52	111.11	58.51	-0.0973	45.04	44.41	-0.23	1.44
556	-	1599.	0.1905	2.286	550.1	139.49	108.73	57.98	-0.0501	43.40	43.26	0.09	0.48
555	-	1602.	0.1902	2.293	559.1	139.50	107.56	57.34	-0.0297	42.85	42.78	-0.20	-0.01
554	-	1595.	0.1908	2.288	570.0	144.47	98.61	53.85	-0.0010	37.67	38.52	11.97	9.52
553	-	1597.	0.1907	2.280	586.8	156.18	80.76	40.06	0.0417	27.88	26.10	37.34	42.66

PRESSURE ------- 2200 PSIA
FLOW RATE ------ 0.50E+6 LBM/SQFT-HR
HEAT FLUX ------ 0.20E+6 BTU/SQFT-HR
CODE ----------- 47

RUN	REF CODE	PRESURE	HEAT FLUX	FLOW RATE	INLET TEMP	GAMMA RATE 1	GAMMA RATE 2	GAMMA RATE 3	QUALITY	DENSITY (GAP)	DENSITY (CENTER)	VOID (GAP)	VOID (CENTER)
558	-	2201.	0.1892	0.509	437.3	142.18	100.20	54.71	-0.1428	38.88	39.90	7.36	4.02
559	-	2201.	0.1887	0.506	460.9	146.01	92.54	53.88	-0.0814	34.65	38.06	16.36	4.37
560	-	2200.	0.1894	0.507	480.4	150.26	80.92	50.57	-0.0287	28.83	34.51	32.96	11.92
561	-	2200.	0.1888	0.505	501.4	156.30	69.11	45.19	0.0274	22.95	29.42	51.10	25.97
562	-	2201.	0.1893	0.504	520.0	162.62	63.53	40.29	0.0804	19.89	25.01	60.01	39.76
563	-	2201.	0.1894	0.505	540.3	168.29	58.89	34.08	0.1375	17.45	20.30	67.08	55.13
564	-	2201.	0.1888	0.505	559.5	172.36	55.27	27.11	0.1918	15.66	15.69	72.24	72.09

PRESSURE ------- 2200 PSIA
FLOW RATE ------ 1.00E+6 LBM/SQFT-HR
HEAT FLUX ------ 0.10E+6 BTU/SQFT-HR
CODE ----------- 48

RUN	REF CODE	PRESURE	HEAT FLUX	FLOW RATE	INLET TEMP	GAMMA RATE 1	GAMMA RATE 2	GAMMA RATE 3	QUALITY	DENSITY (GAP)	DENSITY (CENTER)	VOID (GAP)	VOID (CENTER)
565	-	2208.	0.0945	1.022	590.0	141.46	105.14	55.42	-0.1015	41.22	40.66	-2.96	-1.07
566	-	2200.	0.0943	1.023	596.8	142.83	103.33	54.99	-0.0768	40.07	39.89	-1.32	-0.68
567	-	2202.	0.0944	1.024	609.6	145.07	101.36	52.82	-0.0340	38.66	37.60	-1.01	2.81
568	-	2199.	0.0941	1.019	615.1	146.54	97.59	52.72	-0.0133	36.68	37.08	4.00	2.49
569	-	2193.	0.0938	1.024	620.2	148.45	92.12	49.71	0.0059	33.93	34.43	12.48	10.55
570	-	2195.	0.0935	1.023	625.7	152.82	88.85	45.01	0.0257	31.72	30.10	18.89	25.24

FINAL DATA (ENGLISH UNITS)

PRESSURE ------- 2200 PSIA
FLOW RATE ------ 1.00E+6 LBM/SQFT-HR
HEAT FLUX ------ 0.20E+6 BTU/SQFT-HR
CODE ----------- 49

RUN	REF CODE	PRESURE	HEAT FLUX	FLOW RATE	INLET TEMP	GAMMA RATE 1	GAMMA RATE 2	GAMMA RATE 3	QUALITY	DENSITY (GAP)	DENSITY (CENTER)	VOID (GAP)	VOID (CENTER)
571	-	2202.	0.1908	1.022	531.8	140.42	104.59	55.16	-0.1448	41.26	40.83	0.77	2.15
572	-	2204.	0.1891	1.024	544.7	142.27	102.13	54.69	-0.1115	39.69	39.85	2.73	2.20
573	-	2201.	0.1883	1.025	565.1	144.35	97.84	53.24	-0.0518	37.29	38.13	5.30	2.26
574	-	2203.	0.1879	1.023	575.7	144.35	97.84	53.24	-0.0198	37.26	38.13	1.75	-1.57
575	-	2196.	0.1886	1.022	590.0	154.96	81.98	44.37	0.0283	28.49	29.18	30.75	28.02
576	-	2197.	0.1891	1.023	601.2	160.92	75.45	37.62	0.0657	24.92	23.64	41.81	46.87
577	-	2204.	0.1899	1.024	610.4	164.24	71.19	34.92	0.0959	22.77	21.42	48.36	53.83

PRESSURE ------- 2200 PSIA
FLOW RATE ------ 2.30E+6 LBM/SQFT-HR
HEAT FLUX ------ 0.20E+6 BTU/SQFT-HR
CODE ----------- 50

RUN	REF CODE	PRESURE	HEAT FLUX	FLOW RATE	INLET TEMP	GAMMA RATE 1	GAMMA RATE 2	GAMMA RATE 3	QUALITY	DENSITY (GAP)	DENSITY (CENTER)	VOID (GAP)	VOID (CENTER)
578	-	2202.	0.1893	2.263	598.3	144.03	103.67	54.56	-0.0840	39.95	39.18	-0.11	2.56
579	-	2203.	0.1890	2.247	605.5	145.32	103.90	54.19	-0.0591	39.73	38.50	-2.05	2.36
580	-	2202.	0.1897	2.244	610.3	146.29	101.98	54.79	-0.0419	38.67	38.61	-0.22	-0.01
581	-	2202.	0.1900	2.241	619.4	149.04	98.33	52.53	-0.0090	36.48	36.20	4.24	5.30
582	-	2202.	0.1906	2.130	631.6	157.36	84.14	43.38	0.0442	29.00	28.01	27.78	31.70

PRESSURE ------- 2000 PSIA
FLOW RATE ------ 1.00E+6 LBM/SQFT-HR
HEAT FLUX ------ 0.10E+6 BTU/SQFT-HR
CODE ----------- 51

RUN	REF CODE	PRESURE	HEAT FLUX	FLOW RATE	INLET TEMP	GAMMA RATE 1	GAMMA RATE 2	GAMMA RATE 3	QUALITY	DENSITY (GAP)	DENSITY (CENTER)	VOID (GAP)	VOID (CENTER)
583	-	2000.	0.0951	1.024	552.1	138.90	108.97	57.26	-0.1452	43.66	42.94	-1.03	1.06
584	-	2003.	0.0939	1.023	561.0	139.53	108.92	57.07	-0.1233	43.46	42.57	-2.39	0.27
585	-	2003.	0.0931	1.022	570.6	140.40	106.49	55.94	-0.0972	42.12	41.42	-0.69	1.49
586	-	2000.	0.0932	1.021	586.0	142.01	104.44	54.87	-0.0519	40.78	40.08	-0.82	1.45
587	-	2001.	0.0931	1.024	602.2	145.23	96.45	51.89	-0.0031	36.49	36.89	8.36	6.99
589	-	2001.	0.0934	1.022	609.7	149.52	91.22	46.87	0.0213	33.37	32.18	16.67	20.89
588	-	1999.	0.0934	1.013	618.9	157.04	79.91	39.33	0.0538	27.34	25.45	35.28	41.92

FINAL DATA (ENGLISH UNITS)

PRESSURE ------- 1600 PSIA
FLOW RATE ------ 0.50E+6 LBM/SQFT-HR
HEAT FLUX ------- 0.20E+6 BTU/SQFT-HR
CODE ------------ 52

RUN	REF CODE	PRESURE	HEAT FLUX	FLOW RATE	INLET TEMP	GAMMA RATE 1	GAMMA RATE 2	GAMMA RATE 3	QUALITY	DENSITY (GAP)	DENSITY (CENTER)	VOID (GAP)	VOID (CENTER)
592	-	1603.	0.1896	0.505	370.2	128.21	101.01	57.73	-0.1120	45.28	45.08	-0.88	-0.36
593	-	1603.	0.1900	0.506	385.2	131.21	97.39	56.12	-0.0827	42.58	42.63	3.90	3.76
594	-	1603.	0.1897	0.507	400.1	134.74	87.45	55.39	-0.0542	36.73	40.75	17.61	6.42
595	-	1600.	0.1897	0.505	414.6	139.90	76.57	52.47	-0.0235	30.35	36.90	33.38	14.81
596	-	1601.	0.1893	0.506	429.5	146.18	68.94	43.61	0.0047	25.65	29.10	45.17	35.19
597	-	1600.	0.1898	0.504	453.3	158.24	66.14	22.87	0.0553	22.64	13.87	51.47	77.20

PRESSURE ------- 1000 PSIA
FLOW RATE ------ 0.50E+6 LBM/SQFT-HR
HEAT FLUX ------- 0.20E+6 BTU/SQFT-HR
CODE ------------ 53

RUN	REF CODE	PRESURE	HEAT FLUX	FLOW RATE	INLET TEMP	GAMMA RATE 1	GAMMA RATE 2	GAMMA RATE 3	QUALITY	DENSITY (GAP)	DENSITY (CENTER)	VOID (GAP)	VOID (CENTER)
608	-	1004.	0.1898	0.506	300.3	122.32	95.72	57.68	-0.0805	47.98	47.96	0.99	1.05
606	-	998.	0.1892	0.504	311.5	128.00	87.22	54.78	-0.0613	41.47	43.13	14.52	10.76
605	-	1004.	0.1892	0.503	320.3	131.64	87.00	48.88	-0.0484	40.36	37.21	16.15	23.38
607	-	996.	0.1894	0.503	327.3	136.01	85.63	37.81	-0.0348	38.51	27.68	19.69	44.70
604	-	1000.	0.1905	0.502	333.2	139.54	85.41	33.25	-0.0237	37.55	23.60	21.19	53.70
603	-	1001.	0.1900	0.503	346.9	144.40	76.14	30.19	-0.0036	31.74	20.57	33.71	60.14
602	-	1002.	0.1894	0.504	365.8	153.07	63.36	25.01	0.0248	23.92	15.88	51.14	70.50
601	-	997.	0.1897	0.503	382.8	159.71	54.88	18.63	0.0544	18.99	11.25	62.14	81.08
599	-	1001.	0.1893	0.506	390.6	160.22	52.71	18.10	0.0641	16.63	10.82	67.70	81.99
598	-	1001.	0.1891	0.505	400.0	163.63	50.27	15.35	0.0799	15.24	8.94	70.75	86.32